University of Strathclyde

Strathclyde Institute for Pharmacy and Biomedical Sciences

Division of Physiology and Pharmacology

THE MOLECULAR PHARMACOLOGY OF PROTEINASE-ACTIVATED RECEPTOR 4 (PAR$_4$)

by

MARGARET ROSE CUNNINGHAM

A thesis presented in fulfilment of the requirements for the degree of Doctor of Philosophy

2010

I

Signed: Date:

ABSTRACT

Proteinase-activated receptors (PARs) are a novel G-protein coupled receptor (GPCR) family activated via proteolytic cleavage. Four subtypes exist, PAR_1 through to PAR_4. Whilst PAR_1 and PAR_2 have been thoroughly researched, the pharmacology and function of PAR_4 is less well defined. The aim of this study was to investigate the molecular pharmacology of PAR_4, assessing receptor localisation, intracellular trafficking and interaction with other proteins, namely PAR_2.

In this study PAR_4 was shown to be retained inside the endoplasmic reticulum (ER) in NCTC-2544 cells but expressed at the membrane in HEK293 cells. Analysis of the protein sequence for PAR_4 identified a functional arginine-based (RxR) ER retention sequence in intracellular loop-2 (ICL-2). Mutation of the $R^{183}AR$ retention sequence enhanced the cell surface expression of PAR_4 but rendered the receptor unable to activate ERK MAPK and inositol phosphate responses. Alanine substitution ($A^{183}AA$) allowed PAR_4 to undergo agonist-induced internalisation; a feature not observed during wild type PAR_4 receptor expression. In both cell types, PAR_4 interaction with the ER chaperone calnexin was observed; possibly contributing to ER retention. In HEK293 cells, tunicamycin abolished cell surface expression of PAR_4, thus identifying a potential role for N-linked glycosylation in the trafficking of PAR_4 to the membrane. During co-expression with PAR_2 in NCTC-2544 cells, PAR_4 was able to traffic to the cell surface. Despite this, no FRET was observed between PAR_4 and PAR_2 until treated with TNFα, an effect not observed during PAR_1/PAR_4 co-expression

These findings implicate a regulatory mechanism, distinct from PAR_1 and PAR_2, in the trafficking of PAR_4 to the plasma membrane. In addition, this work highlights a novel role for PAR_2 in the delivery of PAR_4 to the plasma membrane and a potential regulatory role for TNFα in PAR_2/PAR_4 heterodimerisation. This may influence the receptor pharmacology and the function of PAR_4 in normal physiology and disease.

PUBLICATIONS

Original Research Articles

Cunningham, M.R., Pediani, J.D., Robben, J. H., McIntosh, K.A., Gould, G., Milligan, G, and Plevin, R. (2010). *Investigating the endoplasmic reticulum (ER) retention of proteinase-activated receptor 4 (PAR$_4$): Involvement of Calnexin and PAR$_2$ interaction in the subcellular localisation of PAR$_4$.* (In Preparation)

Cadalbert, L.C., Sloss, C.M., **Cunningham, M.R.,** Al-Mutairi, M.S., McIntire, A., Shipley, J., and Plevin, R., (2010). *Differential regulation of MAP kinase activation by a novel splice variant of human MAP kinase phosphatase-2.* Cell Signalling 22 (3):357-65.

McIntosh, K.A., **Cunningham, M.R.,** Cadalbert, L.C., Ferrell, W.R., Lockhart, J., Boyd, G. and Plevin, R. (2010). *Proteinase-activated receptor-2 mediated inhibition of TNFalpha-stimulated JNK activation - A novel paradigm for G(q/11) linked GPCRs.* Cell Signalling 22(2):265-73

Kanke, T., Kabeya, M., Kubo, S., Kondo, S., Yasuoka, K., Tagashira, J., Ishiwata, H., Saka, M., Furuyama, T., Nishiyama, T., Doi, T., Hattori, Y., Kawabata, A., **Cunningham M. R.,** and Plevin R., (2009). *Novel peptide-mimetic antagonists for proteinase-activated receptor 2: inhibition of cellular and vascular responses.* BJP 158**:** 361-371.

Goon Goh, F., Sloss, C.M., **Cunningham, M.R.,** Nilsson, M., Cadalbert, L.C., and Plevin, R., (2008). *G-protein-dependent and -independent pathways regulate proteinase-activated receptor-2 -mediated p65 NFkappaB serine 536 phosphorylation in human keratinocytes.* Cell Signalling. 20 (7):1267-74.

Book Chapter

Cunningham, M.R., and Plevin, R., (2008). *Proteinase-Activated Receptors (PARs)*. Encyclopaedia of Molecular Pharmacology, Springer-Verlag Berlin and

Heidelberg GmbH & Co. K; 2Rev Ed. Editors: Stefan Offermanns & Walter Rosenthal.

Poster Presentations

Cunningham, M.R., Pediani, J.D., Robben, J. H., Gould, G., Milligan, G, and Plevin, R. (2009). *Investigating the endoplasmic reticulum (ER) retention of proteinase-activated receptor 4 (PAR$_4$): Involvement of Calnexin and PAR$_2$ interaction in the subcellular localisation of PAR$_4$.* Gordons Research Conference (GRC) Molecular Pharmacology Meeting, Il Ciocco, Italy.

Cunningham, M.R., Pediani, J.D., Milligan., and Plevin, R. (2008). *TNF-alpha regulation of proteinase-activated receptor 2 and 4 heterodimerisation.* University of Strathclyde Research Day, University of Strathclyde, Glasgow, UK. Poster number: 33.

Cunningham, M.R., Pediani, J.D., Milligan., and Plevin, R. (2008). *TNF-alpha regulation of proteinase-activated receptor 2 and 4 heterodimerisation.* SIPBS 2nd Year Cell Biology Seminars, University of Strathclyde, Glasgow, UK. Poster number: 1.

Cunningham, M.R., Pediani, J.D., Milligan, G., and Plevin, R. (2007). *Proteinase-activated receptor 2 and 4 heterodimerisation.* British Pharmacological Society Winter Meeting, Brighton, UK. Abstract number: P005. Published PA$_2$ online.

Oral Presentations

Cunningham, M.R., Pediani, J.D., Milligan, G., and Plevin, R., (2008). *TNF-alpha regulation of proteinase-activated receptor 2 and 4 heterodimerisation.* Elevated Symposia Presentation. EPHAR Congress Meeting, Manchester, UK. Abstract number: S11.C002.

Cunningham, M.R., Pediani, J.D., Milligan, G., and Plevin, R., (2008). *TNF-alpha regulation of proteinase-activated receptor 2 and 4 heterodimerisation.* Invited

presentation at Professor Graeme Milligan Research Group Seminar, University of Glasgow. July 8th 2008.

Cunningham, M.R., Pediani, J.D., Milligan, G., and Plevin, R., (2007). *Investigating PAR_2/PAR_4 interaction: Far from PARfection…but PAR dead brilliant man!* SIPBS 1st Year Cell Biology Seminars, University of Strathclyde, Glasgow, UK.

Cunningham, M.R., Goh, F.G., Nilsson, M., Sekiguchi, F., & Plevin, R., (2005). *Proteinase-activated receptor 2 mediated phosphorylation of p65 NFkB is regulated by an inhibitory K B kinase and PKC - dependent pathway in keratinocytes*. British Pharmacological Society Winter Meeting, London, UK.   Abstract number: Published PA_2 online.

ACKNOWLEDGEMENTS

To my parents,

       For giving me the confidence, determination and motivation to knock down social class boundaries to gain an education that some would believe was out with my reach. I thank you very much.

To Ian, my fiancé

       Thank you for your love and support over the past decade, especially during my studies. I doubt I would have come this far without your help 'DD'.

To Dylan, my son

       By far the most unexpected result of my whole PhD experience, you were my constant companion during the final year of my PhD.

       This is for you... just don't read it all in one go!

ABBREVIATIONS

AC	Adenylate cyclase
ANOVA	Analysis of variance
AP	Activating peptide
APS	Ammonium persulfate
AYPGKF-NH$_2$	Ala-Tyr-Pro-Gly-Lys-Phe-amidated (NH$_2$) peptide
BSA	Bovine serum albumin
cAMP	Cyclic adenosine-3′, 5′-monophosphate
DAG	Diacylglycerol
DTT	Dithiothreitol
ECFP	Enhanced cyan fluorescent protein
ECL	Enhanced chemiluminescence
ECL-2	Extracellular loop-2
EDTA	Ethylene diamine tetraacetic acid
ER	Endoplasmic reticulum
ERK	Extracellular signal-regulated kinase
EYFP	Enhanced yellow fluorescent protein
FCS	Foetal calf serum
FRET	Fluorescence/Fösters resonance energy transfer
GDP	Guanosine diphosphate
G-protein	Guanine nucleotide-binding protein
GPCR	G-protein-coupled receptor
GRK	G-protein-coupled receptor kinase
GTP	Guanosine triphosphate
HEK	Human embryonic kidney
HRP	Horseradish peroxidase
IP	Inositol phosphate
IP$_3$	Inositol 1,4,5,-triphosphate
JNK	c-jun N-terminal kinase
kDa	kilo-Dalton
mECFP	Monomeric enhanced cyan fluorescent protein
mEYFP	Monomeric enhanced yellow fluorescent protein

PAGE	Polyacrylamide gel electrophoresis
PAR	Proteinase-activated receptor
PBS	Phosphate buffered saline
PCR	Polymerase chain reaction
PDI	Protein disulfide isomerase
PI3K	Phosphatidylinositol-3 kinase
PIP$_2$	Phosphatidylinositol (4,5)-bisphosphate
PIP$_3$	Phosphatidylinositol (3,4,5)-trisphosphate
PKA	Protein kinase A
PKC	Protein kinase C
PLC	Phospholipase C
PTX	Pertussis toxin
SDS	Sodium dodecyl sulphate
SLIGKV-OH	Ser-Leu-Ile-Gly-Lys-Val-hydroxyl (OH)
TEMED	N,N,N',N'-tetramethylenediamine
TFLLR-NH$_2$	Thr-Phe-Leu-Leu-Arg-amidated (NH$_2$)
TNFα	Tumour necrosis factor-alpha
TNFR	Tumour necrosis factor receptor

AMINO ACID ABBREVIATIONS

Amino acid	Three-letter code	One-letter symbol
Alanine	**Ala**	A
Arginine	**Arg**	R
Asparagine	**Asn**	N
Aspartic acid	**Asp**	D
Cysteine	**Cys**	C
Glutamine	**Gln**	Q
Glutamic acid	**Glu**	E
Glycine	**Gly**	G
Histidine	**His**	H
Isoleucine	**Ile**	I
Leucine	**Leu**	L
Lysine	**Lys**	K
Methionine	**Met**	M
Phenylalanine	**Phe**	F
Proline	**Pro**	P
Serine	**Ser**	S
Threonine	**Thr**	T
Tryptophan	**Trp**	W
Tyrosine	**Tyr**	Y
Valine	**Val**	V

CONTENTS

List of Figures

List of Tables

Chapter 1

Chapter 2

CHAPTER 1

GENERAL INTRODUCTION

1. INTRODUCTION

1.1 THE G-PROTEIN-COUPLED RECEPTOR (GPCR) SUPER FAMILY

The G-protein-coupled receptor (GPCR) superfamily exists as integral membrane proteins that represent the most abundant of all of the cell surface receptors in mammalian cells (Foord *et al.,* 2005). GPCRs are synthesised in the endoplasmic reticulum (ER), where they undergo strict processing and folding prior to post-translational modification in the Golgi apparatus followed by export to the cell membrane (Dong *et al.,* 2007).

These proteins share the same overall structural topology, comprised of seven hydrophobic transmembrane spanning helices with an extracellular amino (N-) terminus and an intracellular carboxyl (C-) terminus (illustrated in Figure 1.1). This hallmark structure for GPCRs was initially characterised through the electron diffraction of bacteriorhodopsin (Henderson and Unwin, 1975). Subsequent molecular cloning of bovine rhodopsin (Nathans and Hogness, 1983) and α_1, α_2- and β-adrenergic receptors (Cotecchia *et al.,* 1988; Kobilka *et al.,* 1987; Dixon *et al.,* 1986) provide the structural template for which most GPCRs are now modelled (Henderson and Schertler, 1990).

Interest in the GPCR field has grown tremendously in light of the cellular activity these receptors mediate in response to a vast array of extracellular stimuli. This includes receptor activation in response to stimuli including sensory signals (e.g. olfactory and light), neurotransmitters, hormones, proteases, amongst others (reviewed by Kobilka, 2007). The broad range of GPCR families, together with the multitude of cell signalling cascades that occur downstream of receptor activation, has placed GPCRs as major targets for drug development; accountable for over 40% of all prescription drugs on the market (Filmore and David, 2004). These drugs range from treatment for psychosis to inflammation, obesity, cardiovascular disease and cancer. GPCRs play a role in a whole range of physiological events, a factor that will continue to drive research into identifying new therapeutic targets for drug discovery.

The number of GPCRs characterised to date, in addition to the increasing number of potential GPCR genes identified upon completion of the human genome project (Wise *et al.,* 2004) has enabled a thorough classification system for GPCRs to be devised (Alexander *et al.,* 2008 and 2007; Foord *et al.,* 2005). Within each class of GPCR, families exist based upon related sequence similarity, ligand specificity and receptor function (Alexander *et al.,* 2008). One system, designated by the Nomenclature Committees of the International Union of Pharmacology (NC-IUPHAR), classify GPCRs A-C or 1-3 (Foord *et al.,* 2005), with a fourth group allocated for Frizzled (FZD) family receptors (Schulte and Bryja, 2007). The classification of GPCRs has been further extended to include a series of 'orphan' GPCR genes, similarly grouped A-C (Foord *et al.,* 2005), for which endogenous ligands and functions remain to be fully understood (Chung *et al.,* 2008). Class A GPCRs, the largest of the classes, include rhodopsin-related receptors, adrenoreceptors, muscarinic acetylcholine receptors and the proteinase-activated receptor (PAR) family, among others (see Section 1.3). Class B GPCRs consist of glucagon and calcitonin receptor families. Class C GPCRs comprise of the metabotrophic glutamate-related receptors (mGlu) and $GABA_B$ receptor families.

Despite sharing similarity in the overall seven transmembrane structure, the mode of receptor activation of some Class A GPCRs differs greatly from one GPCR family to the next. It is widely accepted that the exposed N-terminal region and extracellular loops provides the ligand-binding pocket (or interacting sites). This allows cells to convert an array of extracellular stimuli (i.e. neurotransmitters, hormones and serine proteases) into intracellular signalling events. The intracellular domains of the receptor are responsible for the coupling of heterotrimeric guanine nucleotide binding proteins (G-proteins), an event that has the potential to mediate a multitude of second messenger signalling cascades (discussed in Section 1.1.1). Information retrieved from the protein analysis of the bovine opsin (Nathans and Hogness, 1983) and $β_2$-adrenergic receptor (Dixon *et al.,* 1986) and other GPCRs, such as the thrombin receptor, PAR_1 (Vu *et al.,* 1991a and 1991b), have highlighted that GPCR-ligand interactions can vary considerably. Many GPCR families can become reversibly activated through ligand docking within an extracellular binding pocket

(Gershengorn and Osman, 2001). Other modes of GPCR activation include non-ligand receptor activation following exposure to photons, as described for the light-sensitive rhodopsin family (Gershengorn and Osman, 2001). One GPCR family in particular, the PAR family, undergo 'self activation' through irreversible proteolytic cleavage of the N-terminal by serine proteases, revealing a new tethered ligand, which interacts with extracellular loop-2 (Vu *et al.,* 1991a and 1991b). This is discussed in detail in Section 1.3.

The intricate nature of ligand-GPCR and GPCR-G-protein interaction has been of considerable interest in the GPCR field for decades. However the rate limiting step in the progression of this field has been the difficulty in obtaining the crystal structure of GPCRs to provide important high-resolution information on the 3D arrangement of individual GPCRs. Information related to the spatial organisation of GPCRs has long relied upon the crystal structure of light-activated rhodopsin (Palczewski *et al.,* 2000). Improvements in the existing purification methods in Gebhard Schertler's laboratory has resulted in the crystal structures of the turkey β_1-adrenergic receptor (Warne *et al.,* 2008) and the human β_2-adrenergic receptor (Rasmussen *et al.,* 2007) being successfully derived. The crystal structure of the human adenosine A_{2A} receptor has also been recently resolved (Jaakola *et al.,* 2008). So far these studies have provided a structural framework for the understanding of certain agonist-GPCR (active) and antagonist-GPCR (inactive) conformational states. As this list continues to grow (Topiol and Sabio, 2009), so does the potential to study GPCR active and inactive states in other models. Steps have already been taken to establish the conformational changes that take place in transmembrane regions in active GPCR-G-protein bound models, as demonstrated by purified β_2-adrenoreceptor-G_s bound complexes studied in the laboratory of Brian Kobilka and co-workers (Yao *et al.,* 2009). The information that can be gained from GPCR crystallisation has the potential to advance existing knowledge of structure/function relationships. This could give insight into the structural arrangements of various active/inactive states of GPCRs, allosteric modulation of GPCRs and possibly identify specific sites that assist in GPCR dimerisation (Fung *et al.,* 2009). Such

information will provide a better understanding of the molecular mechanisms that underlie GPCR activation and subsequent G-protein coupling.
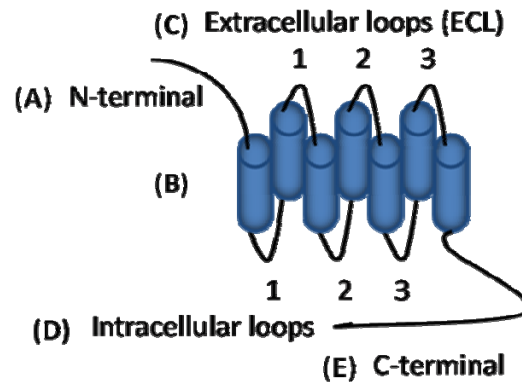
Figure 1.1. The basic structure of a G-protein-coupled receptor (GPCR).

The typical organisation of the GPCR structure, domains and transmembrane arrangement comprising an N-terminal (A), seven transmembrane alpha helices (B), three extracellular loops (C), three intracellular loops (D) and a C-terminal tail (E). Figure adapted from Kobilka, 2007.

1.1.1 G-protein-coupled receptor activation and signalling

GPCRs transmit extracellular stimuli into an intracellular signal primarily, but not exclusively through membrane-associated GTP-sensitive heterotrimeric guanine nucleotide binding proteins, otherwise known as G-proteins (Gilman, 1987; Rodbell, 1971). G-proteins are heterotrimeric in structure, comprised of α (39-46 kDa), β (35-36 kDa) and γ (~8-10 kDa) subunits (reviewed by Milligan and Kostenis, 2006). Over 20 Gα-subunit proteins have been identified to date; the main mammalian families characterised to date include $G\alpha_s$, $G\alpha_i$, $G\alpha_{q/11}$ and $G\alpha_{12/13}$, each of which have a number of splice variant isoforms and differentially regulate specific effectors (Table 1.1). When an agonist binds to a GPCR structural rearrangement within transmembrane helices of the receptor takes place which enables the receptor to switch from an inactive to an active conformation (reviewed by Gether, 2000). Once activated, G-protein couping can take place. Activation of G-proteins involves the exchange of GDP for GTP on the Gα subunit. This exchange causes conformational changes that result in the the dissociation of the GTP-bound Gα subunit from the Gβγ dimer, thus allowing both Gα and Gβγ subunits to freely interact with a diverse array of downstream effectors (Vilardaga *et al* 2009). Inactivation of G-proteins involves hydrolysis of GTP to GDP on the Gα subunit which in turn allows re-assembly of the Gα and Gβγ subunits to form the inactive Gαβγ heterotrimer. These events are facilitated by the GTPase activity of both the Gα subunit and interacting GTPase-accelerating proteins (GAPs) such as regulators of G-protein signalling (RGS) proteins (Xie and Palmer, 2008), the outcome of which is the attenuation of G-protein-mediated signal transduction.

Whilst focus has primarily been placed on targeting GPCRs with the aim to find effective therapeutic targets, increasing interest has now been placed upon heterotrimeric G-protein subunits as potential drug targets (Ayoub *et al.,* 2009). Pan-inhibition of the Gα-subunit, thus targeting all heterotrimeric G-proteins, has been demonstrated through the use of the imidazopirazine containing small molecule BIM-46187 (Ayoub *et al.,* 2009). This small molecule inhibits GDP/GTP exchange through the direct binding of BIM-46187 with Gα-subunit, without affecting the

recruitment of other scaffold proteins such as β-arrestin. Such inhibition strategies would allow for effective distinction between G-protein dependent and independent events downstream of GPCR activation.

i) Current perspectives in G-protein signalling

The development of fluorescent-labelling of proteins and the use of imaging technology (see Section 1.4) has provided great insight into protein localisation, distribution, co-localisation and protein-protein interactions. This has been particularly effective in investigating the intracellular sorting of GPCRs following ligand binding (Lohse *et al.,* 2008a and 2008b). Such studies have managed to pinpoint the kinetics of GPCR activation and signalling from the millisecond (ms) to the second (s) and minute (m) timescale (outlined in Lohse *et al.,* 2008a). The incorporation of optical techniques, such as fluorescence resonance energy transfer (FRET) has enabled researchers to establish the kinetics ($t_{1/2}$) of ligand binding and G-protein coupling to within 30-50 ms, receptor activation to 200-300 ms, and the recruitment of β-arrestin within 5 minutes of ligand binding (Hoffmann *et al.,* 2005; Vilardaga *et al.,* 2003). The actual rate of these steps may differ from GPCR to GPCR. The sensitivity of such approaches has even led to the conventional model of GPCR-G-protein coupling being re-appraised. Contrary to the belief that the G-protein Gα subunit dissociates from its respective Gβγ dimer during activation, as widely accepted for Gαi, evidence resulting from FRET experiments has found that rather than dissociate, the Gαi-Gβγ trimer merely undergoes conformational rearrangement to interact with their respective effectors (Bünemann *et al.,* 2003). However whether this applies to all G-proteins remains to be investigated.

ii) Gα$_s$-mediated signalling events

GPCRs that couple to the stimulatory G-protein subtype, Gα$_s$, activate adenylyl cyclase (AC), resulting in the production of the second messenger cyclic adenosine-3′, 5′-monophosphate (cAMP) and subsequent cAMP-dependent activation of a serine/threonine protein kinase, protein kinase A (PKA), (Dessauer *et al.,* 1996). Cholera toxin has been demonstrated as a useful tool for distinguishing Gα$_s$-mediated signalling events from other G-proteins. Early work found that Cholera

toxin was able to activate $G\alpha_s$ and through ADP-ribosylation, confine $G\alpha_s$ to a GTP-bound active state, resulting in constitutive G-protein activation and stimulation of the effector AC and downstream second messengers (Cassel and Selinger, 1977).

iii) $G\alpha_i$-mediated signalling events

In contrast to $G\alpha_s$-mediated signalling, receptors that couple to $G\alpha_i$ inhibit the activation of AC, resulting in the negative regulation of cAMP and PKA-mediated second messenger responses (Kostenis *et al.,* 2005). $G\alpha_i$ can also signal to small GTPases like Ras through its $G\beta\gamma$-dimer (Luttrell and Lefkowitz, 2002). Upon dissociation of the G-protein trimer, the $G\beta\gamma$-dimer can proceed to induce Src-dependent activation of matrix metalloproteinases (MMPs) at the plasma membrane. These events have been reported to precede transactivation of a receptor tyrosine kinase, such as c-Src, which subsequently activates mitogen-activated protein kinase (MAPK) pathways (reviewed by Bhattacharya *et al.,* 2004; Bar-Sagi and Hall, 2000). Dissociation of the $G\beta\gamma$-dimer upon $G\alpha_{i/o}$ activation has also been implicated in the regulation of potassium (K^+) channel conductance, which can alter cell membrane potential (Krapivinsky *et al.,* 1995). $G\alpha_i$ is pertussis toxin (PTX)-sensitive and therefore the use of this compound is a routine approach to demonstrate $G\alpha_i$-specific events. PTX inactivates $G\alpha_i$ through ADP ribosylation of the $G\alpha$ subunit and prevents the release of bound GDP, thus confining $G\alpha_i$ to an inactive state (reviewed by Hubbard and Hepler, 2006).

iv) $G\alpha_{q/11}$-mediated signalling events

Work by Strathmann and colleagues and others demonstrated that $G\alpha_{q/11}$ stimulates β isoforms of phospholipase C (PLC-β) directly through $G\alpha$-GTP and $G\beta\gamma$ subunits, leading to the hydrolysis of phosphatidylinositol 4,5 bisphosphate (PIP$_2$), (Strathmann and Simon, 1990; Cockcroft and Gomperts, 1985 and Cockcroft *et al.,* 1987). The products of this hydrolysis reaction are the second messengers diacylglycerol (DAG) and inositol 1,4,5-trisphosphate (Ins P$_3$), initially characterised through the work of Berridge and colleagues (Berridge *et al.,* 1983 and Berridge, 1983). Membrane-bound DAG directly activates isoforms of protein kinase C (PKC) whilst Ins P$_3$ mediates the release of calcium from intracellular stores (Streb *et al.,*

1983).   Both PKC and calcium have the potential to trigger multiple cellular responses and therefore have widespread roles as intracellular messengers (Bikle *et al.,* 2001; Mellor and Parker, 1998).   Similar to PKA, PKC is a serine/threonine kinase capable of phosphorylating multiple intracellular proteins including those involved in the MAPK cascade and various transcription factors, resulting in altered gene expression (Naor, 2009).   The recent development of a highly-specific $G\alpha_{q/11}$ inhibitor, cyclic depsipeptide YM-254890, although no longer commercially available, has enabled $G\alpha_{q/11}$ mediated signalling events to be distinguished.   YM-254890 blocks the exchange of GDP for GTP, thus confining $G\alpha_{q/11}$ in an inactive state (Takasaki *et al.,* 2004).

(v) $G\alpha_{12/13}$-mediated signalling events

The features of GPCR-$G\alpha_{12/13}$-coupled signalling have yet to be fully elucidated however, signalling via $G\alpha_{12/13}$ has been shown to involve the interaction of small monomeric G-proteins such as Ras homology (Rho) guanine nucleotide exchange factors (RhoGEFs), among other GTPases such as Rac (Hart *et al.,* 1998).   This has been shown to be important in actin reorganisation and regulation of gene expression (Tanabe *et al.,* 2004).   Subsequently, siRNA and $G\alpha_{13}$-specific knock out approaches have demonstrated the importance of $G\alpha_{13}$ in receptor tyrosine kinase (RTK)-mediated cell migration (Shan *et al.,* 2006), independent of GPCR coupling.

Table 1.1 Typical G-protein family downstream effectors

G-protein	Effectors	Second messengers	Typical responses*	References
$G\alpha_s$	↑ AC	↑ cAMP ↑ PKA	↓ K^+ channel conductance ↑ Na^+ and Cl^- channel conductance Cell metabolism Smooth muscle relaxation Gene expression regulation	Dessauer *et al.,* 1996 Sunahara *et al.,* 1997
$G\alpha_{i/o}$	↓ AC	↓cAMP ↓ PKA	Muscarinic effects	Kostenis *et al.,* 2005
$G\beta\gamma$-dimer	Src K^+ Channel Ca^{2+} Channel	MMPs	Transactivation of EGF/RTK receptors Ras-dependent MAPK activation ↑K^+ channel conductance Change in membrane potential ↓ Ca^{2+}	Luttrell and Lefkowitz, 2002 Prenzel *et al.,* 1999 Bhattacharya *et al.,* 2004 Krapivinsky *et al.,* 1995
$G\alpha_{q/11}$	↑ PLCβ	PIP_2 hydrolysis IP_3 accumulation Ca^{2+} mobilisation PKC activation	Muscle contractility Vasodilatation/constriction Platelet aggregation Altered gene expression Ras-dependent MAPK activation Rho signalling	Berridge *et al.,* 1983 Cockcroft and Gomperts, 1985 & Cockcroft *et al.,* 1987 Hubbard and Hepler, 2006 Streb *et al.,* 1983
$G\alpha_{12/13}$	↑ PLD RhoGEF	RhoA Rac	Cytoskeletal rearrangement RTK-mediated cell migration	Hart *et al.,* 1998 Bhattacharya *et al.,* 2004 Shan *et al.,* 2006

* Note this list is not comprehensive. Typical responses will vary in accordance to the GPCR family in question and tissue/cellular distribution.

1.1.2 GPCR signal termination and downregulation

The central events that underlie GPCR signalling depend upon G-protein coupling to effectors to initiate signal transduction, with G-protein uncoupling required to terminate signalling (Sibley *et al.,* 1987). The most important proteins that have been implicated in GPCR signal termination at the membrane include G-protein receptor kinases (GRKs), (Premont *et al.,* 1995), arrestin proteins (Ma and Pei, 2007; Benovic *et al.,*1987) and regulators of G-protein signalling (RGSs), (for current reviews see Wieland *et al.,* 2003; Hollinger *et al.,* 2002; De Vries *et al.,* 1999).

i) GRK-mediated GPCR desensitisation

Following the work of Lefkowitz and colleagues from the late 1980's, it is now widely accepted that activation of a number of GPCRs including β_2-adrenergic receptors (Benovic *et al.,* 1985) is attenuated, in part, due to phosphorylation (Sibley *et al.,* 1987). Phosphorylation of GPCRs, such as the β_2-adrenergic receptor involves various serine/threonine protein kinases; PKA and PKC (Chuang *et al.,* 1996; Benovic *et al.,* 1985) and G-protein coupled receptor kinases (GRKs), (Attramadal *et al.,* 1992; Sibley *et al.,* 1987; Benovic *et al.,* 1986). The rate at which PKA/PKC phosphorylate GPCRs is somewhat slower ($t_{1/2}$ = 3 minutes) than that of GRK-dependent phosphorylation ($t_{1/2}$ = 15 seconds), (Roth *et al.,* 1991). PKA and PKC are usually associated with agonist-independent GPCR phosphorylation, whilst GRKs usually require agonist activation to mediate receptor phosphorylation. For many GPCRs, the latter model of receptor phosphorylation/dephosphorylation is more widely applicable. This involves GPCR activation and G-protein coupling upon ligand binding, followed by receptor phosphorylation, G-protein uncoupling and GRK recruitment. These events precede β-arrestin binding followed by receptor internalisation, dephosphorylation, receptor sorting and dissociation of receptor/agonist complexes to enable receptor resensitisation and recycling back to the plasma membrane. These events are outlined in Figure 1.2. Generally GRKs exist in an inactive state (Inglese *et al.,* 1993) and target GPCRs when the receptor exists in an agonist-occupied conformation. Initially described for rhodopsin (i.e. GRK1) and β-adrenergic receptors (i.e. βARK, GRK2), more GRK isoforms have since been identified, including βARK2/GRK3 and GRK4-GRK6. Unlike the name

suggests, the specificity of βARK-type GRKs is not limited to adrenergic receptors. These proteins are capable of targeting multiple GPCR families at different sites within the receptor (Willets *et al.,* 2003). GPCR phosphorylation by GRKs was found to be at serine-threonine rich regions, in particular serine residues 355, 356, and 364 on the C-terminal, as described for GRK2 in the β_2-adrenergic receptor (Vaughan *et al.*, 2006; Fredericks *et al.,* 1996). Other receptors, such as the α_2-adrenergic receptor where the C-terminal tail is shorter, have GRK phosphorylation sites located within intracellular loop-3 (Eason *et al.,* 1995; Liggett *et al.,* 1992). GRK-dependent phosphorylation of GPCRs precedes β-arrestin recruitment, resulting in receptor internalisation and signal desensitisation. The distinct mechanism through which GRK activation occurs remains to be fully elucidated (Sterne-Marr *et al.,* 2009) However recent investigation into the activation of GRKs by the chemokine receptor CCR7 has identified the ability of different selective CCR7 agonists to preferentially activate specific GRK isoforms (Zidar *et al.,* 2009) with a significant impact upon the role β-arrestin performs when recruited.

ii) The role of β-arrestin in GPCR trafficking

Studies involving prototypical GPCRs such as rhodopsin and the β-adrenergic receptors, among other families, have demonstrated the recruitment of β-arrestin to the phosphorylated GPCR following GRK-meditated phosphorylation (Oakley *et al.,* 2000; Zhang *et al.*. 1999; Zhang *et al.,* 1997; Ferguson *et al.,* 1996; Gurevich *et al.,* 1995). Arrestins are cytosolic proteins that include visual arrestins, cone arrestins, β-arrestins and D/E-arrestins; each sharing varying degrees of homology (Ferguson *et al.,* 1996a and b). Early studies involving the β-adrenergic receptor family highlighted the role of β-arrestins in receptor trafficking through their ability to uncouple G-proteins and mediate desensitisation (Attramadal *et al.,* 1992). Furthermore, it has been suggested that GRK-mediated phosphorylation promotes high affinity binding of β-arrestin and enhances receptor desensitisation (Freedman *et al.,* 1995). The activity of β-arrestin isoforms is crucial in the transition between receptor activation, desensitisation, internalisation and resensitisation in the GPCR recycling process. The mechanism through which β-arrestin is involved in GPCR recycling has been extensively studied, with many secondary interactions between β-

arrestins and other cellular proteins documented (Lefkowitz and Shenoy, 2005; Goodman *et al.,* 1997). One proposed molecular mechanism of β-arrestin-mediated internalisation involves interaction between β-arrestin and clathrin in coated pits, as detailed in Figure 1.2. This was demonstrated for the β_2-adrenergic receptor where the receptor was observed to co-localise with both β-arrestin and clathrin (Goodman *et al.,* 1996). This co-localisation was further confirmed when studies found that the GPCR-β-arrestin-clathrin interaction was disrupted in the absence of fully functional β-arrestin, which subsequently affected internalisation (Krupnick *et al.,* 1997).

The functional diversity and specificity of the actions of arrestin isoforms have been demonstrated between Class A and Class B GPCRs, as well as families that exist within GPCR Classes (Kohout *et al.,* 2001; Oakley *et al.,* 2000). These studies have demonstrated that a preferential high affinity binding of β-arrestin2 exists among members of Class A GPCRs, resulting in receptor desensitisation, internalisation and signal termination. In addition, it has also been proposed that β-arrestin2 can support receptor internalisation through interaction with the clathrin adaptor protein AP-2 (Laporte *et al.*, 2000; Laporte *et al.,* 1999). Despite this, evidence has emerged suggesting that β-arrestin1 plays a more significant role than β-arrestin2 in the signal termination of some members of Class A GPCRs, namely the proteinase-activated receptors (PAR) family, (Chen *et al.,* 2004). In addition to the role of β-arrestins in receptor desensitisation, studies have since identified a clear β-arrestin-mediated extracellular-related kinase (ERK) pathway, thus highlighting the potential of β-arrestin to serve as a scaffold protein to mediate cell signal transduction in addition to signal termination (see Section 1.1.2. iv).

iii) Regulator of G-protein signalling (RGS) proteins
RGS family proteins are often referred to as GTPase-activating proteins (GAPs), for which there are over 20 family members (Dohlman *et al.*, 1997), subgrouped into families A-F (Zheng *et al.,* 1999). These proteins facilitate in GTP hydrolysis at the Gα subunit to return it to the inactive GDP-bound state. Each RGS subtype display differential activity depending upon the G-protein. Small RGS protein family B members comprise the largest group and include RGS1, RGS4, RGS5, RGS8,

RGS13 and RGS16 which all display intrinsic GTPase activity for $G\alpha_{i/o}$ and $G\alpha_{q/11}$ proteins (Wieland *et al.*, 2003), with no GAP activity observed for $G\alpha_s$ or $G\alpha_{12/13}$ proteins. This preferential GAP activity for $G\alpha_{i/o}$ and $G\alpha_{q/11}$ proteins can be extended to RGS3 family members. However RGS3 subtypes have been shown to also target the $G\beta\gamma$ dimer, thus inactivating $G\beta\gamma$-specific signalling events (Shi *et al.*, 2001). The use of bioluminescence resonance energy transfer (BRET) has identified interaction between RGS2 and $G\alpha_s$ protein, thus resulting in inhibition of cAMP production (Roy *et al.*, 2006). GAP activity for $G\alpha_{12/13}$ has been documented for family D RGS, RGS12 (Snow *et al.*, 1998). Immunoprecipitation techniques have identified instances where RGS subfamilies can directly interact with many GPCRs, independent of G-protein coupling or receptor activation. This has been documented for RGS2 interaction with intracellular loop-3 of M_1 muscarinic receptors (Bernstein *et al.*, 2004) and β_2-adrenergic receptors (Roy *et al.*, 2006).

iv) G-protein-independent signal transduction; β-arrestin as a scaffold protein

The versatility of arrestin proteins as signalling molecules has become apparent in recent years. Whilst previous work has predominantly focussed on the role of β-arrestin isoforms in receptor trafficking, the role of arrestins as adaptor proteins in the scaffolding of mitogenic signalling pathways has emerged (reviewed by Lefkowitz and Whalen, 2004). Conformational rearrangement of β-arrestin and the phosphorylated state of the GPCR is thought to be significant in the transition between β-arrestin interaction in trafficking and functioning as a scaffolding protein in mitogenic cell signalling events (Gurevich and Gurevich, 2004). G-protein-independent activation of ERK has been observed in the Class A GPCR, proteinase-activated receptor-2 (DeFea *et al.*, 2000b) and the Class B GPCR, AT1A angiotensin receptor (Wei *et al.*, 2003) among others, identifying a clear β-arrestin-mediated ERK pathway. Structural analysis of β-arrestin isoforms led to the identification of distinct domains responsible for interaction with multiple proteins such as Src family tyrosine kinases, Raf-1 and MEK, clathrin and AP-2 (Luttrell *et al.*, 2002). Recent proteomic analysis carried out by researchers in Lefkowitz's laboratory found that β-arrestin has the potential to interact with up to 337 different cellular proteins (Xiao *et al.*, 2007). Of these proteins, 173 were shown to interact preferentially with β-

arrestin1, 266 with β-arrestin-2 and 102 for both isoforms. Potential interacting proteins range from those associated with apoptosis to metabolic enzymes and those involved in cellular organisation. This comprehensive study provides an insight into the pivotal role β-arrestin may play in a vast array of major cellular events.
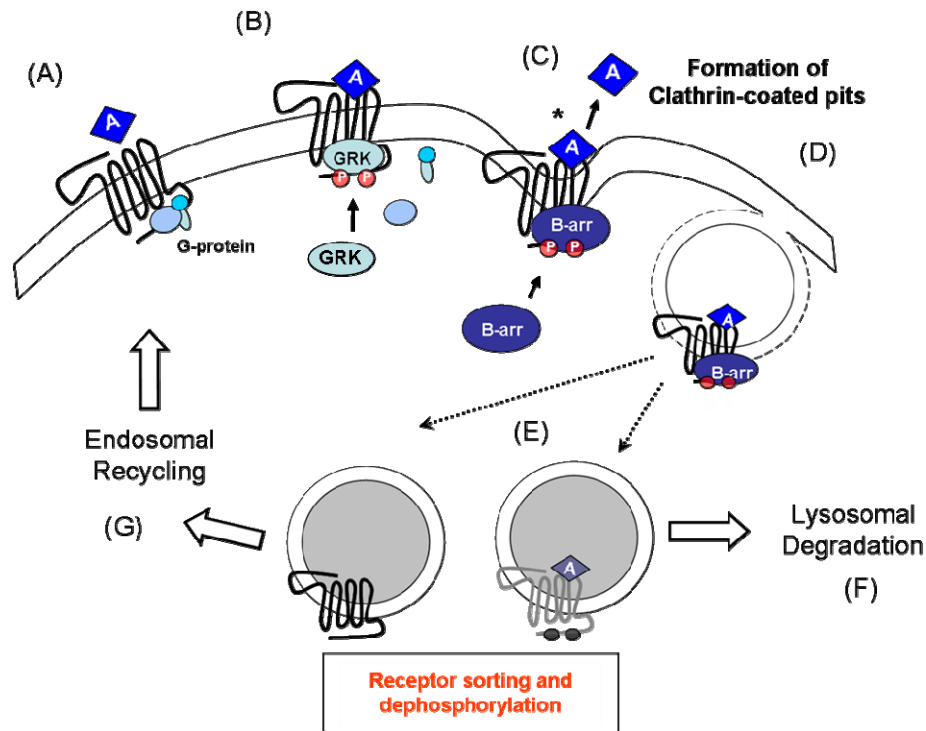
Figure 1.2. Intracellular sorting of Class A GPCRs following receptor activation. Upon agonist binding, GPCR-G-protein coupling takes place (A). In the agonist-occupied state, GRK-mediated receptor phosphorylation and G-protein uncoupling takes place (B) followed by recruitment of β-arrestin (C). This results in receptor desensitisation. *Depending upon the GPCR in question, an agonist may reversibly bind to the GPCR and be released prior to internalisation or be internalised into clathrin coated pits as a GPCR-agonist complex (D). Early endosomes are then formed (E) where receptor sorting and dephosphorylation can take place. This receptor complex can be targeted for lysosomal degradation via ubiquitination (F). Removal of the agonist results in resensitisation and the GPCR can be recycled back to the membrane (G) where agonist responsiveness will be regained. Figure adapted from Ma and Pei, 2007.

1.2 THE ROLE OF THE ER IN GPCR-PROTEIN INTERACTIONS AND GPCR DIMERISATION

1.2.1 Maturation of GPCRs in the ER

Whilst the events that underlie GPCR trafficking from the plasma membrane to intracellular compartments have been extensively studied, very little is known with respect to the pathways that take place in the export of GPCRs to the membrane. GPCR biosynthesis and maturation takes place in the secretory pathway comprised of the ER and Golgi (see Figure 1.3), with properly assembled receptors exported to the plasma membrane (Lippincott-Schwartz *et al.,* 2000).

Many processes take place in the ER, ranging from protein folding and assembly to sorting and degradation (Hirsch *et al.,* 2009). These events are tightly regulated and involve multiple interacting accessory proteins (Cooray *et al.,* 2009). The quality control checkpoint of the ER ensures that ER-resident proteins are sorted distinctly from cargo proteins destined for secretion. Several ER chaperone proteins facilitate in the folding and sorting process in the ER. The role of these proteins is discussed further in Section 1.2.1 i. Specific signal motifs that reside within the synthesised proteins allows efficient sorting of proteins (refer to Section 1.2.1 ii).

i) ER chaperone proteins

ER chaperone proteins such as calnexin and calreticulin, heatshock protein 70 (Hsp70) family member BiP (GRP78) and protein disulfide isomerase (PDI) facilitate in protein folding to ensure that receptors which are not assembled correctly are retained in the ER (Herbert and Molinari*,* 2007). Calnexin is a type I ER membrane protein (Bergeron *et al.,* 1994) known for its ability to target N-linked glycoproteins via a lectin binding site within its protein structure (Vassilakos *et al.,* 1998). Proteins that contain the asparagine (Asn)-Xxx-Ser/Thr motif undergo N-linked glycosylation. N-linked glycosylation has been shown to play an important role in the delivery of certain proteins to the cell surface. This has been demonstrated for dopamine receptor 5 (D_5), (Karpa *et al.,* 1999), where mutagenesis of specific Asn (N) linked motifs resulted in ER retention of the receptor. Calnexin has been linked to both protein retention within the ER and ER export, as further

work demonstrated recently for the dopaminergic GPCR family (Free *et al.,* 2007). Work in their laboratory found a clear role for calnexin in the assembly of D_1/D_2 heterodimers resulting in efficient cell surface delivery of the complex. Inhibition of calnexin caused the complex to be retained in the ER, whilst overexpression of calnexin retained monomeric D_1 receptors in the ER (Free *et al.,* 2007). The reason for retention of D_1 is not yet clear as cell surface delivery of D_1 was not shown to be dependent upon specific N-linked motifs (Karpa *et al.,* 1999). However, this work demonstrates the duality of function that calnexin serves in the ER, both in proper folding and export of dimeric complexes and in retention of proteins in the ER.

The ability of calnexin to bind to proteins, independent of N-linked glycan interaction, has also been studied. Inhibition of N-linked glycosylation by mutagenesis of Asn motifs and treatment with inhibitors, tunicamycin and castanospermine, established a clear glycan-independent interaction between calnexin and nicotinic acetylcholine receptors (AChR), (Wanamaker and Green, 2005). This highlights the potential for calnexin to recognise other protein sorting motifs, other than N-linked glycans.

ii) ER-retention/retrieval motifs in GPCRs

Efficient transport between the ER-Golgi-plasma membrane is facilitated through discrete motifs that reside within the synthesised protein (Gassmann *et al.,* 2005; Michelsen *et al.,* 2005). These signals may behave as ER-retention signals, thus prohibiting export to ER/Golgi intermediate compartment (ERGIC), or ER-retrieval signals targeting proteins to return to the ER from ERGIC via retrograde transport. During the assembly of multimeric proteins, such as GPCR homo/heterodimers, it has been shown that ER motifs, particularly arginine-based ER retention motifs (Michelsen *et al.,* 2005), may be masked to allow proteins to evade the quality control processes in the ER (Boyd *et al.,* 2003; Margeta-Mitrovic *et al.,* 2000), examples are discussed in detail in Section 1.2.2.

Properly assembled proteins are then packaged into coat protein vesicles (COPII) and exported from the ER (Aridor *et al.,* 1995), to the ERGIC, (Schweizer *et al.,* 1990).

The formation of COPII vesicles relies upon the GTPase, Sar1p (Barlowe *et al.*, 1993 and 1994). Another family of proteins called 14-3-3 proteins, located in the ERGIC, are responsible for ensuring that folded proteins are exported to the Golgi (Yuan *et al.,* 2003) whilst misfolded proteins are targeted and diverted back to the ER. 14-3-3 proteins recognise specific arginine ER retention signal motifs (RXR) that reside within some synthesised proteins (see Table 1.2). Misfolded proteins or those containing such signal motifs are shuttled back to the ER via COPI vesicles (Vivithanaporn *et al.,* 2006; Aridor *et al.,* 1995) where they undergo ER-associated degradation (ERAD) through the ubiquitin-proteosomal degradation system. Multimeric proteins possess the ability to evade this quality control checkpoint, allowing ER retention signals to become masked during protein assembly, thus allowing transport to the membrane (Vivithanaporn *et al.,* 2006; Boyd *et al.,* 2003; Margeta-Mitrovic *et al.*, 2000; Zerangue *et al.*, 1999). This has become an area of significant interest in terms of the assembly of GPCR dimers in the ER for export to the membrane, discussed in Section 1.2.2.
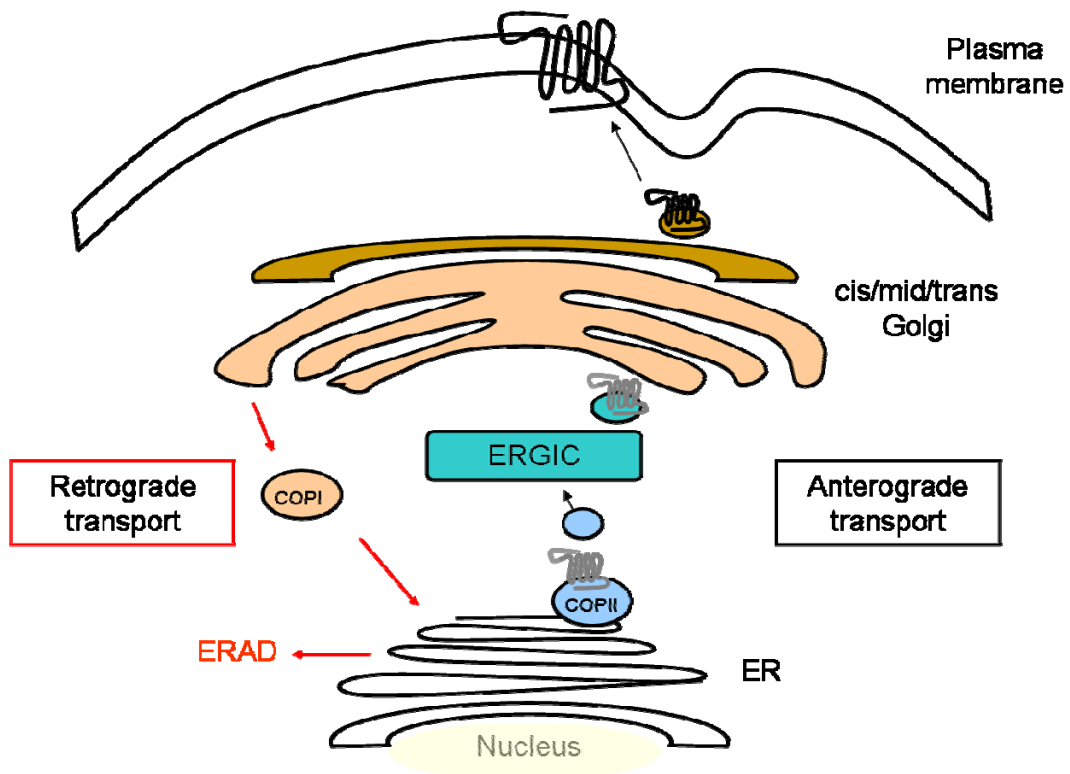
Figure 1.3. GPCR maturation in the secretory pathway.

Proteins synthesised in the ER are sorted by various ER chaperone proteins, with properly assembled proteins packaged for export into COPII vesicles. These vesicles progress to the ER-Golgi intermediate compartment (ERGIC), yet another quality control checkpoint in anterograde transport in the secretory pathway. Here, proteins are further processed and sorted into cargo destined to proceed to the Golgi apparatus or proteins re-delivered back to the ER. Those proteins returned to the ER are packaged into COPI vesicles (known as retrograde transport) and undergo ER-associated degradation (ERAD). Figure adapted from Lippincott-Schwartz *et al.,* 2000.

Table 1.2 ER retention/retrieval motifs within some GPCR families

Receptor	ER retention motif	Localisation	Reference
GABA$_{B1}$	RSRR	C-terminal	Margeta-Mitrovic *et al.,* 2000
5HT$_{3B}$	RAR	Intracellular loop	Boyd *et al.,* 2003
mGluR1	FRRK	C-terminal	Chan *et al.*, 2001
KA1 and KA2 KA2	RRRR RAR	C-terminal Intracellular loop	Ren *et al.,* 2003 Nasu-Nishimura *et al.,* 2006
Vasopressin V2R	RRGR	Intracellular loop	Hermosilla and Schülein, 2001

1.2.2. GPCR dimerisation and receptor surface expression

The classical view of GPCR signal transduction was once thought to follow a sequential pathway in linear cascade upon activation of a GPCR as a single monomeric entity. However, it has now emerged that GPCRs can form dimeric and multimeric complexes at the plasma membrane as well as in intracellular compartments (reviewed by Milligan *et al.,* 2007).

Several studies have envisaged dimerisation as non-covalent association either by lateral interaction or through the swapping of recognised domains (Maggio *et al.,* 1993). However, advances in the crystal structure for rhodopsin have provided a starting point for the identification of potential sites for Class A GPCR dimers to form. The key sites for dimer formation were found to involve transmembrane domains I, IV and V (Fotiadis *et al.,* 2004). Studies have since incorporated mutagenesis approaches to disrupt regions thought to be important for dimeric/oligomeric interaction and define consequential effects (Lopez-Gimenez *et al.,* 2007).

Class A GPCRs, such as the adrenergic receptors, remain the most widely studied family in terms of investigating dimerisation. Common features of Class A heterodimerisation include changes observed in receptor pharmacology, signalling and agonist-induced internalisation (reviewed by Terrillon and Bouvier *et al.,* 2004). However, much of the work carried out for Class A GPCRs remained highly controversial until the examination of the Class C γ-Aminobutyric acid (GABA) family, revealed heterodimerisation between $GABA_{B1}$ and $GABA_{B2}$ (Marshall *et al.,* 1999a and 1999b). When expressed individually, both $GABA_{B1}$ and $GABA_{B2}$ displayed poor cellular expression and signalling capabilities. Heterologous expression of both receptors was shown to result in the formation of a functional $GABA_{B1}/GABA_{B2}$ heterodimeric complex, masking the arginine-based ER retention motif present on the C-terminal of $GABA_{B1}$, and enhancing cell surface localisation, trafficking and downstream signalling events (Margeta-Mitrovic *et al.* 2000). This ER retention motif has also been shown to control the cell surface expression of other receptors such as the 5-hydroxytryptamine Type 3 (5-HT) receptor (Boyd *et al.,* 2003). When $5\text{-}HT_{3B}$ receptors are expressed in isolation, the receptor is retained inside the ER due to the presence of an ER retention signal. However, when $5\text{-}HT_{3A}$ receptors are co-expressed with $5\text{-}HT_{3B}$ receptors, cell surface expression of the complex is observed, thought to result through steric masking of the ER retention signal.

GPCR heterodimerisation has since been documented, with various outcomes, for the majority of GPCRs as shown in Table 1.3, these include dimer formation between oxytocin and vasopressin V1a and V2 receptors (Terrillon *et al.,* 2003 and 2004), adenosine α2A and β₁ adrenoceptors (Xu *et al.,* 2003), adenosine α2A and dopamine D2 receptors (Hillion *et al.,* 2002), dopamine D1 and D2 receptors (O'Dowd *et al.,* 2005), orexin-1 and cannabinoid CB1 receptors (Ellis *et al.,* 2006), PAR_1 and PAR_4 receptors (Leger *et al.,* 2006b) as well as PAR_1 and PAR_3 receptors (McLaughlin *et al.,* 2007). Dimerisation between members of the PAR family is discussed further in Section 1.3.7. Such studies have utilised fluorescence or bioluminescence resonance energy transfer methods (FRET and BRET), as well as co-immunoprecipitation and

cross linking approaches to identify dimeric complex formation. FRET analysis is discussed further in Section 2.7.

The list of GPCR families capable of forming dimeric complexes continues to grow and has led to original work on dimerisation being re-visited. Whilst many studies aim to determine the functional consequences of dimerisation between novel receptor pairs, more recent studies have placed their focus on investigating the existence of higher order oligomers. Recent evidence has emerged proposing that the α_{1b}-adrenoceptor forms higher oligomeric structures, beyond the realm of homodimers and heterodimers (Milligan *et al.,* 2006). Furthermore, it has been found that the oligomeric organisation of the α_{1b}-adrenoceptor, if partially disrupted, can result in inefficient maturation of the receptor complex that can alter the delivery of the complex to the cell surface and promote intracellular retention in the ER/Golgi apparatus (Lopez-Gimenez *et al.,* 2007). Resultant changes in pharmacological properties of heterodimerisation can be considerable, as demonstrated for SSTR5/dopamine D_2 heteromers (Rocheville *et al.,* 2000). Distinct pharmacological differences were observed between this heteromeric complex and SSTR5 and D_2 homodimers. Upon dopamine and SST agonist stimulation, enhanced Gαi-protein coupling to adenylyl cyclase was observed in SSTR5/dopamine D_2 heteromers; synergy attributed to improved ligand binding of SST-14 during D_2 stimulation with quinpirole.

GPCRs are highly important therapeutic targets; therefore the identification of clinically important dimeric complexes may be valuable for the development of more specific drugs.

Table 1.3. Summary of key GPCR families that dimerise.

Receptor Family	Receptor Subtype	Dimer Partner	Effects	Methods	References
GABA	GABA$_{B1}$	GABA$_{B2}$	Enhanced trafficking of GABA$_{B1}$	Co-immunoprecipitation	Marshall *et al.,* 1999a and b
Adrenergic	B$_2$AR	B$_1$AR B$_3$AR	↓internalisation of B$_2$AR ↓ ERK phosphorylation	Co-immunoprecipitation BRET	Lavoie *et al.,* 2002 Breit *et al.,* 2004
Opioid	δ- OPR	κ- OPR μ- OPR	Altered receptor pharmacology Synergistic signalling	Co-immunoprecipitation Cross linking assays	Jordan *et al.,* 1999 George *et al.,* 2000
Purinergic	Adenosine A$_1$R	Dopamine D$_1$R	Co-internalisation Cross-desensitisation	Immunofluorescence Co-immunoprecipitation	Gines *et al.,* 2000
Somatostatin	SSTR5	Dopamine D$_2$R	Enhanced signalling Altered receptor pharmacology	Immunohistochemistry FRET	Rocheville *et al.,*2000
Vasopressin	V1a	V2	Co-internalisation	Co-immunoprecipitation BRET	Terrillon *et al.,* 2004
PAR	PAR1	PAR-4	Co-factoring Synergistic activation	Co-immunoprecipitation FRET	Leger *et al.,* 2006a
	PAR1	PAR-3	Altered G-protein selectivity	BRET	McLaughlin *et al.,* 2007
Cannabinoid	CB1	Orexin-1	Altered receptor localisation	FRET	Ellis *et al.,* 2006

1.3 PROTEINASE-ACTIVATED RECEPTORS

1.3.1. The proteinase-activated receptor (PAR) family

The actions of serine protease enzymes are traditionally thought to be involved in degradative or coagulative processes, however it is now clear that they can function as potent hormone-like signalling molecules (reviewed by Hollenberg *et al.* 2005). Protease enzymes such as thrombin and trypsin induce cell-signalling cascades through a novel family of GPCRs called proteinase-activated receptors (PARs). Four members of the PAR family have been cloned and characterised to date, PAR_1 (Vu *et al.,* 1991a and Rasmussen *et al.,* 1991), PAR_2 (Nystedt *et al.,* 1995a and 1995b), PAR_3 (Ishihara *et al.,* 1997) and PAR_4 (Xu *et al.,* 1998). The functional domains of the PAR family members are illustrated in Figure 1.4. Potential roles for the PAR family have been explored in blood coagulation (reviewed by Cirino *et al.,* 2006), nociception (Vergnolle *et al*., 2001), the central nervous system (Bushell *et al.,* 2006), cardiovascular diseases (reviewed by Steinberg, 2005; Leger *et al.,* 2006a) inflammatory conditions of the skin (Buddenkotte *et al.,* 2005), joint (Ferrell *et al.,* 2003), gastrointestinal tract (reviewed by Vergnolle, 2000 and Kawabata, 2003), cerebrovascular damage (Suo *et al.,* 2003) and in protection of the airways (Cocks *et al.,* 1999 and 2001). The functional diversity of PAR-mediated responses has identified the PAR family members as worthwhile therapeutic targets.

(A)

N-terminal Cleavage Sites

PAR$_1$: LDPR^{41} ↓ S^{42}FLLRN

PAR$_2$: SKGR^{34} ↓ S^{35} LIGKV

PAR$_3$: LPIK^{38} ↓ T^{39} FRGAP

PAR$_4$: PAPR^{47} ↓ G^{48}YPGQV

(B)

Tethered Ligand

SFLLRN

SLIGKV

TFRGAP

GYPGQV

(C)

Extracellular loop 2 (ECL-2)

QTIQVPGLNITTCHDVLNETLLEG

QTIFIPALNITTCHDVLPEQLLVG

QEYYLVQPDITTCHDVHNTCESSS

QTFRLARSDRVLCHDALPLDAQAS

(D)

C-terminal region *

PAR$_1$: SSECQRYVYSILCCKESSDPSSYNSSGQLMASKMDTCSSNLNNSIYKKLLT

PAR$_2$: SHDFRDHAKNALLCRSVRTVKQMQVSLTSKKHSRKSSSYSSSSTTVKTSY

PAR$_3$: SKTRNHSTAYLTK

PAR$_4$: SAEFRDKVRAGLFQRSPGDTVASKASAEGGSRGMGTHSSLLQ

Figure 1.4. The functional domains of the proteinase-activated receptor (PAR) family.
The characterisation of the structure of the PAR family identified important proteolytic cleavage sites at the N-terminal (A). This cleavage forms a unique tethered ligand (B) that interacts at specific sites within extracellular loop-2 (ECL-2) (C). These events result in receptor activation, G-protein coupling and second messenger signal transduction. Finally putative serine/threonine sites (in red) residing within the intracellular C-terminal tail facilitate receptor desensitisation (D) and internalisation. The sequences above represent those obtained for human PAR subtypes. A tyrosine-based motif (Y^{420}KKL^{423}) responsible for PAR$_1$ interaction with AP2, involved in PAR$_1$ trafficking, is present at the C-term of PAR$_1$ (underlined). This sequence also comprises a KK ubiquitination signal motif facilitating cell surface delivery of PAR$_1$. Figure adapted from Macfarlane *et al.,* 2001.

1.2.2. Proteinase-activated receptor 1 (PAR$_1$)

Thrombin was originally identified as a very potent serine protease involved in multiple biological responses including platelet aggregation, clot formation (Kahn *et al.,* 1998 and 1999) and angiogenesis, all of which are important in haemostasis and vascular injury (Leger *et al.,* 2006b). For a long time, the functional receptors through which thrombin mediated its effects were largely unknown until the identification of a functional thrombin receptor (Vu *et al.,* 1991a), latterly termed proteinase activated receptor 1 (PAR$_1$). Work modelled on the thrombin cleavage site of zymogen protein C (LDPR/I), was found to be an important factor in receptor activation of the newly established thrombin receptor, PAR$_1$ (LDPR^{41}S). Mutagenesis of this site rendered the receptor unresponsive to thrombin (Vu *et al.,* 1991a), but retained the ability to bind thrombin.

i) PAR$_1$ agonists

PAR$_1$ was identified as a novel GPCR by virtue of this unique mechanism of activation; irreversible proteolytic cleavage of the extracellular N-terminal in response to thrombin (Vu *et al.,* 1991a and 1991b). This reveals a new tethered ligand region that interacts at conserved regions within extracellular loop 2 (ECL-2), resulting in receptor activation (Vu *et al.,* 1991a; Chen *et al.,* 1994; Nanevicz *et al.,* 1995). The interaction between thrombin and PAR$_1$ takes place at low nanomolar (nM) concentrations through the association of the PAR$_1$ N-terminal hirudin-like domain (D^{51}KYEPF^{56}) with thrombin's anion binding exosite, thus accommodating proteolytic cleavage at the N-terminal LDPR^{41}↓S^{42}FLLRN sequence (Vu *et al.,* 1991b; Ishii *et al.,* 1995; Bouton *et al.,* 1995). Investigation into the receptor pharmacology of PAR$_1$ advanced significantly through the generation of synthetic activating peptides (Scarborough *et al.,* 1992; Sabo *et al.,* 1992; Chao *et al.,* 1992). These peptides correspond to the related tethered ligand domain exposed following proteolytic cleavage; however these peptides directly interact with ECL-2 independent of cleavage, resulting in receptor activation. The kinetics of PAR$_1$ activation differs considerably between endogenous thrombin and synthesised activating peptides (Ishii *et al.,* 1993). Whilst thrombin can elicit maximal cellular signalling activity at low concentrations (0.3U-1U/ml), activating peptides require

higher concentrations (1-400µM) to elicit a signalling (Ishii *et al.,* 1993) or aggregation response of the same magnitude (Chao *et al.,* 1992). Modification of the hexapeptide SFLLRN through amidation of the C-terminal (i.e. SFLLRN-NH$_2$) has been shown to increase the potency of this synthetic peptide 4-fold (Scarborough *et al.,* 1992). Activation via serine proteases versus activating peptide (AP) is outlined in Figure 1.5.

The function of the 41 amino acid cleaved peptide sequence released from the N-terminal following proteolytic cleavage by thrombin was largely unknown until recent investigation. This sequence, termed Parstatin (Zania *et al.,* 2009), has been shown to be cell permeable, due to the hydrophobic composition of the sequence, and acts intracellularly to inhibit VEGF and bFGF-mediated angiogenesis. This work demonstrated the ability of this peptide to inhibit VEGF and bFGF-mediated ERK phosphorylation, DNA synthesis, microvessel formation, cell proliferation and enhance caspase-3 activity and induce endothelial cell death (Zania *et al.,* 2009). Whether the same biological activity is observed for the cleaved peptide sequences of the other PAR family members remains to be elucidated.
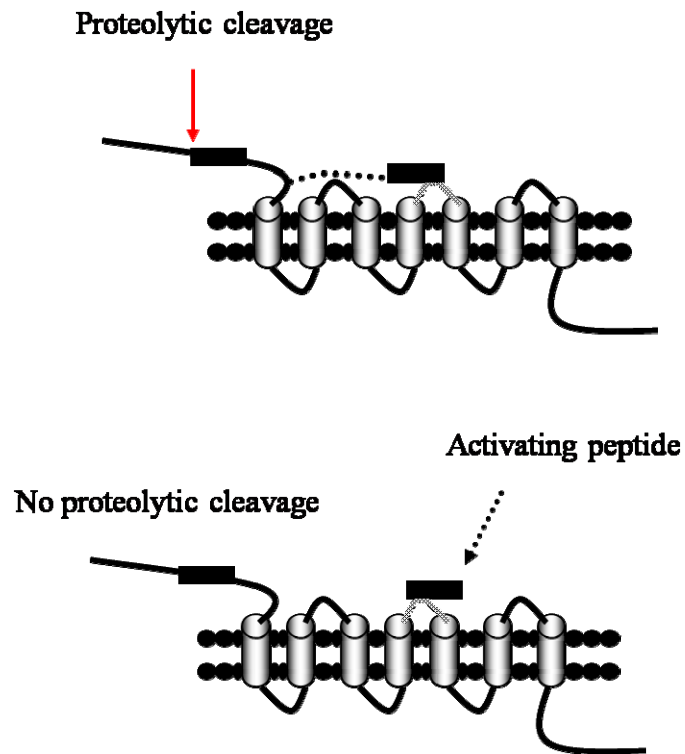
Figure 1.5. Proteinase-activated receptor (PAR) activation.

PAR activation can take place via serine protease-mediated cleavage at the N-terminal resulting in the formation of unique tethered ligand that interacts at sites residing within extracellular loop-2 (ECL-2). Receptor activation can also take place independent of cleavage using activating peptides derived from the tethered ligand sequence, binding directly to ECL-2. Figure adapted from Hollenberg *et al.,* 2005.

ii) The distribution of PAR$_1$

Characterisation of human PAR$_1$ and subsequent Northern blot analysis successfully identified PAR$_1$ mRNA expression in the brain, heart, lung, kidney, stomach, colon and testis (Vu *et al.,* 1991a). Further PCR analysis confirmed differential mRNA expression levels of PAR$_1$ in human platelets, vascular endothelium (Vu *et al.,* 1991a), vascular smooth muscle, (O'Brien *et al.,* 2000), epithelium, leukocytes (Major *et al.,* 2003), neurones and astrocytes (Hollenberg, 2002). The distribution of PAR$_1$ is indicative of the diverse physiological roles PAR$_1$ may have *in vivo*. The widespread tissue distribution, cell localisation and potential physiological roles of PAR$_1$ are outlined in Table 1.4.

iii) PAR$_1$ signal transduction

Early studies have already established that thrombin activation of PAR$_1$ couples to phospholipase C-β1 (PLC-β1) activation and the inhibition of cAMP accumulation (Rasmussen *et al.,* 1991; Brass *et al.,* 1991). Experiments using transfected cell systems have also confirmed the capability of PAR$_1$ to couple to G$\alpha_{q/11}$, G$\alpha_{i/o}$ and G$\alpha_{12/13}$ heterotrimeric G-proteins in response to thrombin (Offermanns *et al.,* 1994; Swift *et al.,* 2000; Marinissen *et al.,* 2003). PAR$_1$ coupling to G$\alpha_{i/o}$ was demonstrated through the use of pertussis toxin (PTX) whereby thrombin-mediated inositol phosphate accumulation and calcium mobilisation was reduced (Babich *et al.,* 1990; Brass *et al.,* 1991). This pathway, in part, was also latterly shown to be responsible for PAR$_1$ mediated activation of the MAP kinase pathway. However, a possible role for pp60^{src} (Chen *et al.,* 1994b), independent of PAR$_1$-Gα_i-coupling, has been identified in PAR$_1$-mediated ERK activation. Further investigation into the nature of PAR$_1$ coupling to Gα_i has recently implicated the possibility of pre-assembly of GPCR-G-protein complexes prior to signal transduction. This was confirmed using bioluminescence resonance energy transfer (BRET) technology (Ayoub *et al.* 2007). Recent evidence has suggested that activation of PAR$_1$ using activating peptides results in the preferential activation of G$\alpha_{q/11}$ over G$\alpha_{12/13}$ (McLaughlin *et al.,* 2005). The nature of this biased agonism may reflect the homo or heterodimeric status of PAR$_1$. The signalling capabilities of PAR$_1$ are outlined in Table 1.5.

iv) The role of PAR$_1$

Thrombin is a highly potent coagulative serine protease and, as such, its actions mediated through PAR$_1$ have been well established in relation to platelet activation (Kahn *et al.,* 1998 and 1999). Platelet activation is a vital process in maintaining haemostasis but can also participate in inflammation during vascular damage. Thrombin activation of PAR$_1$ mediates platelet aggregation and has been further implicated in the pathophysiology of arterial thrombosis (Leger *et al.,* 2006a and 2006b). Multiple aspects of PAR$_1$ signalling have been investigated in response to thrombin in platelets. Thrombin activation of PAR$_1$ in platelets stimulates thromboxane A$_2$ (TXA$_2$) and serotonin (5-HT) release and contributes to the activation of GPIIb/IIIa, the latter a result of PAR$_1$ coupling to Gα_i and G$\alpha_{12/13}$ (Dorsam *et al.,* 2002). Depending upon the condition of the vessel wall these events can either be protective or damaging. The accessibility of thrombin in the circulation coupled with PAR$_1$ expression in other cells of the vasculature (i.e. endothelial cells and smooth muscle cells) further expands the role of PAR$_1$ in vascular damage in the cardiovascular system.

Functional expression of PAR$_1$ in endothelial cells has been implicated in leukocyte recruitment in inflammation (reviewed by Major *et al.,* 2003). In response to injury, leukocytes are recruited to the site of injury and transmigrate through the endothelial barrier to the underlying smooth muscle cells (reviewed by Kaneider *et al.,* 2006). Different types of leukocytes are involved in inflammatory responses. Neutrophils release matrix metalloproteinases (MMPs), cathepsins and other enzymes that further contribute to inflammatory conditions including sepsis. Monocytes contribute towards the pathogenesis of cardiovascular conditions such as atherosclerosis through their role in plaque formation. PAR$_1$ was initially believed to be in part responsible for this leukocyte-endothelial interaction; however, the discovery of additional PAR family thrombin receptors has resulted in the role of PAR$_1$ being revised (Vergnolle *et al.,* 2002).

The development of PAR$_1$ knock-out mice models have been invaluable in elucidating phenotypic features of PAR$_1$ deficiency, thereby establishing the

potential roles of PAR_1 in function and disease. One study in particular identified embryonic lethality in mice as a consequence of PAR_1 gene deletion (Connolly et al., 1996). PAR_1 deficiency resulted in fatal bleeding, a phenotype that was manifest in part due to the lack of haemostatic control. Using this model it also became apparent that despite functional expression of PAR_1 in human platelets, mouse platelets lacking PAR_1 still responded to thrombin, albeit less efficiently (Connolly et al., 1994 and 1996). This research was the first to acknowledge the possibility of the existence of another thrombin-responsive receptor, other than PAR_1. This is discussed further in Section 1.3.4.

1.3.3. Proteinase-activated receptor 2 (PAR_2)

The characterisation of proteinase-activated receptor 2 (PAR_2) was achieved through molecular cloning, with the identification of a similar DNA sequence to the thrombin receptor PAR_1 (Nystedt et al., 1994, 1995a and 1995b). PAR_2 was identified through its partial homology to PAR_1, sharing ~30% amino acid identity with PAR_1, with the presence of a putative proteolytic cleavage consensus sequence characteristic of PAR activation.

i) PAR_2 agonists

The main difference between PAR_1 and PAR_2 was the relative inability of thrombin to activate PAR_2. However, PAR_2 activation was evident in response to proteolytic cleavage by low concentrations (1-10nM) of the serine protease trypsin at the N-terminal $SKGR^{34}\downarrow S^{35}$ LIGKV sequence, which fails to activate PAR_1 unless used at higher concentrations (>100nM) (Nystedt et al., 1994). Other physiological activators of PAR_2 have been identified such as mast cell tryptase (Ma et al., 2006), acrosin (Fox et al, 1997), cathepsin G (Molino et al., 1997a and 1997b) and trypsin IV (Cottrell et al., 2004). Other circulating coagulation factors such as factor VIIa have also been demonstrated to activate PAR_2 in endothelial cells (Camerer et al., 2000).

As with PAR_1, synthetic activating peptides have been developed corresponding to related tethered ligand regions of rodent PAR_2, SLIGRL-NH_2 (Nystedt et al., 1995a;

Santulli *et al.,* 1995) and human PAR$_2$ (Nystedt *et al.,* 1995b), SLIGKV. Further modification of these agonist peptides have identified more potent sequences; features such as the amidation of the C-terminal of the peptide, i.e. SLIGKV-NH$_2$ (Blackhart *et al.,* 1996; Hollenberg *et al.,* 1997) or the substitution of the N-terminal serine with a furoyl group, i.e. 2f-LIGKV-NH$_2$ (Ferrell *et al* 2003; Kawabata *et al.,* 2004 and 2005). These agonist peptides have facilitated in the exploration of the functional relevance of PAR$_2$ expression in various cells types, thus defining cell-specific roles for PAR$_2$.

ii) The distribution of PAR$_2$

Northern blot analysis demonstrated that PAR$_2$ is widely expressed in the kidney, pancreas, liver, the small intestine and colon (Nystedt *et al.,* 1994 and 1995b). Subsequent studies have demonstrated functional PAR$_2$ expression in human keratinocytes (Santulli *et al.,* 1995; Hou, *et al.,* 1998), endothelial cells (Molino *et al.,* 1997a), vascular smooth muscle cells, intestinal epithelium (Molino *et al.,* 1997b), neutrophils (Howells *et al.,* 1997), airway epithelium (Cocks *et al.,* 1999), hippocampal neurones and astrocytes (Bushell *et al.,* 2006). The tissue distribution, cell localisation and potential physiological roles are outlined in Table 1.4.

iii) PAR$_2$ signal transduction

As with PAR$_1$, PAR$_2$ also couples to the heterotrimeric G-proteins G$\alpha_{q/11}$, Gα_i and G$\alpha_{12/13,}$ resulting in the production of second messenger signalling cascades (reviewed by Kanke *et al.,* 2005b). Activation of PAR$_2$ is coupled to the cell-specific activation of multiple kinase cascades, namely the extracellular signal-related kinase (ERK) pathway, the P38 MAP kinase pathway, the c-Jun N-terminal kinase (JNK) pathway and the nuclear-factor kappa B (NFκB) pathway (Kanke *et al.,* 2001; Goon Goh *et al.,* 2007), all of which have been well established as cellular mediators of inflammation. The cell signalling capabilities of PAR$_2$ are outlined in Table 1.5.

iv) The role of PAR$_2$

Although PAR$_2$ is widely expressed in most tissues, the challenge remains in defining physiological roles for PAR$_2$ where both PAR$_2$ is expressed and endogenous

activators of PAR_2 exist. So far, roles for PAR_2 have been largely based upon the use of PAR_2 selective activating peptides and PAR_2 knock-out mice models (Kelso *et al.,* 2006), nonetheless such studies have found important potential roles in the cardiovascular, gastrointestinal and respiratory systems (Vergnolle, 2000; Kawabata and Kuroda, 2000; Cocks and Moffatt, 2001) as well as processes involved in nociception (Hoogerwerf *et al.,* 2001) and joint inflammation (reviewed by McIntosh *et al.,* 2007). Furthermore, studies in these areas have implicated PAR_2 in both anti-inflammatory (Cocks *et al.,* 1999) and pro-inflammatory processes (Kelso *et al.,* 2006), with unique downstream signalling and receptor cross-talk events mediated upon PAR_2 activation possibly responsible for this duality of function.

1.3.4. Proteinase-activated receptor 3 (PAR_3)

A third PAR family member was first described by Coughlin and colleagues in 1996 when PAR_1 gene knock-out experiments observed a secondary low level Ins P_3 response when treated with thrombin (Connolly *et al.* 1996). This research group proceeded to characterise this second thrombin-related receptor, PAR_3 (Ishihara *et al.,* 1997), with expression observed in mouse platelets and spleen megakaryocytes, and human bone marrow. PAR_3 was found to be relatively shorter than both PAR_1 and PAR_2 family members, as shown in Figure 1.3. (Macfarlane *et al.,* 2001), however it retained ~27% amino acid sequence identity with both PAR_1 and PAR_2. As with the other PAR members, proteolytic cleavage of PAR_3 by thrombin was evident at the N-terminal, at $LPIK^{38} \downarrow T^{39}$ FRGAP exosite, however unlike the other PAR members, PAR_3 activation independent of cleavage was not evident with synthetic activating peptides that correspond to its tethered ligand domain (Ishihara *et al.,* 1997). Further examination of the PAR_3 structure also identified a distinct truncation of the intracellular C-terminal when aligned with other PAR family members (Ishihara *et al.,* 1997). Sequence alignment also found that PAR_3 retained the hirudin-like domain, important for thrombin interaction and significant sequence homology at the important extracellular loop-2 (ECL-2) region, responsible for receptor activation (refer to Figure 1.3).

Similar to PAR$_1$, a role for PAR$_3$ was implicated in platelet aggregation; however PAR$_3$ knock-out strategies in mice models identified a significant secondary aggregative response to thrombin in platelets (Kahn *et al.,* 1998 and 1999). As PAR$_1$ is not expressed in mouse platelets, this response implicated the existence of a third thrombin receptor and possible fourth PAR member (Kahn *et al.,* 1998), latterly identified as PAR$_4$ (see below). Despite the ability of thrombin to activate mouse platelets via PAR$_3$, no downstream signalling events have been characterised for PAR$_3$. Although the receptor pharmacology of PAR$_3$ has been hindered by the lack of selective peptide agonists, this receptor subtype appears to be unable to signal. Despite this, mutagenesis studies carried out in COS-7 cells expressing PAR$_3$ and PAR$_4$ highlighted a significant interaction between these two receptors. PAR$_3$ was shown to enhance the efficiency of thrombin-mediated PAR$_4$ activation, serving as a co-factor for PAR$_4$ (Nakanishi-Matsui *et al.,* 2000). This is discussed in detail in Section 1.3.7.

1.3.5. Proteinase-activated receptor 4 (PAR$_4$)

Proteinase-activated receptor 4 (PAR$_4$) was the fourth family member to be identified (Xu *et al.,* 1998; Kahn *et al.,* 1998) sharing ~33% identity with the other PAR family members and displaying similar proteolytic activation through N-terminal cleavage at the PAPR^{47}↓G^{48}YPGQV sequence. The protein sequence of PAR$_4$ was shown to lack the necessary hirudin domain; a feature present on both PAR$_1$ and PAR$_3$ which confers high affinity for thrombin binding. As a result PAR$_4$ was found to function as a low affinity thrombin receptor, requiring high concentrations of thrombin for receptor activation (3-5 U/ml). PAR$_4$ was also found to respond to trypsin (EC$_{50}$ 5 nM), as well as the tethered ligand activating peptide GYPGQV (EC$_{50}$ 100 μM), (Xu *et al.,* 1998). Further physiological activators of PAR$_4$ include the neutrophil protease cathepsin G (Sambrano *et al.,* 2000) and trypsin IV (Cottrell *et al.,* 2004).

The tissue distribution of PAR$_4$ was elucidated through Northern blot analysis, with high expression evident in human platelets, lung, pancreas, thyroid, testis and small intestine (Xu *et al.,* 1998). At the cellular level, expression of PAR$_4$ has been observed in vascular endothelial cells and leukocytes (Vergnolle *et al.,* 2002),

hippocampal neurones (Suo *et al.,* 2003) and cardiomyocytes (Sabri *et al.,* 2003). The widespread distribution of PAR$_4$ expression and potential physiological roles are outlined in Table 1.4.

The discovery of PAR$_4$ has meant that physiological roles previously associated with PAR$_1$ activation, such as platelet activation and aggregation, had to be revised. Experiments using α-thrombin and γ-thrombin demonstrated clearly that PAR$_4$ lacks the N-terminal hirudin-like domain that is present on both PAR$_1$ and PAR$_3$, (Xu *et al.,* 1998). This work recognised that the interaction of thrombin with PAR$_4$ was distinct from the other PAR family members. Kuliopulos and colleagues addressed the issue regarding thrombin recognition and cleavage (Jacques *et al.,* 2003). This research group identified discrete domains on PAR$_4$, namely dual prolines at P^4 and P^2 and an anionic cluster at D^{57}DED on the N-terminal that facilitates thrombin interaction. This may also explain in part why the kinetics of PAR$_4$ activation by thrombin differs considerably to that of PAR$_1$ activation. Together, these receptors form a dual thrombin receptor system for human platelet aggregation, whilst PAR$_4$ and PAR$_3$ perform the same role in murine platelets (Kahn *et al.,* 1998). Vergnolle and colleagues identified a significant role for PAR$_4$ in leukocyte-endothelial interaction involved in inflammation mediated by thrombin, previously attributed to PAR$_1$ (Vergnolle *et al,* 2002).

As with other PAR family members, PAR$_4$-mediated responses have been implicated to involve signalling coupled to heterotrimeric G-proteins Gα$_{q/11}$, and Gα$_{12/13}$ (Faruqi *et al.,* 2000), as outlined in Table 1.5. Subsequent studies have since found that PAR$_4$ also couples to Gα$_{i/o}$ in response to thrombin. This work identified Gα$_{i/o}$-dependent, calcium-independent nitric oxide (NO) production which resulted in relaxation of bovine aortic endothelial cells (Momota *et al.,* 2006). This research group further found that whilst PAR$_4$ mediated NO production was calcium-independent; it was however dependent upon activation of the phosphatidylinositol-3 kinase-Akt pathway (Hirano, 2007). These events are somewhat distinct from PAR$_1$-mediated NO production, where NO production was shown to be both calcium-dependent and –independent, with coupling of PAR$_1$ to Gα$_{q/11}$ in part responsible.

The inflammatory potential of PAR_4 was explored in cardiomyocytes (Sabri *et al.,* 2003), again a role attributed to PAR_1 (Sabri *et al.,* 2000). This research group have identified a clear $G\alpha_{q/11}$ pathway linked to early and late ERK activation. However in this cell type a low level, delayed phospholipase C (PLC) and ERK response were observed upon PAR_4 activation. A sustained PAR_4-mediated Src-dependent activation of p38 MAPK signal was observed, independent of $G\alpha_i$ $G\beta\gamma$ dimer or PAR_1 activation.

1.3.6 PAR antagonists

The widespread distribution and major physiological roles that the PAR family participate in highlight the therapeutic potential of this GPCR family. The use of various knock-out mouse approaches and PAR-specific agonists have been useful in implicating PAR expression and activation in the progression of various disease states, including arthritis (McIntosh *et al.,* 2007) and cardiovascular disease (Leger *et al.,* 2006a). However, the development of adequately potent PAR-specific antagonists remains the Achilles heel of PAR research. With the exception of PAR_1, where various antagonists have been documented, the availability of antagonists for the remaining PAR family members are limited to low affinity compounds (see Table 1.5).

Peptide mimetic PAR_1 antagonists such as BMS-200261 and RWJ-56110 have been documented as selective inhibitors of PAR_1 (Kuliopulos and Covic, 2003; Leger *et al.,* 2006a and 2006b). Recently developed antagonists that have shown promise are palmitoylated peptides, referred to as cell permeable pepducins, which inhibit in the micromolar (μM) range (Covic *et al.,* 2002). Pepducins act by targeting intracellular loops of the receptor, thus blocking GPCR-G-protein signal transduction. Pepducin antagonists have been reported for PAR_1 and PAR_4, namely P1pal-12 and P4pal-i1 respectively (Covic *et al.,* 2002; Leger *et al.,* 2006b). This work has shown dual inhibition of PAR_1 with RWJ-56110 and PAR_4 with P4pal-i1 as an effective anti-thrombotic therapy.

The development of PAR$_2$ antagonists is still ongoing. So far only low-to-moderately potent inhibitors have been reported, these include the small molecule inhibitor ENMD-1068 (Kelso *et al.,* 2006) and the peptide mimetic K-14585 (Kanke *et al.,* 2009). These compounds have both provided insight into their effectiveness in the treatment of PAR$_2$-mediated inflammation through their ability to block PAR$_2$ responses in the mM-μM range. Whilst these antagonists provide a structural template for effective PAR$_2$ antagonism, further work is required to develop more potent antagonists with improved solubility.

Table 1.4 Proteinase-activated receptor (PAR) family tissue distribution, cellular localisation and physiological roles.

Receptor	Tissue Distribution	Cell Localisation	Physiological Roles*	References
PAR$_1$	Brain, colon, heart, kidney, lung, stomach, testis	Platelets, Megakaryoctyes Leukocytes Vascular endothelium Keratinocytes Neurons and astrocytes	Platelet activation Inflammation Embryonic lethality Cell proliferation Modulation of vascular tone Cerebrovascular damage	Vu *et al.,* 1991a and 1991b Rasmussen *et al.,* 1991 Santulli *et al.,* 1995 O'Brien *et al.,* 2000 Marinissen *et al.,* 2003
PAR$_2$	Colon, kidney, liver, pancreas, prostate, small intestine, trachea	Vascular endothelium Keratinocytes Leukocytes Epithelium Neurons and astrocytes Neutrophils	Inflammatory conditions Nociception Airway protection Modulation of vascular tone	Nystedt *et al.,* 1994 and 1995b Santulli *et al.,* 1995b Molino *et al.,* 1997 Howells *et al.,* 1997 Cocks *et al.,* 1999 O'Brien *et al.,* 2000
PAR$_3$	Bone marrow, spleen, stomach, small intestine, trachea low levels in brain and lung	Platelets (m) Megakaryoctyes Smooth muscle (airway) Vascular Endothelium (low)	Cofactor for PAR$_4$ platelet activation (m)	Ishihara *et al.,* 1997 Schmidt *et al.,* 1998
PAR$_4$	Lung, pancreas, small intestine, spleen, testis, thyroid, Low levels in adrenal gland, colon, lymph node, placenta, prostate, skeletal muscle and uterus	Platelets Megakaryoctyes Neurons Cardiomyocytes Vascular endothelium Leukocytes	Platelet activation Inflammation Cerebrovascular damage	Xu *et al.,* 1998 Kahn *et al.,* 1998 Vergnolle *et al.,* 2002 Suo *et al.,* 2003 Sabri *et al.,* 2003

Note: This is not a comprehensive list. Tissue distribution based upon Northern blot analysis experiments in literature.

*Includes both known and potential roles.

Table 1.5 Proteinase-activated receptor (PAR) family activators and typical signal transduction.

Receptor	Proteases	Activating Peptides[*]	Transduction	Effectors	Deactivators	References
PAR_1	Thrombin Factors Xa Plasmin	SFLLRN-NH_2 (h) TFLLRN-NH_2 SFFLRN (r, m)	$G\alpha_{i/o}$ $G\alpha_{q/11}$ $G\alpha_{12/13}$ Via EGF receptor	↓AC, ↓cAMP, PLA_2, PGI_2 ERK PLCβ; - DAG, PKC activation - IP_3, Ca^{2+} mobilisation MAPK cascades Rho-GEFs MAP kinase MAP kinase	Cathepsin G BMS200261 RWJ-561100 SCH-79797 FR-171113	Rassmussen et al.,1991 Grand et al., 1996 Molino et al., 1997a & b Marinissen et al., 2003
PAR_2	Trypsin Tryptase Trypsin IV Acrosin Cathepsin G Factors Xa/VIIa	SLIGKV-NH_2 (h) SLIGRL-NH_2 (m) 2f-LIGKV-NH_2	$G\alpha_{i/o}$ $G\alpha_{q/11}$	↓AC, ↓cAMP, PLA_2 ↑Nitric oxide PLCβ; - DAG, PKC activation - IP_3 accumulation, - Ca^{2+} mobilisation -NFκB activation	FSY-NH_2 LS-NH_2 Cathepsin G ENMD-1068 K-14585	Santulli et al., 1995 Molino et al., 1997a & b Camerer et al., 2000 Kawabata et al., 2001 Al-Ani et al., 2002a Cottrell et al.,2004 Kanke et al., 2005a & 2009 Goon Goh et al., 2008 Kelso et al., 2006
PAR_3	Thrombin	None	Influences PAR1-G-protein coupling	?	Cathepsin G	Ishihara et al., 1997 McLaughlin et al., 2007
PAR_4	Thrombin Trypsin Cathepsin G Plasmin	GYPGKF-NH_2 (m) GYPGQV-NH_2 (h) AYPGKF-NH_2[*]	$G\alpha_{i/o}$ $G\alpha_{q/11}$	↑Nitric oxide PLCβ; - DAG, PKC activation - IP_3, Ca^{2+} mobilisation Src, MAPK cascades	YD-3 tcYPGKF-NH_2 P4pal-il (pepducin)	Xu et al., 1998 Kahn et al.,1998 Sabri et al., 2003 Momota et al., 2006 Leger et al., 2006b

* Denotes synthetic activators of PAR signalling based on related tethered ligand sequence. Cross-reactivity of the SFLLRN activating peptide is evident with PAR_2.

1.3.7. The regulation of proteinase-activated receptor activation

Receptor desensitisation occurs to enable a cell to attenuate signal transduction mediated after receptor activation takes place. In the case of GPCR desensitisation, this involves uncoupling of G-proteins followed by receptor internalisation (Kelly *et al.*, 2008), see Section 1.1. As with other GPCRs, PAR$_1$ activation is shortly followed by agonist-dependent desensitisation and internalisation (Hoxie *et al.*, 1993). The molecular mechanism of PAR$_1$ desensitisation is facilitated through receptor phosphorylation by GRKs, namely GRK-3 and GRK-5 (Déry *et al.*, 1999; Tiruppathi *et al.*, 2000), at the putative residues upon the cytoplasmic C-terminal tail (refer back to Figure 1.4) that supports the recruitment of β-arrestins (Shapiro *et al.*, 1996). β-arrestin1 has been implicated as the preferential candidate for PAR$_1$ desensitisation based upon its ability to uncouple PAR$_1$/Gα$_q$-coupled signalling more effectively than β-arrestin2 (Paing *et al.*, 2002; Chen *et al.*, 2004). However, the utilisation of β-arrestin-specific knockout studies undertaken in the same laboratory subsequently identified an alternative, β-arrestin-independent mode for PAR$_1$ internalisation (Paing *et al.*, 2002). Recent reports have since highlighted that phosphorylation of the C-terminal is not a prerequisite for β-arrestin binding, as previously thought (Chen *et al.*, 2004). This introduces an alternative means of signal termination through β-arrestin, independent of receptor phosphorylation (Chen *et al.*, 2004).

PAR$_1$ rapidly internalises via clathrin-coated pits within minutes of activation (outlined in Figure 1.6). Studies have indicated a GTPase dynamin-dependent mode of PAR$_1$ internalisation (Trejo *et al.*, 2000; Paing *et al.*, 2002). Whilst a small proportion of receptors are recycled back to the cell membrane, most receptors are sorted into lysosomes for degradation and signal termination (Hein *et al.*, 1994; Brass *et al.*, 1991; Trejo *et al.*, 1998). Cellular trafficking proteins called sorting nexins (SNX), in particular SNX1 and possibly SNX2, have been identified as important regulators for targeting PAR$_1$ receptors for lysosomal degradation (Wang *et al.*, 2002). When PAR$_1$ is recycled back to the membrane, the receptor is unresponsive to thrombin whilst retaining the capability to respond to the activating peptide SFLLRN (Hoxie, *et al.*, 1993). This feature is attributed to the irreversible

nature of receptor activation by proteolytic cleavage. In order to restore the responsiveness of PAR_1 to agonist stimulation, new receptors have to be synthesised in the ER/Golgi and exported to the membrane (Hein *et al.,* 1994). Cell surface replenishment of PAR_1 also involves the tonic cycling of non-activated receptors between the plasma membrane and intracellular receptor stores (Shapiro *et al.,* 1998). Recent studies incorporating RNA interference, have managed to define a role for the clathrin adaptor protein AP2 in the regulation of tonic cycling of internalised non-activated PAR_1 receptors (Paing *et al.,* 2006). Silencing the cellular activity of AP2 in endothelial cells led to the inhibition of the tonic cycling of non-activated receptors and cellular responsiveness to thrombin, thus defining a clear regulatory role for AP2. Further studies have found a tyrosine-based motif, $Y^{420}KKL^{423}$, on the extreme C-terminal of PAR_1 (Wolfe *et al.,* 2007). This was identified as a site of interaction between PAR_1 and AP2, with the $K^{421}K$ demonstrated as a site of ubiquitination required for cell surface expression of PAR_1 (refer to Figure 1.4). In smooth muscle cells, constitutive cycling of PAR_1 was also shown to be regulated via a Rho/Rac1 dependent mechanism (Yufu *et al.,* 2005). Dysregulation of PAR_1 trafficking events have been observed in breast carcinoma, resulting in sustained mitogenic cell signalling responses (Booden *et al.,* 2004; Arora *et al.,* 2007).
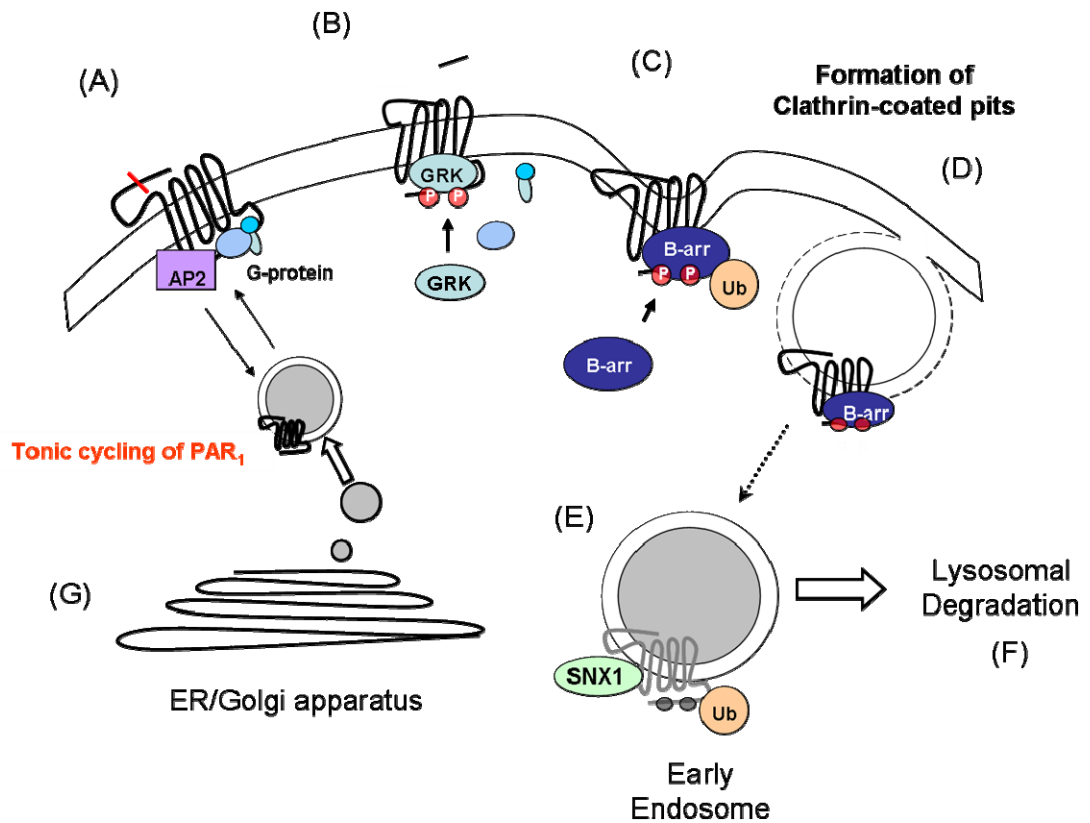
Figure 1.6. Intracellular sorting of PAR$_1$ following receptor activation.
Upon proteolytic cleavage, PAR1-G-protein coupling takes place (A). This is
followed by GRK-mediated receptor phosphorylation and G-protein uncoupling (B)
and interaction with β-arrestin (C) resulting in receptor desensitisation. PAR1 is then
internalised into clathrin coated pits (D), forming early endosomes (E) where
receptor sorting and dephosphorylation takes place for lysosomal degradation (F).
This process involves ubiquitination and SNX1. Replenishment of membrane
receptors requires re-synthesis of new receptors and mobilisation from Golgi stores
(G). AP2 participates in tonic cycling of non-activated PAR1 between plasma
membrane and intracellular receptor stores. Figure adapted from Hoxie et al., 1993
and Hein et al., 1994.

The features of PAR_1 trafficking events have provided a good basis for research into the regulation of other PAR family members. Studies carried out investigating the regulation of PAR_2 signal termination identified similar trafficking patterns to PAR_1 (Böhm *et al.,* 1996), refer to Figure 1.7. As with PAR_1, PAR_2 receptors are trafficked to endosomes prior to minimal membrane recycling and then targeted for lysosomal degradation; however the defined GRK phosphorylation events remain to be elucidated (Böhm *et al.,* 1996). Real-time analysis of the molecular interactions that occur during PAR_2 internalisation led to the identification of a distinct calcium-dependent interaction between β-arrestin1 and PAR_2 (Déry *et al.,* 1999). Small GTPase Rab5 and Rab11a have been shown to play a role in agonist-induced endocytosis of PAR_2 (Roosterman *et al.,* 2003). Rab5 was found to participate in β-arrestin1/dynamin dependent PAR_2 endocytosis; a process that was restricted in the presence of dominant negative Rab5 expression. A role for Rab11a was identified in the trafficking of PAR_2 from Golgi stores to the plasma membrane (Roosterman *et al.,* 2003). These trafficking events coincide with those documented for dopaminergic D_2 receptors (Iwata *et al.,* 1999) and $β_2$-adrenoreceptors (Seachrist *et al.,* 2000), among others.

The molecular mechanism underlying PAR_2 resensitisation at the plasma membrane has been one of interest in recent years. Work carried out in Georg Reiser's laboratory has added a further dimension to the existing literature surrounding the trafficking of PAR_2 back to the plasma membrane from Golgi receptor stores (Luo *et al.,* 2007). These studies have recognised PAR_2 as a cargo protein for p24A, a Type I transmembrane protein localised in the ER/Golgi apparatus. Interaction between PAR_2 and p24A was found to take place at sites on the N-terminus of p24A and the ECL-2 of PAR_2, to confine PAR_2 in the Golgi. Activation of PAR_2 resulted in the recruitment of the small GTPase, ADP-ribosylation factor-1 (ARF-1) to the Golgi where it becomes activated by guanine nucleotide exchange factors (GEF). These events have been shown to disrupt the interaction between PAR_2 and p24A, thus allowing PAR_2 to be exported to the membrane to replenish cell surface expression (Luo *et al.,* 2007).

PAR$_2$ mutagenesis studies have demonstrated β-arrestin recruitment to PAR$_2$ as a major contributing factor to the induction of mitogenic responses and cell migration, through β-arrestin–dependent cytosolic ERK activation (DeFea *et al.,* 2000b). Further analysis using PAR$_2$ C-terminal truncated mutants has defined the significance of the C-terminal to the stability of β-arrestin binding (Stalheim *et al.,* 2005). These studies have identified a clear link to PAR$_2$-β-arrestin binding post-internalisation, with particular importance in signalling for ERK activation as well as participating in desensitisation. Recent evidence by DeFea and colleagues has demonstrated the importance of the PAR$_2$-β-arrestin scaffold in the dephosphorylation and activation of the cofilin pathway, a pathway that results in augmented cell motility and tumour metastasis (Zoudilova *et al.,* 2007). This work highlights the importance of G-protein-independent, β-arrestin-dependent signalling events that results upon PAR$_2$ activation, which may be accountable for previous observations where PAR$_2$ activation resulted in enhanced tumour metastasis (Shi *et al.,* 2004).

In addition to agonist-dependent desensitisation, as defined for PAR$_1$ and PAR$_2$, there also appears to be a degree of concomitant agonist-independent desensitisation via the self-limiting effects of the second messenger PKC that results in the phosphorylation of the receptor (Böhm, *et al.,* 1996).
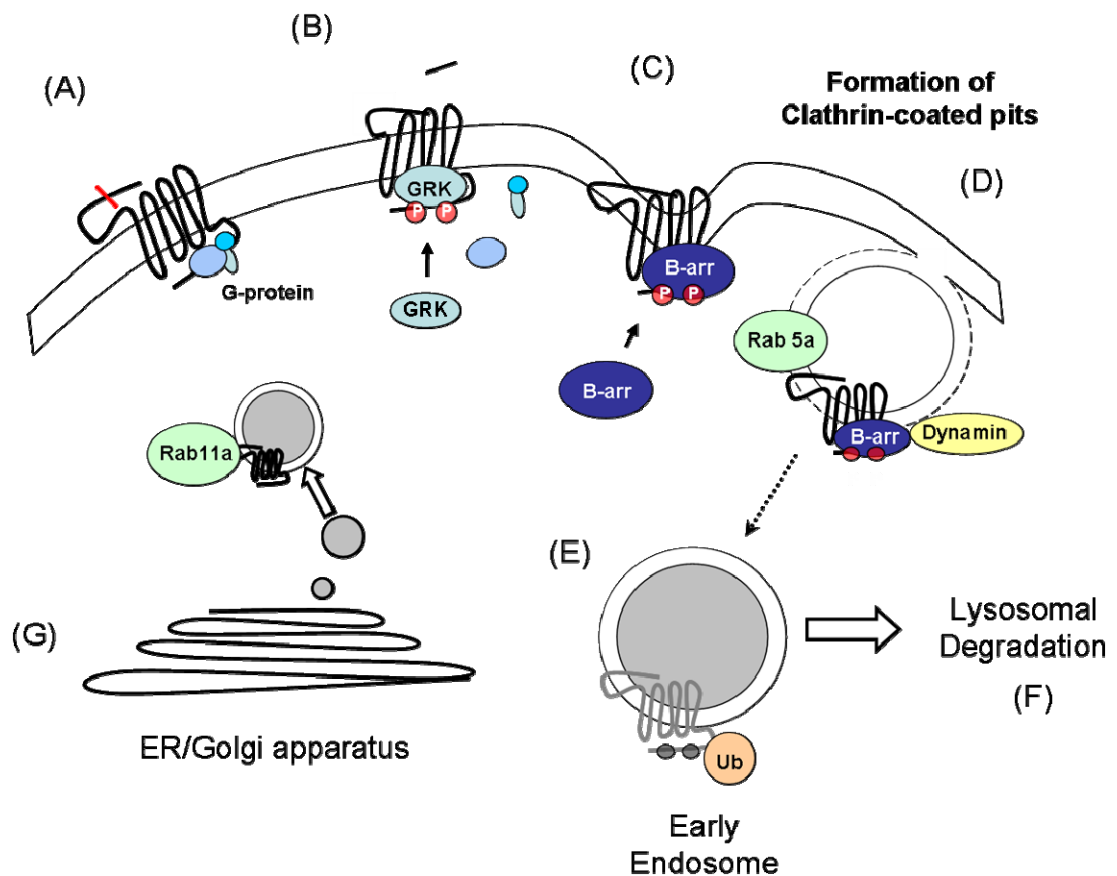
Figure 1.7. Intracellular sorting of PAR$_2$ following receptor activation.

Upon proteolytic cleavage, PAR$_2$-G-protein coupling takes place (A). This is followed by GRK-mediated receptor phosphorylation and G-protein uncoupling (B) and interaction with β-arrestin1 (C) resulting in receptor desensitisation. PAR$_2$ is then internalised into clathrin coated pits (D), forming early endosomes (E). This requires both Rab5a and dynamin. Receptor sorting and dephosphorylation takes place, with the receptors ubiquitinated being targeted for lysosomal degradation (F). This Replenishment of membrane receptors requires re-synthesis of new receptors and mobilisation from Golgi stores (G). Rab11a participates the trafficking of PAR$_2$ from Golgi receptor stores to the plasma membrane. Figure adapted from Déry *et al.,* 1999.

The regulation of PAR_3 and PAR_4 activation has yet to be elucidated. However, the striking feature of PAR_4 activation is the longevity of various signalling events, such as calcium signalling, inositol phosphate accumulation, and the relative lack of desensitisation observed upon receptor activation (Shapiro *et al.,* 2000). These responses were observed in rat fibroblasts stably expressing PAR_4, with responses compared to those obtained from thrombin-mediated PAR_1 activation. Mutagenesis of amino acid residues at putative phosphorylation sites within the C-terminus of PAR_1 resulted in dysregulation of cell signal termination, thus allowing prolonged PAR_1-mediated cell signalling. Similar mutagenesis did not alter PAR_4-dependent cell signalling responses. This suggests that PAR_4 has a regulatory control distinct from the other PARs. Whilst the receptor trafficking events have been studied in great detail for both PAR_1 and PAR_2, no such work has been undertaken to elucidate the events that follow PAR_4 activation.

The fidelity of serine protease signalling relies upon desensitisation, internalisation, receptor recycling and resensitisation processes for the fine-tuning of cell signalling events. Herein lies the need for further investigation into the cellular trafficking of PAR_4.

1.3.8. PAR-PAR and PAR-other receptor interactions

The emergence of GPCR dimerisation has encouraged many researchers to review previously published results regarding the receptor pharmacology of this super family. Early studies involving the PAR family, identified at the time, unexplainable interactions between PAR members. Synergistic PAR activity was observed in platelet activation in what was described at that time as a 'dual thrombin receptor system' (Kahn *et al.,* 1998). Through the years, small advances have been made to elucidate PAR-PAR interactions. Coughlin and colleagues initially raised the question of PAR interaction indirectly in the mouse model. This research group showed that PAR_3 acted as a cofactor in thrombin mediated PAR_4 activation (Nakanishi-Matsui *et al.,* 2000). Thrombin-cleavage of PAR_4, as previously discussed in Section 1.3.5, was regarded as rather inefficient when compared to PAR_1 and PAR_3. It was found that PAR_3 enhanced PAR_4 activation by providing the

necessary hirudin-binding domains; a feature PAR_4 lacks, to enable thrombin cleavage of PAR_4 to occur more efficiently. This partnership enabled thrombin to act as a bivalent agonist, capable of interacting with PAR_3 at its hirudin-like domain whilst interacting with PAR_4 via its anionic-binding exosite. This interaction significantly enhanced mouse platelet activation at low concentrations of thrombin, an event not possible when PAR_4 was expressed in isolation. This was later investigated (Owen, 2003) and further demonstrated in the context of thrombin mediated PAR_1 and PAR_4 activation in human platelets (Leger *et al.,* 2006b). This work identified PAR_1/PAR_4 heterodimerisation, responsible for thrombin-mediated platelet activation. Preliminary findings suggested that targeting of this heterodimeric complex may prove to be beneficial in improving existing anti-thrombotic therapies.

More recently, constitutive heterodimers were found to exist between PAR_1 and PAR_3 when expressed in endothelial cells (McLaughlin *et al.,* 2007). The significance of this interaction was demonstrated when a shift in the preferential coupling of PAR_1 to $G\alpha_{q/11}$ was observed, with PAR_1/PAR_3 heterodimers favourably coupling to $G\alpha_{13}$. In essence, within this heterodimeric complex, PAR_3 was observed to allosterically regulate PAR_1 G-protein selectivity in response to thrombin. In addition, activation of this heterodimer also resulted in increased endothelial cell permeability, a crucial stage in the development of vascular inflammation. It was hypothesised that by targeting the heterodimer complex, the effects of thrombin may be minimised to the extent where vascular inflammation can be prevented.

Earlier studies have also proposed some level of interaction between PAR_1 and PAR_2 in thrombin-mediated tumour cell migration, even though thrombin does not cleave PAR_2 (Shi *et al.,* 2004). Thrombin-induced metastasis through PAR_1 was shown to be enhanced in the presence of PAR_2, through a cleavage-independent mechanism, possibly involving PAR_1/PAR_2 heterodimer formation. This was further explored, with PAR_1 transactivation of PAR_2 observed as having an important protective role in the progression of PAR_1/LPS-mediated sepsis. This suggests that targeting the

PAR_1/PAR_2 heterodimer with appropriate agonists could be effective in the treatment of late sepsis, through activating a Gi(βγ)-dependent pathway, promoting endothelial barrier protection (Kaneider *et al.,* 2007).

Recently work carried out by Hollenberg and colleagues have shown interaction between PAR_2 and the toll-like receptor, TLR-4 (Rallabhandi *et al.,* 2008), highlighting the potential of receptor cooperativity in inflammation. Studies conducted to date have also established a clear link between inflammation and the upregulation of PAR expression levels, PAR_2 in particular (Ferrell *et al.,* 2003; Abe *et al.,* 2006; Xiang *et al.,* 2006). In contrast, a dual role for PAR_2 and PAR_4 has not been explored further in the context of inflammation. This is despite the fact that both receptors respond to trypsin and become up-regulated in inflammation. This has been demonstrated in our laboratory, as well as others, in endothelial cells during pro-inflammatory challenge with tumour necrosis factor (TNFα), (Ritchie *et al.,* 2007). This was first demonstrated in 2001, when Cocks and colleagues identified increased PAR_2 and PAR_4 expression in coronary artery endothelium during similar challenge (Hamilton *et al.,* 2001a). This presents a potential physiological setting where PAR_2/PAR_4 heterodimerisation may prove to be significant.

1.4 AIMS

Unlike the extensive research into the receptor signalling and trafficking events following PAR_1 and PAR_2, similar investigation into the trafficking of PAR_4, the most recent PAR member, is somewhat lacking. The distinct sustained signalling responses and subsequent lack of receptor desensitisation that PAR_4 displays in comparison to both PAR_1 and PAR_2 is intriguing (Shapiro *et* al 2000) and thus warrants further investigation.

Furthermore recent studies have demonstrated the capability of PAR_4 to form heterodimers with PAR_1 and PAR_3 in physiologically important contexts. Previous RT-PCR studies in our laboratory, as well as others, have shown that PAR_2 and PAR_4 become dual-upregulated following inflammatory challenge with TNFα (Ritchie *et al.,* 2007). This provides a physiologically important model whereby PAR_2 and PAR_4 may interact similarly, in the context of inflammation.

The aims of this study were to;

1. Investigate the cellular expression of PAR_4 relative to that of PAR_2 through the use of fluorescence imaging techniques to monitor cellular systems expressing C-terminal GFP-variant tagged PAR constructs.

2. Assess the relative contribution of the possible ER retention motifs upon PAR_4 subcellular localisation and signal transduction and investigate co-expression with other PAR family members.

3. Through the application of FRET, identify if PAR_4 and PAR_2 form constitutive heterodimers and investigate the consequence of interaction.

CHAPTER 2

MATERIALS AND METHODS

2.1 MATERIALS

2.1.1 General reagents

All reagents used were of the highest commercial grade possible and solutions were prepared in deionised water.

BioRad Laboratories (Hertfordshire, UK)

BioRad AG® 1-X8 Resin, Protein Assay Dye Reagent Concentrate (500-0006)

Fisher Scientific (Leicestershire, UK)

Hydrochloric acid

Insight Biotechnology Ltd (Wembley, UK)

Recombinant TNF-alpha

Invitrogen Ltd (Paisley, UK)

Fura-2-AM cell permeant (Molecular Probes)

NEN Dupont (Hertfordshire, UK)

Myo-[2-^{3}H(N)]-inositol (10-25Ci/mmol)

Sigma-Aldrich Co Ltd (Poole, Dorset, UK)

Ammonium Formate, EDTA, Formic Acid, Glycerol, Isopropanol, Protein A-Sepharose® beads (from *Staphylococcus aureus*) Protein G-Sepharose® beads (4B Fast Flow recombinant protein G in 20% ethanol), Sodium tetraborate, Trizma HCl, Tryptone, Tunicamycin (from *Streptomyces*, T7765) and Yeast Extract.

Wallac UK (Milton Keynes, UK)

Optiphase Hi-safe™ scintillant

β-scintillation counter

2.1.2   Fluorescent plasmid DNA constructs

All fluorescent PAR constructs were generated by Advantagen Ltd (Dundee, UK) unless otherwise stated. The fluorescence resonance energy transfer (FRET) positive control ECFP-EYFP tandem plasmid was a generous gift from Prof. Graeme Milligan, (University of Glasgow, Glasgow, UK). EYFP-Calnexin and ECFP-Calnexin plasmid DNA constructs were kindly provided by Dr Michael Freissmuth (Centre of Bimolecular Medicine and Pharmacology, Institute of Pharmacology, Medical University of Vienna).

2.1.3 PAR-specific agonists

Sigma-Aldrich Co Ltd (Poole, Dorset, UK)

α-Thrombin (Human Plasma), Trypsin (from Bovine Pancreas)

University of Calgary Peptide Service, Calgary, Canada

Ala-Tyr-Pro-Gly-Lys-Phe-amidated (NH_2) peptide (AYPGKF-NH_2)

Ser-Leu-Ile-Gly-Lys-Val-hydroxyl (OH) peptide (SLIGKV-OH)

2.1.4 Reagents for molecular biology and cellular transfection

Amaxa Biosystems GmbH (Germany, Europe)

Cell line Nucleofector Kit V

GE Healthcare UK Ltd, (Buckinghamshire, UK)

Illustra Plasmid Prep Mini Spin Kit

Invitrogen Ltd (Paisley, UK)

D5α-T1 chemically competent cells, Gene Tailor™ Site-Directed Mutagenesis System, Lipofectamine 2000™, PCR Primers and TOP10 Competent Cells.

Polysciences Inc., (Warrington, UK)

Polyethylenimine (PEI), (Linear MW~25,000, 23966)

Promega UK Ltd (Hampshire, UK)

Restriction Enzymes

Qiagen (West Sussex, UK)

Endofree Plasmid Maxi Kit

Stratagene, (Agilent Technologies UK Ltd, Cheshire, UK)

QuikChange® Multi-Site-Directed Mutagenesis Kit

2.1.5 Tissue culture consumables

All tissue culture flasks, plates, dishes and graduated pipettes were obtained from Corning Costar (Buckinghamshire, UK).

Gibco BRL (Paisley, UK)

Foetal calf serum (FCS), L-glutamine, Geneticin (G418), Medium 199 with Earls salts (M199), Minimal Essential Medium (x10), Non-essential amino acids, Opti-MEM® I Reduced Serum media, Penicillin/Streptomycin, Sodium Bicarbonate.

Lonza Wokingham Ltd, (Berkshire, UK)

HEPES Buffered Saline Solution

Sigma-Aldrich Co Ltd (Poole, Dorset, UK)

Dimethyl sulfoxide (DMSO), Optiprep Density Gradient Medium and ethanol.

2.1.6 Reagents for Western blotting

Amersham International Plc (Aylsbury, Buckinghamshire, UK)

ECL detection reagents

Bio-Rad Laboratories (Hertfordshire, UK)

Pre-stained SDS-PAGE Molecular Weight Marker

Bio-Rad Mini PROTEAN III^{TM} electrophoresis system

Boehringer Mannheim Ltd. (East Sussex, UK)

Bovine Serum Albumin (BSA), Dithiothreitol (DTT)

GE Healthcare Ltd (Buckinghamshire, UK)

Amersham™ Hybond™ -ECL nitrocellulose membrane

Sigma-Aldrich Co Ltd (Poole, Dorset, UK)

Acrylamide, Ammonium Persulfate (APS), Glycerol, Glycine, Kodak X-OMAT LS X-ray film, methanol, Sodium Chloride, Sodium Dodecyl Sulphate (SDS), N,N,N',N'-tetramethylenediamine (TEMED), TWEEN-20, and Trizma Base.

Whatmann (Kent, UK)

17 CHR Chromatography Paper

2.1.7 Antibodies

Abcam plc. (Cambridge, UK)

Anti-Calnexin (ab10286, rabbit polyclonal)

Anti-Calnexin (ab31290, mouse monoclonal)

Biosource Europe SA, Invitrogen Ltd (Paisley, UK)

Anti-phospho-p38 MAP kinase (44684-G, rabbit polyclonal)

Cell Signalling Technology, Inc. (New England Biolabs, UK)

Anti-Na, K-ATPase alpha1 (30105, rabbit polyclonal)

Clontech-Takara Bio Europe (France, EU)

Living Colours ® Full length A.v. GFP (632460, rabbit polyclonal)

Jackson ImmunoResearch Laboratories Inc., (PA, USA)

Horseradish peroxidase (HRP)-conjugated AffiniPure goat anti-rabbit IgG (111-035-144)

HRP-conjugated AffiniPure donkey anti-mouse IgG (715-035-150)

HRP-conjugated AffiniPure $F(ab^1)_2$ Fragment donkey anti-goat (705-036-147)

Texas Red® dye-conjugated AffiniPure donkey anti-mouse IgG (715-075-150)

Texas Red® dye-conjugated AffiniPure $F(ab^1)_2$ Fragment donkey anti-goat (705-076-147).

Santa Cruz Biotech. Inc. (CA, USA)

Anti-ERK (sc-94, rabbit polyclonal, K23)

Anti-p38 MAP kinase (sc-728, rabbit polyclonal, N20)

Anti-PAR$_4$ (sc-8482, goat polyclonal, M-20)

Anti-phospho-ERK (sc-7383, mouse monoclonal, E-4)

Sigma-Aldrich Co Ltd (Poole, Dorset, UK)

Anti-VSV-G (V4888, rabbit polyclonal)

Fluorescein (FITC)-conjugated goat anti-rabbit IgG (F-0382)

Fluorescein (FITC)-conjugated goat anti-mouse IgG (F-0257)

Zymed Laboratories Inc USA (Invitrogen Ltd, Paisley, UK)

Anti-Human Transferrin Receptor (13-6800, mouse monoclonal, Clone H68.4)

2.1.8 Microscopy

Merck-Calbiochem (Nottingham, UK)

Mowiol

Leica Microsystems (Milton Keynes, UK)

Leica DM6000 Confocal Fixed Stage (CFS) microscope

Molecular Devices Corp. (Downingtown, PA, USA)

MetaMorph Imaging Series software (version 7.0 or 7.6.4)

Nikon Instruments (New York, USA)

Nikon TE-300 Epifluorescence microscope

Nikon Eclipse TE2000-E inverted Epifluorescence microscope

40 x or 100 x oil-immersion Plan Fluor Objective Lens, NA=1.3

VWR International Ltd (Leicestershire, UK)

No. 0, (0.09-0.13 mm thick), circular glass 13 or 22 mm diameter coverslips.

0.8-1.0mm thick glass microscopy slides

2.2 GENERATION OF FLUORESCENT-TAGGED PAR CONSTRUCTS

All PAR constructs were fluorescently tagged at the extreme C-terminal and sequenced to ensure 100% sequence identity. The plasmid DNA was then amplified and extracted by Endofree Plasmid Maxi kit (Qiagen Ltd, UK) to produce transfection grade plasmid DNA. The constructs were then transiently expressed and functionally characterised in various mammalian cell lines.

2.2.1 pPAR$_1$-EGFP and pPAR$_1$-EYFP (Advantagen Ltd, Dundee, UK)

Human PAR$_1$ was amplified from pcDNA 3.1(+)-PAR$_1$ by PCR, prior to insertion into a pEGFP/pEYFP-N1 vector (Clontech) to create C-terminal hPAR$_1$-EGFP and hPAR$_1$-EYFP fluorescent constructs. The hPAR$_1$ insert was digested with EcoRI and BamHI restriction enzymes and subsequently ligated into the respective restriction sites within the multiple cloning region of pEGFP/pEYFP-N1 expression vector. The following primers were used;

Forward primer (T7 primer): 5'ATTGTAATACGACTCACTATAGGG
Reverse primer: 5' GTGGATCCCGAGTTAACAGCTTTTTGTATATGCTG

2.2.2 pPAR$_2$-EYFP (Advantagen Ltd, Dundee, UK)

Human PAR$_2$ was amplified from pRSV-PAR$_2$ by PCR. The PAR$_2$ insert was digested with HindIII and BamHI and ligated into the respective sites of the pEYFP-N1 expression vector. The following primers were used;

Forward primer: 5' TCAAGCTTACCATGCGGAGCCCCAGCGC
Reverse primer adg426: 5' CTGGATCCATAGGAGGTCTTAACAGTGGTTG

2.2.3 pPAR$_4$-ECFP and VSV-G-pPAR$_4$-ECFP (Advantagen Ltd, Dundee, UK)

Human PAR-4 was amplified from a pcDNA 3.1 (+)-hPAR$_4$ plasmid. The PAR$_4$ insert was digested with Kpn-AgeI restriction enzymes. ECFP was amplified from an ECFP-N1 vector (Clontech) and digested with Age and XbaI. PAR$_4$ and ECFP were ligated and inserted into the KpnI-XbaI sites of a pcDNA 3.1 (+) vector. The following primers were used;

Forward primer (T7 primer): 5' ATTGTAATACGACTCACTATAGGG

Reverse primer: 5'AGACCGGTGGCTGG AGCAAAGAG GAGTGGG

2.3 SITE-DIRECTED MUTAGENESIS

2.3.1 Generation of monomeric fluorescent protein constructs ($A_{206}K$ point mutation)

Monomeric GFP variants were generated by amino acid substitution of the primary sequence at position Ala_{206} in the GFP protein through site-directed mutagenesis, as indicated by Zacharias *et al.,* 2002. Mutagenesis was carried out by PCR (Techne Touchgene Gradient PCR machine, Fisher Scientific Ltd, Leicestershire, UK) using a Gene Tailor ™ Site-Directed Mutagenesis kit (Invitrogen Ltd, UK) following manufacturer's guidelines. Plasmid DNA (100 ng) was methylated for an hour at 37ºC in the presence of DNA methylase and S-adenosylmethionine (1xSAM). In order to introduce the desired mutation into the construct, the methylated DNA (5 µl) was amplified by PCR using a high fidelity Platinum® *Pfx* DNA Polymerase (Invitrogen Ltd, UK). The following primers were designed for this mutagenesis PCR reaction, resulting in the successful amino acid substitution of Alanine (A) to Lysine (K) at position 206 of each GFP, YFP and CFP construct;

Forward primer:

CAGTCC<u>AAG</u>CTGAGCAAAGACCCCAACGAGAAGCGCGAT CAC

Reverse primer:

GTCATCGCGCTTCTCGTTGGGGTCTTTGCTCAG<u>CTT</u>GGA CTG

The cycling parameters used for the PCR reaction involved an initial hot start step of 94ºC for 2 minutes followed by thermal cycling of 30 seconds at 94ºC (denaturation step), 30 seconds at 55ºC (annealing) and 8 minutes at 68ºC (extension step) for 20 cycles. A final extension period of 10 minutes at 72ºC was included at the end of the PCR program. Bacterial transformation of the PCR product was carried out in D5α™-T1® chemically competent cells (Invitrogen Ltd). The transformation procedure involved incubation of 2 µl of mutagenesis PCR reaction with the competent cells on ice for 30 minutes. This was followed by heat shock treatment of

the cell mix for 45 seconds at 42ºC followed by ice incubation for 2 minutes. The cell mix was then transferred into 5 ml of pre-warmed antibiotic-free Luria-Beltane (LB) culture medium (1% Try tone, 0.5% Yeast Extract and 1% Sodium Chloride) and placed in a C24 Incubator (New Brunswick Scientific, Edison, NJ, USA) to shake at 190 rpm at 37ºC for 1 hour. A small volume of the transformation reaction (100 µl) was then spread on pre-warmed LB-agar plates (with antibiotic for selection pressure); the plates were inverted and incubated at 37ºC for 16 hours. Colonies present on the plates were selected and grown in LB culture medium (with antibiotics) shaking at 190 rpm at 37ºC for 8 hours. Mini plasmid DNA was extracted and purified from the cultures using an Illustra plasmid prep mini spin kit (GE Healthcare UK Ltd, Buckinghamshire, UK) in accordance to manufacturer's guidelines. The constructs were then sequenced to ensure that the mutation was present. The plasmid DNA was then extracted and purified by Endofree Plasmid Maxi kit (Qiagen Ltd, UK), following the manufacturer's instruction, to produce transfection grade plasmid DNA. Plasmid DNA was quantified by GeneQuant pro UV/visible spectrophotometry (Amersham Biosciences).

2.3.2 Generation of PAR$_4$-ECFP endoplasmic reticulum (ER) motif mutants.

Two arginine (R)-based endoplasmic reticulum (ER) retention motifs, located within the protein sequence of pPAR$_4$-ECFP, were mutated using site-directed mutagenesis as described in 2.3.1 using a QuikChange® Multi-Site-Directed Mutagenesis Kit (Stratagene). Arginine residues were substituted for alanine amino acids at positions R^{183}AR (to create A^{183}AA) and R^{188}GRR (to create A^{188}GAA). A third construct was also generated incorporating alanine substitutions into both motifs simultaneously. The following primers were used to incorporate the necessary amino acid substitutions;

'R^{183} AR→AAA' Forward primer:
CAC CCG CTG GCG GCC GCC GCC CTG CG
'R^{183}AR→AAA' Reverse primer:
CGCAGG GCG GCG GCC GCC AGC GGG TG

'R[188] GRR→AGAA' Forward primer:

GCG CCC TGG CTG GCG CGG CCC TGG CCC

'R[188] GRR→AGAA' Reverse primer:

GGG CCA GGG CCG CGC CAG CCA GGG CGC

'R[183] AR AL R[188]GRR→AAA AL AGAA' Forward primer:

CAC CCG CTG GCG GCC GCC GCC CTG GCT GGC GCG GCC CTG GCC C

'R[183] AR AL R[188]GRR→AAA AL AGAA' Reverse primer:

GGG CCA GGG CCG CGC CAG CCA GGG CGG CGG CCG CCA GCG GGT G

2.4 CELL CULTURE

All cell culture was carried out in a Class II laminar flow hood under aseptic conditions.

2.4.1 Human Embryonic Kidney (HEK) 293 cells

Human embryonic kidney (HEK) 293 cells were maintained in Minimal Essential Medium (MEM) with Earle's salts (GIBCO®, Invitrogen Ltd) supplemented with 10% (v/v) foetal calf serum (FCS), penicillin (250 units/ml), streptomycin (100 μg/ml), L-glutamine (27 mg/ml), 1x (v/v) non-essential amino acids and 0.375% (v/v) sodium bicarbonate (all GIBCO®, Invitrogen Ltd). At 90% confluence, the HEK293 cells were washed once with phosphate buffered saline (PBS), (PBS; 150 nM NaCl, 5.4 mM KCl, 10 mM Na_2PO_4, 1.5 mM KH_2PO_4, pH7.4) and passaged using 1x sodium citrate (1x SSC, pH7.4). The cells were then collected in media, centrifuged at 700 rpm for 5 minutes and transferred to a fresh T75 flask and/or 12 well plates, depending upon the experimental procedure. Cells where then incubated at 37°C in a humidified atmosphere with 5% CO_2 with media replaced every second day. Cells were used for experimentation between passage 30 and 55.

2.4.2 Human Keratinocyte NCTC-2544 cells and NCTC-2544 cells expressing PAR$_2$ (NCTC-PAR$_2$)

Human keratinocyte NCTC-2544 cells were maintained in Medium 199 (M199) containing Earles salts (Sigma-Aldrich Co Ltd) supplemented with 10% (v/v) FCS, penicillin (250 units/ml), streptomycin (100 µg/ml), L-glutamine (27 mg/ml). At 90% confluence, cells were washed once with PBS, passaged using Versene (0.2 g/L EDTA prepared in sterile PBS), centrifuged at 700 rpm for 5 minutes and seeded as required. Cells were incubated at 37°C in a humidified atmosphere with 5% CO_2 with the media replaced every second day. Cells were used for experimentation between passage 4 and passage 20. Cells for experimentation were serum starved in serum-free M199 media for 24 hours prior to agonist treatment.

2.5 TRANSIENT TRANSFECTION

2.5.1. Lipofectamine™ 2000 Transfection

HEK293 cells were maintained as indicated in 2.4.1. Cells were grown to 80-90% confluence in 12 well plates with or without coverslips prior to transient transfection of 1 µg of Endofree plasmid DNA using the Lipofectamine™ 2000 transfection reagent (Invitrogen Ltd) in accordance to manufacturer's guidelines. Optimisation of the manufacturer's protocol found that a DNA/Lipofectamine™ 2000 ratio of 1 µg/2 µl per well of a 12 well plate was sufficient for maximal gene expression with minimal cytotoxicity in both HEK239 and NCTC-2544 cell lines. The complex was prepared in Opti-MEM® I reduced serum medium (Invitrogen Ltd). Plasmid DNA (1 µg) was resuspended in 100 µl of Opti-MEM® whilst 2 µl of Lipofectamine™ 2000 was added to a fresh eppendorf containing another 100 µl of Opti-MEM®. Both individual tubes were incubated at room temperature for 5 minutes. The DNA was carefully transferred to the tube containing Lipofectamine™ 2000 reagent and the complex was left at room temperature for a further 25 minutes. The adherent cells in the 12 well plates were washed once with PBS and the media replaced with 0.8 ml of Opti-MEM®. The complex was then added to the cells and incubated for 4 hours at 37ºC in a humidified atmosphere with 5% CO_2, after which time the Opti-MEM® was replaced with fresh media. Maximal gene expression was observed at 24-48 hours post-transfection.

2.5.2 Nucleofection® DNA Delivery

NCTC-2544 cells were maintained as indicated in Section 2.4.2. Cells were grown to 90% confluence in T75 cm flasks prior to Nucleofection® (Amaxa Biosystems GmbH, Lonza Wokingham Ltd, UK) in accordance to the manufacturer's guidelines (Cell line Nucleofector® Kit V). Optimisation of the manufacturer's general protocol found that each Nucleofection® reaction could be performed in either a 6 well or 12 well plate. Optimal conditions for a 6 well plate was 2 μg of DNA/$0.5x10^6$ cells/well per Nucleofection® reaction, with the same conditions adopted for the 12 well format but the contents of the reaction equally divided between 2 wells of a 12 well plate. The program used for optimal Nucleofection® in NCTC-2544 cells was program A-023 using a Nucleofector™ II machine. Briefly, 1.5 ml Eppendorf tubes were prepared containing the desired DNA concentration (2 μg) per reaction. Cells were passaged as outlined in Section 2.4.2. Using a haemocytometer, cells were counted and the total number of cells required to perform all the required reactions were transferred to a sterile 15 ml tube. The cells were centrifuged at 700 rpm for 5 minutes at room temperature. The supernatant was discarded and Solution V (Lonza Cologne's Nucleofector® Technology patent application number PCT/DE02/0148) was added to the cell pellet (100 μl per reaction). The cells were mixed and 100 μl from this was transferred to each of the tubes containing DNA. The cells and DNA were mixed and transferred to a sterile Nucleofection® cuvette and subsequently placed into the holding chamber of the Nucleofector™ II device and set to nucleofect at program A-023. The cells in the cuvette were removed with the addition of 1 ml of M199 media. The media/cells were then transferred by Pasteur pipette to one well of a 6 well plate (or 2 wells of a 12 well plate) containing pre-warmed M199 media. The cells were then given time to recover overnight at 37ºC in a humidified atmosphere with 5% CO_2, after which time the contents of the plate was replaced with fresh media. Maximal gene expression was observed at 24-48 hours post-nucleofection.

2.5.3 Polyethylenimine (PEI) Transfection

HEK293 cells and NCTC-2544 cells were seeded into 12 well plates as outlined in Section 2.4.1 and 2.4.2. Cells were grown to 80-90% confluence in 12 well plates

with or without coverslips prior to transient transfection of 1 µg of Endofree plasmid DNA using Polyethylenimine (PEI, Polysciences Inc., Warrington, UK). Optimal transfection with maximal gene expression and low cytotoxicity was achieved using a DNA/PEI ratio of 1 µg of DNA/5.7 µl of PEI (PEI Stock; 1 mg/ml in deionised water, heated until dissolved, filtered and stored at -80ºC). Briefly, 1 µg of Endofree plasmid DNA was added to an Eppendorf tube with 5.7 µl of PEI and 100 µl of complete growth medium. The contents of the tube were mixed by pipette and left to incubate at room temperature for 10 minutes. The media in the wells were replaced with 0.9 ml of complete growth medium and the contents of the tube transferred drop wise to the cells. The cells were left to incubate overnight at 37ºC in a humidified atmosphere with 5% CO_2, after which time the media was replaced with fresh media. Maximal gene expression was observed at 24-48 hours post-transfection.

2.6 FLUORESCENCE MICROSCOPY

2.6.1 Direct Immunofluorescence

Sterile round glass coverslips, (diameter 13 mm, thickness No.0), located in 12 well plates were used to culture HEK293 or NCTC-2544 cells. After a 24 hour growth period the cells were transiently transfected as indicated in Section 2.5. Prior to agonist treatment (where applicable), cells were serum starved for 24 hours in serum free medium. After stimulation, the cells on the coverslips were washed gently with ice cold PBS followed by fixation with ice cold 3% paraformaldehyde or methanol for 15 minutes at room temperature in the dark. The cells were washed twice in ice cold PBS and then incubated at room temperature in the dark for 5 minutes with 1 ml of PBS containing 100 ng/ml of the specific fluorescent nuclear marker 4',6-diamidino-2-phenylindole (DAPI). The cells were washed twice with PBS and the coverslips were mounted on to glass microscope slides with 15 µl Mowiol (2.4 g of Mowiol added to 25% glycerol prepared in 0.1M Tris-HCl). The microscope slides were then stored in the dark at 4ºC overnight to allow the coverslips to dry. Cells were visualised using a Nikon TE300-E upright epifluorescence microscope. Cells were imaged at x100 or x40 magnification with an oil-immersion Plan Fluor objective lens. Images were collected using a digital Cool Snap-HQ CCD camera (Roper Scientific, Photometrics, Tucson, AZ). MetaMorph Imaging Series 7.0

(Molecular Devices Corp., Downington, PA, USA) was used for control of image acquisition, processing and modification of all image data. The background average statistical correction editing function in MetaMorph was used to produce background corrected images. This was achieved by determining the average background level of fluorescence from regions of interest drawn adjacent to cells expressing fluorescence.

2.6.2 Indirect Immunofluorescence: VSV-G epitope detection

HEK293 cells and NCTC-2544 cells were grown to 70-80% confluence on 13mm glass coverslips as indicated in Section 2.4. Both transiently transfected cells (outlined in Section 2.5) and untransfected cells were used. Cells were serum starved for 24 hours in serum free medium prior to indirect staining. Cells were washed in ice cold PBS twice prior to fixation with ice cold methanol or 3% paraformaldehyde at room temperature as outlined in Section 2.6.1. After fixation, cells were washed twice with PBS and permeabilised with 0.3% SDS prepared in PBS containing 0.1% BSA for 10 minutes at room temperature. The coverslips were then incubated for 15 minutes at room temperature in 1 ml of 50 mM NH_4Cl prepared in PBS. The cells were washed firstly in PBS and then in 0.3% TritonX-100 (prepared in PBS containing 0.1% BSA). The cells were then blocked for 30 minutes in 1 ml of goat serum dilution buffer (GSDB: 16% goat serum, 0.3% TritonX-100, 0.3 M NaCl prepared in PBS) or 1% BSA in PBS. After blocking, the coverslip was placed cell side down onto 30 µl of primary antibody (1:100 dilution in GSDB) overnight in the dark at 4ºC in a humidified chamber to minimise evaporation. The cells were washed three times in 0.3% TritonX-100 permeabilisation buffer and the coverslip placed cell side down onto 30 µl of FITC or Texas Red conjugated secondary antibody (1:100 dilution in GSDB) for 1 hour at room temperature in the dark. The cells were then washed a further 2 times in permeabilisation buffer followed by incubation at room temperature in the dark for 5 minutes with 1 ml of PBS containing 100 ng/ml of DAPI. The cells were then washed with PBS and the coverslips were placed cell side down on to glass microscope slides containing 15 µl Mowiol. The microscope slides were then stored in the dark at 4ºC overnight to allow the coverslips to dry. The microscope slides were then processed as outlined in Section 2.6.1.

2.6.3 Indirect Immunofluorescence: Calnexin Abcam antibodies

Cells were fixed at room temperature as outlined in Section 2.6.2, then washed twice with ice cold PBS prior to permeabilisation for 10 minutes with 0.25% TritonX-100 in PBS (PBST) at room temperature. The coverslips were carefully washed three times with PBS, with an interval of 5 minutes between each wash. The cells were blocked in 1% BSA in PBST for 30 minutes. After blocking, the coverslips were placed cell side down onto 30 µl of primary antibody (1:100 dilution in 1% BSA in PBST) and stored overnight in the dark at 4ºC in a humidified chamber to minimise evaporation. The coverslips were carefully washed three times with PBS as before. The coverslips were then placed cell side down onto 30 µl of FITC or Texas Red conjugated secondary antibody (1:100 dilution in 1% BSA in PBST) for 1 hour at room temperature in the dark. The cells were then washed three times in PBS as before followed by incubation at room temperature in the dark for 5 minutes with 1 ml of PBS containing 100 ng/ml of DAPI. After washing with PBS, the coverslips were placed cell side down on to glass microscope slides containing 15 µl of Mowiol. The microscope slides were then stored in the dark at 4ºC overnight to allow the coverslips to dry. The microscope slides were then processed as outlined in Section 2.6.1.

2.7 FLUORESCENT TECHNOLOGY USED FOR STUDYING PROTEIN-PROTEIN INTERACTION

For years researchers have been continually striving to advance upon existing techniques available to study the dynamics of protein-protein interaction. Researchers have relied upon immunoprecipitation techniques as a means to confirm protein-protein interactions in cellular systems. Many of the tools available now incorporate novel fluorescent reporter proteins to detect such interactions, monitor protein localisation and movement in living cells (Chapman *et al.*, 2005). Advances in molecular imaging technology have resulted in the development of highly sophisticated methods to directly measure protein-protein interaction real time in live cells (reviewed by Day and Schaufel, 2005).   These powerful experimental approaches have worked towards providing a better understanding of the proteome at subnanometer resolution.   One of the imaging techniques in the forefront of

monitoring protein interactions in recent years has been fluorescence (Förster) resonance energy transfer (FRET). So far this technique has been used to identify interaction of proteins localised in the nucleus (Voss *et al.,* 2005), endoplasmic reticulum (Verrier *et al.,* 2008), cytosol (Dowal *et al.,* 2006), and plasma membrane (Wilson *et al.,* 2005). FRET can be carried out in live cells by wide-field, confocal, multiphoton and life time imaging microscopy (Tadross *et al.,* 2009). Common fluorescent tags used for FRET are those derived from *Aequorea victoria* green fluorescent protein (*A.v.* GFP), reviewed by Pollok and Heim in 1999 and Zhang *et al* in 2002. The most widely used FRET pair is cyan fluorescent protein (CFP; donor) and yellow fluorescent protein (YFP; acceptor), Zhang *et al.,* 2002.

At the moment GFP-based expression systems remain the first method of choice for many researchers studying protein localisation, trafficking and interaction. GFP is a 238 amino acid protein isolated from the jellyfish *Aequoria victoria*, with an excitation/emission spectrum peak of 489 nm/508 nm (Yang *et al.,* 1996). Since the molecular cloning of GFP cDNA by Ward and colleagues (Chalfie *et al.,* 1994), many recombinant GFP variant proteins have been developed as shown in Table 2.1. The major drawback of the use of these proteins to monitor cellular proteins is the large size of the fluorophore, which when fused together with the protein of interest, can result in the loss of normal protein function. The development of fluorescent-based techniques that minimise the loss of protein function has been ongoing for years, with smaller fluorescent probes such as the FlAsH tag, being more favourable (Hoffman *et al.,* 2005). As imaging technology becomes more advanced, an increasing number of researchers have been striving to create highly quantitative approaches in order to validate protein interaction.

Table 2.1. Spectrally different GFP variant proteins and common FRET pairs

Fluorescent Protein (FP)	Wavelength (λ) Ex/Em (nm)
Enhanced Green (EGFP)	489/508
Enhanced Cyan (ECFP)	434/477
Enhanced Yellow (EYFP)	514/527
Enhanced Blue (EBFP)	380/440
Common FRET pairs	
Donor (Ex/Em peaks in nm)	**Acceptor (Ex/Em peaks in nm)**
ECFP (434/477)	EYFP (514/527)
EBFP (380/440)	EGFP (489/508)
ECFP (434/477)	DsRed (558/583)
Cy3 (550/570)	Cy5 (650/670)
FITC (492/520)	TRITC
Alexa488	Alexa555
Alexa488	Cy3 (550/570)
EGFP2 (410/510)	EYFP (514/527)

References: Lippincott-Schwartz *et al.,* 2001; Kenworthy, 2001; Harrison and van der Graaf, 2006.

2.7.1 Wide-Field Fluorescence Resonance Energy Transfer (FRET) Microscopy

The basic principles of FRET relies on fluorescence microscopy to measure molecular interaction based upon the distance between two fluorophores that will allow energy to transfer from one fluorophore (the donor) to the other (the acceptor). Typically, for optimal energy transfer to occur, the donor (Don) and the acceptor (Acc) fluorophores have to be within close proximity (1-100Å), share a degree of spectral overlap (i.e. acceptor excitation spectrum must overlap with the donor emission spectrum) and have parallel transition dipole orientations to enable efficient non-radioactive dipole-dipole interaction to take place (for review see Takanishi *et al.,* 2006).   Table 2.1 shows commonly used fluorophores for FRET analysis; however the most established methods for GFP-based FRET imaging use the ECFP (Don)-EYFP (Acc) spectral variants as the donor and acceptor pair (Grailhe *et al.,*

2006). The better the spectral overlap between donor and acceptor fluorophores, the better the FRET efficiency, which makes ECFP-EYFP the most favourable FRET pair to date (as shown in Figure 2.1).

Generally, FRET efficiency can be quantified through acceptor photobleaching or based upon sensitised emission measurements (Berney *et al.,* 2003). Acceptor photobleaching results when donor excitation takes place and the subsequent light emitted is measured before and after acceptor photobleaching. The quantification of sensitised emission requires the measurement of light emitted from the donor or acceptor upon donor excitation. The features of sensitised FRET are observed when a decrease in donor emission coincides with an increase in acceptor emission. Despite this simplistic overview, the quantitative aspects of FRET are far from simple and require extensive knowledge of the fluorescence microscopy equipment and applications as well as an appropriate FRET efficiency quantification method. The basis of most of the quantification methods rely upon appropriately controlled experimental conditions in order for experimental FRET data to be reliably corrected and interpreted (Berney *et al.,* 2003). Factors that can result in the contamination and misinterpretation of the FRET signal have to be taken into consideration in the experimental design, these include determination of fluorophore excitation cross-talk, spectral bleed-through, non-specific FRET, mixed fluorophore populations and variable fluorophore expression levels (for review see Tankanishi *et al.,* 2006).
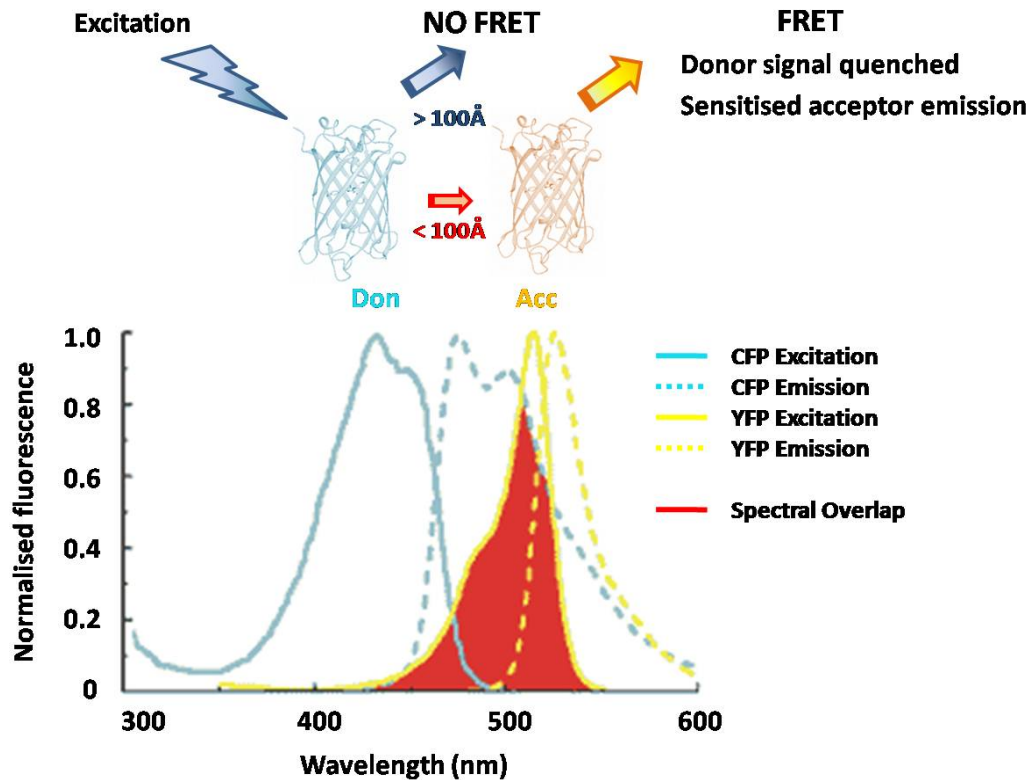
Figure 2.1. Overview of the typical requirements for FRET.

The spectral overlap between CFP emission and YFP excitation is shown (Red shaded area). Other considerations for FRET include the distance between the Don and Acc (1-100Å). Distances out with this (>100Å) results in donor emission but no energy transfer (i.e. no FRET). Clear indicators of FRET occurrence include a decrease in donor signal coupled with increased acceptor emission. Adapted from Chen *et al.* 2005

2.7.2 Wide-Field FRET Method
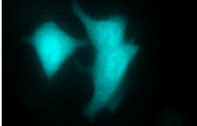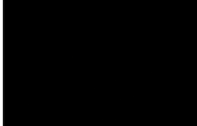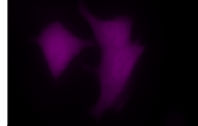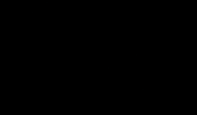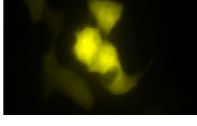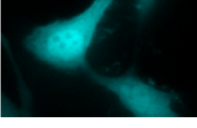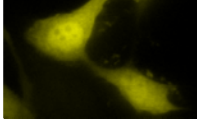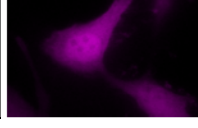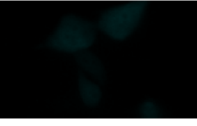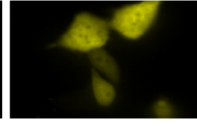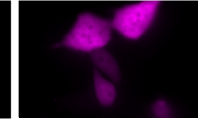
Sterile circular glass coverslips, (diameter 22 mm, thickness No.0), positioned in 6 well plates were used to culture the cells. After 24 hours growth, the cells were transiently transfected as previously described in Section 2.5. The following experimental control assays were then set up:

i.   Cells were transfected with ECFP (donor protein) only to determine bleedthrough coefficient values for the amount of bleedthrough of the cyan donor into the FRET and acceptor channel.

ii.   EYFP (acceptor protein) was expressed only in cells to quantify bleedthrough constant values for the amount of bleedthrough of the yellow acceptor into the FRET and donor channel.

iii.   Cells were co-transfected with ECFP and EYFP, (negative control), to determine random collisional FRET interactions.

iv.   An ECFP-EYFP tandem (positive control for FRET), was expressed only in cells. On expression, the donor and acceptor molecules are fused to generate a FRET signal.

Various proteins of interest tagged with ECFP (donor protein) or EYFP (acceptor protein) were expressed individually in cells and co-expressed to measure FRET between the donor and acceptor pairs. Fluorescence resonance energy transfer (FRET) was measured in single cells co-expressing acceptor/donor pairs. The following FRET experiments were carried out in cells co-expressing; PAR_2 EYFP and PAR_4 ECFP, PAR_2 EYFP and ECFP-Calnexin, EYFP-Calnexin and PAR_4 ECFP, PAR_2 EYFP and PAR_4 ECFP ER mutants (described in Section 2.3.2). The coverslips were transferred to a microscope chamber containing physiological HEPES-buffered saline solution (130 mM NaCl, 5 mM KCl, 1 mM $CaCl_2$, 1 mM $MgCl_2$, 20 mM HEPES, and 10 mM D-glucose, pH 7.4).

FRET was performed at room temperature (20-22 ºC) in living cells prepared on coverslips using wide-field FRET microscopy (see Wilson *et al.,* 2005; Ellis *et al.,* 2006; Lopez-Gimenez *et al.,* 2007) on a Nikon TE2000-E inverted microscope (Nikon Instruments, Melville, NY). Epifluorescence imaging was carried out using a

40x (numerical aperture; NA 1.3) oil immersion Fluor lens. Emitted fluorescence was detected using a photometric Cool Snap-HQ monochrome camera (Roper Scientific, Trenton, NJ) set up in 12-bit mode (0-4095 grey tones). MetaMorph software, (version 7.6.4) was used to control both the microscopy hardware and multi-wavelength fluorescence image acquisition required for intermolecular FRET detection. Donor 430 nm or acceptor 500 nm excitation light was generated using a computer controlled Optoscan monochromator (Cairn Research) which was coupled to a 103/W2 mercury (Hg) arc lamp source (Cairn Research, Faversham, Kent, UK). Optimisation of excitation centre wavelength and bandpass settings was necessary to ensure that the signal-to-noise ratio was optimal and no recorded pixels within the images were saturated, i.e. above the 4095 grey intensity level. The risk of motion occurring during the sequential FRET imaging process was minimised by using a high-speed filter wheel (Prior Scientific Instruments, Cambridge, UK). The following emission filters were used for detecting donor, acceptor and FRET emissions respectively: donor Em, HQ470/30 nm; acceptor and FRET Em, HQ535/30 nm. The three filter channel combinations used to detect FRET were; **ECFP donor**: Ex 430 nm/Em 470 nm; **EYFP acceptor**: Ex 500/ Em 535 nm; **ECFP/EYFP/FRET**: Ex 430/Em 535 nm. All images were recorded in 2 x 2 binning format and the illumination exposure time was 250 msec. The emitted fluorescence detected in the acceptor, donor and FRET channels for each experimental group were acquired using identical excitation illumination settings and exposure times. The filter combinations used for the FRET experiments allowed images to be taken from cells expressing each of the individual protein fluorophores (i.e. acceptor and donor only expressing cells) and generate the uncorrected (raw) FRET image, see below in Figure 2.2.

Fluorophore Expressed	Images acquired		
	Donor	Acceptor	uFRET
Donor only			
Acceptor only			
Donor + Acceptor			
Donor-Acceptor concatamer			

uFRET = uncorrected (raw) FRET channel containing spectral bleedthrough contamination from Acceptor and Donor fluorescence.

Figure 2.2. Typical images acquired for FRET analysis.

The images recorded in each channel from the different experimental groups above were used to carry out pixel-by-pixel based correction of background fluorescence and spectral bleedthrough (SBT) of the acceptor fluorescence present in donor (AD) and FRET (AF) images, as well as correct for donor fluorescence present in acceptor (DA) and FRET (DF) images. Correction was based upon the pixel intensity of defined regions of interest (ROI) created at the same points across all three images (donor, acceptor and FRET). Metamorph imaging software was used to process the acquired images and correct SBT present in uncorrected FRET images. This software provided a specified bleedthrough correction algorithm, which when applied was capable of correcting raw FRET images to produce corrected FRET images and measurements. The ratio between the fluorescence signal detected in the

FRET image and the image for each fluorophore were defined as bleedthrough coefficients (see below).

Typical bleedthrough coefficients calculated from FRET experiments were;

FRET/DONOR (DF) = 0.63 and FRET/ACCEPTOR (AF) = 0.12

The FRET measurements obtained were normalised and ratiometric FRET (RFRET) values were calculated. This involved taking the measurements from raw FRET fluorescence and dividing this value by the total SBT (total spillover) of the acceptor and donor into the FRET channel. The following equation was used to calculate RFRET;

Raw FRET, Acceptor and Donor images shown above correspond to the respective background corrected images acquired through the relevant filter channels, whilst [a] and [b] correspond to the bleedthrough coefficient values calculated for EYFP (AF coefficient) and ECFP (DF coefficient), shown previously.

In the absence of energy transfer (i.e. no FRET occurrence), the RFRET value obtained would be 1, values greater than 1 would represent the occurrence of FRET, thus indicative of protein interaction. Quantified RFRET values were graphed using GraphPad Prism 4 Software.

2.8 DETECTION AND ANALYSIS OF PROTEINS

2.8.1 Preparation of samples for Western blotting

Cells in 12 well plates (as prepared in Section 2.4) were serum starved for 24 hours prior to agonist treatment. The cells were then washed twice with ice cold PBS and killed in 150 µl of pre-heated (~85°C) 1x Laemmli sample buffer (63 mM tris HCl, 2 mM $Na_4P_2O_7$, 5 mM EDTA, 10% (v/v) glycerol, 2% (w/v) SDS, 0.007% (w/v) bromophenol blue) supplemented with 50 mM DTT. The cells were scraped on ice and the whole cell lysates collected using a 1 ml syringe attached to a 16-guage needle. The cells were drawn up and down repeatedly through the syringe prior to transfer into a 1.5 ml Eppendorf tube. The samples were then boiled for 5 minutes in a boiling bath and stored at -20°C until required.

2.8.2 Western blotting

Whole cell lysates were prepared as indicated in 2.8.1. The Bio-Rad Mini PROTEAN III^{TM} electrophoresis system (Bio-Rad Laboratories, Hertfordshire, UK) was used for Western blotting (see Goon Goh *et al.,* 2008). Proteins (10-20µg per lane) were separated on SDS-PAGE resolving gels (acrylamide:N'-methylenebis-acrylamide (30%:0.8%) in 0.375 M Tris pH8.8, 0.1% (w/v) SDS). Polymerisation of the resolving gel was achieved through the addition of 0.5% (w/v) ammonium persulfate (APS) and 0.05% (v/v) N,N,N,N', N'-tetramethylethylenediamine (TEMED). These components were added to the other resolving gel components and mixed immediately prior to pouring into clean pre-assembled 1 mm (medium) or 1.5 mm (thick) glass plates (Bio-Rad). An overlay of 0.1% SDS (~500 µl) was added carefully to the top of the resolving gel to allow the gel to set straight and provide a separate liquid interface to provide an indication as to when the resolving gel was set. This SDS interface was removed and the resolving gel was topped with a 4% stacking gel solution (Acrylamide: N'-methylenebis-acrylamide (30%:0.8%) solution, in 125 mM Tris pH6.8, 0.1% (w/v) SDS and 0.5% (w/v) APS and 0.05% (v/v) TEMED. Once the stacking gel solution was poured, a Teflon comb (10 well or 15 well) was carefully inserted between the glass plates and into the stacking gel solution. Once the stacking gel was set, the combs were removed and the wells rinsed with sterile water. The glass plates containing the SDS-PAGE gels were

assembled into PROTEAN III^{TM} electrophoresis holders, which were then inserted into a Western blotting tank. The tank was filled with electrophoresis running buffer (25 nM Tris, 19 mM Glycine, 0.1% (w/v) SDS). The whole cell lysates were loaded into the wells through a Hamilton micro-syringe alongside a pre-stained molecular weight marker (Bio-Rad) and set to run at 120 volts until the bromophenol blue sample dye ran off the bottom of the gel.

The resolved proteins were then transferred onto pre-cut Amersham™ Hybond™ - ECL nitrocellulose membrane in a transfer cassette arranged as follows; black side of cassette followed by 1x sponge pad, 1x 3 MM Whatmann filter paper, nitrocellulose membrane, resolving gel, 1x 3MM filter paper, and 1x sponge pad . All components in the cassette were pre-soaked in transfer buffer (25 mM Tris, 19 mM Glycine, 20% (v/v) methanol) prior to assembly. The prepared cassette(s) were then inserted into a Bio-Rad trans-blot tank and immersed in transfer buffer, with an ice reservoir to keep the tank cool. The transfer apparatus was connected to a power pack set at a constant current of 290 mA for 1 hour 45 minutes. The membranes were then removed from the cassette and blocked for non-specific protein binding in 2% BSA (w/v) prepared in NATT buffer (50 mM Tris-HCl, 150 mM NaCl, 0.2% (v/v) Tween-20). The blocking buffer was then removed and blots were then incubated overnight with primary antibody prepared in 0.2% BSA (w/v) in NATT buffer. The blots were washed at 15 minute intervals with NATT buffer for a total duration of 90 minutes prior to incubation with HRP-conjugated secondary antibody prepared in 0.2% BSA (w/v) in NATT buffer for a further 2 hours. A further series of NATT washes was undertaken (as before). Finally the blots were subjected to enhanced chemiluminescence (ECL) reagent for 2 minutes, blotted to remove excess ECL and then transferred to an exposure cassette. In the dark room, the blots in the cassette were exposed to Kodak X-OMAT LS film for the appropriate time, with the exposed film developed through a Kodak M35-M X-OMAT processor.

2.8.3 Nitrocellulose membrane stripping and reprobing

Nitrocellulose membranes processed through Western blotting were reprobed for the subsequent detection of other cellular proteins. This involved stripping the

membrane of any previous antibody using a stripping buffer (0.05 M Tris-HCL, 2% SDS, and 0.1 M of β-mercaptoethanol). The membrane was incubated in 15 ml of stripping buffer for 60 minutes at 70°C in an incubator/shaker (Stuart Science Equipment). The stripping buffer was discarded in a fume hood sink and the membrane washed six times with NATT buffer at 15 minute intervals to remove residual stripping buffer. After the final NATT wash, membranes were then incubated overnight with primary antibody prepared in 0.2% BSA (w/v) in NATT buffer. The membranes were then processed as outlined in Section 2.8.2.

2.8.4 Determination of protein concentration by Bradford's assay

Cells were prepared as outlined in Section 2.4. Quantification of the protein concentration in the cells was determined through the application of the Bradford method using Bio-Rad protein assay dye reagent. The protein assay reagent was prepared from concentrate, diluted 1:5 in distilled water. A BSA protein standard curve was prepared using 0, 5, 10 and 20 μg/ml concentration points and made to a total volume of 1 ml with the prepared protein assay reagent. A small volume of the cell sample (5 μl) was added to a 1.5 μl Eppendorf and mixed with 995 μl of the protein assay reagent. The contents were then transferred to a cuvette and left to incubate for 15 minutes at room temperature. The cuvettes were then placed inside a calibrated UV/visible spectrophotometer (Ultrospec 2000®, Amersham Pharmacia Biotech., GE Healthcare Ltd, Buckinghamshire, UK) and the protein content determined through measuring the absorbance at a wavelength of 595 nm (i.e. A595). The absorbance values obtained for each test sample were then measured against those obtained for the BSA standard curve. The final protein concentration of each sample was then calculated from the BSA standard curve.

2.8.5 Co-immunoprecipitation

Cells were grown to 90% confluence in T75 cm tissue culture flasks prior to transient transfection as outlined in Section 2.5. The cells were harvested using versene to detach the cells from the flask and collected together with growth media in a sterile 50 ml centrifuge tube. The cells were centrifuged at room temperature at 1000 rpm for 10 minutes and the cell pellet solubilised in 500 μl solubilisation buffer (20 mM

HEPES, 50 mM NaCl, 0.1 mM EDTA, 1% TritonX-100 supplemented with 25 µg/ml leupeptin, 10 µg/ml aprotinin and 1 µg/ml PMSF, pH7.6 prepared in distilled water). The solubilised cells were mixed by vortex and left to incubate on ice for 30 minutes prior to clarification by centrifugation. After incubation, the protein concentration of the solubilised sample was determined using the Bradford assay as described in Section 2.8.4.

Prior to solubilisation, 15 µl of Protein G-Sepharose beads (Sigma-Aldrich Co Ltd, Poole, Dorset, UK) or 50 µl of Protein A-Sepharose beads (5 mg/tube) were transferred into 1.5 ml Eppendorf tubes. The beads were washed with solubilisation buffer once, centrifuged at 14,000 rpm for 5 minutes at 4°C and the aqueous phase aspirated carefully by syringe to leave the bead pellet. The beads were pre-coupled with 1 µg/ml of primary antibody in a total volume of 50 µl solubilisation buffer. The beads/antibody was incubated at 4°C on a rotor shaker, set to shake at 1250 rpm for 2 hours. After incubation, the beads were washed twice in ice cold PBS and 2.5 mg/ml of protein added to the beads in a total volume of 500 µl. The pre-coupled beads and protein sample was incubated overnight on a rotary mixer at 4ºC. The tubes were then centrifuged at 14,000 rpm for 5 minutes and the aqueous phase aspirated by syringe. The beads were then washed three times with solubilisation buffer with centrifugation for 14,000 rpm for 5 minutes in between each wash. On the final spin, the aqueous phase was aspirated and replaced with 50 µl of solubilisation buffer and 50 µl of 2x Laemmli sample buffer. The samples were vortexed then boiled for 5 minutes in a boiling bath and centrifuged at 14,000 rpm for 1 minute. The sample was then carefully transferred to a fresh Eppendorf and resolved by Western blotting as described in Section 2.8.2.

2.8.6 Subcellular fractionation of ER and plasma membrane compartments

Cells were grown to 90% confluence in 5x T150 cm tissue culture flasks prior to transient transfection as outlined in Section 2.5. The cells were harvested as described in Section 2.4. The cells were centrifuged at room temperature at 1000 rpm for 10 minutes. The growth media was discarded and the cell pellet resuspended in 3 ml of HES buffer (25 mM HEPES, 1 mM EDTA and 250 mM sucrose, pH 7.4

prepared in distilled water) supplemented with protease inhibitors (25 µg/ml leupeptin, 10 µg/ml aprotinin and 1 µg/ml PMSF).

The resuspended cell sample was homogenised using a pre-cooled (~4°C) cell homogeniser (Isobiotec Precision Engineering, Germany German Patent Office under No. 202 09 547.9) fitted with a size 10 or 12 micron clearance tungsten carbide ball bearing. The sample was passed through the cell homogeniser 10 times and collected in 1.5 ml Eppendorf tubes. To remove the nuclei from the cell homogenate the sample was centrifuged at 500g for 2 minutes at 4°C on a benchtop centrifuge.

The supernatant was transferred to a fresh tube and resuspended in Opti-prep density gradient medium (60% w/v solution in water) to create a 45% (v/v) density sample solution (500 µl of sample to 1500 µl Opti-prep medium). The 45% density sample (2ml) was transferred to an ultra-centrifuge tube (Beckman). A density gradient starting from 30%-10% (30% [600 µl], 25% [600 µl], 20% [750 µl], 15% [750 µl] and 10% [750 µl]) was prepared using Opti-prep medium mixed in HES buffer. Each phase of the gradient was carefully added to an ultra-centrifuge tube (Beckman, in sequence starting at 30% and finishing with 10%. The volumes of each gradient added are indicated above. The density gradient then underwent differential centrifugation at 72,000 rpm for 4 hours at 4°C to separate plasma membrane, endosomal and endoplasmic reticulum (ER) fractions (Proctor *et al.,* 2006).

The fractions of the density gradient were collected in 300 µl sample volumes (~ 16 fractions) and transferred to 1.5 ml Eppendorf tubes containing 50 µl of 37.5% TCA. The tubes were mixed by vortex for 2-3 seconds and then incubated on ice for 15 minutes. The samples were centrifuged at 14,000 rpm for 15 minutes at 4°C. The supernatant was removed and the remaining pellet resuspended in 2x Laemmli sample buffer supplemented with 1M urea. Residual TCA from the previous step can often result in the sample buffer changing colour to yellow. This was rectified through the addition of 5 µl of saturated tris solution to the affected tube followed by votexing to mix.

The cell fractions were then resolved by Western blotting, as outlined in Section 2.8.2. Successful subcellular fractionation of ER and plasma membrane cell compartments was determined using Na^+/K^+ ATPase, transferrin receptor and calnexin antibodies as markers for plasma membrane, endosomal and ER fractions.

2.9. MEASUREMENT OF [^{3}H]-INOSITOL PHOSPHATE ACCUMULATION

Cells were maintained as described in Section 2.4 and grown to confluence in 12 well or 6 well plates. Following transient transfection (as outlined in Section 2.5), with fluorescent PAR constructs (Section 2.2) for 24 hours, cells were serum starved for a further 24 hours in serum free media supplemented with myo-[2-^{3}H-(N)]-inositol (0.25 μCi/well; 1 Ci = 37 GBq). Measurement of total inositol phosphate accumulation was carried out in accordance to the method published by Plevin *et al.*, 1994.

In order to inhibit the breakdown of inositol polyphosphates ($InsP_{1-4}$) in the cells, lithium chloride (LiCl) was added to the wells at a final concentration of 10 mM for 15 minutes at 37ºC in a humidified atmosphere with 5% CO_2. The cells were then stimulated with agonist for 45 minutes at 37ºC and then washed with PBS twice on ice. The PBS was removed and replaced with 1 ml of methanol and the cells scraped and transferred into 5 ml scintillant vials on ice. 0.5 ml of chloroform was added to each of the vials to give a 2:1 methanol: chloroform mix. The samples were vortexed and incubated on ice for 90 minutes, after which time 0.8 ml of sterile water and 0.5 ml of chloroform was added to each vial and vortexed. The vials were left at 4°C in order to allow the cells to settle and different aqueous phases to form. During incubation, 1 volume of BioRad AG® 1-X8 Ion exchange resin (DOWEX) was prepared in 2 volumes of sterile water and stirred thoroughly to ensure the resin was evenly mixed. 1 ml of DOWEX was then transferred into a fresh scintillant vial for each sample and allowed to settle at room temperature. The liquid phase of the resin was aspirated and replaced with 2.5 ml of sterile water. Once the resin had settled the water was removed and replaced with1 ml of the upper aqueous phase of the sample. The vials were vortexed and the resin left to settle at room temperature for 20 minutes. The aqueous phase was aspirated and the resin washed with 2.5 ml of

sterile water, followed by 2.5 ml of sodium tetraborate (5 mM $Na_2B_4O_7.10H_2O$, 60 mM ammonium formate prepared to 500 ml in distilled water) and then 2.5 ml of sterile water. In between each wash the resin was allowed to settle and the liquid phase aspirated prior to the addition of the next wash solution. In order to elute total inositol phosphate ($[^3H]$-IP_{1-4}) from the resin, 1 ml of ammonium formate elution buffer (1 M ammonium formate, 0.1 M formic acid prepared to 500 ml in distilled water) was added to each vial and the contents of the vial mixed by vortex. Whilst the resin was allowed to settle, a fresh scintillant vial was prepared for each sample and 1 ml of the aqueous phase transferred to the fresh vial. Optiphase Hi-safe™ scintillant (4 ml) was then added to the fresh vial containing the sample and mixed before being read on a liquid β-scintillation counter (Wallac, USA) for 2 minutes.

2.10 RATIOMETRIC FURA-2 AM CALCIUM (Ca^{2+}) IMAGING

Cells were grown on 22 mm diameter glass coverslips prepared in 6 well culture plates as described in Section 2.4. Following transient transfection with various fluorescent PAR constructs (Section 2.2) for 24 hours, cells were serum starved for a further 24 hours prior to calcium imaging (Bushell *et al.,* 2006). The cells were loaded with 6 µM of fura-2 AM cell permeant (a calcium sensitive ion indicator with a stoichiometry of 1:1, i.e. 1 fura 2 molecule binds 1 calcium ion) and left to incubate in the dark at room temperature for 60 minutes. The fura-2 loaded cells were then transferred to control HEPES buffered saline solution and left in the dark for 30 minutes to ensure that all of the loaded fura-2 AM had been converted to its free acid form via intrinsic esterase activity. After 30 minutes, the loaded cells were then transferred to a 1ml perfusion chamber mounted on a Zeiss Axioskop FS epifluorescence microscope containing control HEPES-buffered saline. Imaging was carried out using a 40x (numerical aperture; NA 1.3) oil immersion Superfluor lens with 1x binning and 1x gain.

The cells were perfused at room temperature at a constant rate of 1.5 ml/minute with HEPES-buffered saline (130 mM NaCl, 10 mM HEPES, 5.4 mM KCl, 1 mM $CaCl_2$, 1 mM $MgCl_2$ and 25 mM d-glucose prepared in distilled water, pH7.4). The cells were then perfused with various agonists prepared in HEPES-buffered saline (HBS)

for 2 minutes and then washed with HBS until the calcium response returned to basal. Calcium transients were measured from stimulated cells expressing PAR$_2$-EYFP and PAR$_4$-ECFP visualised at 488/25 nm and compared to responses obtained from non-transfected parental cells. Ratiometric images (340/380 nm) were acquired every 2-5 seconds using WinFluor V3.0.8 software (created by John Dempster, University of Strathclyde) to control image acquisition. Elevation of intracellular free calcium was distinguishable when a decrease in fluorescence was observed at 380 nm, which coincided with an increase in fluorescence at 340 nm. The background average statistical correction editing function in WinFluor was used to produce 340 and 380 nm background corrected images prior to the quantification and graphing of the 340/380 nm ratio. Agonist-evoked $[Ca^{2+}]_i$ transients were quantified as the difference between the baseline resting fura-2 340/380 nm ratio level and that attained at the maximum peak response.

2.11 CELL SURFACE VSV-G ELISA

Cells were transiently transfected in 6 well plates with VSV-PAR$_4$-ECFP, as outlined in Section 2.5. Twenty four hours post-transfection, the cells were harvested and evenly distributed into wells of a poly-D-lysine coated 96 well plate (1x 6 well: 8x 96 wells). The cells were left to settle for a further 24 hours at 37°C in a humidified atmosphere with 5% CO_2. Cell surface receptors were detected using a VSV-G cell surface ELISA on intact cells (Ellis *et al.,* 2006). The media was replaced with fresh media supplemented with anti-VSV-G antibody (1:1000) for 30 minutes at 37°C. The wells were washed twice in fresh growth medium and replaced with media supplemented with HRP-conjugated anti-rabbit IgG (1:1000) for 30 minutes at 37°C. The cells were washed three times in PBS and incubated with 100 µl SureBlue TMB peroxidase substrate (Insight Biotechnology) in the dark for 5 minutes at room temperature. The plate was then read at 620 nm in a SpectraMax 190 ROM v3.13 microplate spectrometer (Molecular Devices, Sunnyvale, CA). TMB stop solution was added to each of the wells and incubated in the dark at room temperature for 5 minutes to stop the reaction and then the plate was read at 450 nm. The 620 nm O.D. values were then tabulated.

2.12 SCANNING DENSITOMETRY

Autoradiography films for Western blotting were scanned on an Epson Perfection 1640SU scanner with the device accessed through Adobe Photoshop CS3 Software Version 10 (Adobe Systems Incorporated, USA) using TWAIN 2.0 as an interface between the device and software. The captured images were then quantified using Scion Image Densitometry Software 1.0.0.1 (Scion Corporation, Maryland, USA).

2.13 DATA ANALYSIS

The values obtained from FRET analysis were firstly exported into an Excel spreadsheet for the application of the necessary equations. The tabulated data was then transferred into PRISM 4.03 (GraphPad Software) where the data was expressed as the mean ± S.E.M and graphed accordingly. Statistical analysis was carried out using one-way ANOVA with Post Dunnett's test. Differences were considered significant at $P < 0.05$.

CHAPTER 3

THE EFFECT OF FLUORESCENT TAGGING UPON PAR$_2$ AND PAR$_4$ LOCALISATION, INTERNALISATION AND SIGNALLING

3.1 INTRODUCTION

Many of the original studies investigating the trafficking events following PAR_1 (Hein *et al.,* 1994) and PAR_2 (Böhm *et al.,* 1996) activation largely depended upon epitope tagging (FLAG tag; DYKDDDDK or 12CA5 hemagglutinin (HA) epitope; YPYDVPDYA) to monitor receptor localisation in overexpression cell models. These studies used indirect immunofluorescence as the method of choice to detect receptor localisation in fixed cells using antibodies directed against the expressing epitope. This was necessary as the commercial antibodies available for PARs were largely non-specific. The specificity of commercial PAR antibodies continues to be problematic. As a result the decision was made to fluorescently label human PAR_2 and PAR_4 with EGFP variant fluorescent proteins, EYFP and ECFP respectively. Due to the nature of PAR activation with N-terminal proteolytic cleavage, these fluorescent proteins were incorporated into the extreme C-terminus of the PAR receptor for the experiments carried out in this study. This strategy for monitoring receptor expression had the added advantage of allowing receptors to be monitored by direct immunofluorescence, with the opportunity of following events in living cells. However, the limitation of using epitope tagging to monitor protein localisation is the potential for the fluorescent protein to alter protein localisation and function. For this reason, characterisation of PAR localisation and cell signal transduction was required to ensure that the fluorescently tagged constructs were functional. PAR_2 localisation has been previously observed at the plasma membrane when expressed in kirsten murine sarcoma virus-transformed rat kidney (KNRK) epithelial cells (Böhm *et al.,* 1996) and human embryonic kidney (HEK293) cells (Hasdemir *et al.,* 2009), among other cell lines. Upon activation by tryspin or activating peptide, PAR_2 internalisation takes place, with decreased cell surface expression observed in KNRK cells within 5 to 30 minutes post-stimulation. Typical downstream cell signal transduction following PAR_2 activation include Ca^{2+} and $InsP_{1-4}$ responses, as well as mitogenic signalling and pro-inflammatory signalling through ERK MAPK, p38 MAPK and NFκB pathways (Bretschneider *et al.,* 1999, Macfarlane *et al.,* 2005, Kanke *et al.,* 2001). PAR_2-mediated ERK MAP kinase activation has been shown to be partly β-arrestin-dependent, an event that takes place at the C-terminal of PAR_2 and is pivotal to both PAR_2 activated ERK MAP kinase

signalling and receptor desensitisation (Kumar *et al.,* 2007). Many of these signalling events have been characterised in various epithelial-derived cell models including hBRIE 380 cells, a polarised intestinal epithelial cell line, KNRK cells (Böhm *et al.,* 1996) and human keratinocyte NCTC-2544 cells (Kanke *et al.,* 2001). PAR_4 activation has been found to result in Ca^{2+} mobilisation (Ando *et al.,* 2007) and $InsP_3$ accumulation (Kataoka *et al.,* 2003), phosphorylation of p38 MAP kinase (Fujiwara *et al.,* 2005) and ERK MAP kinase (Kataoka *et al.,* 2003). However, studies describing PAR_4 internalisation remain to be published therefore the experiments conducted in this study were modelled on those events observed for PAR_2, which in turn were originally based on those events observed for PAR_1.

The aim of this chapter was to use PAR_2 EYFP and PAR_4 ECFP fluorescent constructs to monitor receptor localisation and internalisation. In addition experiments were carried out to ensure that the downstream signalling events that take place upon PAR activation were not affected by the presence of the fluorescent protein. The main signalling events tested were PAR-mediated phosphorylation of ERK, $InsP_{1-4}$ and calcium responses.

3.2 Characterisation of PAR_2 mEYFP and PAR_4 mECFP expression in HEK293 cells.

Prior to the functional characterisation of the fluorescent PAR constructs, considerations had to be made regarding their use in future experiments. One of the main concerns with the use of ECFP and EYFP fluorophores, particularly if used for protein interaction studies such as FRET (see Chapter 5), is the propensity for the beta barrel structures of both ECFP and EYFP to form natural dimers (Zacharias *et al.,* 2002). The impact of beta barrel dimerisation would produce artifactual FRET results, thus obscuring actual FRET signals between two proteins of interest. To overcome this, a single point mutation was introduced (see Chapter 2, Section 2.3.1) into the GFP variant tagged constructs, substituting alanine (A) to lysine (K) at position 206 of the GFP protein sequence ($A^{206}K$). This resulted in the generation of non-dimerising monomeric human PAR_2 EYFP (PAR_2 mEYFP) and human PAR_4 EYFP (PAR_4 mECFP) fluorescent constructs. The ability of these constructs to

respond to their respective agonists was then tested. The effect of known activators of PAR_2 and PAR_4, such as trypsin and the PAR_2-specific activating peptide (AP) SLIGKV-OH, and thrombin and PAR_4-specific AP AYPGKF-NH_2, was assessed in parental HEK293 cells. Cells over-expressing either PAR_2 mEYFP or PAR_4 mECFP were treated with agonist and the respective responses compared to cells over-expressing human wild type (WT) PAR_2 and WT PAR_4 (without the C-terminal YFP/CFP tag).

3.2.1 Experiments to assess membrane localisation and internalisation of PAR_2 and PAR_4.

As a marker of receptor activation, the ability of PAR_2 mEYFP and PAR_4 mECFP to internalise in a HEK293 cell transient expression model was assessed following agonist treatment with trypsin and SLIGKV-OH for PAR_2 and thrombin and AYPGKF-NH_2 for PAR_4. Receptor localisation was observed through epifluorescence microscopy. Figure 3.1 illustrates the expression of PAR_2 mEYFP in fixed HEK293 cells following stimulation with trypsin (50 nM) or SLIGKV-OH (100 µM) over a period of 30 minutes. Membrane localisation of PAR_2 mEYFP was clearly apparent in unstimulated control cells (white arrows), with punctate intracellular receptor stores present (red arrows). Upon agonist stimulation, receptor internalisation was evident with almost complete loss of cell surface expression observed 30 minutes post-stimulation (red arrows). PAR_4 localisation and internalisation was similarly assessed following agonist treatment. Unlike PAR_2, PAR_4 mECFP was predominantly localised in stores inside the cell (red arrows), with a low level of receptor expressed on the plasma membrane (white arrows), as shown in the control unstimulated image in Figure 3.2.A. Following treatment with thrombin (3 U/ml) or AYPGKF-NH_2 (100 µM), internalisation of membrane expressed PAR_4 was not observed at the 5 or 30 minute time points. Even after 60, 120 or 180 minutes of agonist treatment, no obvious internalisation of PAR_4 mECFP was observed, as shown in Figure 3.2.
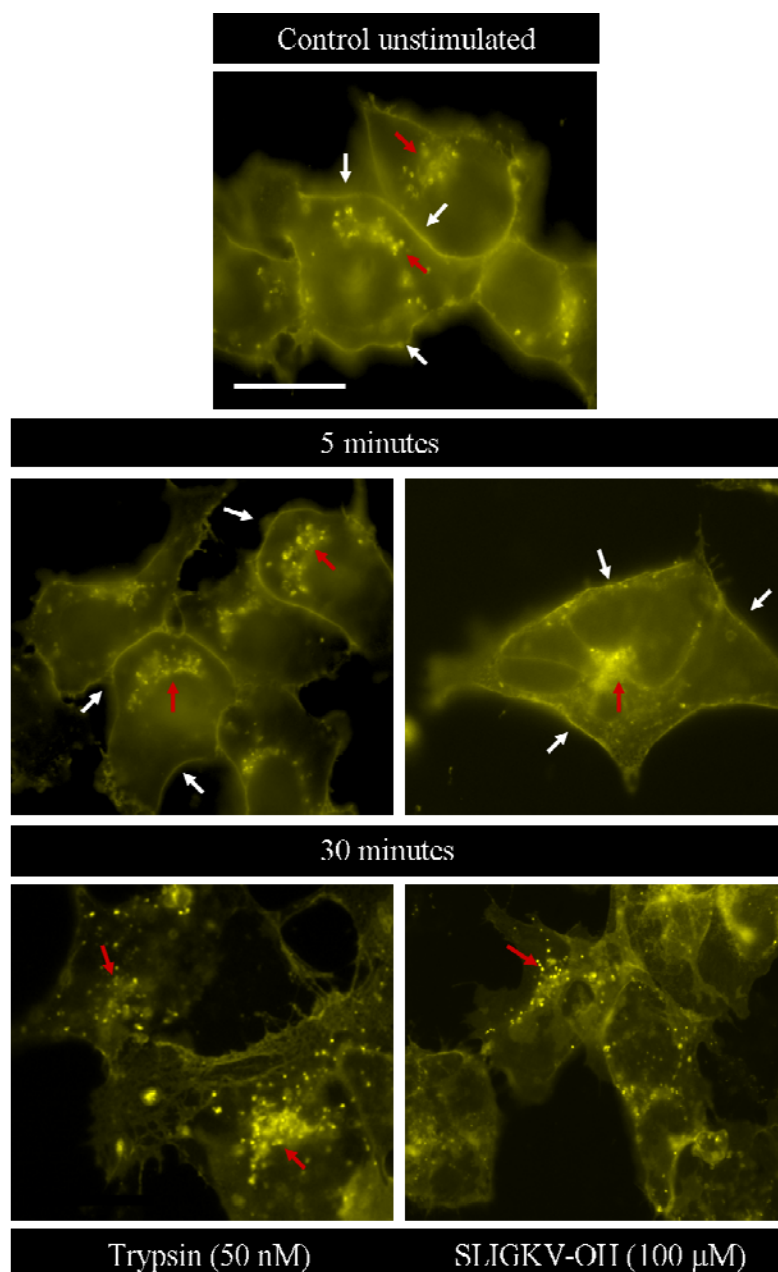
Figure 3.1. PAR$_2$ mEYFP localisation and internalisation in HEK293 cells.

HEK293 cells were grown on coverslips and transiently transfected with PAR$_2$ mEYFP for 24 hours as outlined in Chapter 2.5. Cells were serum starved for a further 24 hours prior to stimulation with trypsin (50 nM) or SLIGKV-OH (100 μM) for the indicated time periods. PAR$_2$ mEYFP expression was monitored using epifluorescence microscopy as described in Chapter 2.6.1 with images acquired at 100x magnification (scale bar = 10 μm). White arrows represent PAR$_2$ membrane expression whilst the red arrows indicate intracellular receptor stores. Images are representative of at least 3 experiments.

Control unstimulated
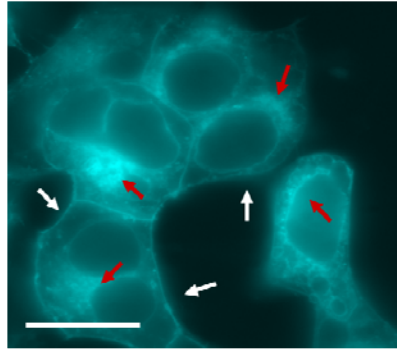
5 minutes
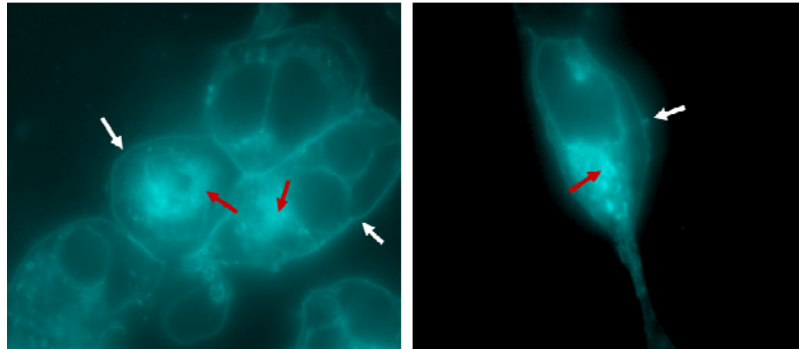
30 minutes

Thrombin (3 U/ml)   AYPGKF-NH$_2$ (100 µM)

87
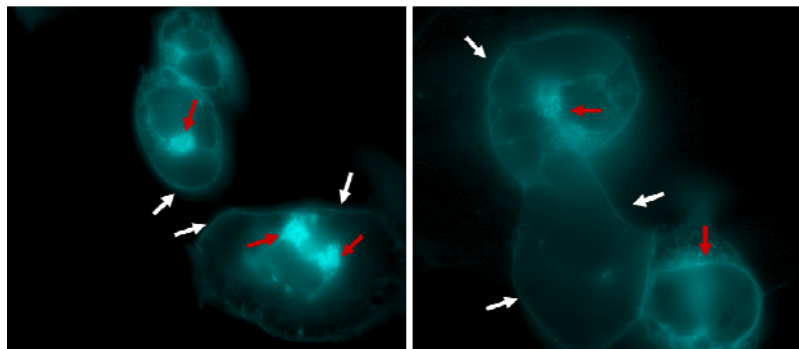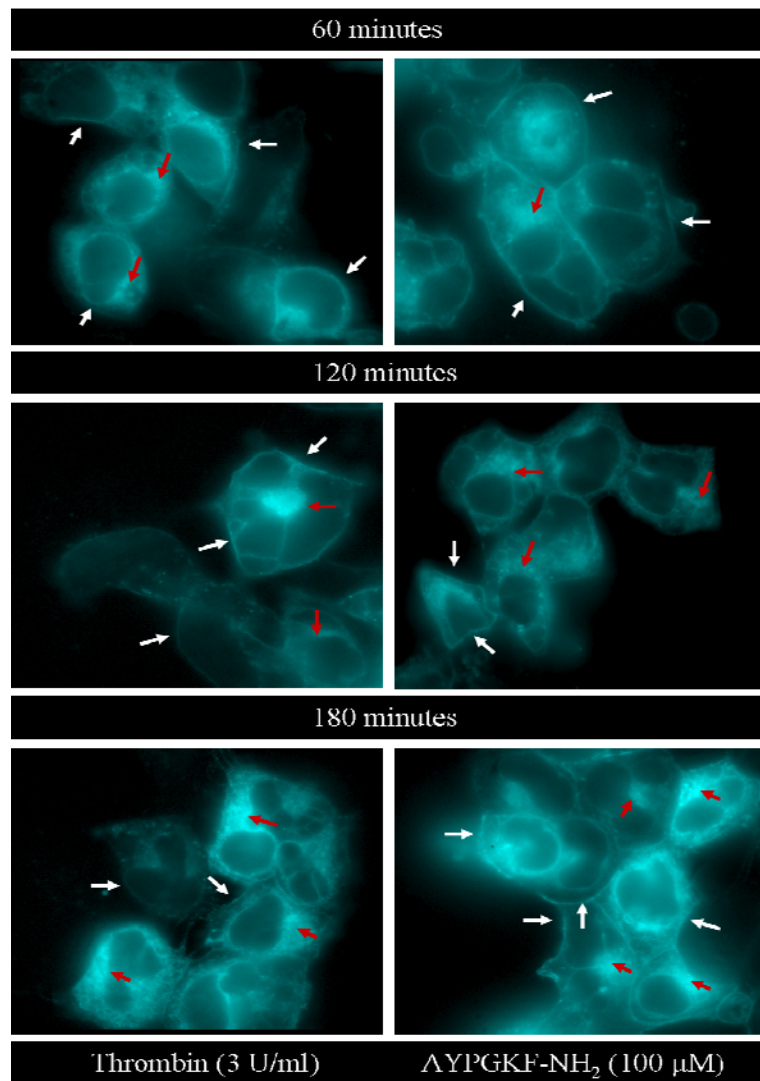
Figure 3.2. PAR$_4$ mECFP localisation following agonist treatment in HEK293 cells.

HEK293 cells were grown on coverslips and transiently transfected with PAR$_4$ mECFP for 24 hours as outlined in Chapter 2.5. Cells were serum starved for a further 24 hours prior to stimulation with thrombin (3 U/ml) or AYPGKF-NH$_2$ (100 μM). PAR$_4$ mECFP expression was monitored as in Figure 3.1 with images acquired at 100x magnification (scale bar = 10 μm). PAR$_4$ localisation was monitored following treatment with agonist for 5, 30, 60, 120 and 180 minutes. Membrane PAR$_4$ (white arrows) and intracellular receptor stores (red arrows) are highlighted. Images are representative of at least 3 experiments.

3.2.2 PAR2 mEYFP and PAR4 mECFP-mediated [3H]-inositol phosphate accumulation.

Whilst PAR_2 activation was associated with receptor internalisation, it was clear from the experiments carried out in Section 3.2.1, that activation of PAR_4 did not result in receptor internalisation. Following from these experiments, the effect of PAR-specific agonist treatment upon total [^{3}H]-inositol phosphate accumulation was assessed in transfected HEK293 cells. The responses generated from agonist-treated parental HEK293 cells were compared with those cells transiently expressing WT PAR_2 or WT PAR_4, which in turn were then compared with cells expressing PAR_2 mEYFP or PAR_4 mECFP.

Figure 3.3 shows trypsin (50 nM) and SLIGKV-OH (100 μM)-mediated [^{3}H]-inositol phosphate responses generated 1 hour post-activation in non-transfected HEK293 cells and HEK293 cells transiently expressing WT or PAR_2 mEYFP. A significant increase in total [^{3}H]-inositol phosphate accumulation was observed in trypsin-stimulated cells expressing PAR_2 mEYFP (28.02 ± 8.44 fold of basal) when compared to both parental HEK293 cell (7.59 ± 3.63) and WT PAR_2 (12.53 ± 3.74) cellular responses. However, the response generated from SLIGKV-OH-treated PAR_2 mEYFP expressing cells was considerably lower than that observed in the presence of trypsin, only 6.13 ± 1.71 fold of basal, with no statistical difference observed between parental HEK293, WT PAR_2 or PAR_2 mEYFP responses. PAR_4-mediated [^{3}H]-inositol phosphate accumulation obtained for parental cells and cells expressing WT PAR_4 and PAR_4 mECFP is illustrated in Figure 3.4. Upon treatment with thrombin (3 U/ml) or PAR_4 specific activating peptide (AP), AYPGKF-NH$_2$ (100 μM), a significant increase in total [^{3}H]-inositol phosphate accumulation was observed in cells expressing either WT PAR_4 (Th = 28.21 ± 1.217, AP = 23.85 ± 1.6 fold of basal control) or PAR_4 mECFP (Th = 24.17 ± 3.35, AP = 21.16 ± 3.7) compared to parental HEK293 cell responses (Th = 1.36 ± 0.06, AP = 0.85 ± 0.35). Unlike the results observed for PAR_2 activation, no significant difference was observed between WT and PAR_4 mECFP-mediated responses or between thrombin and AP treatment.
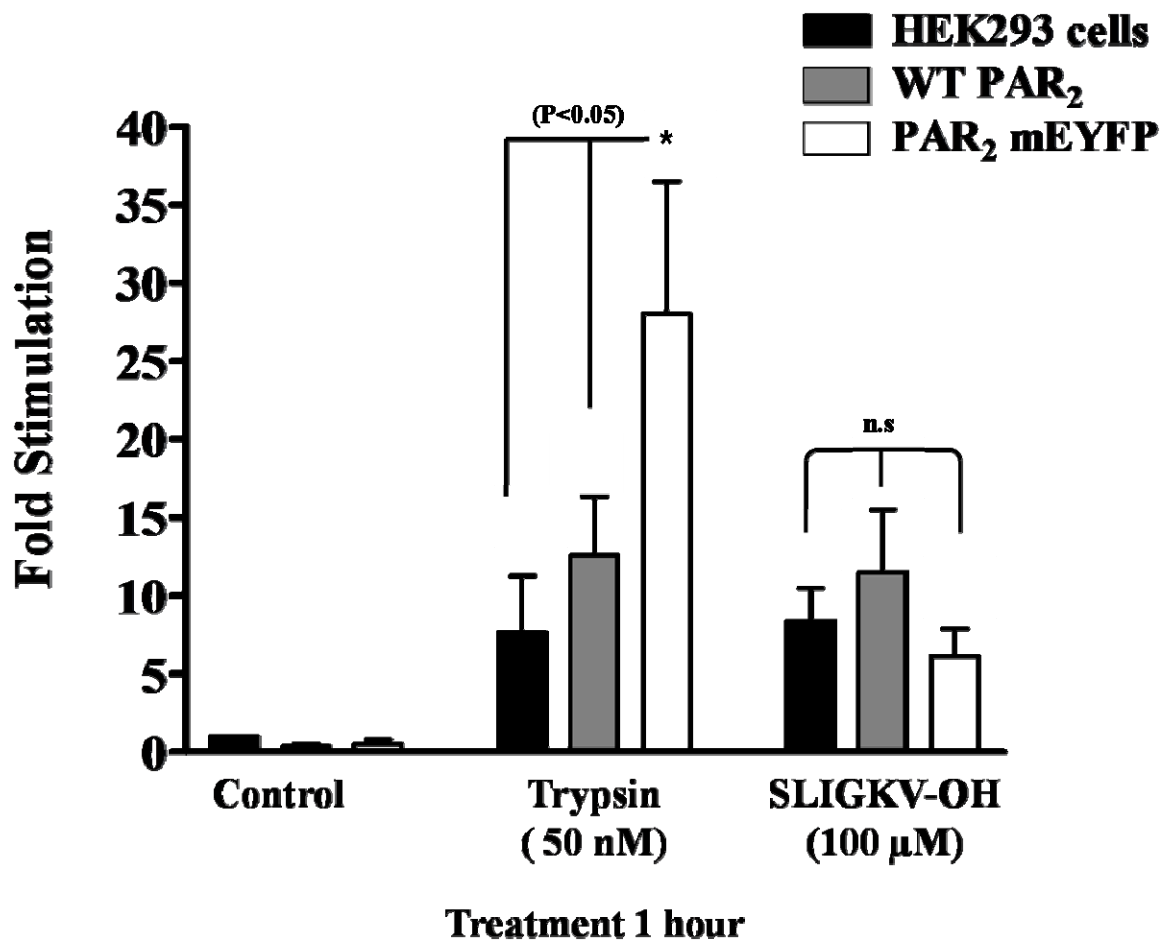
Figure 3.3. PAR$_2$ mediated [^{3}H]-inositol phosphate accumulation in HEK293 cells.

HEK293 cells were transiently transfected with WT PAR2 (grey) or PAR2 mEYFP (white) for 24 hours as described in Chapter 2.5. After which time the media was replaced with serum free media supplemented with [3H]-2-myo-inositol (0.25 μCi/well) for a further 24 hours. The cells were pre-treated with 10 mM lithium chloride for 15 minutes then stimulated for 1 hour with trypsin (50 nM) or SLIGKV-OH (100 μM). Accumulation of total [3H]-inositol phosphate (InsP1-4) was measured as outlined in Chapter 2.9. Each value represents the mean ± s.e.m. from three separate experiments performed in triplicate, (*P<0.05, n.s = not significant P>0.05).
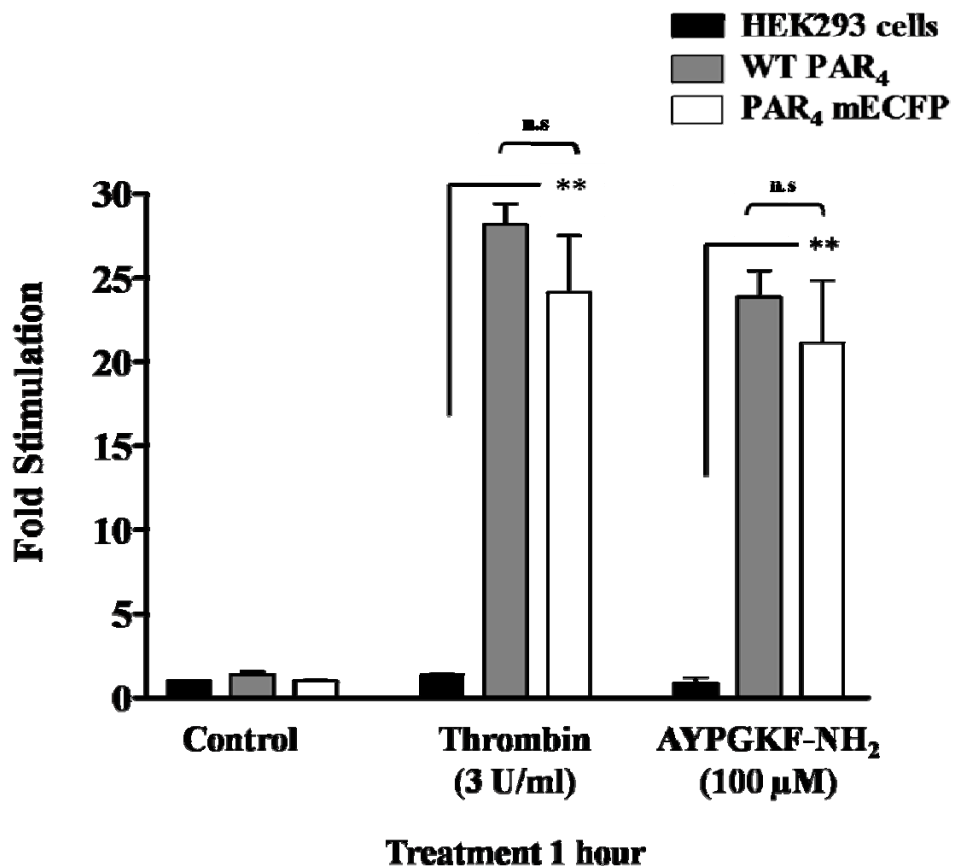
Figure 3.4. PAR$_4$-mediated [^{3}H]-inositol phosphate accumulation in HEK293 cells.

HEK293 cells were transiently transfected with WT PAR4 (grey) or PAR4 mECFP (white) as outlined in Chapter 2.5 for 24 hours, after which time the media was replaced with serum free media supplemented with [3H]-2-myo-inositol (0.25 μCi/well) for a further 24 hours. The cells were pretreated with 10 mM lithium chloride and then stimulated for 1 hour with thrombin (3 U/ml) or AYPGKF-NH2 (100 μM). Accumulation of total [3H]-inositol phosphate (InsP1-4) was measured as outlined in Chapter 2.9. Each value represents the mean ± s.e.m. from three separate experiments performed in triplicate (**P<0.01, n.s. = not significant P>0.05).

3.2.3 PAR$_2$ mEYFP and PAR$_4$ mECFP-mediated calcium response.

Generally signal transduction via the inositol phosphate (InsP) pathway, as demonstrated in the experiments carried out in Section 3.2.2, coincides with the release of intracellular calcium. In order to provide further confirmation that the InsP$_3$/diacylglycerol (DAG) pathway was intact in transfected cells, the ability of PAR$_2$ and PAR$_4$ fluorescent constructs to mediate calcium signalling was tested in HEK293 cells upon receptor activation.

Figures 3.5 and 3.6 highlight the typical changes in fura-2 ratio (F340/F380) in response to trypsin (50 nM) in parental HEK293 cells and cells that express PAR$_2$ mEYFP respectively. The calcium trace obtained for HEK293 cells showed elevated levels of calcium following trypsin treatment, peaking within 1 minute (F340/F380 ratio = 1.433 ± 0.147), gradually returning to basal levels (F340/380 ratio = 0.491 ± 0.184) by 2 minutes post-agonist treatment. A similar calcium trace was obtained for cells expressing PAR$_2$ mEYFP. As Figure 3.6 illustrates, a transient calcium signal (F340/F380 ratio = 1.364 ± 0.244) was observed that also peaked within 1 minute of agonist treatment. Whilst a significant increase in the F340/F380 ratio was observed for stimulated HEK293 cells and cells expressing PAR$_2$ mEYFP when compared to basal, no significant difference was observed between the non-transfected and PAR$_2$ mEYFP expressing cells, as shown in Figure 3.7.

Figures 3.8 and 3.9 shows the calcium trace and peak fura-2 ratios obtained following the treatment of parental HEK293 cells with PAR$_4$ AP, AYPGKF-NH$_2$ (100 μM) followed by stimulation with thrombin (1 U/ml). Upon AP treatment, no increase in cellular calcium was observed (basal F340/F380 ratio = 0.35 ± 0.02, AP = 0.35 ± 0.02) until treatment with thrombin (F340/F380 ratio = 1.25 ± 0.18). This was a short-lived calcium signal that peaked 1 minute post-thrombin treatment, returning to basal immediately thereafter.

Transient transfection of HEK293 cells with PAR$_4$ mECFP, as shown in Figure 3.10, resulted in a more prolonged, yet lower, calcium signal than previously observed in the calcium trace obtained for stimulated parental cells in Figure 3.8. Following

stimulation with AYPGKF-NH$_2$ (100 µM), peak calcium levels (F340/F380 ratio = 1.301 ± 0.148) were reached within 1 minute of agonist treatment returning to basal (0.359 ± 0.01) only upon superfusion with fresh extracellular solution. Further treatment with thrombin (3 U/ml) resulted in a transient calcium signal as previously observed in Figure 3.8, which increased significantly 1.59 ± 0.45 in comparison to basal.
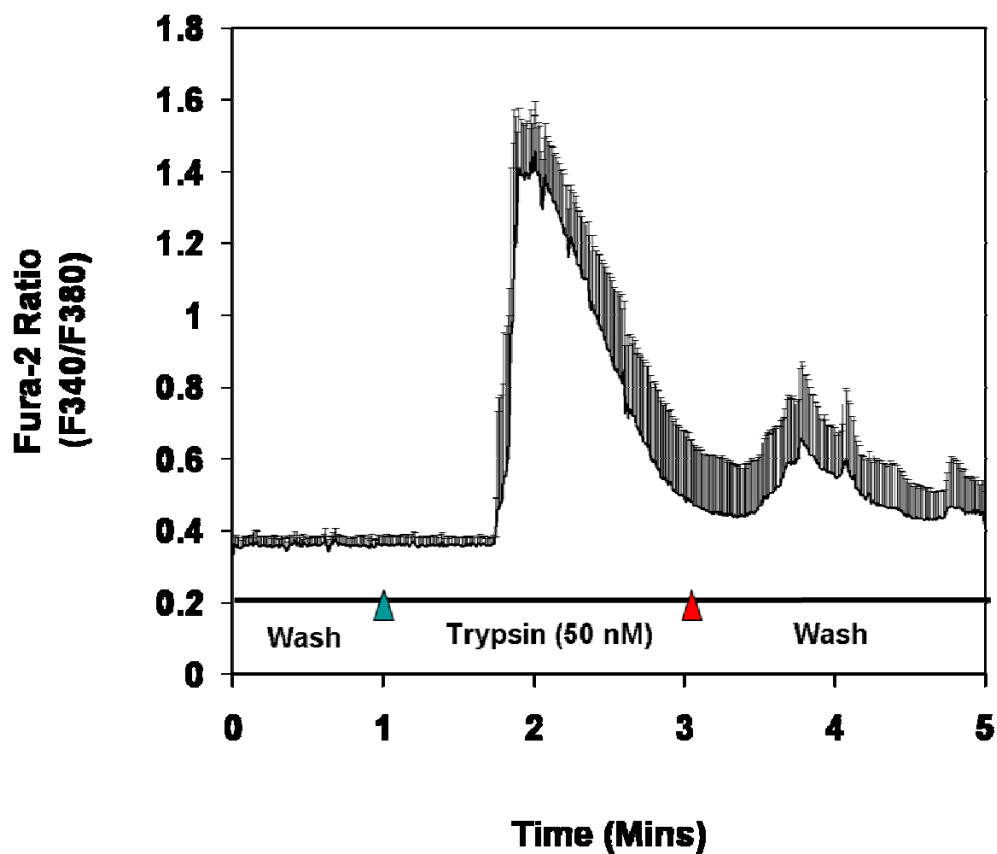
Figure 3.5. Characterisation of calcium signalling in parental HEK293 cells following PAR$_2$ agonist treatment.

HEK293 cells were serum starved for 24 hours then loaded with the Ca^{2+}-sensitive dye, fura-2 AM (6 µM) for 1 hour at room temperature. Calcium imaging was carried out at 40x magnification as outlined in Chapter 2.10. Ratiometric images (340/380 nm) were acquired every 2-5 seconds from parental HEK293 cells following perfusion with extracellular solution then treatment with trypsin (50 nM) for 2 minutes. The data represents the changes in the fluorescence ratio taken from two separate experiments (mean ± s.e.m. from 20 cell measurements).
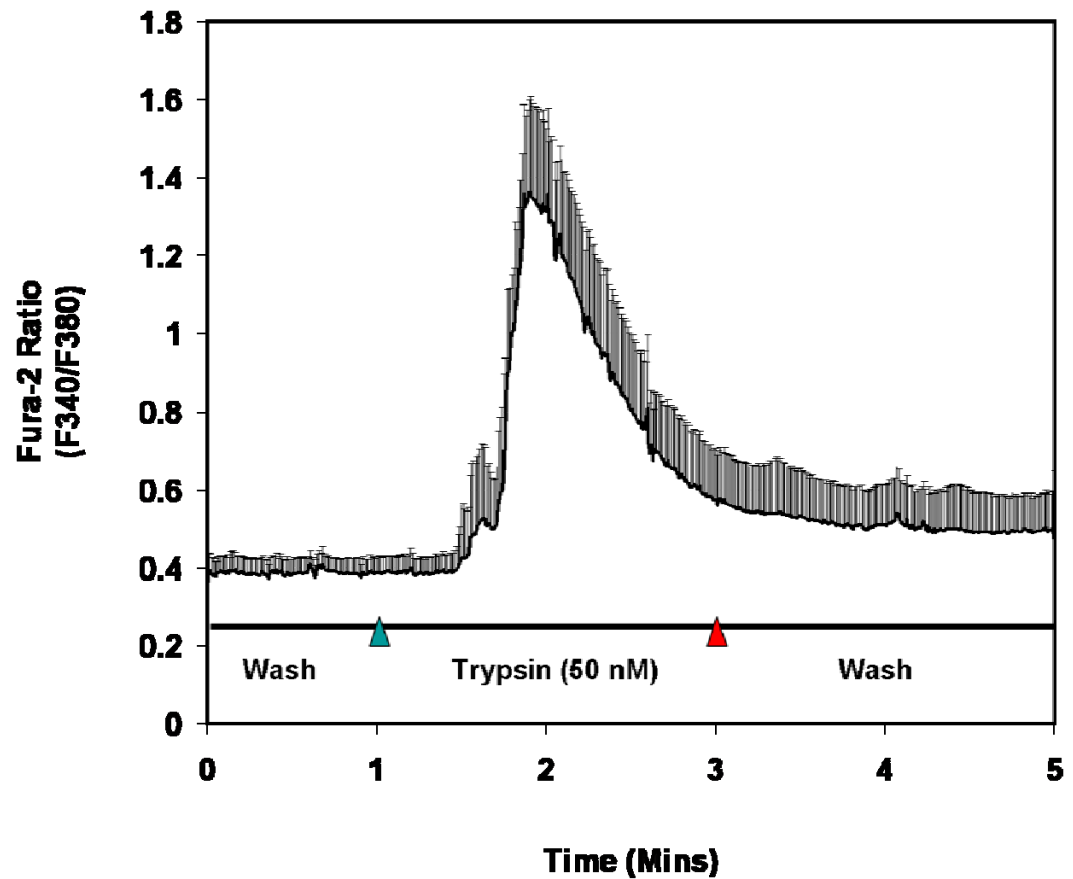
Figure 3.6. Characterisation of calcium signalling in HEK293 cells expressing PAR$_2$ mEYFP following PAR$_2$ agonist treatment.

HEK293 cells transiently transfected with PAR2 mEYFP for 24 hours as described in Chapter 2.5, serum starved for a further 24 hours then loaded with the Ca2+-sensitive dye, fura-2 AM (6 μM) for 1 hour at room temperature. Calcium imaging was carried out at 40x magnification as outlined in Chapter 2.10. Ratiometric images (340/380 nm) were acquired every 2-5 seconds following perfusion with extracellular solution then treatment with trypsin (50 nM) for 2 minutes. The data represents the fluorescence ratio taken from two separate experiments (mean ± s.e.m. from 20 cell measurements).
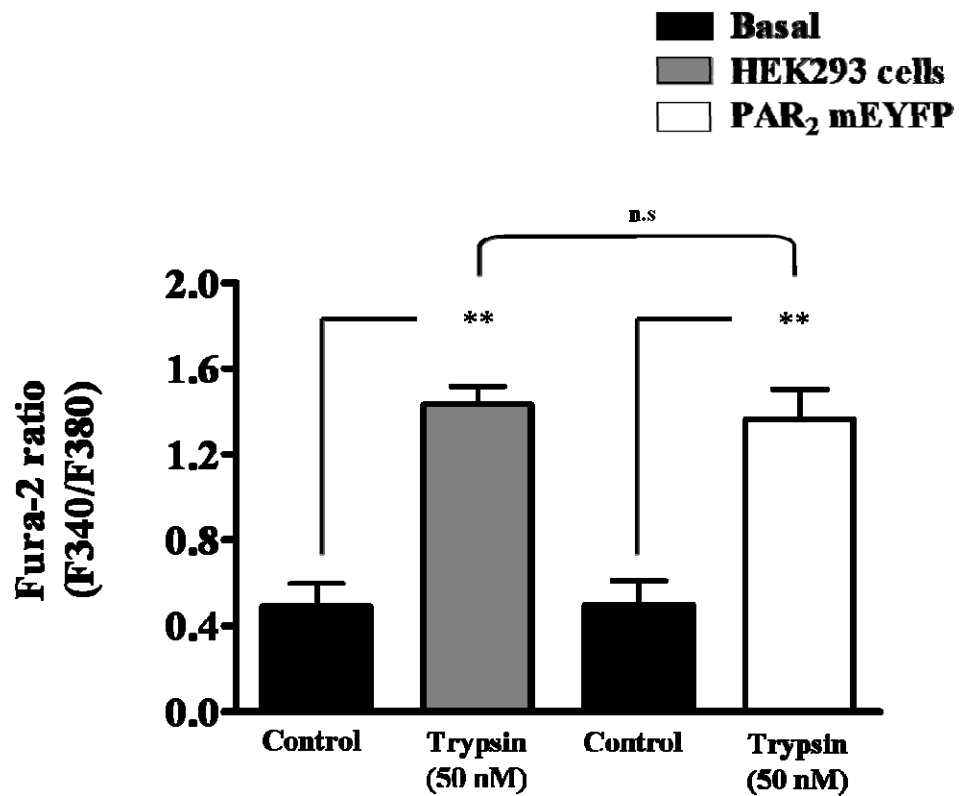
Figure 3.7. Peak Fura-2 ratios obtained from calcium traces following trypsin treatment of parental HEK293 cells and PAR$_2$ mEYFP expressing cells.

Following calcium imaging using Fura-2-AM as outlined in Chapter 2.10, peak Fura-2 (F340/F380) ratios were taken from calcium traces at basal (black) and following trypsin treatment of parental HEK293 cells (grey) and cells expressing PAR$_2$ mEYFP (white). The data above represents the ratios obtained from the traces observed in Figure 3.5 and 3.6 taken from two separate experiments (mean ± s.e.m from 20 cell measurements, **P<0.01 compared to basal control ratio, n.s. = not significant P>0,05).
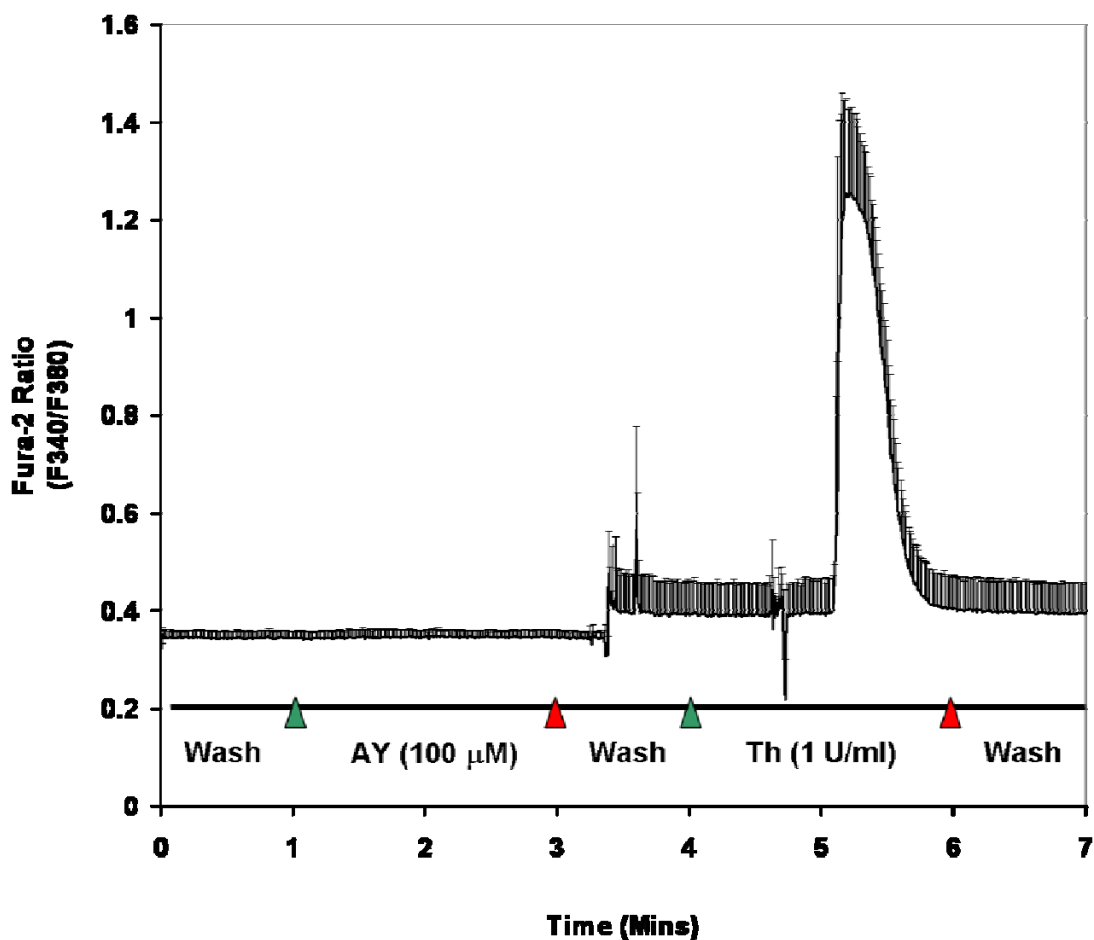
Figure 3.8. Characterisation of calcium signalling in parental HEK293 cells following PAR$_4$ agonist treatment.

HEK293 cells were serum starved for 24 hours then loaded with the Ca^{2+}-sensitive dye, fura-2 AM (6 µM) for 1 hour at room temperature. Calcium imaging was carried out at 40x magnification as described in Chapter 2.10. Ratiometric images (340/380 nm) were acquired every 2-5 seconds from parental HEK293 cells following perfusion with extracellular solution then treatment with AYPGKF-NH$_2$ (100 µM) for 2 minutes and then Thrombin (1 U/ml), as indicated. The calcium trace provided represents the fluorescence ratio taken from two separate experiments (mean ± s.e.m. from 20 cell measurements).
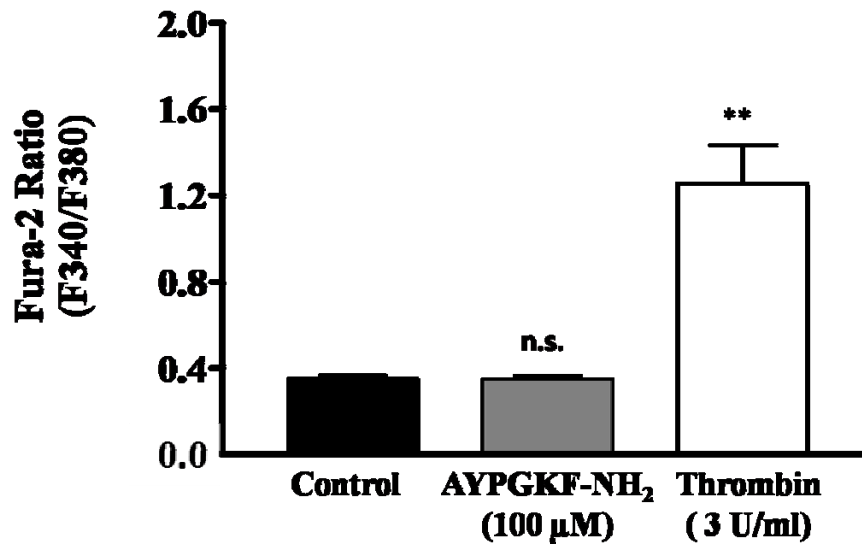
Figure 3.9. Peak Fura-2 ratios obtained from calcium traces following agonist treatment of parental HEK293 cells.

Following calcium imaging using Fura-2-AM as outlined in Chapter 2.10, peak Fura-2 (F340/F380) ratios were taken from calcium traces at basal (black) and following AYPGKF-NH$_2$ (grey) and Thrombin (black) treatment of parental HEK293 cells. The data above represents the ratios obtained from the trace observed in Figure 3.8 taken from two separate experiments (mean ± s.e.m from 20 cell measurements, **P<0.01 compared to basal control ratio, n.s. = not significant P>0.05).
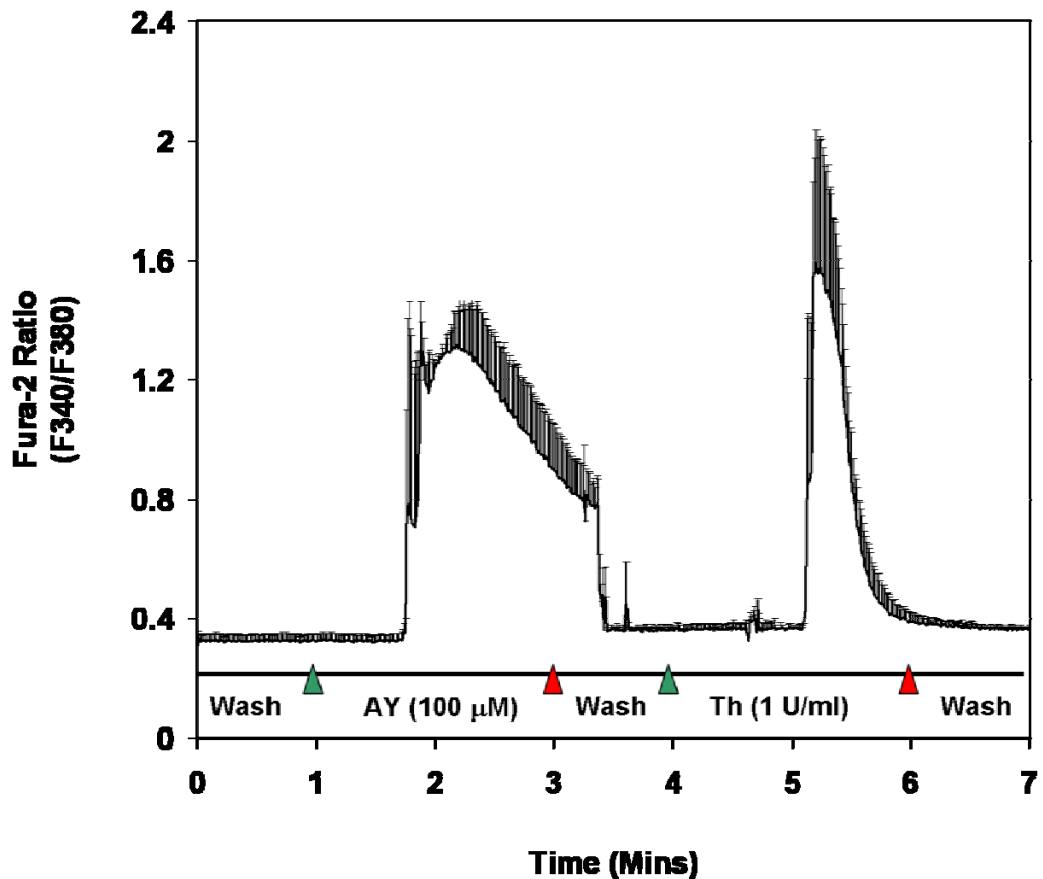
Figure 3.10. Characterisation of calcium signalling in HEK293 cells expressing PAR₄ mECFP following PAR₄ agonist treatment.

HEK293 cells were transiently transfected with PAR$_4$ mECFP for 24 hours as outlined in Chapter 2.5, serum starved for a further 24 hours then loaded with the Ca^{2+}-sensitive dye, fura-2 AM (6 µM) for 1 hour at room temperature. Calcium imaging was carried out at 40x magnification as described in Chapter 2.10. Ratiometric images (340/380 nm) were acquired every 2-5 seconds following perfusion with extracellular solution then treatment with AYPGKF-NH$_2$ (100 µM) for 2 minutes and then Thrombin (1 U/ml), as indicated. The calcium trace provided is representative of the average of 20 cell measurements (mean ± s.e.m).
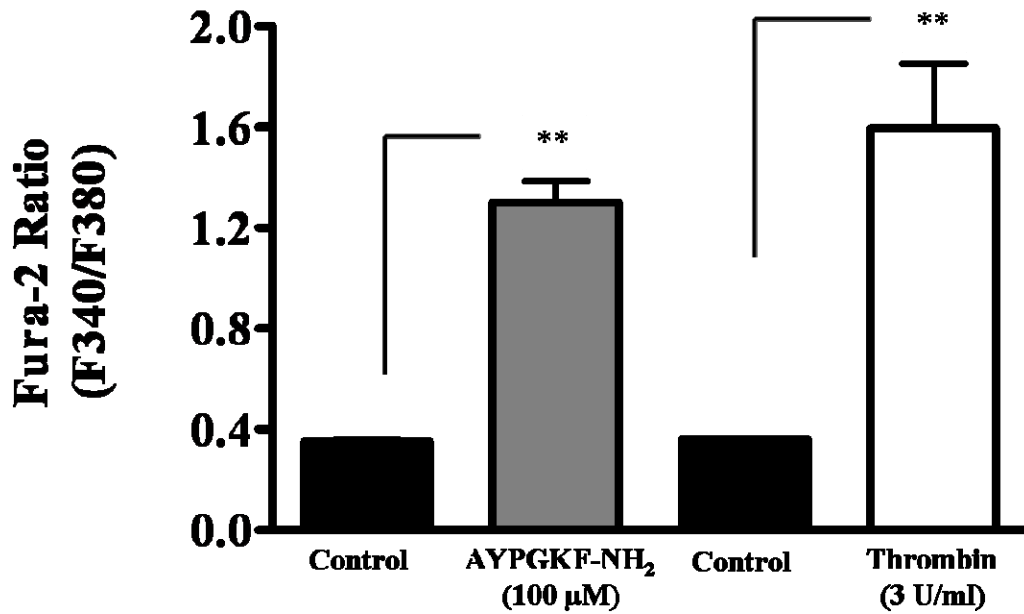
Figure 3.11. Peak Fura-2 ratios obtained from calcium traces following agonist treatment of HEK293 cells expressing PAR$_4$ mECFP.

Following calcium imaging using Fura-2-AM as outlined in Chapter 2.10, peak Fura-2 (F340/F380) ratios were taken from calcium traces at basal (black) and following AYPGKF-NH$_2$ (grey) and Thrombin (black) treatment of HEK293 cells expressing PAR$_4$ mECFP. The data above represents the ratios obtained from the trace observed in Figure 3.10 taken from two separate experiments (mean ± s.e.m from 20 cell measurements, **P<0.01 compared to the basal control ratio).

3.2.4 PAR$_2$ mEYFP and PAR$_4$ mECFP-mediated activation of ERK MAPK

With the confidence that both PAR$_2$ mEYFP and PAR$_4$ mECFP could signal effectively through the InsP/DAG pathway, other pathways downstream of receptor activation were assessed. The characterisation of PAR$_2$ mEYFP and PAR$_4$ mECFP activation was investigated further in terms of the phosphorylation of the classical MAP kinase pathway, extracellular signal-regulated kinase (ERK). Using Western blot analysis, activation of ERK1/2 isoforms were characterised in parental HEK293 cells, as well as cells expressing empty vector, WT PAR$_2$, WT PAR$_4$, PAR$_2$ mEYFP or PAR$_4$ mECFP.

Figure 3.12 shows the duration of PAR$_2$-mediated ERK1/2 phosphorylation in response to (A) trypsin (50 nM) and (B) SLIGKV-OH (100 μM). A weak, transient ERK signal was observed in parental HEK293 cells in response to trypsin, which peaked at 5 minutes (2.301 ± 0.100 fold of basal), returning to basal within 15 minutes of agonist treatment. An increase in trypsin-mediated ERK phosphorylation was observed in PAR$_2$ mEYFP expressing cells (7.505 ± 0.63 fold), peaking between 5-15 minutes, returning to basal levels thereafter. These results were consistent with cells expressing WT PAR$_2$ (6.9 ± 0.8 fold). Responses observed upon treatment with PAR$_2$ AP SLIGKV-OH for 5 minutes were greater in magnitude in parental HEK293 cells (9.708 ± 0.02 fold) and more prolonged, only returning to near-basal levels at time points beyond 30 minutes post-treatment. A similar trend in AP-mediated ERK signal duration was observed in cells expressing the EYFP-N1 vector (9.1 ± 0.10 fold), WT PAR$_2$ (10.1 ± 0.34 fold) and PAR$_2$ mEYFP (13.18 ± 2.68 fold).

PAR$_4$-mediated ERK phosphorylation in response to (A) thrombin (3 U/ml) and (B) AYPGKF-OH (100 μM) is shown in Figure 3.13. A low level, transient thrombin-mediated ERK1/2 phosphorylation was observed in parental cells (2.4 ± 0.01 fold of basal), which was undetectable in cells treated with PAR$_4$-specific activating peptide AYPGKF-NH$_2$ (1.1 ± 0.01 fold). Similar results were obtained for cells over-expressing ECFP-N1 vector without PAR$_4$ (Thrombin; 2.37 ± 0.101 and AP; 1.5 ± 0.01 fold respectively). Further investigation confirmed that this weak ERK signal in response to thrombin was mediated through the activation of endogenous PAR$_1$

expressed in HEK293 cells (not shown). However in cells expressing PAR_4 mECFP, treatment with thrombin (3 U/ml) and the activating peptide AYPGKF-NH_2 (100 μM), induced a sustained ERK1/2 response. These responses peaked at 5 minutes (thrombin; 13.04 ± 1.10 fold and AP; 14.58 ± 0.83 fold), however rather than return to basal, the response was still observed, albeit at a lower level, 60 minutes post-stimulation. These results were higher than those responses observed in cells expressing WT PAR_4 (thrombin; 6.9 ± 1.7 fold and AP; 6.92 ± 0.80 fold), possibly a feature of different transfection efficiency between these two PAR_4 constructs.

(A)
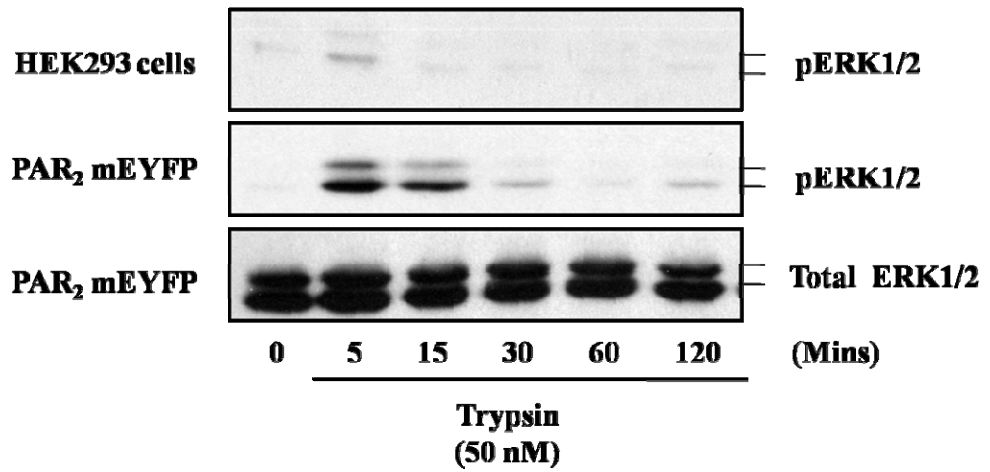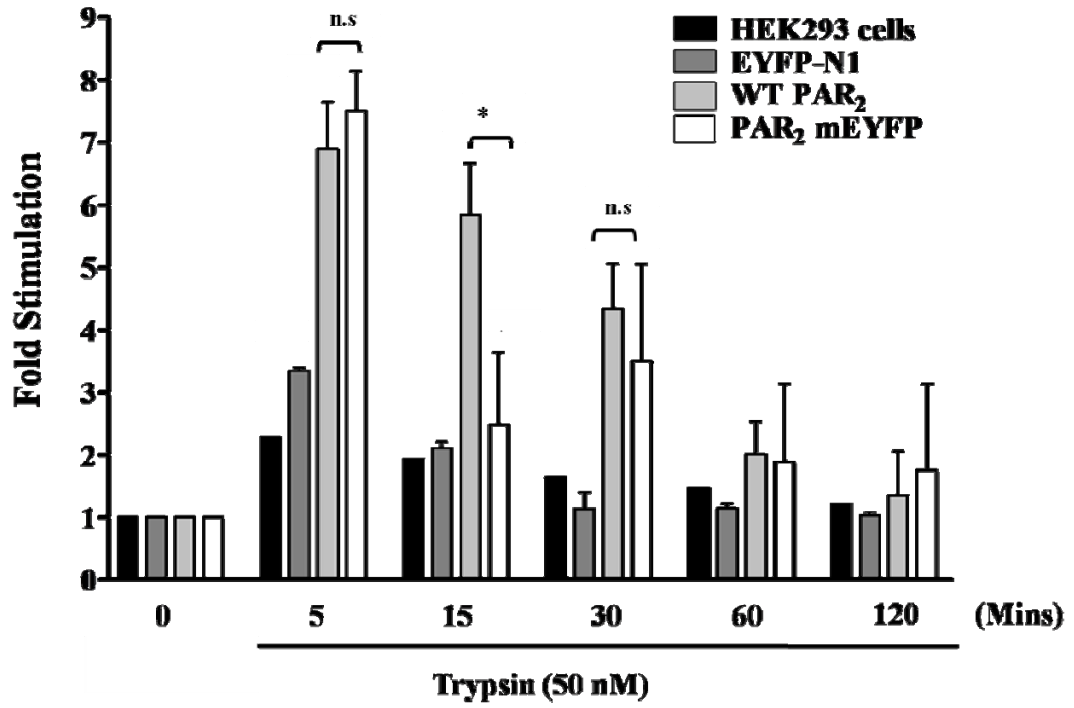
(B)
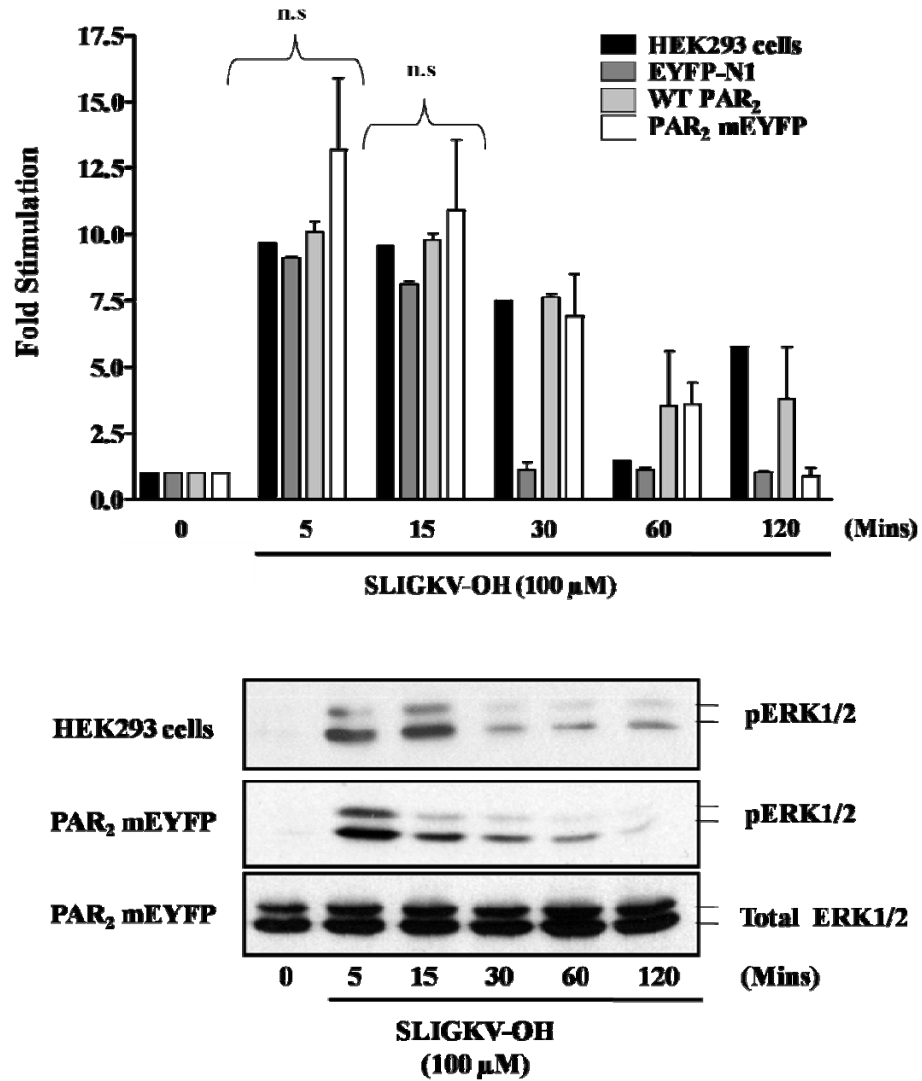
Figure 3.12. PAR$_2$-mediated phosphorylation of ERK in HEK293 cells following PAR$_2$ activation.

HEK293 cells were transiently transfected with EYFP-N1 vector, WT PAR$_2$ or PAR$_2$ mEYFP for 24 hours and serum starved for a further 24 hours. Cells were then stimulated with (A) trypsin (50 nM) or (B) SLIGKV-OH (100 μM) as indicated. ERK1/2 phosphorylation (42/44 kDa bands) was measured in whole cell lysates resolved by Western blotting as outlined in Chapter 2.8.2 and the immunoblots were quantified by scan densitometry. Blots shown are representative of three others. (*P<0.05, n.s. = not significant).

(A)
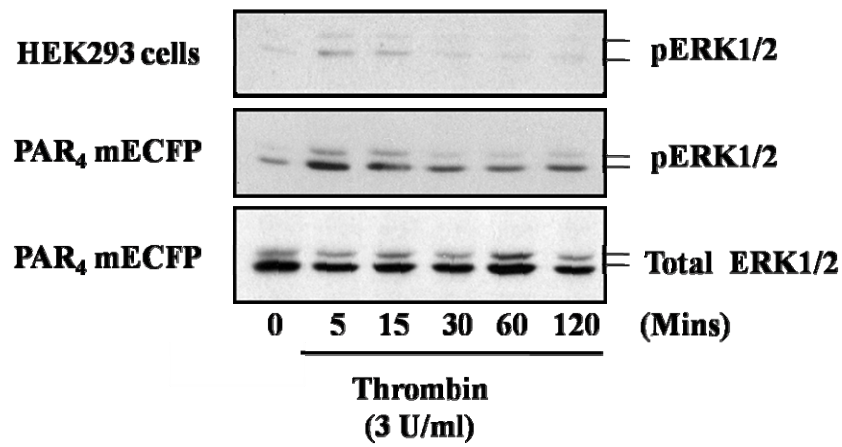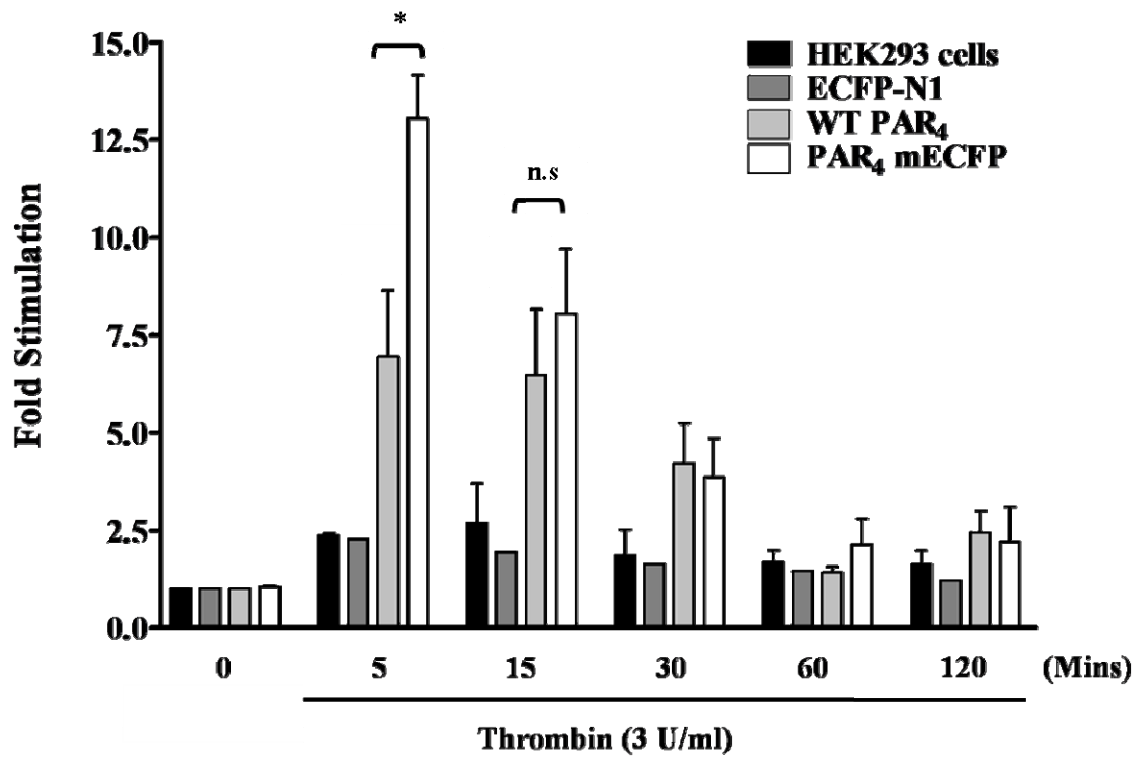
(B)
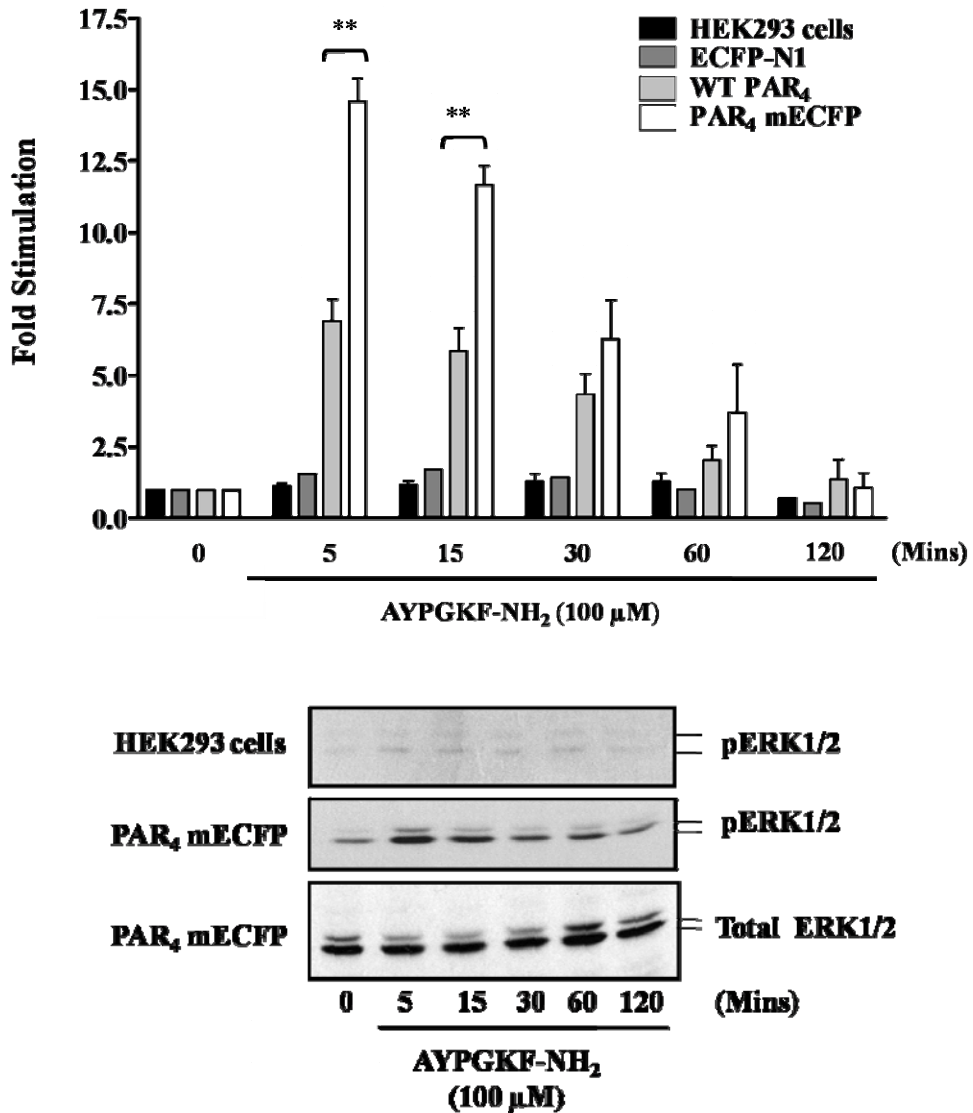
Figure 3.13. PAR$_4$-mediated phosphorylation of ERK MAPK in HEK293 cells following PAR$_4$ activation.

HEK293 cells were transiently transfected with ECFP-N1 vector, WT PAR$_4$ or PAR$_4$ mECFP for 24 hours then serum starved for a further 24 hours. Cells were stimulated with (A) thrombin (3 U/ml) or (B) AYPGKF-NH$_2$ (100 µM) as indicated. ERK1/2 phosphorylation (42/44 kDa) was measured in whole cell lysates resolved by Western blotting as described in Chapter 2.8.2 and the immunoblots were quantified by scan densitometry. Blots shown are representative of three others. (*P<0.05, **P<0.01, n.s. = not significant).

106

3.3 Characterisation of PAR$_2$ mEYFP and PAR$_4$ mECFP expression in a PAR-null cell line.

The results obtained in Section 3.2 highlighted a potential problem with the HEK293 cell model. Endogenous levels of PAR$_1$ and PAR$_2$ present in HEK293 cells were clearly demonstrated through the trypsin and thrombin-mediated signalling observed in the parental cells. The lack of response to PAR$_4$-specific AP AYPGKF-NH$_2$ in parental HEK293 cells confirmed the lack of endogenous PAR$_4$ in the cell model. The various responses observed in HEK293 cells expressing PAR$_4$ mECFP provided confidence that the ECFP fluorophore did not interfere with normal PAR$_4$-mediated signalling downstream of receptor activation. However due to the endogenous PAR$_2$-mediated signal transduction witnessed in the HEK293 model it was necessary to find a cell line with minimal or no PAR expression in order to confirm that the PAR$_2$ mEYFP construct was functional. The human keratinocyte cell line, NCTC-2544, has previously been used in our laboratory and others, and exhibits no detectable PAR$_2$ mRNA (Kawabata *et al.,* 2004) or signalling response to trypsin, with only a weak PAR$_1$-mediated signal observed in response to thrombin (Kanke *et al.,* 2001). This cell line provided an alternative model to ensure that the EYFP fluorophore within PAR$_2$ did not interfere with PAR$_2$-mediated cell signal transduction.

3.3.1 PAR$_2$ mEYFP mediated calcium signalling in NCTC-2544 cells.

The endogenous level of PAR$_2$ in NCTC-2544 cells was assessed through the ability of trypsin to mediate a calcium response. Figure 3.14 (A) demonstrates the typical calcium signal in parental NCTC-2544 cells in response to trypsin (50 nM). Upon agonist treatment for 5 minutes, no significant calcium response was observed in parental NCTC-2544 cells (basal F340/F380 ratio = 0.436 ± 0.0124, Tr F340/F380 ratio = 0.5100 ± 0.0313). Following expression of PAR$_2$ mEYFP, a transient calcium response was observed upon treatment with trypsin (50nM) or PAR$_2$ AP SLIGKV-OH (100 μM), as demonstrated in Figure 3.14 (B and C) respectively. NCTC-2544 cells expressing PAR$_2$ mEYFP demonstrated an increase in calcium that peaked within 1 minute of agonist treatment (AP F340/F380 ratio = 1.210 ± 0.244, Tr F340/380 ratio = 1.285 ± 0.477) followed by a delayed phase which gradually

returned to near-basal levels (F340/F380 ratio = 0.534 ± 0.064) upon perfusion with extracellular solution. The peak Fura-2 ratios obtained for each calcium trace is shown in Figure 3.15.

3.3.2 PAR$_2$ mEYFP-mediated inositol phosphate response in NCTC-2544 cells.

The ability of PAR$_2$ mEYFP to signal to inositol phosphate was demonstrated in the null PAR NCTC-2544 cell line following treatment with trypsin (50 nM) and SLIGKV-OH (100 μM). Figure 3.16 clearly shows a low level response in parental NCTC-2544 cells following treatment with trypsin (4.026 ±0.139 fold of basal), which was not observed in response to activating peptide (1.555 ± 0.229 fold of basal). Following transient transfection with WT PAR$_2$ or PAR$_2$ mEYFP, stimulation with trypsin resulted in the generation of an appreciable inositol phosphate response (7.312 ± 1.273 and 16.191 ± 0.804 respectively). Not surprising, responses to SLIGKV-OH were rather poor in cells transiently expressing WT PAR$_2$ and PAR$_2$ mEYFP (3.310 ± 0.217 and 1.758 ± 0.229 respectively), as previously observed in the HEK293 cell model. NCTC-2544 cells stably expressing PAR$_2$ (NCTC PAR$_2$ cells) generated a significant increase in inositol phosphate upon treatment with trypsin (11.018 ± 0.063) and SLIGKV-OH (11.102 ± 0.701).

In contrast to proteolytic cleavage by native serine proteases such as trypsin, the potency of the synthetic activating peptides available for PARs are considerably lower, functioning variably at micromolar levels depending upon the assay tested. As demonstrated in Section 3.2 and 3.3, the results obtained from inositol phosphate assays have found the PAR$_2$-specific activating peptide SLIGKV-OH to be poor in the transfected cell models used. Certain modifications of this peptide agonist have resulted in increased potency, namely the addition of a furoyl group in the place of the serine residue, thus creating 2f-LIGKV-OH (Kawabata *et al.,* 2004).

The ability of the 2f-LIGKV-OH peptide to mediate an inositol phosphate response was demonstrated in Figure 3.17. Parental NCTC-2544 cells did not respond to 100 μM of either 2f-LIGKV-OH (1.115 ± 0.050 fold of basal control) or SLIGKV-OH (1.138 ± 0.060 fold of basal) treatment. Cells expressing PAR$_2$ mEYFP showed in a

significant increase in inositol phosphate following stimulation with 2f-LIGKV-OH (5.173 ± 0.462), with a considerably lower response observed following activation with SLIGKV-OH (2.053 ± 0.111).

(A)
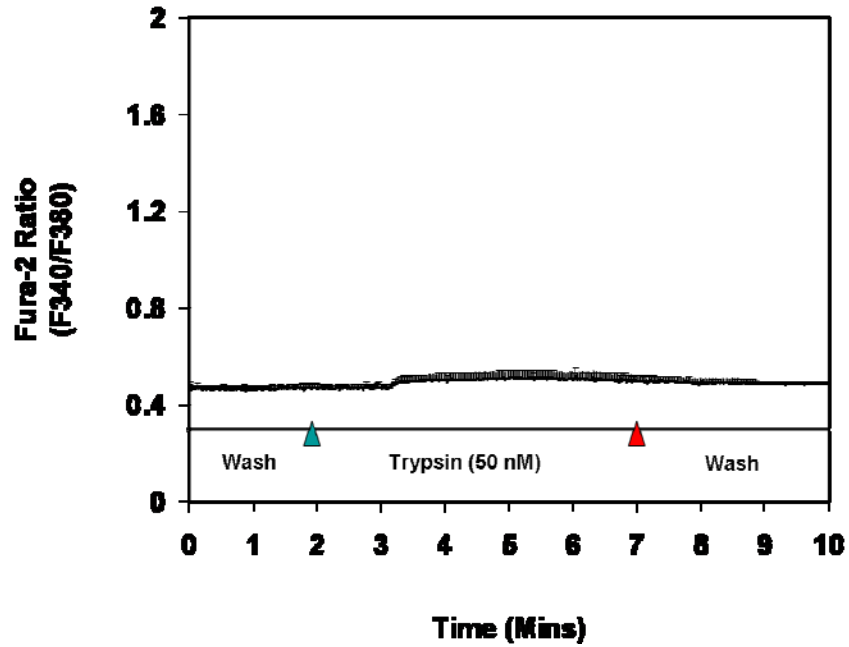
(B)
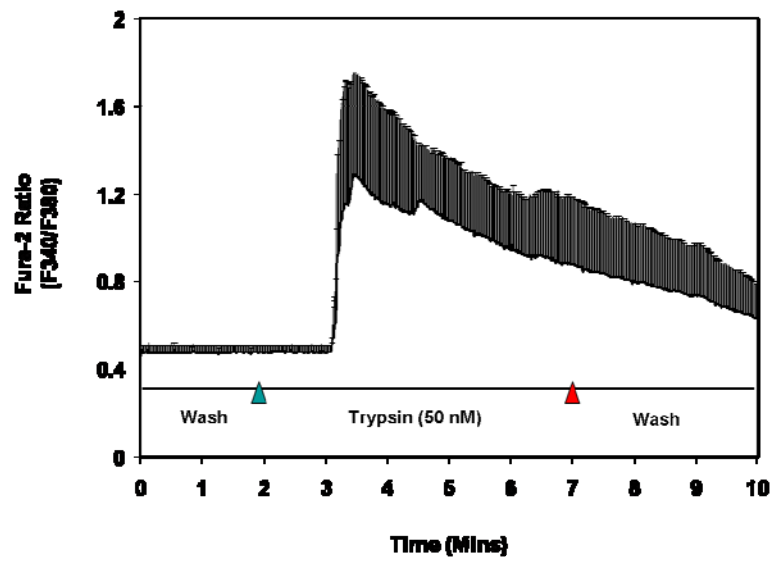
(C)
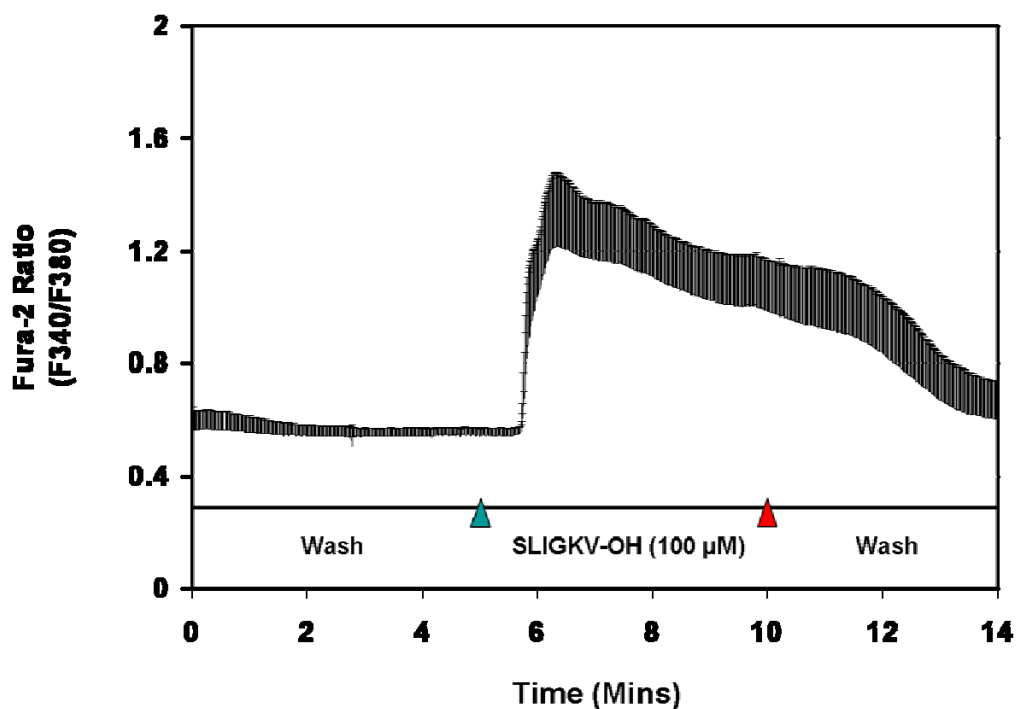
Figure 3.14. The characterisation of calcium signalling in parental NCTC-2544 cells and PAR$_2$ mEYFP expressing cells following PAR$_2$ agonist treatment.
NCTC-2544 cells were transiently transfected with PAR$_2$ mEYFP for 24 hours as outlined in Chapter 2.5. The cells were serum starved for a further 24 hours then loaded with the Ca^{2+}-sensitive dye, fura-2 AM (6 µM) for 1 hour at room temperature. Calcium imaging was carried out at 40x magnification as described in Chapter 2.10. Ratiometric images (340/380 nm) were acquired every 2-5 seconds from parental cells (A) or cells expressing PAR$_2$ mEYFP following perfusion with extracellular solution then treatment with (B) trypsin (50 nM) or (C) SLIGKV-OH (100 µM) for 5 minutes. The calcium traces provided represent the fluorescence ratios taken from two separate experiments (mean ± s.e.m from 20 cell measurements).
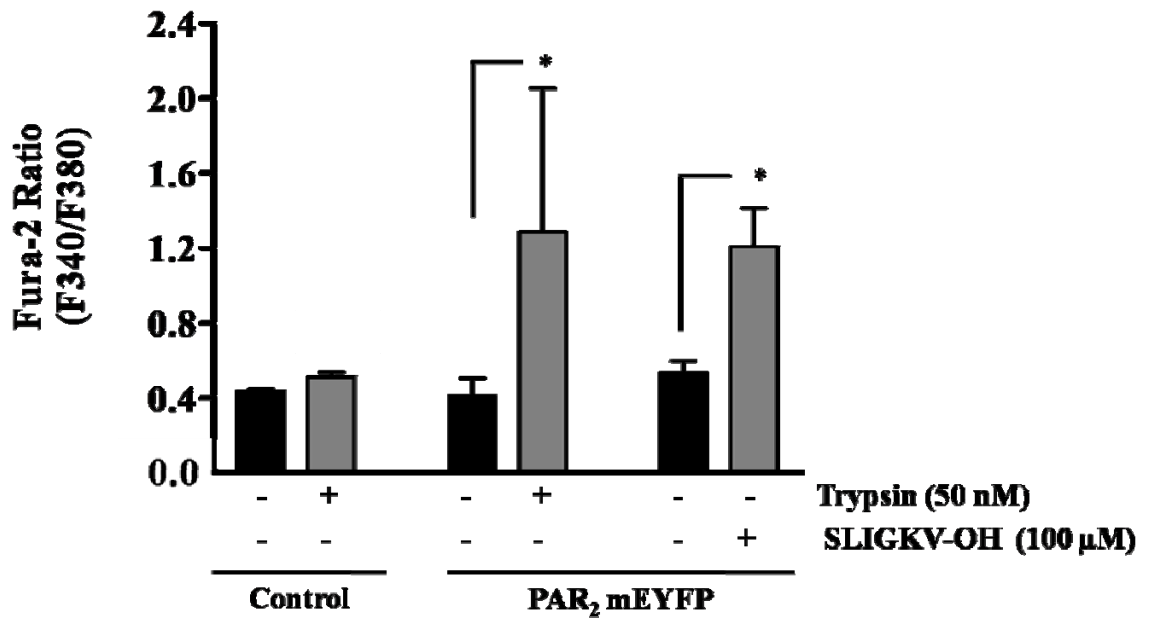
Figure 3.15. Peak Fura-2 ratios obtained from calcium traces following agonist treatment of parental NCTC-2544 cells and cells expressing PAR$_2$ mEYFP.
Following calcium imaging using Fura-2-AM as outlined in Chapter 2.10, peak Fura-2 (F340/F380) ratios were taken from calcium traces at basal (black) and following PAR$_2$ agonist treatment (grey) in NCTC-2544 cells (control) and cells expressing PAR$_2$ mEYFP. Cells were treated with trypsin (50 nM) or SLIGKV-OH (100 μM) as indicated. The data above represents the peak Fura-2 ratios obtained from the calcium traces observed in Figure 3.14 taken from two separate experiments (mean ± s.e.m from 20 cell measurements, *p=<0.05).
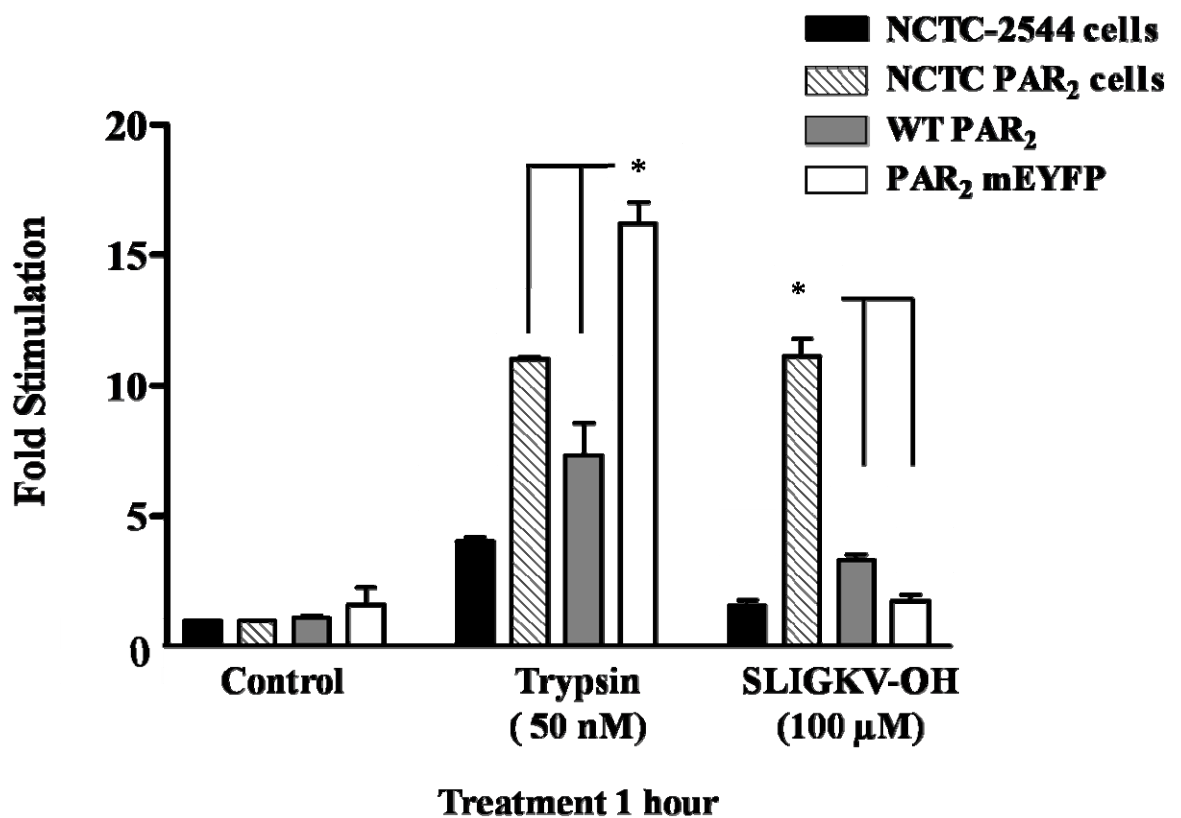
Figure 3.16. PAR$_2$-mediated [^{3}H]-inositol phosphate accumulation in NCTC-2544 cells.

NCTC-2544 cells were transfected with WT PAR$_2$ or PAR$_2$ mEYFP for 24 hours, as outlined in Chapter 2.5, after which time the media was replaced with serum free media supplemented with [^{3}H]-2-myo-inositol (0.25 µCi/well) for a further 24 hours. Total inositol phosphate accumulation was measured as shown in Chapter 2.9 in parental NCTC-2544 cells (black) or NCTC cells stably expressing PAR$_2$ (striped) and cells transiently expressing WT (grey) or PAR$_2$ mEYFP (white). The cells were pretreated with 10 mM lithium chloride and then stimulated for 1 hour with trypsin (50 nM) or SLIGKV-OH (100µM). Each value represents the mean ± s.e.m. from two separate experiments performed in triplicate (*p=<0.05).
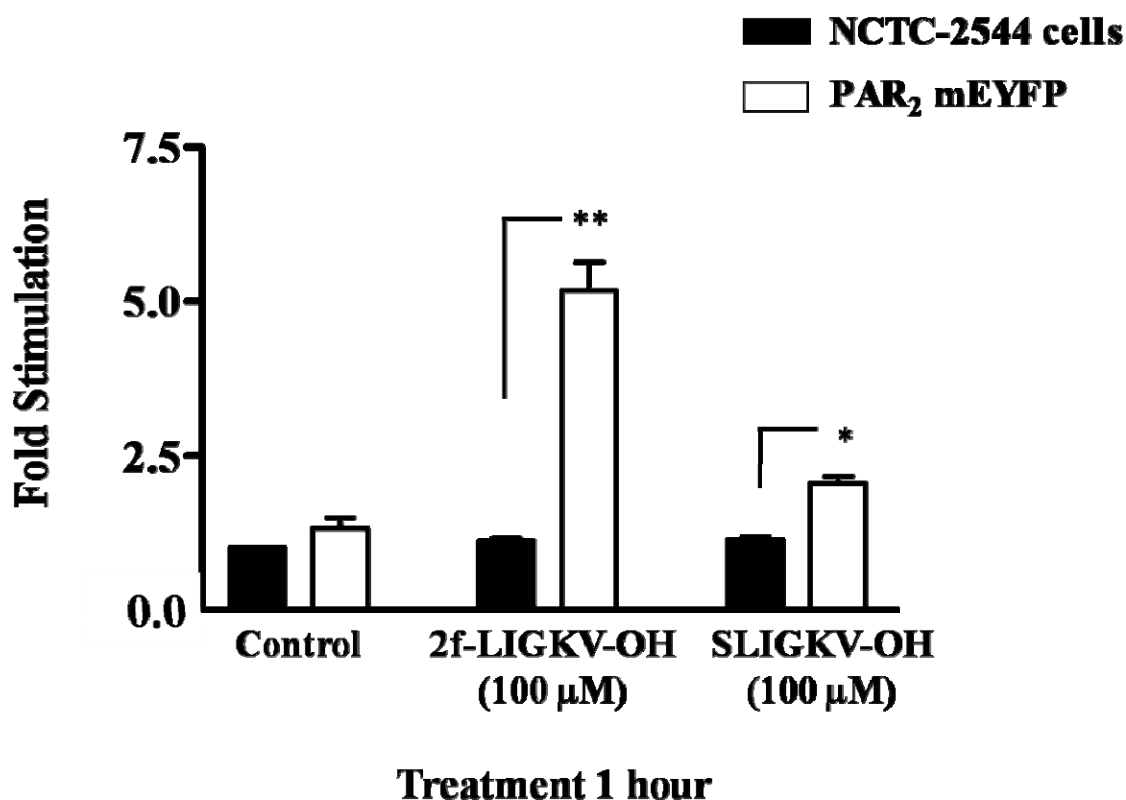
Figure 3.17. 2-fl-SLIGKV-OH-mediated [^{3}H]-inositol phosphate accumulation in NCTC-2544 cells.

NCTC-2544 cells were transfected with PAR$_2$ mEYFP for 24 hours as described in Chapter 2.5, after which time the media was replaced with serum free media supplemented with [^{3}H]-2-myo-inositol (0.25 μCi/well) for a further 24 hours. The cells were pretreated with 10 mM lithium chloride and then stimulated for 1 hour with 2f-SLIGKV-OH (100 μM) or SLIGKV-OH (100 μM). Accumulation of total [^{3}H]-inositol phosphate (InsP$_{1-4}$) was measured in parental NCTC-2544 cells and PAR$_2$ mEYFP expressing cells as outlined in Chapter 2.9. Each value represents the mean ± s.e.m. from three separate experiments performed in triplicate (*p=<0.05, **p=<0.01).

3.4 Investigating the cellular localisation of PAR$_4$ mECFP in the null PAR NCTC-2544 cell line.

A striking feature of PAR$_4$ mECFP expression, in comparison to PAR$_2$ mEYFP in the HEK293 cell line, as shown in Section 3.2, was the weak membrane localisation with high level of intracellular retention. Treatment with PAR$_4$ agonists highlighted the capability of PAR$_4$ to mediate various cell signalling cascades despite the low level of PAR$_4$ expressed on the plasma membrane. Intracellular retention of PAR$_4$ was investigated further in the NCTC-2544 cell model. NCTC-2544 cells provided a valuable model to study PAR$_4$ localisation in isolation due to the lack of endogenous PAR expressed in this cell line.

3.4.1 Investigating the cellular localisation of PAR$_4$ mECFP in NCTC-2544 cells.

Using confocal microscopy (Lieca Corps), the expression of PAR$_4$ mECFP in NCTC-2544 cells was investigated. Figure 3.18 clearly shows PAR$_4$ mECFP expression to be predominantly intracellular (red arrows), with only a small number of cells expressing PAR$_4$ at the plasma membrane (white arrows). Similar to experiments carried out in HEK293 cells, PAR$_2$ mEYFP was expressed at the plasma membrane (white arrows) in the NCTC-2544 cells with punctate intracellular pools (red arrows) present, as shown in Figure 3.19.
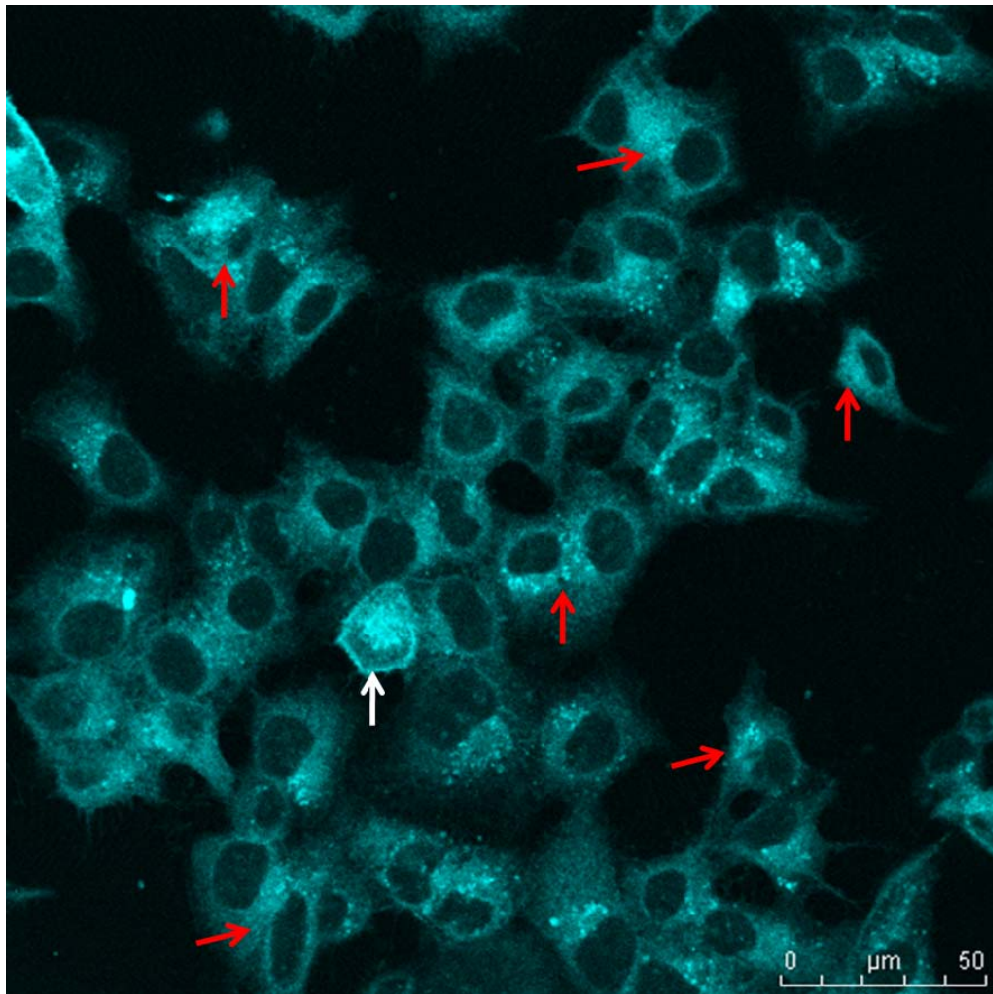
Figure 3.18. PAR$_4$ mECFP expression in NCTC-2544 cells monitored by confocal microscopy.

NCTC-2544 cells were grown on coverslips then transfected with PAR$_4$ mECFP for 24 hours. The cells were serum starved for a further 24 hours prior to fixation by methanol as outlined in Chapter 2.6.1 and then the coverslips were mounted on glass microscope slides with Mowiol. PAR$_4$ mECFP expressing cells were visualised by confocal microscopy (Lieca Corps) using ECFP wavelength settings (Ex: 430 nm). Cells expressing intracellular PAR$_4$ are indicated by red arrows whilst membrane expressing cells are highlighted by white arrows (Scale bar = 50 μm). Image representative of at least 4 experiments.
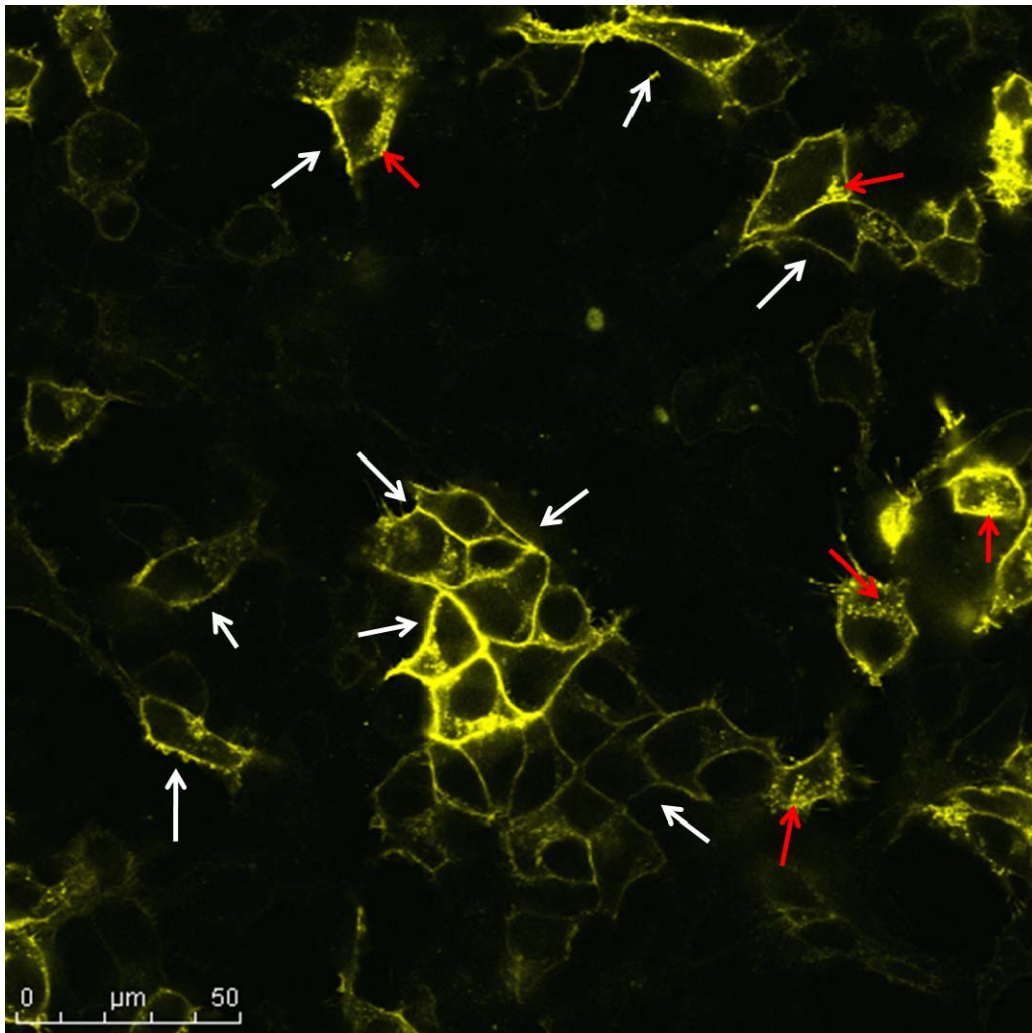
Figure 3.19. PAR$_2$ mEYFP expression in NCTC-2544 cells monitored by confocal microscopy.

NCTC-2544 cells were grown on coverslips then transfected with PAR$_2$ mEYFP for 24 hours. The cells were serum starved for a further 24 hours prior to fixation by methanol as described in Chapter 6.2.1. The coverslips were mounted on glass microscope slides with Mowiol and PAR$_2$ mEYFP expressing cells were visualised by confocal microscopy using EYFP wavelength settings (Ex: 505 nm). Cells expressing PAR$_2$ at the plasma membrane are indicated with white arrows, whilst intracellular pools of receptor are indicated by red arrows (Scale bar = 50 μm). Image representative of at least 4 experiments.

3.4.2 Intracellular retention of PAR$_4$ mECFP in the endoplasmic reticulum (ER).

The distinctive intracellular expression of PAR$_4$ in both cell models tested raised the question as to where the receptor population was retained within the cell. As described in Chapter 1, GPCRs are synthesised in the endoplasmic reticulum (ER), where they are transported to the Golgi via interaction with chaperone proteins then undergo various post-translational modifications in order to become maturely expressed at the plasma membrane. As PAR$_4$ expression was predominantly observed inside the cell, with rather inefficient delivery to the cell surface, it was necessary to identify the location where PAR$_4$ was being retained.

To identify if PAR$_4$ was retained in the ER, PAR$_4$ co-localisation with the ER protein calnexin was investigated in NCTC-2544 cells transiently expressing PAR$_4$ mECFP. Using indirect immunostaining, a calnexin-specific antibody and Texas red-conjugated secondary antibody was used to detect endogenous calnexin protein in the ER of NCTC2544 cells, as shown in Figure 3.20. Co-localisation between PAR$_4$ mECFP and calnexin was carried out using confocal microscopy. Figure 3.21 clearly shows intracellular PAR$_4$ mECFP expression (cyan image, top) and calnexin staining (red image, middle) with co-localisation, as indicated by the white arrows, observed between PAR$_4$ mECFP and calnexin in the merged image (yellow image, bottom).
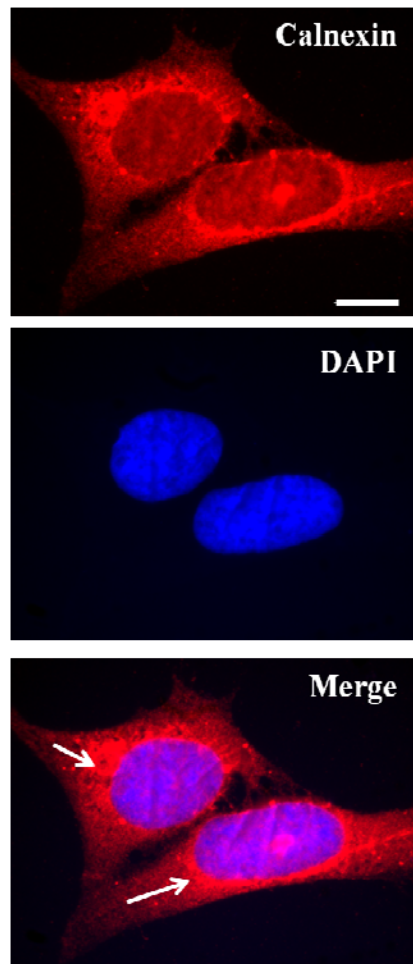
Figure 3.20. Indirect immunofluorescence for the detection of the ER protein marker calnexin in NCTC-2544 cells.

NCTC-2544 cells were grown on coverslips until 70% confluence then subjected to indirect immunostaining for endogenous calnexin expression in fixed cells as outlined in Chapter 2.6.3. Using epifluorescence microscopy, cells were visualised at 100x magnification (scale bar = 10 µm) using Texas red (Ex: 605 nm) filter settings to detect calnexin and a 380 nm wavelength to detect DAPI nuclear stain. Immunofluorescence staining for calnexin (Red) is shown alongside DAPI (blue) with both images merged to highlight distinct ER/nuclei compartments. White arrows point to the areas of calnexin expression, indicative of ER localisation. Image set representative of three separate experiments.
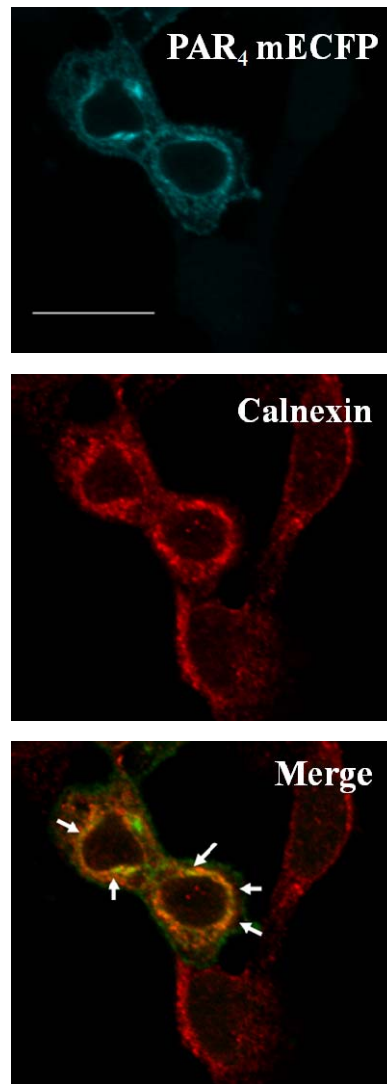
Figure 3.21. Co-localisation of PAR$_4$ mECFP with the ER protein marker calnexin in NCTC-2544 cells.

NCTC-2544 cells were transiently transfected with PAR4 mECFP for 24 hours prior to serum starvation for a further 24 hours followed by indirect immunostaining for endogenous calnexin as described in Chapter 2.6.3. Using confocal microscopy, cells were visualised at 60x magnification (scale bar = 20 µm) using ECFP (Ex: 430 nm) and Texas red (Ex: 605 nm) filter settings. PAR4 mECFP expression (Cyan) and calnexin (Red) is shown alongside colour combined PAR4 mECFP and calnexin images (merge). White arrows indicate areas of co-localisation between PAR4 and calnexin. Image set representative of three separate experiments.

3.5 Discussion

To date, much of the work published relating to GPCR expression, localisation, function and potential interaction have depended on monitoring receptor expression using epitope tagging or fluorescent fusion proteins engineered to the receptor of interest (see Lohse *et al.,* 2008b. As a result, the common approach adopted to characterise receptor function involves the generation of relevant transfected expression systems encoding 'tagged' receptor populations. This has been particularly true for early research investigating PAR distribution and receptor trafficking (Böhm *et al*., 1996; Déry *et al.,* 1999). Even now, epitope-tagged PAR over-expression systems are still adopted due to the poor specificity of commercial antibodies available to detect endogenous PAR expression. The major drawback of using epitope tagged receptors in studies has been the 'artificial' nature of the expression systems investigated and the potential for the fusion tag to influence the behaviour of the tagged protein of interest. For this reason it was necessary to functionally characterise the PAR constructs used in the present study.

Overall, the results in Section 3.2 and 3.3 detailing the functional characterisation of the fluorescent PAR constructs confirmed that expression and signalling capabilities of PAR_2 mEYFP and PAR_4 mECFP were intact and not influenced by the presence of the C-terminal fusion of EYFP or ECFP. By combining the results obtained from the two cell models utilised, namely HEK293 cells and NCTC-2544 cells the data presented clearly shows typical receptor expression for PAR_2. However the very nature of PAR_4 expression is an area that requires further investigation. Phospholipase C (PLC) activity, as demonstrated from the inositol phosphate assays, calcium signalling studies and the activation of ERK, were all shown to be unaffected by epitope tagging. All of which were clearly functional downstream of PAR_2 mEYFP and PAR_4 mECFP activation.

PAR_2 signalling has been well characterised in terms of the ability of trypsin and PAR_2 specific activating peptides (AP) to stimulate PLC-mediated inositol phosphate and calcium responses providing confirmation of PAR_2 coupling with $G\alpha_{q/11}$ (Nystedt *et al.,*1995a and 1995b; Molino *et al.,* 1997; Seatter *et al.,*2004). Studies in

our laboratory, using the $G\alpha_{q/11}$ selective inhibitor YM 254890, have demonstrated clear PAR_2-$G\alpha_{q/11}$ coupling downstream of receptor activation and upstream of PLC-mediated signal transduction, (Goon Goh *et al.,* 2008).

Activation of PAR_2 has also been shown to signal to MAP kinase pathways such as ERK, p38 and JNK (Belham *et al.,* 1996; DeFea *et al.,* 2000b; Kanke *et al.,* 2001), however the direct route through which these pathways become activated are more complicated. PAR_2-mediated ERK activation has been previously shown to involve a β-arrestin scaffold via a G-protein-independent mechanism (DeFea *et al.,* 2000b), in addition to a possible EGFR-transactivation-dependent mechanism. In this chapter several features of receptor activation was explored. Agonist-induced receptor internalisation of PAR_2 mEYFP, as shown in Figure 3.1, was consistent with the typical features published in original PAR_2 trafficking studies (Böhm *et al.,* 1996; Déry *et al.* 1999), outlining vesicular trafficking followed by a loss of cell surface expression. Internalisation of PAR_2 was achieved within 30 minutes of agonist treatment. The time frame of these receptor trafficking events corresponded well with the attenuation of several PAR_2-mediated signal events. Following receptor activation, transient calcium responses were observed (Figures 3.5, 3.6 and 3.14). PAR_2-mediated ERK phosphorylation responses (Figure 3.12) were somewhat more prolonged, however returned to basal levels by 30 minutes post-agonist treatment, thus consistent with the kinetics of receptor internalisation.

Trypsin-mediated inositol phosphate and calcium responses implied that the modulation of PAR_2-induced PLC activity was intact, thus C-terminal tagging did not affect G-protein coupling, as demonstrated through the efficient activation of $G_{\alpha q/11}$-specific signalling events. Despite this, the inositol phosphate responses generated using the PAR_2-specific activating peptide SLIGKV-OH were consistently poor for both cell lines tested, yet appeared to mediate a strong calcium and ERK signal when tested. A possible rationale for the differences between the signal transduction profile mediated by trypsin and SLIGKV-OH may be due to different sites of action through which both agonists act, thus the conformational changes that might occur within the receptor may differ from one mode of receptor activation to

the other. This has the potential to influence the ability of certain G-proteins or non-G-protein scaffolds to couple effectively upon receptor activation, which in turn may result in the preferential activation of certain downstream second messengers over others. This may explain the different responses observed downstream of trypsin-mediated receptor activation versus peptide activation. Investigation into the nature of such biased agonism or 'functional selectivity' (Urban *et al.,* 2007) has been a hot topic in the GPCR field for some time now. Work in this area has identified receptor families, such as the opioid receptor family, where some agonists may mediate receptor activation or preferentially function to facilitate in desensitisation due to biased agonism (reviewed by Kelly *et al.,* 2008). Characterisation of a recent novel PAR$_2$ peptide, K-14585 (Kanke *et al.,* 2009) found that as well as displaying distinct antagonist activity towards various PAR$_2$-mediated signalling pathways, at different concentrations this compound may function as an agonist (Goh *et al.,* 2009). Whilst this is only one example of biased agonism for PAR peptides, the idea that members of the PAR family may exist in various active states depending upon the mode of activation has been previously described for PAR$_1$ (McLaughlin *et al.,* 2005) and PAR$_2$ (Al-ani *et al.,* 2002a and 2002b).   However, a more simplistic explanation for the results observed in the present study may be due to trypsin-mediated receptor cleavage and the formation of the receptors own tethered ligand resulting in a more efficient accumulation of inositol phosphate.   In this case receptor activation independent of cleavage through peptide binding would be naturally less efficient due to the ability of one molecule of peptide to bind one receptor at a time, thus the rate limiting step would be the supply of agonist, which over time would be depleted.

The poor potency of PAR-selective activating peptides has been well documented in comparison to the native serine proteases for this receptor family (discussed in Chapter 1.3). This has led the way for the development of more potent agonist peptides. Unlike the poor inositol phosphate response observed following SLIGKV-OH treatment, the use of the modified peptide 2f-LIGKV-OH (Kawabata *et al.,* 2004) resulted in an enhanced signal upon receptor activation. The improved activity of this peptide has been attributed to the substitution of the serine residue for a furoyl group which is thought to improve the stability of the peptide by preventing

aminopeptidase degradation. The improved activity of this peptide agonist for PAR_2 has been characterised for various signalling pathways, with more prolonged responses observed in comparison to trypsin stimulation (Goon Goh *et al.,* 2008).

The fact that PAR_2 internalisation proceeded alongside an efficient ERK response confirmed that C-terminal tagging did not affect any possible β-arrestin-dependent signalling scaffold, thought to be involved in both PAR_2 trafficking events and signalling to ERK (Defea *et al.,* 2000b).

The cellular localisation and trafficking of PAR_4 has been studied in less detail, with very little published in terms of receptor trafficking events. Unlike PAR_2, PAR_4 did not internalise in response to thrombin or the PAR_4-specific activating peptide, AYPGKF-NH_2, even at higher agonist concentrations or longer incubation times. One possible explanation for this may be the lack of serine/threonine phosphorylation sites present on the C-terminal tail of the receptor (see Chapter 1.2). These phosphorylation sites have been demonstrated to contribute greatly towards PAR_1 and PAR_2 trafficking events; sites which are thought to be crucial for GRK/β-arrestin binding for receptor internalisation and desensitisation (Shapiro *et al.,* 1996 and Stalheim *et al.,* 2005). Despite the relative lack of internalisation in the cell models used in this study, internalisation of PAR_4 has been reported in platelets using biotinylation to measure changes in cell surface protein expression following receptor activation by thrombin (Harper and Sage, 2006). However, the lack of PAR_4 internalisation observed in this study coincided with the longevity of PAR_4-mediated signalling events observed in the corresponding signalling experiments. This was demonstrated both in terms of the delayed decay in the calcium signal and the sustained ERK activation following receptor activation with thrombin and AYPGKF-NH_2. The prolonged calcium response observed was characteristic of PAR_4-mediated calcium signalling studies carried out in other cells, including platelets (Jardin *et al.,* 2007), alveolar epithelial cells (Ando *et al.,* 2007), among other cell lines tested to date. However, some literature published has found calcium responses to be negligible upon PAR_4 activation, as demonstrated in hippocampal

cultures (Bushell *et al.,* 2006), or sensory neurones where receptor activation actually resulted in the inhibition of KCl-mediated calcium mobilisation (Asfaha *et al.,* 2007).

As with signalling observed for PAR$_2$, PAR$_4$ coupling to G$\alpha_{q/11}$-specific signalling events appeared to be intact, efficiently signalling to both calcium and inositol phosphate, with signals consistent with cells expressing WT PAR$_4$ without the fluorescent fusion protein. The sustained ERK responses observed in these studies also correlated well with those responses documented in smooth muscle cells (Bretschneider *et al.,* 2001). The results obtained in the present study are consistent with the mounting evidence that has previously demonstrated the longevity of PAR$_4$-mediated responses, with relative lack of desensitisation, when compared with the other PAR family members (Covic *et al.,* 2000 and Shapiro *et al.,* 2000). However, based upon the lack of PAR$_4$ internalisation, this suggests that the attenuation of PAR$_4$-mediated signalling may be regulated by an alternative, yet unknown mechanism.

As discussed previously in Chapter 1, the trafficking studies of other PAR members have found pronounced membrane localisation with constitutive expression of receptors in intracellular pools, namely the Golgi, where newly synthesised receptors can be exported to the membrane when required (Déry *et al.,*1999). However, the cellular localisation of PAR$_4$ mECFP observed in both the HEK293 and NCTC-2544 cell models, highlighted novel features of receptor expression and trafficking distinct from both PAR$_1$ and PAR$_2$. Both cell lines tested provided insight into the cellular localisation of PAR$_4$. Expression of PAR$_4$ was observed predominantly inside the cell with very little receptor expressed at the cell surface. Whilst this may have been attributed to the presence of the C-terminal fusion protein, corresponding signalling studies carried out demonstrated that fusion with ECFP did not affect PAR$_4$ activation or cell signal transduction, despite the relatively low level of receptor present at the plasma membrane. Further investigation found that PAR$_4$ was predominantly localised in the endoplasmic reticulum (ER), as demonstrated through co-localisation with the ER resident chaperone protein, calnexin.

These preliminary experiments were carried out with the aim to characterise the functional capacity of PAR_2 mEYFP and PAR_4 mECFP for use in future experiments. In carrying out these preliminary characterisation experiments, these results have highlighted major areas of investigation into the nature of PAR_4 expression in the cell. ER retention and subsequent inefficient delivery of PAR_4 to the plasma membrane implicates a different regulatory process in receptor sorting and maturation, distinct from the other PAR family members. These distinct features raise the question as to why PAR_4 is largely retained in the ER in the NCTC-2544 cell line and most importantly through what means does PAR_4 become expressed at the membrane, as observed in the HEK293 cell model.

This thesis aims to provide a rationale for the distinct features of ER retention of PAR_4 and subsequent delivery of PAR_4 to the cell surface.

CHAPTER 4
INVESTIGATING THE NATURE OF PAR4 ER LOCALISATION

4.1 INTRODUCTION

The characterisation studies carried out in Chapter 3 highlighted novel features of PAR$_4$ expression, distinct from observations made in original studies investigating PAR$_1$ or PAR$_2$ localisation. Unlike the other PAR family members, PAR$_4$ was found to be both expressed at the plasma membrane and ER in HEK293 cells but predominantly ER retained in the NCTC-2544 cell model. When the protein sequence of PAR$_4$ was investigated further, two potential arginine-based ER retention/retrieval motifs (RxR) were found (Figure 4.1). Based upon the original cloning, characterisation and identification of the protein organisation of PAR$_4$ (Xu *et al.,* 1998) these motifs were found at position R^{183}AR and R^{188}GRR (in red), residing within the intracellular loop-2 (ICL-2) of the receptor. When the protein sequences of the three functional PAR family members, PAR$_1$, PAR$_2$ and PAR$_4$ were aligned using Clustal W multiple alignment software (Figure 4.2), these motifs were found to be specific to PAR$_4$. As discussed previously in Chapter 1.2, functional arginine-based ER retention motifs have been found to exist in many GPCRs, with those present at the C-terminal of the GABA$_{B1}$ receptor (Margeta-Mitrovic *et al.,* 2000) being highly significant to the receptor localisation and function.

In addition to the presence of these motifs, post translational modification of GPCRs, for example, N-linked glycosylation has been shown to play an important role in the delivery of certain proteins to the cell surface, as demonstrated for the dopamine receptor 5 (D$_5$) receptor (Karpa *et al.,* 1999). Further analysis of the protein sequence of PAR$_4$ found that the receptor has an asparagine (Asn)-Xxx-Ser/Thr motif, located at position N^{56}DS at the N-terminal of the receptor, thus suggesting that the receptor may undergo N-linked glycosylation to allow expression at the plasma membrane.

An additional factor that may influence receptor maturation to the plasma membrane would be interaction with the various ER chaperone proteins that facilitate in protein folding, assembly and sorting for ER export (Hirsch *et al.,* 2009). As discussed in Chapter 1.2.1, the ER chaperone protein calnexin has proven to be a significant player in the regulation of GPCR cell surface expression. Calnexin interaction with

N-linked glycoproteins has also been previously shown (Vassilakos *et al.,* 1998). Work published in 2007 highlighted the capacity of calnexin to serve a dual role in facilitating membrane expression of D_1/D_2 heterodimers whilst retaining monomeric D_1 receptors in the ER (Free *et al.,* 2007).

The experiments carried out in this chapter aim to identify the nature of PAR_4 localisation, firstly through the characterisation of the potential ER retention motifs and secondly through the possible N-linked glycosylation and interaction with the ER chaperone calnexin.
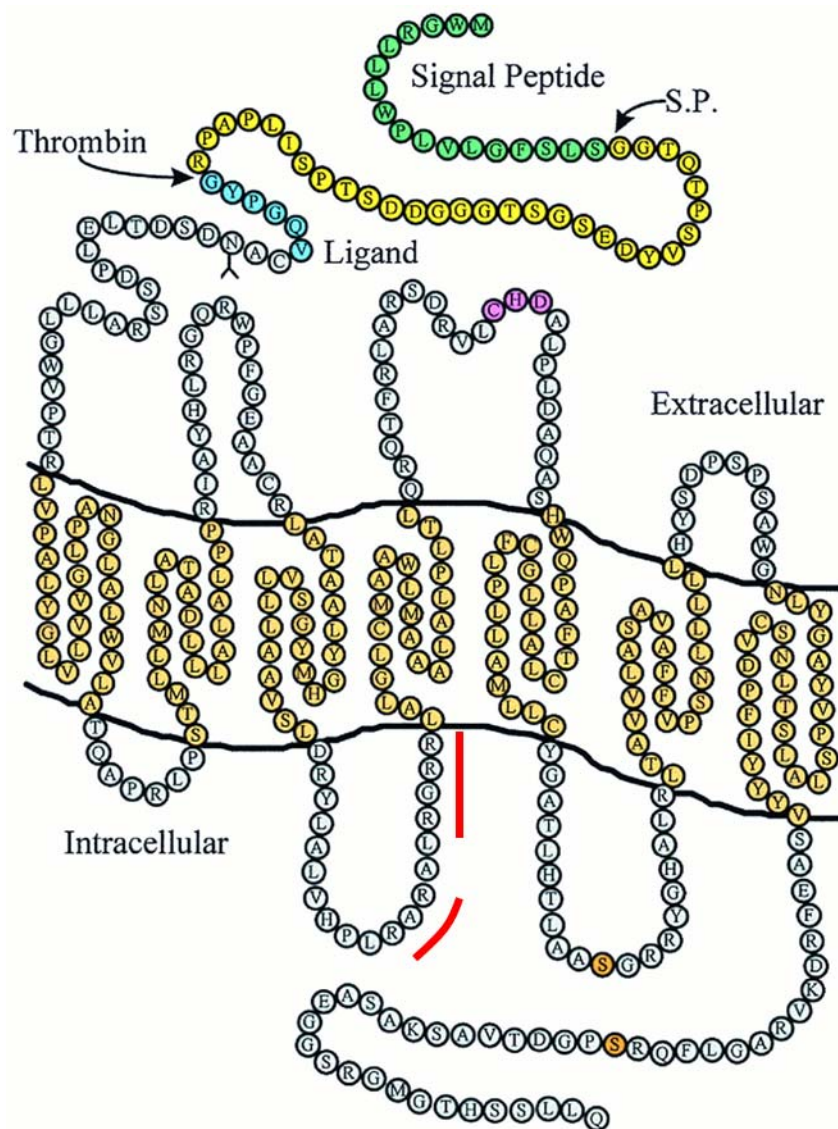
Figure 4.1. Proposed organisation of the protein structure for PAR₄.

The protein organisation of PAR₄, originally published by Xu *et al.,* in 1998, is shown above. Further analysis of the protein sequence found the existence of two potential arginine (R)-based ER retention motifs. These 'RxR' motifs are positioned close together at $R^{183}AR$ and $R^{188}GRR$ within intracellular loop-2 (ICL-2) of the receptor (highlighted in red).

N-term

```
PAR1   -MGPRRLLLVAACFSLCGPLLSARTRARRPESKATNATLDPRSFLLRNPNDKYEPFWEDE  59
PAR2   ------MRSPSAAWLLGAAILLAASLSCSGTIQGTNRSSKGRSLIGKVDG--------TS  46
PAR3   --------MKALIFAAAGLLLLLPTFCQSGMENDTNNLAKPTLPIKTFRGAPPNSFEEFP  52
PAR4   MWGRLLLWPLVLGFSLSGGTQTPSVYDESGSTGGGDDSTPSILPAP------------RF  48
             :    .                         :
```
                                                              TM1
```
PAR1   EKNESGLTEYRLVSINKSSPLQKQLPAFISEDASGYLTSSWLTLFVPSVYTGVFVVSLPL  119
PAR2   HVTGKGVTVETVFSVDEFS-------------ASVLTGKLTTVFLPIVYTIVFVVGLPS  92
PAR3   FSALEGWTGATITVKIKCPE-ESASHLHVKNATMGYLTSSLSTKLIPAIYLLVFVVGVPA  111
PAR4   KPGQVCANDSDTLELPDSSR-------------ALLLGWVPTRLVPALYGLVLVVGLPA  94
              .  .              . *  .   * ::* :*  *:**.:*
```
          ICL-1   TM2   ECL-1
```
PAR1   NIMAIVVFILKMKVKKPAVVYMLHLATADVLFVSVLPFKISYYFSGSDWQFGSELCRFVT  179
PAR2   NGMALWVFLFRTKKKHPAVIYMANLALADLLSVIWFPLKIAYHIHGNNWIYGEALCNVLI  152
PAR3   NAVTLWMLFFRTRSICTTVFYTN-LAIADFLFCVTLPFKIAYHLNGNNWVFGEVLCRATT  170
PAR4   NGLALWVLATQAPRLPSTMLMN-LATADLLLALALPPRIAYHLRGQRWPFGEAACRLAT  153
          * ::: ::  :     .::.    ** **.*    :* :*:*:: *. * :*.  *.
```
        TM3   ICL-2   TM4
```
PAR1   AAFYCNMYASILLMTVISIDRFLAVVYPMQSLSWRTLGRASFTCLAIWALAIAGVVPLVL  239
PAR2   GFFYGNMYCSILFMTCLSVQRYWVIVNPMG-HSRKKANIAIGISLAIWLLILLVTIPLYV  211
PAR3   VIFYGNMYCSILLLACISINRYLAIVHPFTYRGLPKHTYALVTCGLVWATVFLYMLPFFI  230
PAR4   AALYGHMYGSVLLLAAVSLDRYLALVHPLRARALRGRRLALGLCMAAWLMAAALALPLTL  213
          :* :** *:*::: :*::*: .:* *:   .       *   .  *      :*: :
```
          ECL-2   TM5
```
PAR1   KEQTIQVPGLNITTCHDVLNETLLEG-YYAYYFSAFSAVFFFVPLIISTVCYVSIIRCLS  298
PAR2   VKQTIFIPALNITTCHDVLPEQLLVG-DMFNYFLSLAIGVFLFPAFLTASAYVLMIRMLR  270
PAR3   LKQEYYLVQPDITTCHDVHNTCESSSPFQLYYFISLAFFGFLIPFVLIIYCYAAIIRTLN  290
PAR4   QRQTFRLARSDRVLCHDALPLDAQAS-HWQPAFTCLALLGCFLPLLAMLLCYGATLHTLA  272
          .*   :   :  . ***.          .      * .::    :.* .    .*   :: *
```
          ICL-3   TM6   ECL-3
```
PAR1   SSAVANRS--KKSRALFLSAAVFCIFIICFGPTNVLLIAHYSFLSHTSTTEAAYFAYLLC  356
PAR2   SSAMDENSEKKRKRAIKLIVTVLAMYLICFTPSNLLLVVHY-FLIKSQGQSHVYALYIVA  329
PAR3   AYDH------RWLWYVKASLLILVIFTICFAPSNIILIHHANYYYNN-TDGLYFIYLIA  343
PAR4   ASGR------RYGHALRLTAVVLASAVAFFVPSNLLLLLHYSDPSPSA-WGNLYGAYVPS  325
          :          :      :      ::     * *:*::*: *:  .    * *: .
```
          TM7   C-term
```
PAR1   VCVSSISSCIDPLIYYYASSECQRYVYSILCCKESSDPSSYNSSGQLMASKMDTCSSNLN  416
PAR2   LCLSTLNSCIDPFVYYFVSHDFRDHAKNALLCRSVRTVKQMQVSLTSKKHSRKSSSYSSS  389
PAR3   LCLGSLNSCLDPFLYFLMSKTRNHSTAYLTK---------------------------  374
PAR4   LALSTLNSCVDPFIYYYVSAEFRDKVRAGLFQRSPGDTVASKASAEGGSRGMGTHSSLLQ  385
          :.:.::.**:**::*:  *    .  .
```

```
PAR1   NSIYKKLLT  425
PAR2   STTVKTSY-  397
PAR3   ---------
PAR4   ---------
```

Figure 4.2. Multiple sequence alignment of the PAR family using CLUSTAL W software.

The presence of arginine-based ER retention/retrieval motifs was assessed in the protein sequences of all PAR family members. A protein sequence alignment was carried out using CLUSTAL W software. Conserved amino acids are shown above (**.** and **:** indicate residues similar across two of the three proteins whist * highlights residues common to all three proteins). The putative sites for proteolytic cleavage have been underlined and highlighted in blue. Of the three proteins, only the PAR$_4$ sequence appears to contain the RxR motifs (shown in red). A potential N-linked glycosylation site for PAR$_4$ is shown in pink.

4.2 Investigating the cellular localisation of PAR$_4$ in HEK293 cells following mutation of the potential ER retention motifs

Using site-directed mutagenesis, the arginine residues in both ER retention motifs were replaced and substituted with alanine residues, thus creating R^{183}AR → A^{183}AA (RAR mut), R^{188}GRR → A^{188}GAA (RGRR mut) and a double mutant R^{183}AR xx R^{188}GRR → A^{183}AA xx A^{188}GAA (DM mut) within the VSV-PAR$_4$ mECFP construct, as shown in Figure 4.3. The influence of motif mutation upon PAR$_4$ expression was investigated further with the aim to identify if motif mutation had any effect upon the cellular localisation or signalling of PAR$_4$. This was investigated in both HEK293 cells and in NCTC-2544 cells.

Firstly, the levels of PAR$_4$ mECFP transiently expressed in HEK293 cells was monitored through Western blotting, using a GFP antibody to detect protein expression, as shown in Figure 4.4. An increase in the concentration of DNA transfected (0-1.5 μg/ml) in the cells resulted in an increase in the expression of two bands (A). The lower band resolved at a protein size of around 65 kDa; around the predicted size for PAR$_4$ (38 kDa) expressing the mECFP (27 kDa) fluorophore. However a second band resolved slightly higher than the predicted 65 kDa band (~70-70 kDa). The cellular localisation of PAR$_4$ mECFP in HEK293 cells was also monitored through confocal microscopy (B). In the HEK293 cells two distinct populations of receptor are observed, one at the membrane (white arrows) and the other in the ER (red arrows).

The possibility that the resolved band may reflect these distinct receptor populations was investigated further using subcellular fractionation (SCF) to isolate plasma membrane, endosomal and ER compartments from the HEK293 cells. Optimisation of the fractionation procedure was required to ensure that sufficient separation of the cellular compartments could be successfully achieved. This was carried out firstly in parental HEK293 cells expressing only ECFP-N1 empty vector, as shown in Figure 4.5, using Na$^+$, K$^+$ATPase, transferrin and calnexin as markers of plasma membrane, endosomal and ER fractions respectively. Separation of membrane material was found to be best around fractions 1-5 with fraction 2 containing the highest level.

Endosomal compartments were found across all 8 fractions, whilst ER isolation was found between fractions 4-7. A positive control for PAR_4 was loaded to demonstrate that no non-specific bands for GFP were detectable at the 65 kDa resolving size for PAR_4 and as expected ECFP was detected through all fractions.

The specificity of the antibodies used for the fractionation experiments were also assessed through indirect immunofluorescence, as shown in Figure 4.6. The images acquired clearly showed endogenous calnexin in pools surrounding the nucleus, whilst transferrin was observed in vesicular structures throughout the cell with Na^+, K^+ ATPase localised at the plasma membrane.

Fractionation of HEK293 cells expressing PAR_4 mECFP is shown in Figure 4.7. Efficient separation of the distinct plasma membrane, endosomal and ER compartments was observed. Transfection of PAR_4 mECFP resulted in the same two band pattern of expression observed previously, however fractionation resulted in the separation of these two bands into different subcellular compartments. The expression of the top band coincided with Na^+, K^+ ATPase membrane fractions 1-2 whilst the lower 65 kDa band was observed across all the fractions with the band intensity increasing in ER/endosomal fractions. This was demonstrated weakly using a low affinity commercial PAR_4-specific antibody but more clearly with a commercial GFP antibody capable of detecting the ECFP tag fused to PAR_4.

```
  1 MWGRLLLWPL VLGFSLSGGT QTPSVYDESG STGGGDDSTP SILPAPRGYP GQVCANDSDT
 61 LELPDSSRAL LLGWVPTRLV PALYGLVLVV GLPANGLALW VLATQAPRLP STMLLMNLAA
121 ADLLLALALP PRIAYHLRGQ RWPFGEAACR LATAALYGHM YGSVLLLAAV SLDRYLALVH


181 PLRARALRGR RLALGLCMAA WLMAAALALP LTLQRQTFRL ARSDRVLCHD ALPLDAQASH
        ↓ ↓   ↓ ↓ ↓
181 PLAAAALAGA ALALGLCMAA WLMAAALALP LTLQRQTFRL ARSDRVLCHD ALPLDAQASH



241 WQPAFTCLAL LGCFLPLLAM LLCYGATLHT LAASGRRYGH ALRLTAVVLA SAVAFFVPSN
301 LLLLLHYSDP SPSAWGNLYG AYVPSLALST LNSCVDPFIY YYVSAEFRDK VRAGLFQRSP
361 GDTVASKASA EGGSRGMGTH SSLLQ
```

Figure 4.3. Site directed mutagenesis of R^{183}AR and R^{188}GRR ER retention motifs located within ICL-2 of VSV-PAR$_4$ mECFP.

Amino acid substitution from arginine to alanine (R→A) was achieved through site directed mutagenesis as outlined in Chapter 2.3.2. This was carried out at the indicated sites (red) within the PAR$_4$ protein sequence in a VSV-PAR$_4$ mECFP fluorescent construct to create R^{183}AR →A^{183}AA (RAR mut), R^{188}GRR →AGAA (RGRR mut) and a double motif mutant R^{183}AR xx R^{188}GRR → A^{183}AA xx A^{188}GAA (DM mut).

(A)
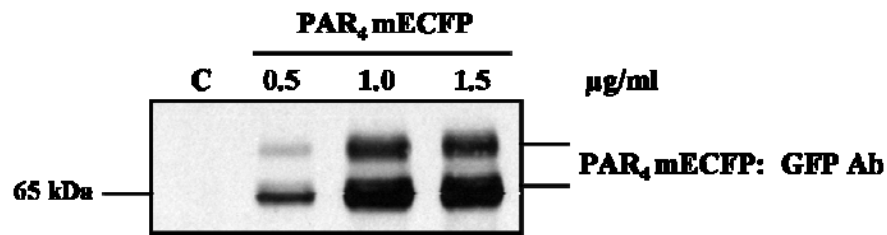
(B)
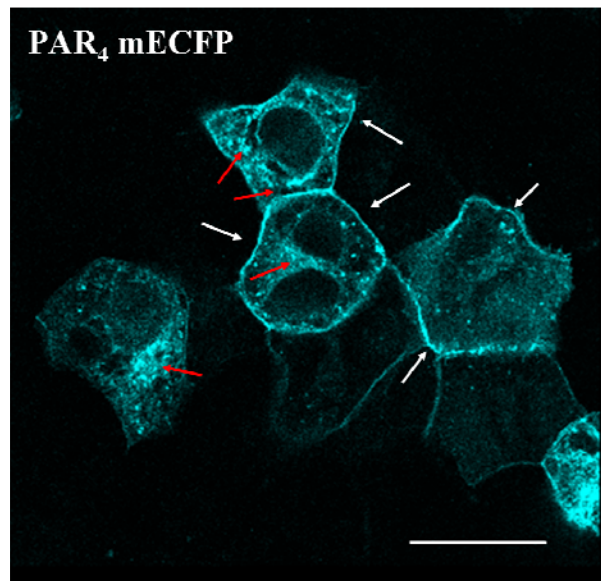
Figure 4.4. Expression of PAR$_4$ mECFP in HEK293 cells.

PAR$_4$ mECFP was transiently transfected as indicated for 24 hours in (A) HEK293 cells as outlined in Chapter 2.5, prior to serum starvation for a further 24 hours. Whole cell lysates were prepared and resolved by Western blotting as described in Chapter 2.8.2. PAR$_4$ mECFP (predicted band size ~65 kDa) was detected using a polyclonal GFP antibody capable of recognising the ECFP at the C-terminal of PAR$_4$. (B) The different receptor populations of PAR$_4$ mECFP was monitored by confocal microscopy (scale bar = 10 μm) as outlined in Chapter 2.6. Membrane expression was highlighted by white arrows whilst the red arrows represent intracellular retained receptor. These blots and images are representative of at least three independent experiments.
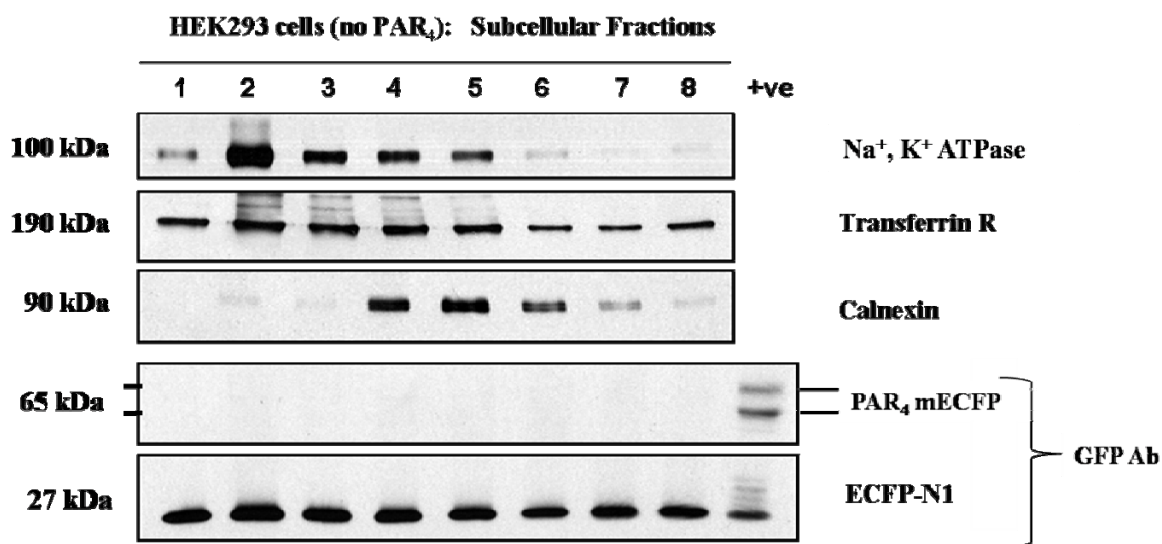
Figure 4.5. Subcellular fractionation (SCF) of plasma membrane, endosomal and endoplasmic reticulum (ER) compartments in HEK293 cells.

Subcellular fractionation was carried out in HEK293 cells expressing ECFP-N1 using differential ultra-centrifugation on a density gradient as outlined in Chapter 2.8.6. Fractions of 300 µl (1-8 shown above) were resolved by Western blotting as described in Chapter 2.8.2. Na^+, K^+ ATPase (~100 kDa), transferrin receptor (~190 kDa) and calnexin (90 ~kDa) antibodies were used for the detection of membrane, endosomal and ER compartments respectively. ECFP (~27 kDa) was detected using GFP antibody. A positive control (HEK293 cells expressing PAR$_4$ mECFP) was loaded to demonstrate specificity of the GFP antibody. These blots are representative of at least two independent experiments.
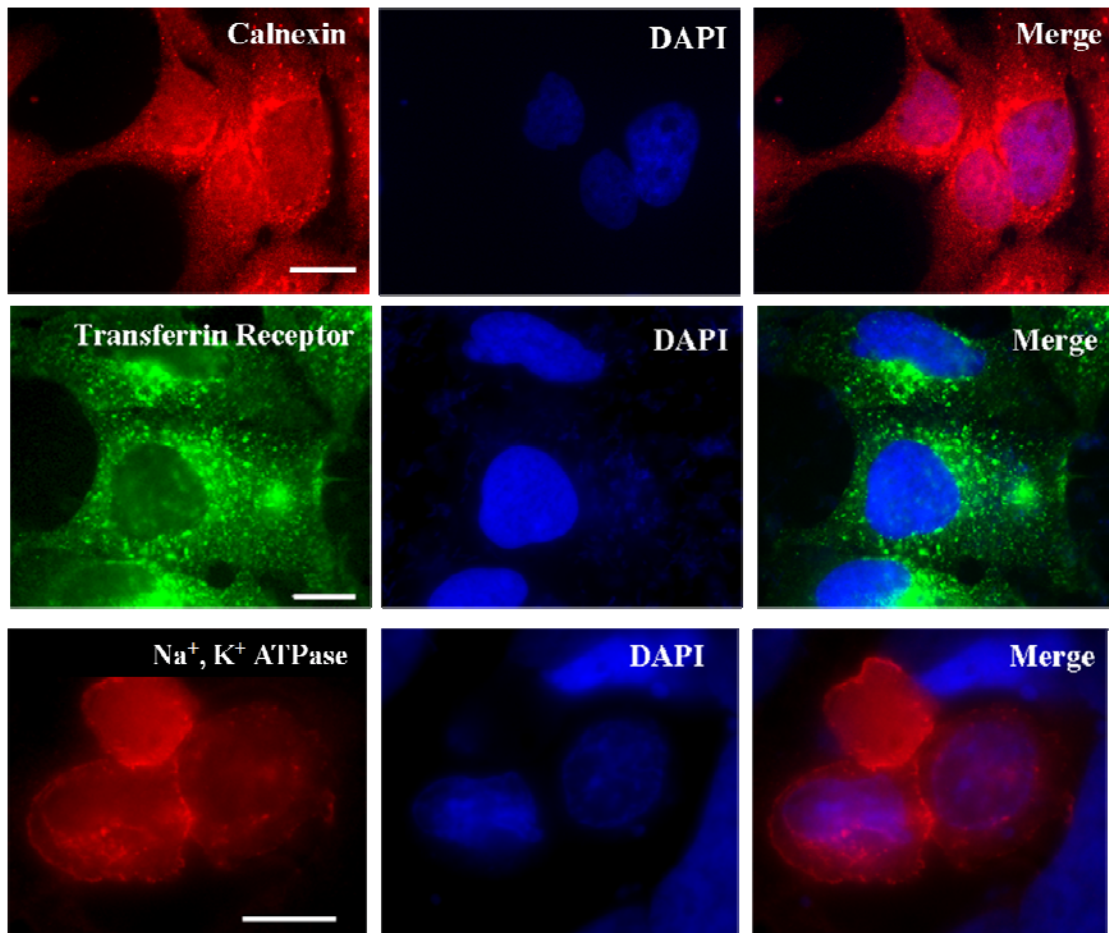
Figure 4.6. Indirect Immunofluorescence to detect endogenous Na$^+$, K$^+$ ATPase, transferrin receptor and calnexin in HEK293 cells.

HEK293 cells were grown to 80% confluence on coverslips, serum starved for 24 hours prior to indirect immunofluorescence as outlined in Chapter 2.6.3. Na$^+$, K$^+$ ATPase, transferrin receptor and calnexin antibodies were used to demonstrate the plasma membrane, endosomal and ER localisation of the respective proteins in HEK293 cells. Images were acquired using epifluorescence microscopy at 100x magnification (scale bar = 10 μm). Images are representative of at least two independent experiments.
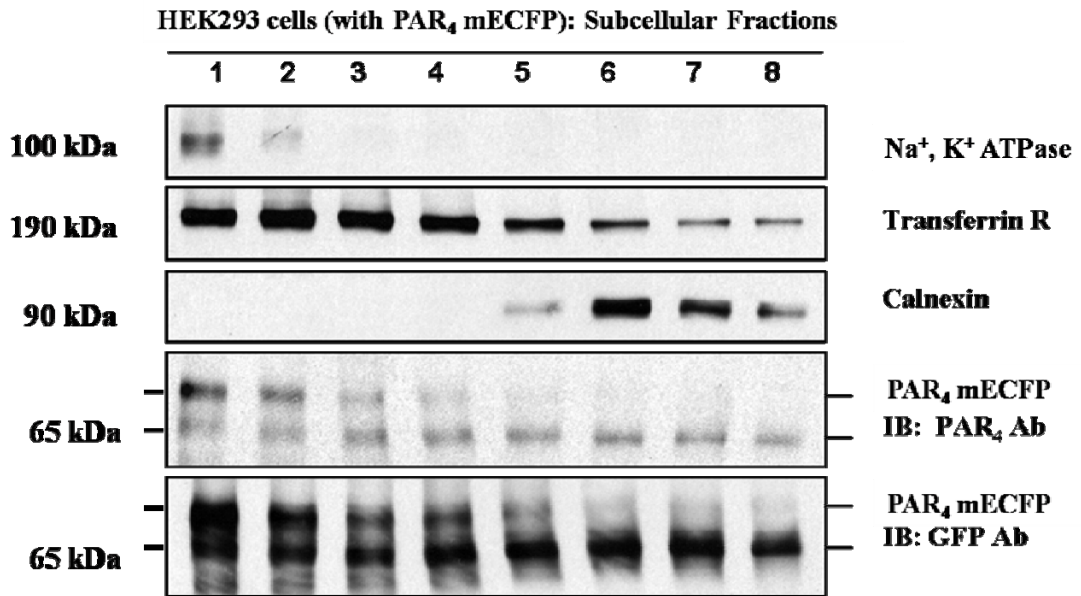
Figure 4.7. Fractionation of membrane, endosomal and ER compartments in HEK293 cells expressing PAR₄ mECFP.

HEK293 cells were transiently transfected with PAR₄ mECFP for 24 hours, serum starved for a further 24 hours prior to subcellular fractionation as described in Chapter 2.8.6. Fractions of 300 μl (1-8 as shown above) were resolved by Western blotting as outlined in Chapter 2.8.2. Na⁺, K⁺ ATPase (~100 kDa), transferrin receptor (~190 kDa) and calnexin (90 ~kDa) antibodies were used for the detection of plasma membrane, endosomal and ER fractions. PAR₄ mECFP (predicted band size of ~65 kDa) was detected using a PAR₄-specific antibody and a GFP antibody. These blots are representative of at least two independent experiments.

4.2.1 Investigating the protein expression of the ER motif mutants in HEK293 cells

The expression pattern of VSV-PAR$_4$ mECFP was compared to the corresponding ER motif mutants. Using the VSV-PAR$_4$ mECFP and ER motif mutated variants, the pattern of protein expression of PAR$_4$ was assessed in HEK293 whole cell lysates resolved through Western blotting. As Figure 4.8 (A) shows, unmodified wild type (WT) VSV-PAR$_4$ mECFP transfection resulted in the two forms of PAR$_4$; the 65 kDa band and the higher band resolving around 70-80 kDa, as previously observed in Figure 4.4. Transfection of the RAR mutant resulted in a similar band pattern, however the upper band appeared to be expressed less in comparison to WT. Following transfection of the RGRR motif mutant and the double motif mutant (DM) PAR$_4$ constructs only the 65 kDa protein band was expressed, with no expression of the upper band detected. Corresponding microscopy experiments, as shown in Figure 4.8 (B) demonstrated that whilst WT and RAR mutated PAR$_4$ protein was expressed both at the membrane (white arrows) and in the ER (red arrows), only ER retained PAR$_4$ was observed when RGRR or the DM mutants were expressed.

(A)

(B)
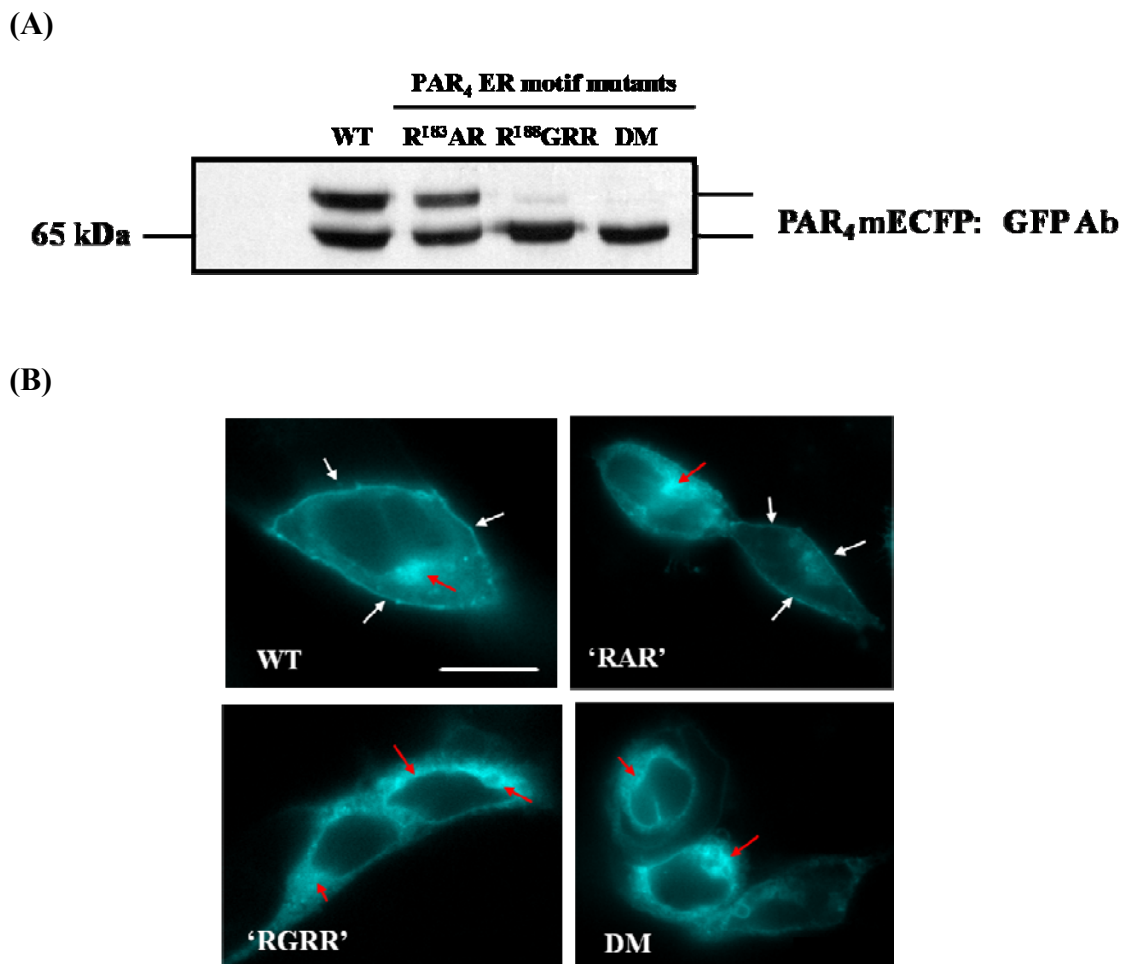
Figure 4.8. Expression of ER retention motif mutants in HEK293 cells.

HEK293 cells grown in plates and on coverslips and transiently transfected with PAR$_4$ mECFP or ER motif mutant constructs as indicated above, for 24 hours prior to serum starvation for a further 24 hours. (A) Whole cell lysates were prepared and resolved by Western blotting as outlined in Chapter 2.8.2. PAR$_4$ receptor expression (~65 kDa and/or 73 kDa) was detected using a GFP antibody. (B) The transfected cells grown on coverslips were also prepared for epifluorescence microscopy as outlined in Chapter 2.6.1. Corresponding images were acquired at 100x magnification (scale bar = 10 μm). The localisation of the ER mutants was compared to wild type (WT) VSV-PAR$_4$ mECFP with membrane (white arrows) and intracellular expression (red arrows) highlighted. Experiments are representative of at least three others.

4.3 Investigating the signalling capacity of PAR$_4$ in HEK293 cells following mutation of the potential ER retention motifs

Following the microscopy experiments carried out previously, the ability of the ER motif mutant PAR$_4$ proteins to mediate signal transduction was tested in HEK293 cells following agonist treatment with PAR$_4$ activating peptide AYPGKF-NH$_2$ or thrombin. Measurement of total inositol phosphate (InsP$_{1-4}$) accumulation and ERK1/2 phosphorylation were used as markers of receptor activation.

Figure 4.9 shows AYPGKF-NH$_2$-mediated inositol phosphate responses in HEK293 cells expressing VSV-PAR$_4$ mECFP, RAR, RGRR or DM mutant PAR$_4$ proteins. Following stimulation with various concentrations of activating peptide (AP), an increase in the total inositol phosphate response was observed in cells expressing VSV-PAR$_4$ mECFP. This response was maximal following treatment with AP (50 μM), with an increase in inositol phosphate observed around 33.498 ± 2.080 fold of basal. Despite membrane expression of the RAR mutant in previous microscopy experiments, the response following receptor activation was negligible, with an increase of 2.355 ± 0.730 fold of basal observed following treatment with 100 μM of AP. As expected, no increase in inositol phosphate was observed downstream of RGRR and DM mutant activation at all AP concentrations tested (max concentration responses = 0.602 ± 0.130 and 0.806 ± 0.019 fold respectively).

A similar approach was adopted to measure thrombin-mediated inositol phosphate responses. As Figure 4.10 shows, increasing the concentration of thrombin resulted in an increase in the total inositol phosphate accumulation in cells expressingVSV-PAR$_4$ mECFP (peak response at 5 U/ml = 17.456 ± 7.362 fold). Unlike the responses observed for the AP, the RAR mutant resulted in a small increase in inositol phosphate response when stimulated with thrombin at all concentrations tested (peak response at 3 U/ml = 7.781 ± 4.888 fold). Again, as demonstrated in the previous experiment the inositol phosphate responses observed following stimulation of cells expressing the RGRR or DM mutant were negligible (peak responses at 5 U/ml = 2.370 ± 0.640 and 1.891 ± 0.294 fold respectively).

Following on from the inositol phosphate experiments carried out, the ability of the PAR_4 ER mutants to signal to ERK following receptor activation was tested in HEK293 cells, as shown in Figure 4.11. Stimulation of parental HEK293 cells (A) with various concentrations of thrombin for 5 minutes resulted in clear PAR_1-mediated ERK activation, even at low concentrations of thrombin treatment (0.1 U/ml). Over-expression of VSV-PAR_4 mECFP (B) resulted in ERK1/2 phosphorylation, with maximum responses observed following 3-5 U/ml of thrombin treatment. This increase was similarly observed in RAR mutant-expressing cells (C) which peaked following 3 U/ml thrombin treatment. Agoinst treatment of cells expressing the PAR_4 RGRR mutant (D) resulted in an ERK response that peaked initially at 0.3 U/ml then again following 3 U/ml thrombin treatment. DM mutant expression (E) resulted in an ERK response corresponding to that observed in parental HEK293 cells following thrombin treatment.

Due to the lack of membrane expression and loss of cell signal transduction observed in cells expressing either RGRR or DM motif mutants, only cells expressing the RAR mutant were investigated further in the HEK293 cell model. The endogenous PAR_1 expressed in the HEK293 cell model made interpretation of ER mutant expression difficult in terms of the effect of receptor activation following thrombin stimulation. As a result, only signal transduction downstream of AP-mediated receptor activation was assessed. In addition the duration of PAR_4-mediated responses was addressed and compared to the corresponding RAR mutant signal. This time the markers of receptor activation included PAR_4-mediated JNK, p38 and ERK phosphorylation, as shown in Figure 4.12. In comparison to parental HEK293 cells, cells expressing WT PAR_4 (without the CFP tag) resulted in an increase in JNK1/2 activation, reaching maximal levels within 5 minutes and with no obvious sign of signal termination even at 120 minutes of AYPGKF-NH_2 treatment. Following similar treatment in cells expressing either VSV-PAR_4 mECFP or the RAR mutant JNK activation was not observed until between 60 and 120 minutes post agonist treatment.

A similar approach was adopted in assessing activation of p38 MAP kinase. As shown in Figure 4.12 (B), treatment with AYPGKF-NH$_2$ (100 µM) resulted in a p38 response in VSV-PAR$_4$ mECFP expressing cells, reaching maximal levels within 15 minutes of receptor activation. Cells expressing either VSV-PAR$_4$ mECFP or the RAR mutant resulted in an increase in the basal p38 levels which remained unchanged following receptor activation.

The most notable difference in signalling between VSV-PAR$_4$ mECFP and the RAR mutant was observed during AYPGKF-NH$_2$-mediated ERK phosphorylation. As Figure 4.12 (C) demonstrates, following agonist stimulation of either WT PAR$_4$ or VSV-PAR$_4$ mECFP expressing cells, the onset of ERK activation occurs within 5 minutes of treatment with the signal only reaching near-basal levels after 120 minutes. In contrast, ERK phosphorylation downstream of RAR mutant activation with AP resulted in a low-level response at 30 minutes returning to basal levels thereafter. In order to ensure that the differences in signalling observed were not a result of variable receptor expression level following transient transfection, the corresponding PAR$_4$ protein levels were determined through reprobe with a GFP antibody, Figure 4.12 (D). The two forms of PAR$_4$ (65 kDa and 73 kDa bands) were clearly observed with no change in the expression of either band detected following agonist treatment. In addition, the levels of expression between WT VSV-PAR$_4$ mECFP and the RAR mutant were the same.
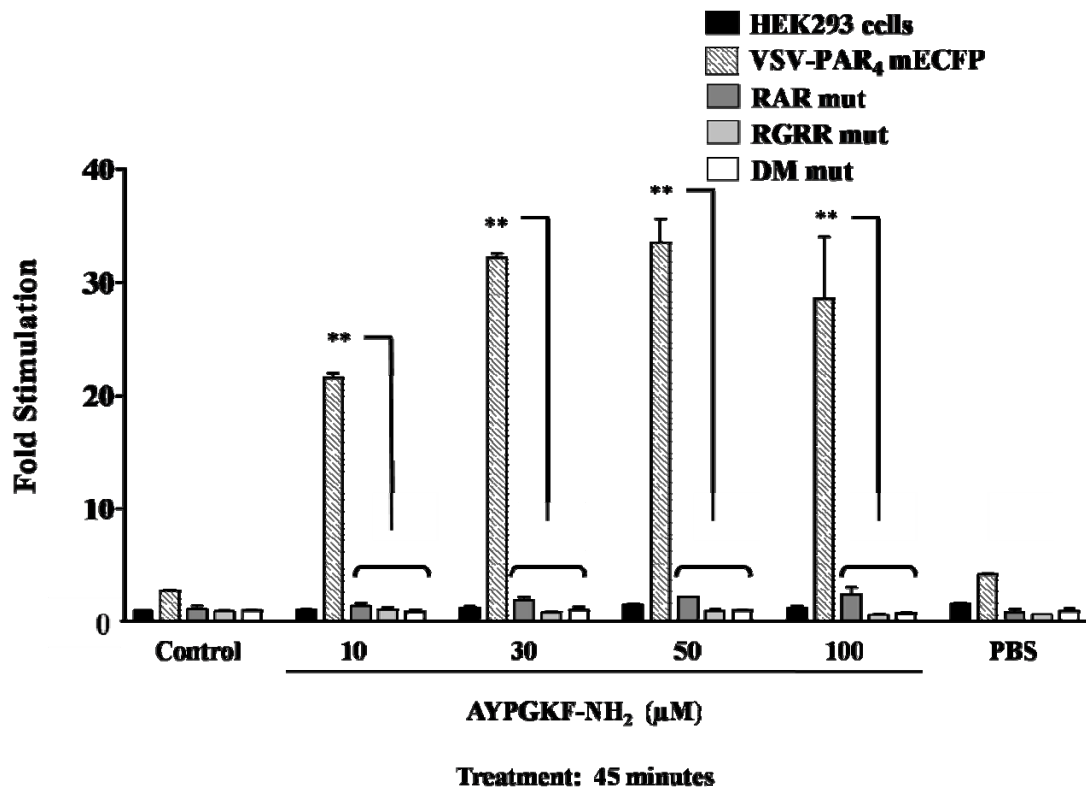
Figure 4.9. AYPGKF-NH$_2$-mediated [^{3}H]-inositol phosphate accumulation in HEK293 cells expressing WT or ER mutant VSV-PAR$_4$ mECFP constructs.
HEK293 cells were transiently transfected for 24 hours with VSV-PAR$_4$ mECFP or ER motif mutants (1 μg/ml) shown above, as outlined in Chapter 2.5. The media was replaced with serum free growth media supplemented with 0.25 μCi of [^{3}H]-2-myo-inositol for a further 24 hours. Cells were pre-treated with 10 mM lithium chloride for 15 minutes prior to stimulation with AYPGKF-NH$_2$ as indicated. Total inositol phosphate (InsP$_{1-4}$) accumulation was measured as described in Chapter 2.9. The data presented represent values measured in triplicate (mean ± s.e.m.) over two independent experiments (**p=<0.01, n.s. = not significant relative to HEK293 control unstimulated cells).
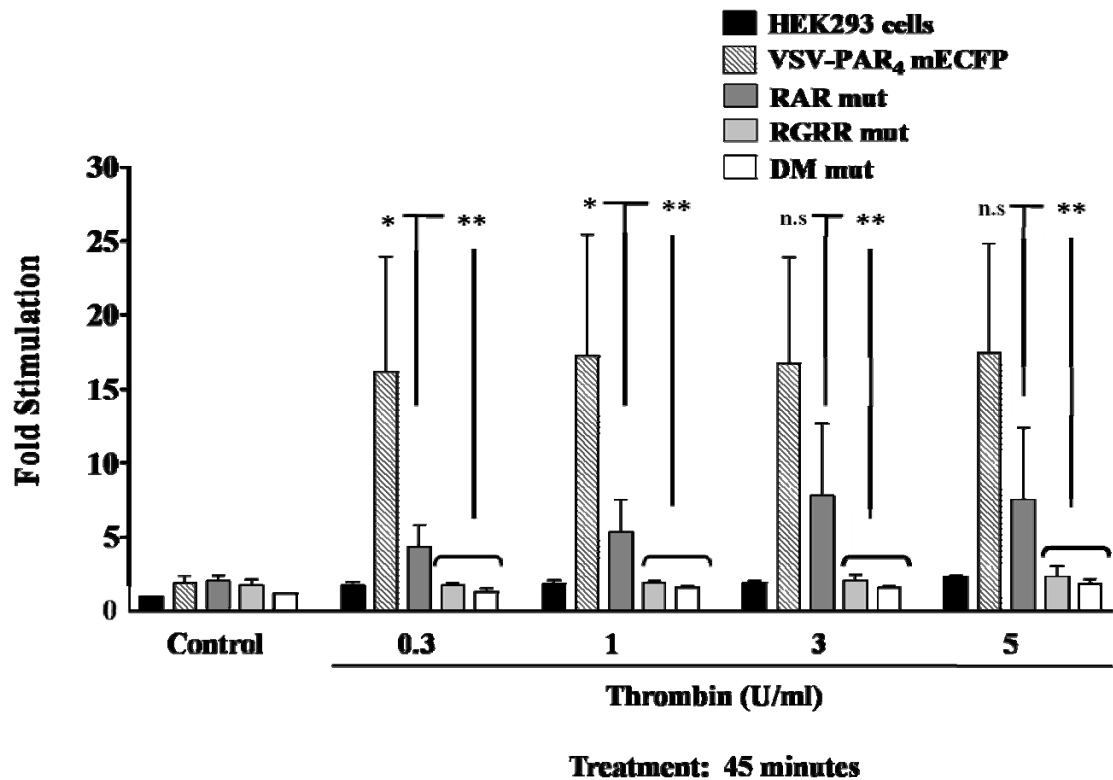
Figure 4.10. Thrombin-mediated [³H]-inositol phosphate accumulation in HEK293 cells expressing WT or ER mutant VSV-PAR₄ mECFP constructs.

HEK293 cells were transiently transfected for 24 hours with VSV-PAR₄ mECFP or ER motif mutants (1 µg/ml) shown above, as outlined in Chapter 2.5. The media was replaced with serum free growth media supplemented with 0.25 µCi of [³H]-2-myo-inositol for a further 24 hours. Cells were pre-treated with 10 mM lithium chloride for 15 minutes prior to stimulation with thrombin as indicated. Total inositol phosphate ($InsP_{1-4}$) accumulation was measured as described in Chapter 2.9. The data represents values measured in triplicate (mean ± s.e.m.) over three independent experiments (*p=<0.05, **p=<0.01, n.s. = not significant).

(A) Parental HEK293 cells

pERK1/2

Total ERK1/2

C   0.1   0.3   1   3   5   (U/ml)

Thrombin (5 minutes)
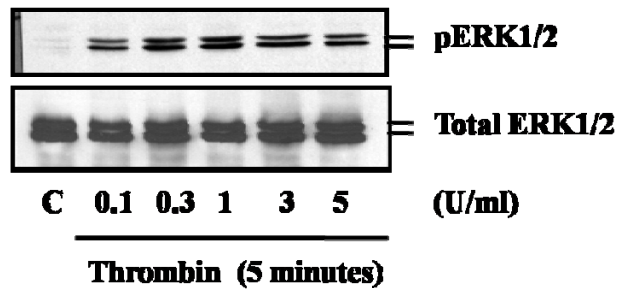
(B) VSV-PAR₄ ECFP expressed in HEK293 cells

pERK1/2

Total ERK1/2

VSV-PAR₄ mECFP

C   0.1   0.3   1   3   5   (U/ml)

Thrombin (5 minutes)

(C) RAR motif mutant expressed in HEK293 cells

pERK1/2

Total ERK1/2

VSV-PAR₄ mECFP

C   0.1   0.3   1   3   5   (U/ml)
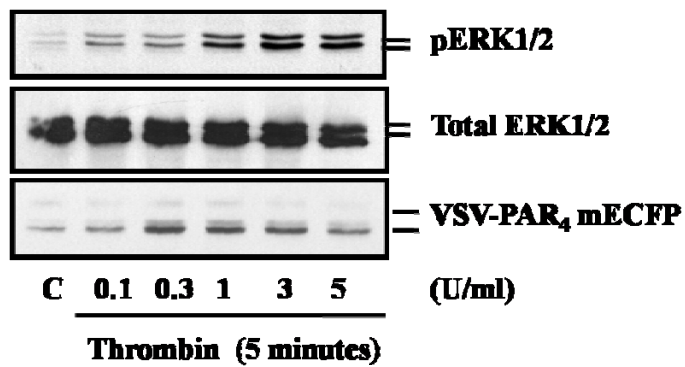
Thrombin (5 minutes)
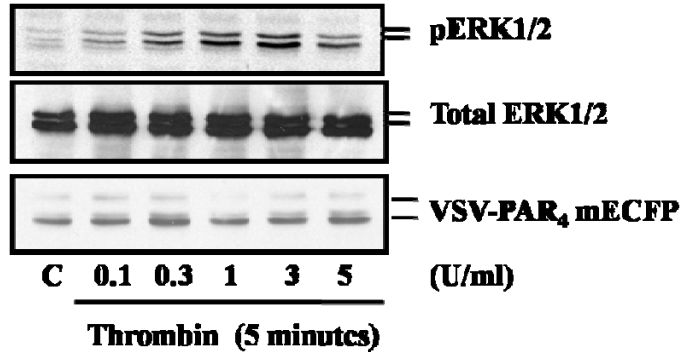
(D) RGRR motif mutant expressed in HEK293 cells
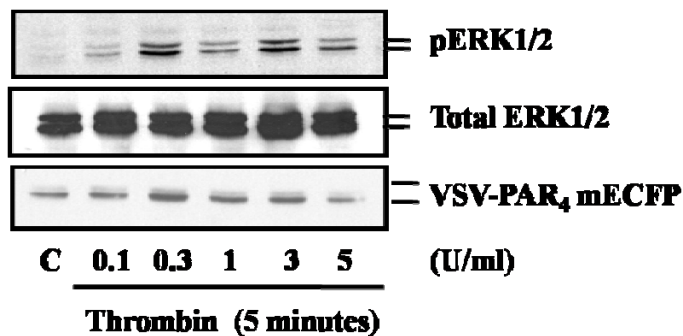
(E) DM mutant expressed in HEK293 cells
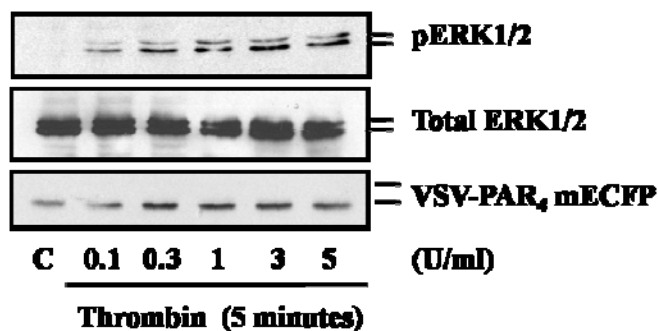
Figure 4.11. Thrombin-mediated phosphorylation of ERK in HEK293 cells expressing VSV-PAR$_4$ mECFP or ER motif mutants.

HEK293 cells were grown in plates and transiently transfected for 24 hours with VSV-PAR$_4$ mECFP or ER motif mutants (1 µg/ml) as outlined in Chapter 2.5. Cells were serum starved for a further 24 hours prior to stimulation with thrombin (U/ml) as indicated for 5 minutes. Whole cell lysates were prepared and proteins resolved by Western blotting as described in Chapter 2.8.2. Activation of ERK (A-E) was detected through use of a phospho-ERK1/2 specific antibody (44/42 kDa protein bands) with membranes reprobed for total ERK1/2 as an indicator of equal protein load (A-E). Expression of VSV-PAR$_4$ mECFP (~65 kDa) and corresponding ER motif mutants were measured through detection of the attached ECFP tag by a GFP antibody (B-E). Experiments are representative of two others.

(A)
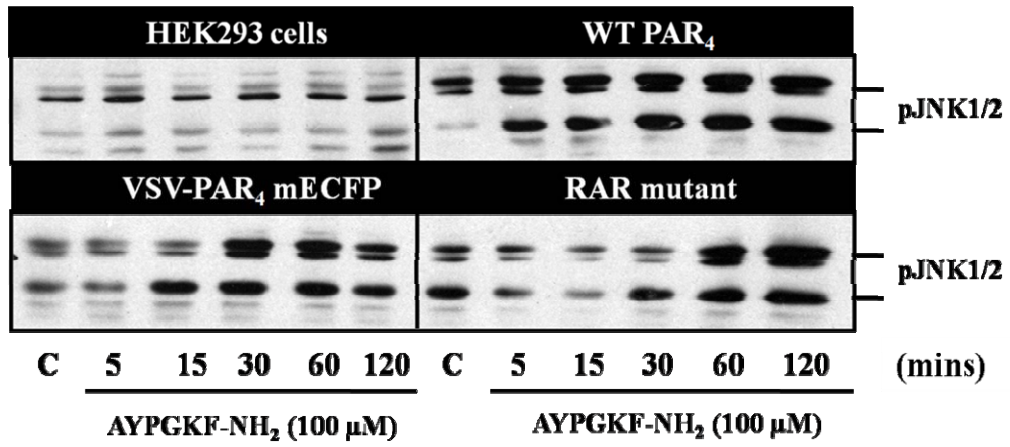
(B)
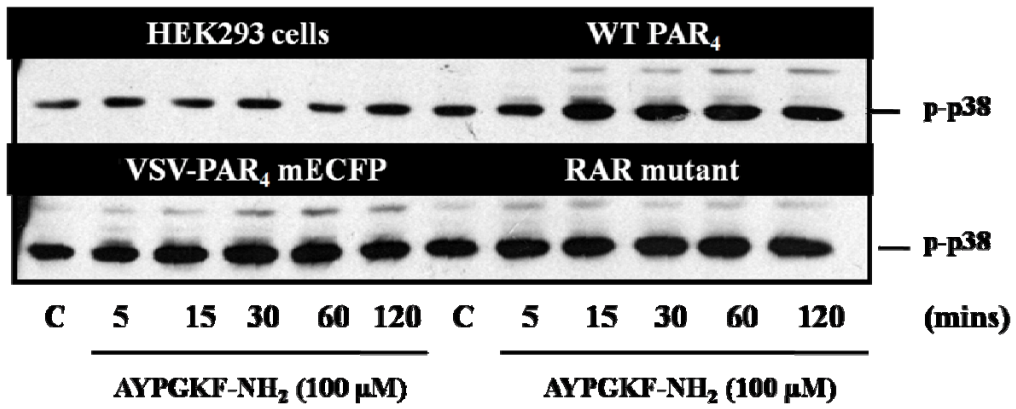
(C)
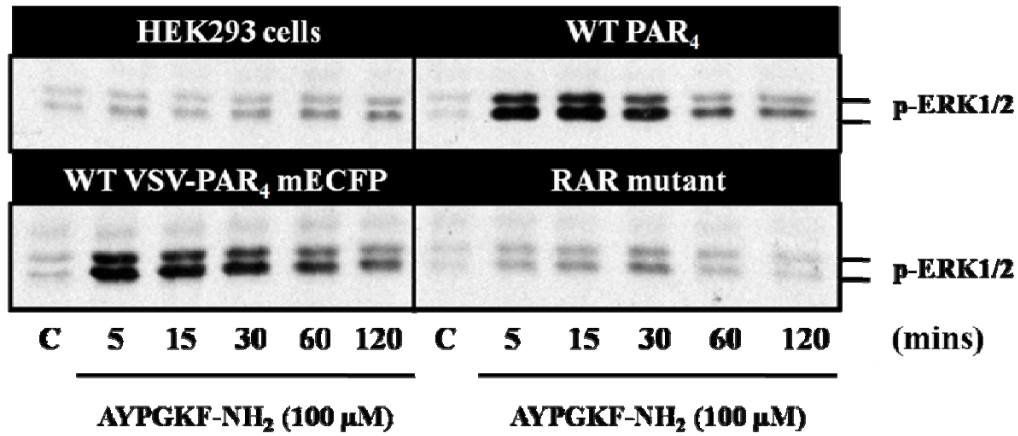
(D)
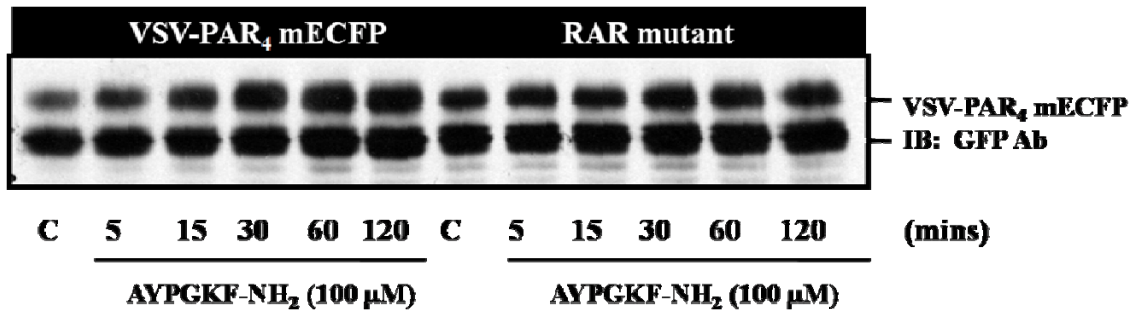
Figure 4.12. AYPGKF-NH₂-mediated phosphorylation of JNK, p38 MAPK and ERK in HEK293 cells expressing VSV-PAR₄ mECFP or the RAR motif mutant.
HEK293 cells were grown in plates and transiently transfected for 24 hours with WT PAR₄, VSV-PAR₄ mECFP or the RAR motif mutant (1 µg/ml) as outlined in Chapter 2.5. Cells were serum starved for a further 24 hours prior to stimulation with AYPGKF-NH₂ (100 µM) as indicated. Whole cell lysates were prepared and proteins resolved by Western blotting as described in Chapter 2.8.2. Activation of JNK (A), p38 MAP kinase (B) and ERK (C) were detected through use of phospho-specific antibodies with membranes reprobed for GFP as an indicator of transfection efficiency (D). Experiments are representative of at least two others.

148

4.4 PAR$_4$ localisation and signalling in NCTC-2544 cells

Having established that the ER motif mutants differ considerably in terms of receptor expression and signalling capabilities, the effect of ER motif mutation was similarly investigated in the NCTC-2544 cell line. Initially the expression of VSV-PAR$_4$ mECFP was assessed in NCTC-2544 cells following transient transfection, with protein expression levels determined through Western blot analysis.

As illustrated in Figure 4.13 (A), increasing the concentration of PAR$_4$ mECFP DNA in the NCTC-2544 cells resulted in an increase in the expression of the 65 kDa band being resolved, similar to that observed in the HEK293 cell expression model. However, one notable feature of PAR$_4$ protein expression in the NCTC-2544 cells was the absence of the upper band that was observed following similar expression in HEK293 cells. Using confocal microscopy (B), the expression of PAR$_4$ was predominantly intracellular (indicated by red arrow) in the NCTC-2544 cells, as previously demonstrated in Chapter 3, with very minimal membrane expression detected. Based upon the pattern of PAR$_4$ protein expressed in NCTC-2544 cells, the signalling capacity of PAR$_4$ was investigated further in this cell type.

Using the inositol phosphate assay as a marker for receptor activation, treatment of parental NCTC-2544 cells with thrombin or AYPGKF-NH$_2$ did not result in a significant increase in the inositol phosphate signal (1.868 ± 0.431 and 1.270 ± 0.215 fold of basal respectively). As shown in Figure 4.14, stable expression of PAR$_4$ in NCTC-2544 cells (NCTC PAR$_4$ cells) resulted in a low level signal in response to thrombin (4.184 ± 0.826) or AYPGKF-NH$_2$ (3.147 ± 0.900) treatment. NCTC-2544 cells transiently expressing WT PAR$_4$ or PAR$_4$ mECFP generated the highest inositol phosphate responses following activation with thrombin (10.571 ± 1.613 and 8.802 ± 2.611) or AP (8.815 ± 0.783 and 7.754 ± 2.364). Whilst these responses appear to be substantial when taking into consideration the low level of membrane receptor detected in this cell type, they are considerably lower than those responses observed in similar experiments carried out in the HEK293 cell model (typical responses between 20-30 fold of basal), where PAR$_4$ at the cell surface was notably higher.

In addition to the inositol phosphate assay, PAR_4 mediated signalling was investigated further in NCTC-2544 cells. As shown in Figure 4.15 A and B, ERK1/2 phosphorylation was negligible (peak response at 15 minutes, 1.611 ± 0.141 fold of basal) in parental cells following treatment with $AYPGKF-NH_2$ (100 μM). In cells expressing PAR_4 mECFP, a transient ERK1/2 response was observed following agonist treatment, which peaked at 5 minutes (4.497 ± 0.309 fold) returning to basal thereafter. Similar to the results observed in the inositol phosphate assay, these ERK responses were lower than those observed in the HEK293 cell line (typical values >10-15 fold of basal)

(A)
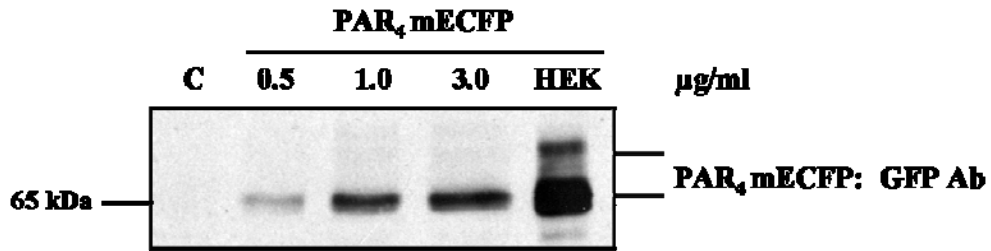
(B)
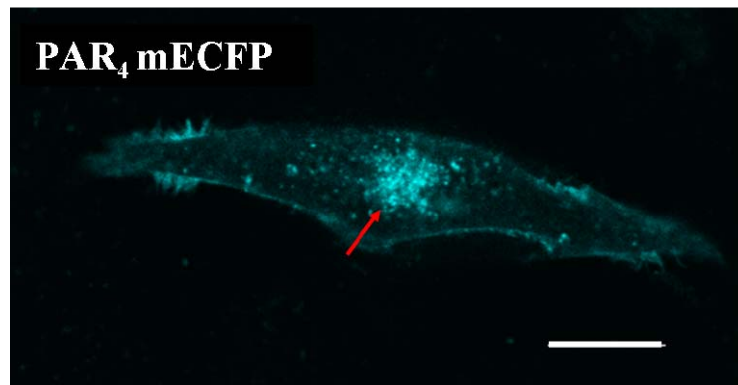
Figure 4.13. Expression of PAR$_4$ mECFP in NCTC-2544 cells.

PAR$_4$ mECFP was transiently transfected as indicated for 24 hours in (A) NCTC-2544 cells as outlined in Chapter 2.5, prior to serum starvation for a further 24 hours. Whole cell lysates were prepared and resolved by Western blotting as described in Chapter 2.8.2. PAR$_4$ mECFP (predicted band size ~65 kDa) was detected using a polyclonal GFP antibody capable of recognising the ECFP at the C-terminal of PAR$_4$. A HEK293 cell sample expressing PAR$_4$ mECFP (1 µg/ml) was loaded alongside samples prepared for NCTC-2544 cells as a positive control. (B) The expression of PAR$_4$ mECFP was monitored by confocal microscopy (scale bar = 10 µm) as outlined in Chapter 2.6. Intracellular expression (red arrow) has been highlighted. These blots and image are representative of at least three independent experiments.
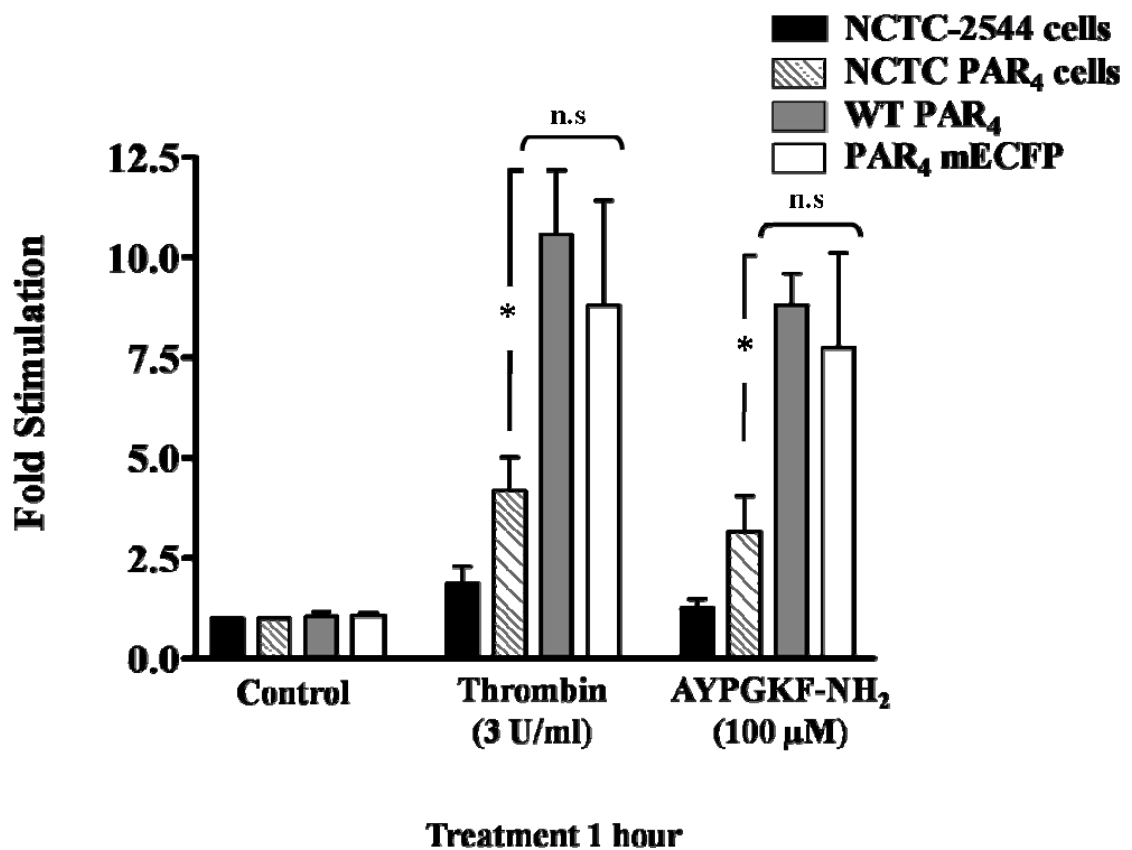
Figure 4.14. PAR$_4$-mediated [^{3}H]-inositol phosphate accumulation in NCTC-2544 cells.

NCTC-2544 cells were transiently transfected for 24 hours with WT PAR$_4$ or PAR$_4$ mECFP shown above, as outlined in Chapter 2.5. The media was replaced with serum free growth media supplemented with 0.25 µCi of [^{3}H]-2-myo-inositol for a further 24 hours prior. Cells were pre-treated with 10 mM lithium chloride for 15 minutes prior to stimulation with thrombin or AYPGKF-NH$_2$ as indicated. Total inositol phosphate (InsP$_{1-4}$) accumulation was measured through anion exchange as described in Chapter 2.9. The data presented represent values taken in triplicate (mean ± s.e.m.) over three independent experiments(*p=<0.05, **p=<0.01).

(A)
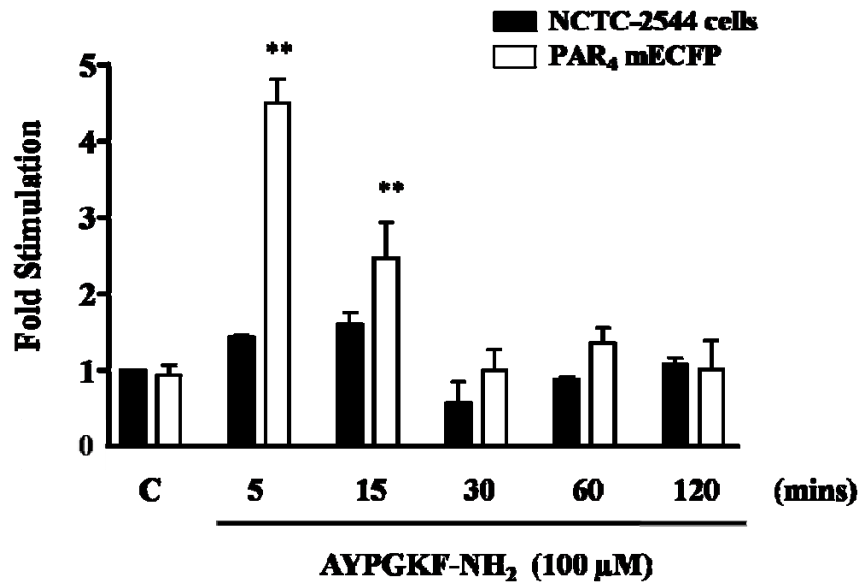
(B)
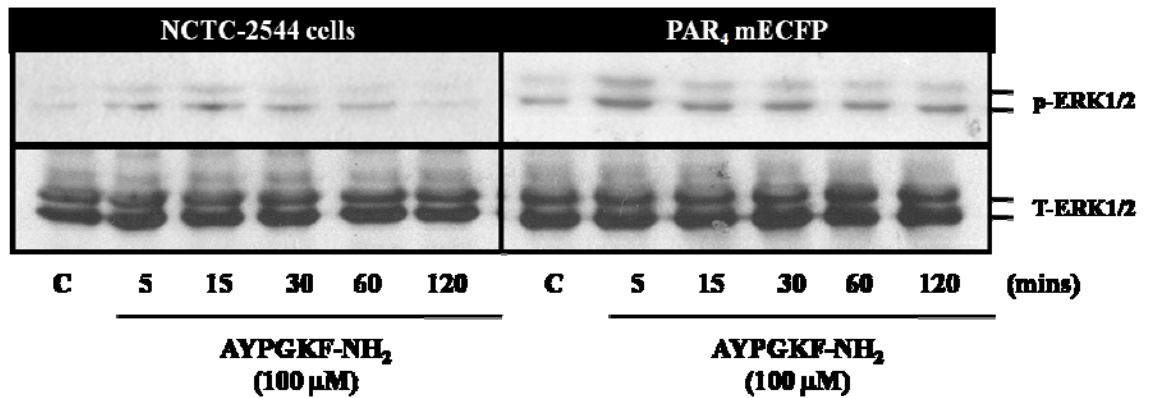
Figure 4.15. PAR₄-mediated phosphorylation of ERK in NCTC-2544 cells

NCTC-2544 cells were transiently transfected with PAR₄ mECFP for 24 hours as outlined in Chapter 2.5. The media was replaced with serum free media for a further 24 hours prior to stimulation with AYPGKF-NH₂ (100 μM) as indicated. ERK1/2 activation was measured in whole cell lysates resolved by Western blotting, as described in Chapter 2.8.2. This was carried out in parental NCTC-2544 (black bars) and in cells expressing PAR₄ mECFP (white bars). Blots shown are representative of at least two others (**p=<0.01).

4.5 Investigating the cellular localisation of PAR$_4$ in NCTC-2544 cells following mutation of the potential ER retention motifs

The cell specific differences in PAR$_4$ expression have been clearly demonstrated between the HEK293 and NCTC-2544 cell models used in this study (see Chapter 3). As a result, the expression of the ER mutants had to be investigated in NCTC-2544 cells similar to those experiments carried out in the HEK293 cell model.

Figure 4.16 (A) highlights the protein bands resolved in HEK293 cells expressing VSV-PAR$_4$ mECFP or the ER motif mutants. When resolved, the 65 kDa protein band was observed for all constructs tested, however the expression level between PAR$_4$ mECFP and the ER mutants was considerably different. When PAR$_4$ mECFP was expressed this time a faint band was observed just above the 65 kDa band, which was also observed for the RAR mutant. The 65 kDa band for the RAR mutant was expressed less well than the PAR$_4$ mECFP protein. This in turn was even lower for the RGRR mutant, with the lowest expression level observed for the DM mutant.

A surprising feature of the ER mutants was noted during fluorescence microscopy experiments carried out for cells expressing the ER mutants, shown in Figure 4.16 (B). As previously observed, PAR$_4$ mECFP was found to exist predominantly in the ER, however expression of the RAR mutant was found to be distinctly at the plasma membrane. Both RGRR and DM mutants were retained inside the cell. However it should be noted that over all of the microscopy experiments carried out for the ER mutants, the DM mutant protein was poorly expressed in the NCTC-2544 cells.

The intriguing nature of RAR mutant expression, i.e. one clear band resolved by Western blotting yet distinctive membrane expression observed in the microscopy experiments resulted in the Western blotting experiments being re-visited. The effect of increasing the concentration of RAR mutant DNA transfected into the NCTC-2544 cells was observed by Western blotting, as shown in Figure 4.17 (A). As the concentration of DNA transfected increased, so did the expression of the PAR$_4$ 65 kDa band. However, above this band a second diffuse band was resolved, not unlike the one observed for HEK293 cell expression. In addition, protein expression at the

65 kDa marker appeared to highlight two bands very close together, as indicated by the red arrow (see 0.5 µg/ml); a feature that may affect the subsequent localisation of PAR$_4$. When the expression of the RAR mutant was assessed using confocal microscopy (B), a notable increase in PAR$_4$ was observed at the plasma membrane when compared to PAR$_4$ mECFP expression. Subsequent subcellular fractionation of NCTC-2544 cells expressing PAR$_4$ mECFP or the PAR$_4$ RAR ER motif mutant (Figure 4.17 C) identified differences in the localisation of the molecular species of the protein bands resolved for PAR$_4$. The 65 kDa band for both appeared to correspond with calnexin/tranferrin fractions, indicative of ER/endosomal localisation, with lower levels of protein in plasma membrane fractions. However the higher molecular weight band resolved in cells expressing the RAR motif mutant was more pronounced in endosomal/plasma membrane fractions containing transferrin/Na$^+$,K$^+$ATPase with only weak levels detected in ER fractions, thus corresponding well with observations made in previous confocal experiments.

(A)

(B)
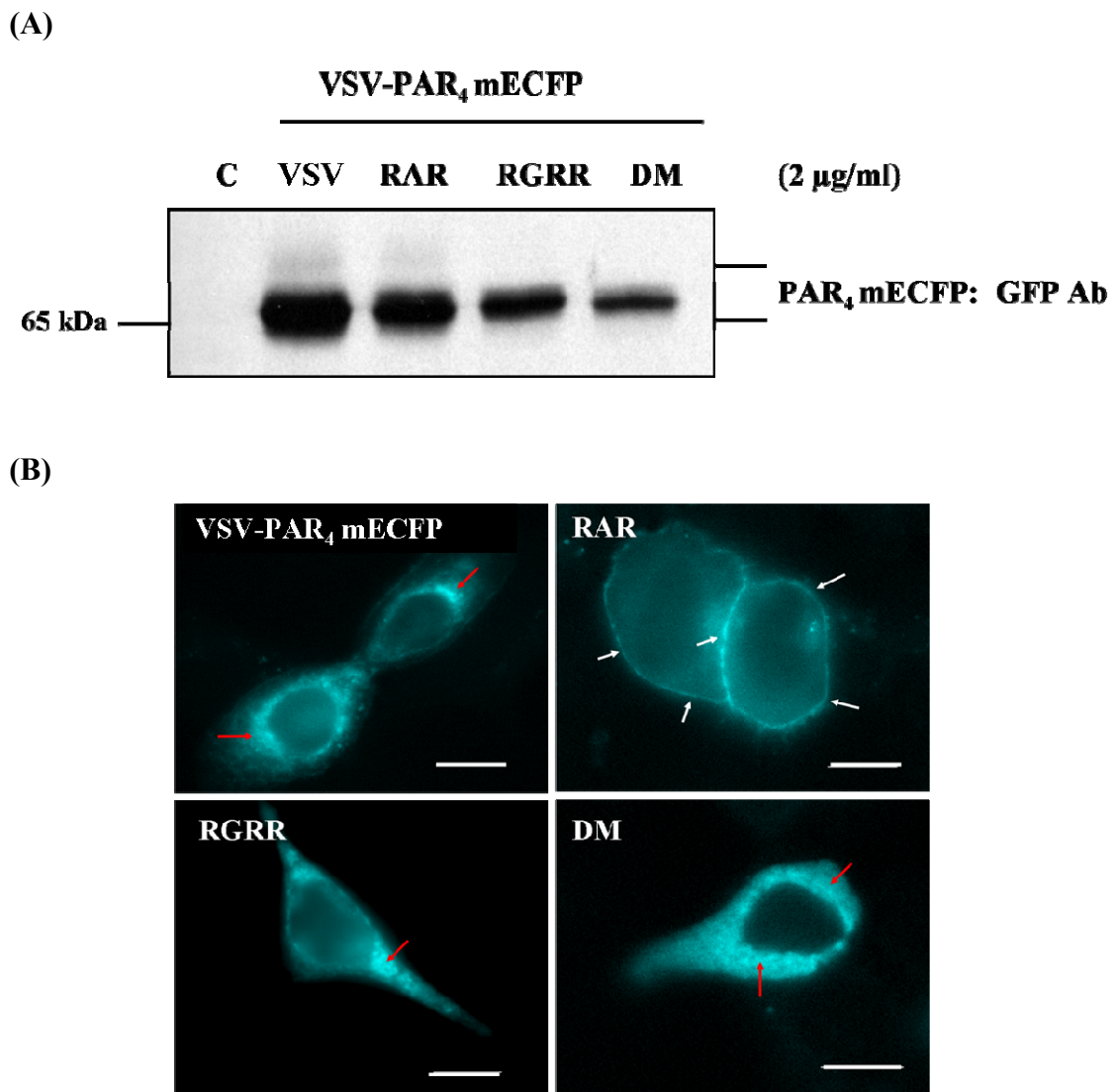
Figure 4.16. Expression of ER retention motif mutants in NCTC-2544 cells.
NCTC-2544 cells were grown in plates and on coverslips and transiently transfected with VSV-PAR$_4$ mECFP (VSV) or ER motif mutant constructs as indicated above, for 24 hours prior to serum starvation for a further 24 hours. (A) Whole cell lysates were prepared and resolved by Western blotting as outlined in Chapter 2.8.2. PAR$_4$ receptor expression (~65 kDa) was detected using a GFP antibody. (B) Transfected cells grown on coverslips were prepared for epifluorescence microscopy as outlined in Chapter 2.6.1. Corresponding images were acquired at 100x magnification (scale bar = 10 μm). The localisation of the ER mutants was compared to VSV-PAR$_4$ mECFP with membrane (white arrows) and intracellular expression (red arrows) highlighted. These experiments are representative of at least three others.

(A)
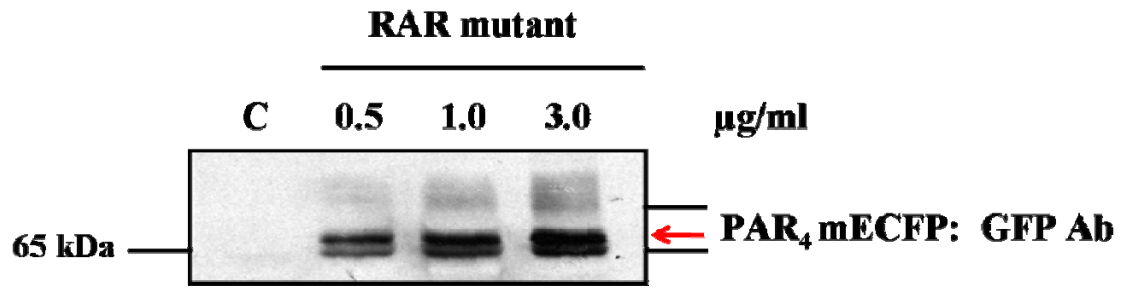
(B)
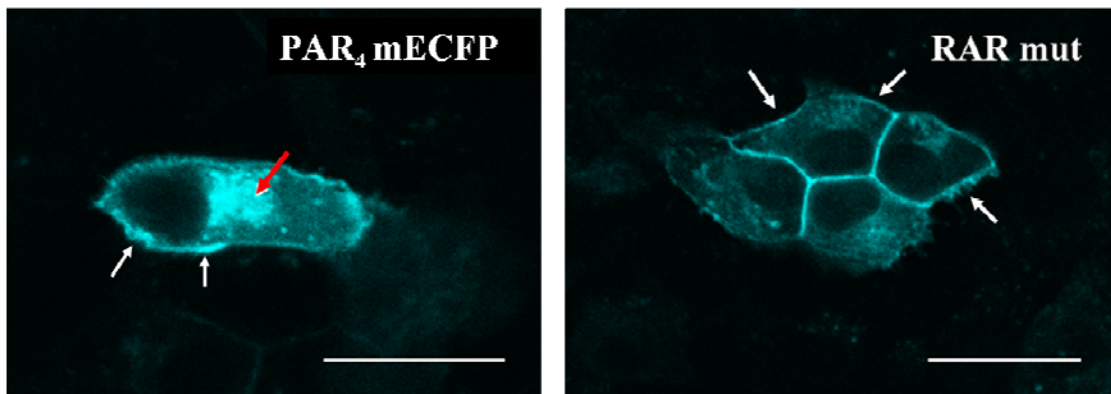
(C)
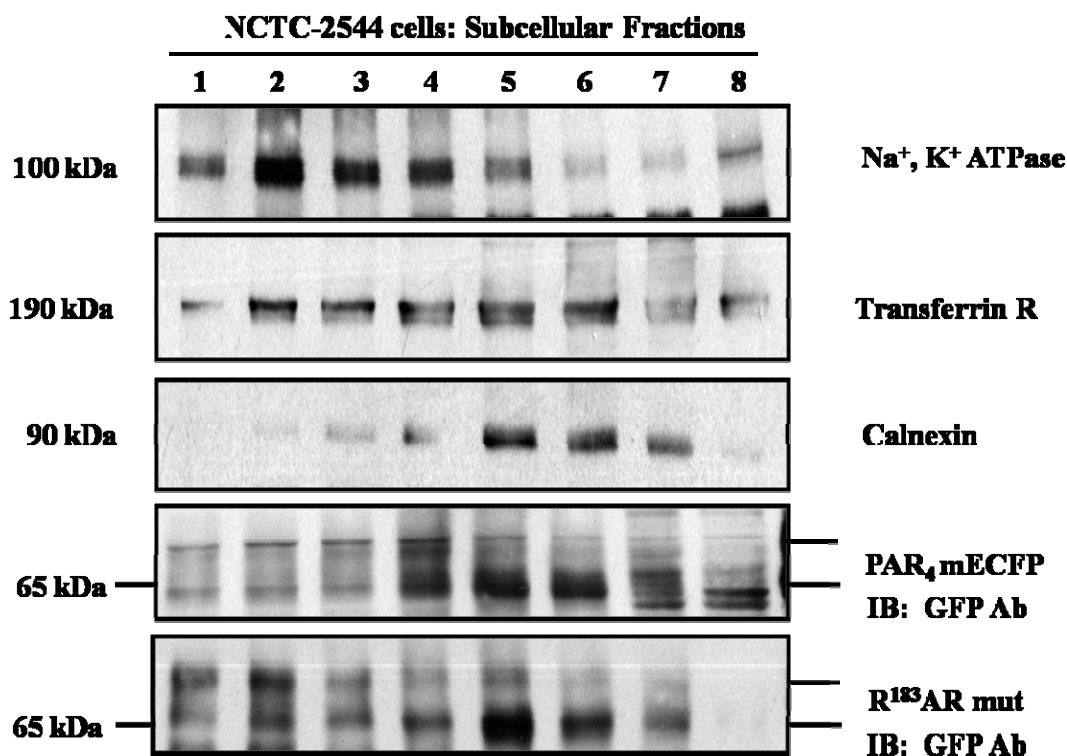
Figure 4.17. Expression of ER retention motif mutant 'RAR' in NCTC-2544 cells.

NCTC-2544 cells were grown in plates and on coverslips and transiently transfected with VSV-PAR$_4$ mECFP or 'RAR' ER motif mutant construct as indicated above, for 24 hours prior to serum starvation for a further 24 hours. (A) Whole cell lysates were prepared and resolved by Western blotting as outlined in Chapter 2.8.2. PAR$_4$ receptor expression (~65 kDa) was detected using a GFP antibody. (B) Transfected cells grown on coverslips were prepared for epifluorescence microscopy as outlined in Chapter 2.6.1. Corresponding images were acquired at 100x magnification (scale bar = 10 μm). The localisation of the 'RAR' mutant was compared to VSV-PAR$_4$ mECFP with membrane (white arrows) and intracellular expression (red arrows) highlighted. (C) Subcellular fractionation was carried in cells expressing either PAR$_4$ mECFP or R^{183}AR mutant as outlined in Chapter 2.8.6. These experiments are representative of at least three others.

4.6 Investigating the signalling capabilities of PAR$_4$ in NCTC-2544 cells following mutation of the ER retention motifs

The experiments carried out in the HEK293 cell model in Section 4.3 highlighted the fact that the ER mutants did not respond well to agonist treatment when compared to PAR$_4$ mECFP responses. This was demonstrated using an inositol phosphate assay and ERK activation, despite comparable membrane localisation of the RAR motif mutant with PAR$_4$ mECFP expressed in these cells. The ability of these mutants to respond to agonist treatment was investigated in the NCTC-2544 cell line using inositol phosphate accumulation as a marker of receptor activation.

The responses observed following agonist treatment of NCTC-2544 cells expressing the ER motif mutants reflected those obtained in Section 4.3. As demonstrated in Figure 4.18, a significant increase in the basal inositol phosphate response was observed in cells expressing VSV-PAR$_4$ mECFP (4.59 ± 0.32 fold of non-transfected cell basal). Receptor activation with thrombin or AYPGKF-NH$_2$ resulted in a further increase in the inositol phosphate response (7.80 ± 0.33 and 9.48 ± 1.73 fold respectively). Agonist treatment of cells expressing RAR, RGRR or the DM motif mutants had little impact upon the respective inositol phosphate responses when compared to the basal responses. This was surprising considering the level of PAR$_4$ expressed at the membrane in NCTC-2544 cells expressing the RAR mutant, as observed in previous confocal experiments in Section 4.5. Experiments assessing PAR$_4$-mediated ERK phosphorylation in the ER mutants resulted in the same outcome observed in the HEK293 cells, with a substantial decrease in ERK activation in cells expressing RAR, RGRR and DM mutants (not shown).

One unique feature of RAR mutant expression was the ability of PAR$_4$ to internalise following receptor activation with thrombin. Figure 4.19 (A) illustrates the effect of thrombin (3 U/ml) treatment upon the localisation of VSV-PAR$_4$ mECFP expressed in NCTC-2544 cells. No change in the distribution of PAR$_4$ was observed following agonist treatment for 30 minutes, with PAR$_4$ expressed intracellularly both before and after stimulation. Membrane localisation of PAR$_4$ was observed when the RAR mutant was expressed in the NCTC-2544 cell model (B). Receptor activation with

thrombin resulted in the formation of punctate vesicles at the membrane as well as inside the cell with a loss of cell surface expression observed. Even in the original characterisation experiments in Chapter 3, internalisation of membrane PAR_4 was not observed in HEK293 cells following stimulation, even after 180 minutes of agonist treatment.
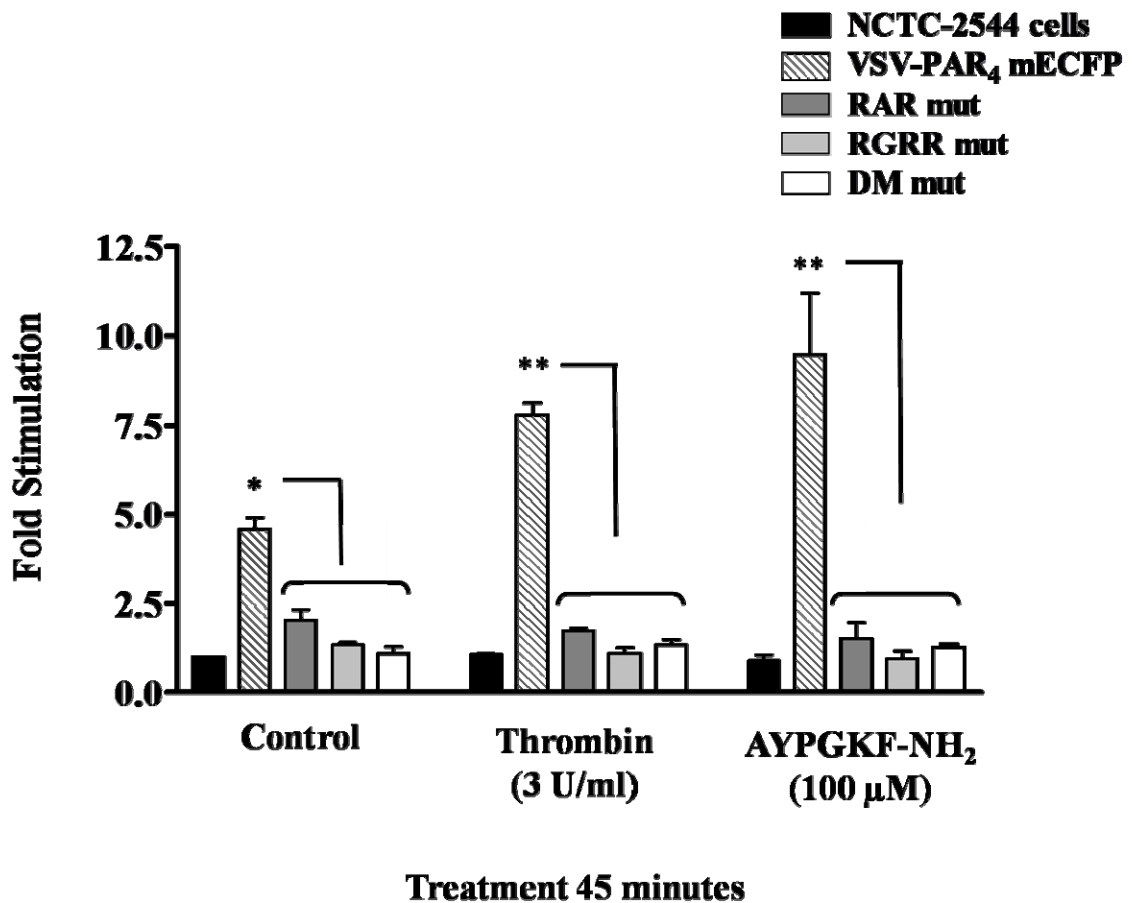
Figure 4.18. PAR$_4$-mediated [^{3}H]-inositol phosphate accumulation in NCTC-2544 cells expressing WT VSV-PAR$_4$ mECFP or the ER motif mutants.
NCTC-2544 cells were transiently transfected for 24 hours with VSV-PAR$_4$ mECFP or the ER motif mutants (2 μg/ml) shown above, as outlined in Chapter 2.5. The media was replaced with serum free growth media supplemented with 0.25 μCi of [^{3}H]-2-myo-inositol for a further 24 hours prior. Cells were pre-treated with 10 mM lithium chloride for 15 minutes prior to stimulation with thrombin or AYPGKF-NH$_2$ as indicated. Total inositol phosphate (InsP$_{1-4}$) accumulation was measured as described in Chapter 2.9. The data presented represent values measured in duplicate (mean ± s.e.m.) over two independent experiments (*p=<0.05, **p=<0.01).

(A)
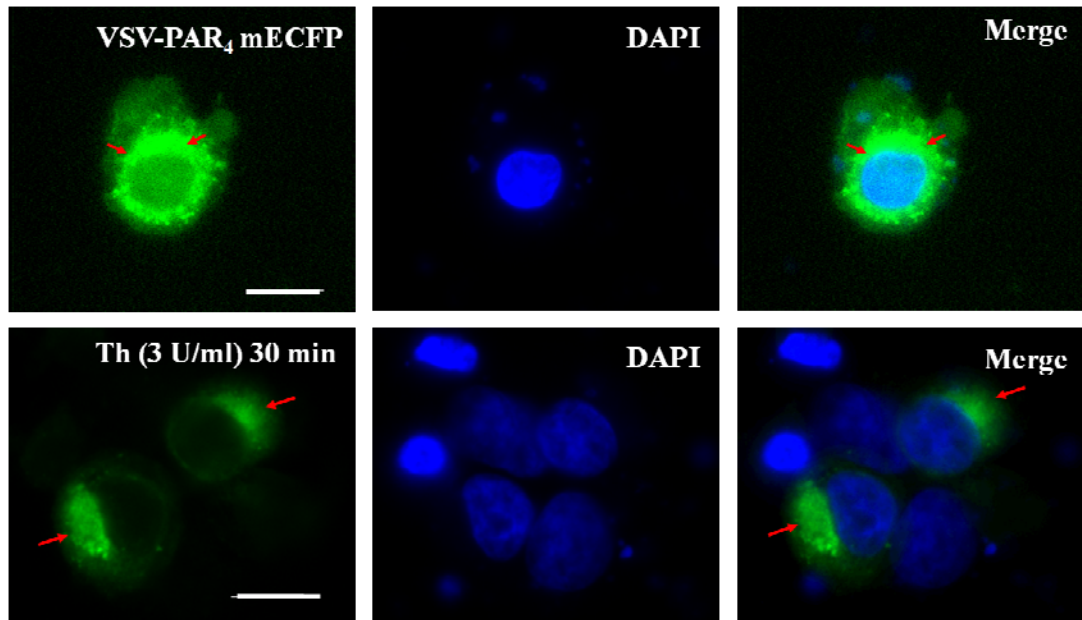
(B)
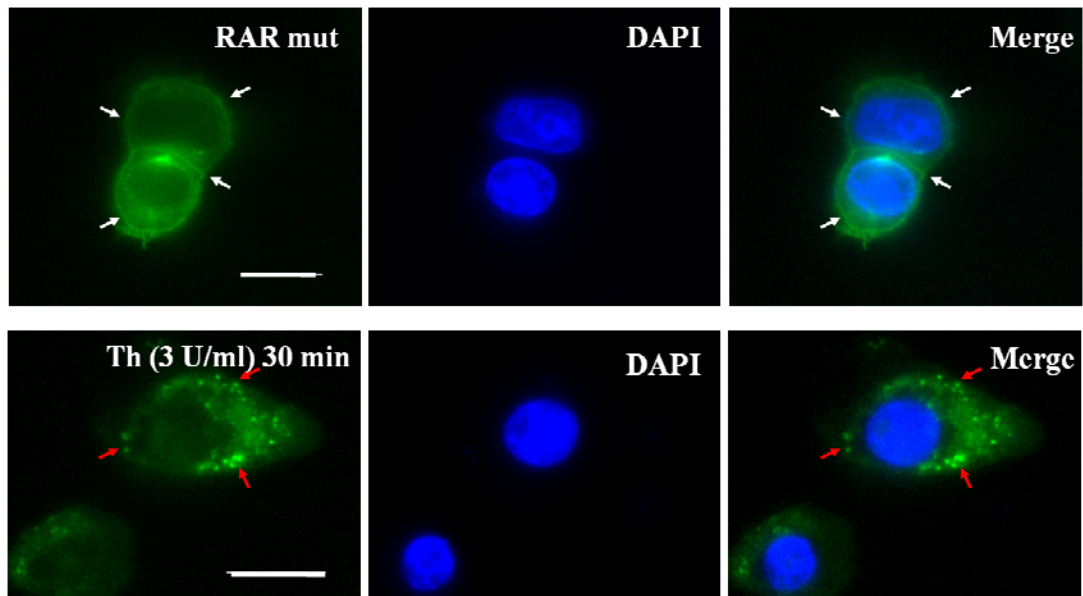
Figure 4.19. Internalisation of PAR$_4$ following receptor activation with thrombin in NCTC-2544 cells expressing the RAR motif mutant.

NCTC-2544 cells were grown on coverslips and transiently transfected, as outlined in Chapter 2.5, with VSV-PAR$_4$ mECFP (A) or RAR ER motif mutant (B) constructs for 24 hours prior to serum starvation for a further 24 hours. Cells were stimulated with thrombin (3 U/ml) for 30 minutes and the coverslips prepared as described in Chapter 2.6.1. Images were acquired at 100x magnification (scale bar = 10 µm). Membrane (white arrows) and intracellular (red arrows) receptor expression is highlighted.   Images shown are representative of at least three independent experiments.

Attempts were made in order to accurately quantify the level of PAR$_4$ expressed at the plasma membrane between VSV-PAR$_4$ mECFP and the ER mutants. Using cell surface ELISA, an antibody directed against the VSV epitope was used to detect VSV-PAR$_4$ mECFP expressed in HEK293 cells.

Figure 4.20 (A) illustrates the values obtained from the ELISA experiments. Increasing the expression of VSV-PAR$_4$ mECFP in HEK293 cells had no effect upon the level of VSV detected at the cell surface relative to control values. However, as a control, expression of another cell surface GPCR, namely the muscarinic M$_3$ receptor (VSV-Muscarinic M$_3$) was detected. When increasing levels of VSV-M$_3$ DNA were transfected in HEK293 cells, a significant concentration-dependent increase in VSV was measured at the cell surface, indicating that the conditions of the assay were optimal for cell surface analysis. The ability of the VSV antibody to detect VSV-PAR$_4$ mECFP was further explored using indirect immunofluorescence, Figure 4.20 (B). Whilst the VSV antibody was unable to detect membrane PAR$_4$, a strong intracellular VSV signal was observed in HEK293 cells. This suggested that PAR$_4$ may undergo post-translational modification, such as N-linked glycosylation, to reach the cell surface; a factor that may impair efficient detection of the VSV epitope expressed on the N-terminal of the receptor.

(A)
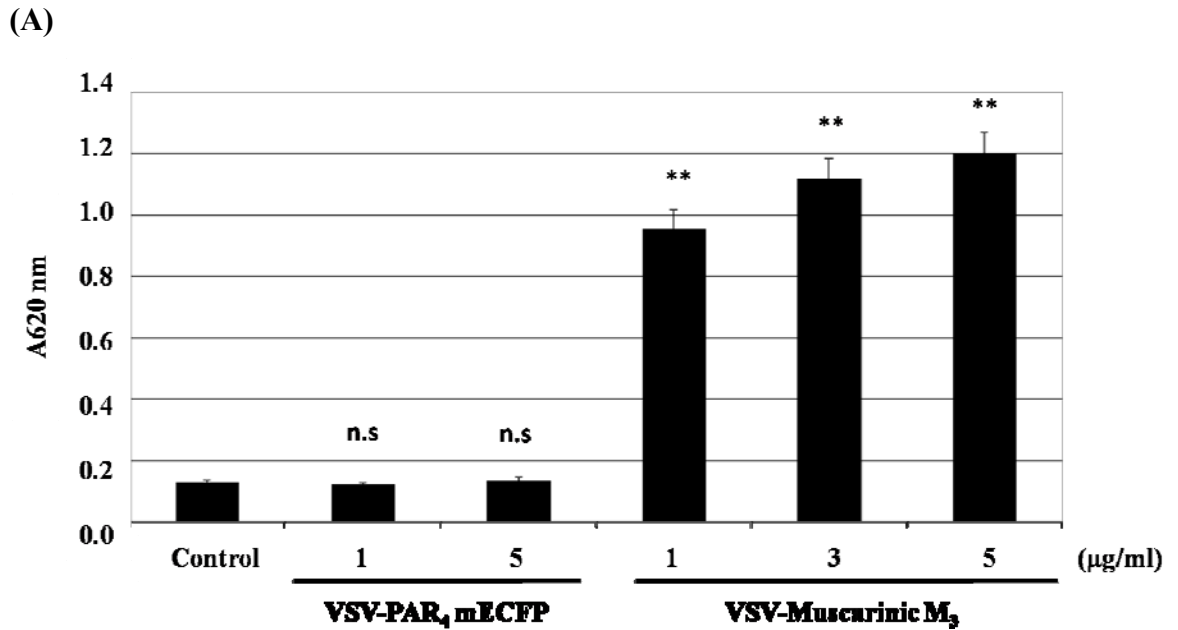
(B)
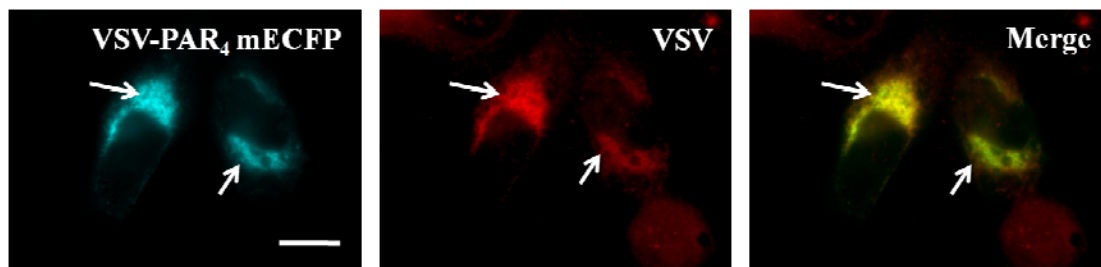
Figure 4.20. Cell surface VSV ELISA to detect membrane expression of VSV-PAR$_4$ mECFP.

HEK293 cells were transiently transfected with increasing concentrations of either VSV-PAR$_4$ mECFP or VSV-Muscarinic M$_3$ DNA as outlined in Chapter 2.5. Cell surface ELISA was performed as described in Chapter 2.11. The assay plates were read at an absorbance wavelength of 620 (A620 nm) and the absorbance values were plotted above. These values are representative of two independent experiments performed in quadruplicate (**p=<0.01, n.s = not significant). (B) Indirect immunofluorescence was also carried out as described in Chapter 2.6.2 (scale bar = 10 μm). Co-localisation between VSV-PAR$_4$ mECFP and the VSV antibody is indicated (white arrows). Images representative of three experiments.

4.7   The effect of deglycosylation upon the cellular localisation of PAR$_4$ and corresponding ER mutants in HEK293 cells.

Of the two cell lines explored in terms of PAR$_4$ localisation, HEK293 cells appeared to be the only model where the effect of deglycosylation would be ideally monitored. This was due to the two distinct populations of receptor observed in the cellular model. Firstly, the effect of tunicamycin (2 μg/ml) upon PAR$_4$ protein expression was observed in HEK293 cells following treatment for 16 hours. This was tested in cells expressing PAR$_4$ mECFP or ER mutant proteins using Western blotting and epifluorescence microscopy. As shown in Figure 4.21 (A), cells expressing VSV-PAR$_4$ mECFP or the RAR mutant resulted in the typical two band pattern observed in previous experiments. Following treatment with tunicamycin (TUN) the mupper PAR$_4$ band was no longer expressed, however a lower band resolving just above the 65 kDa band was observed for both. No changes in the expression pattern of RGRR or DM were observed following deglycosylation, with only the 65 kDa band evident upon expression and tunicamycin treatment.

Corresponding epifluorescence images are shown in Figure 4.21 (B-E). A clear loss in cell surface expression of both VSV-PAR$_4$ mECFP (B) and the RAR mutant (C) was observed following treatment with tunicamycin. No distinct changes were observed for the localisation of RGRR mutant (D) or DM mutant (E), corresponding with the protein expression results obtained from the Western blotting experiments.

(A)

(B)

(C)

167
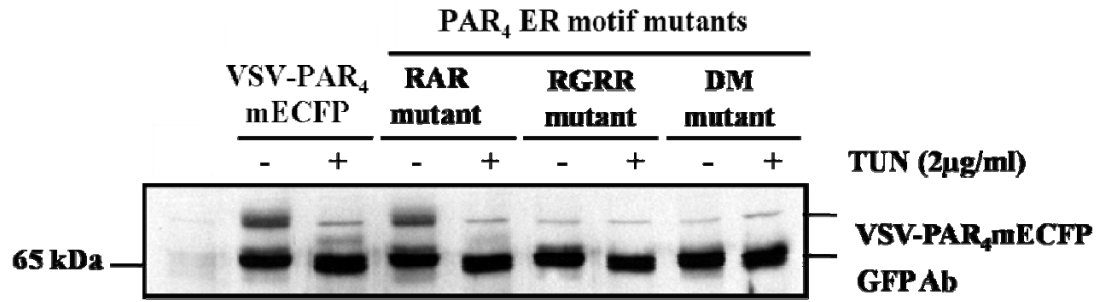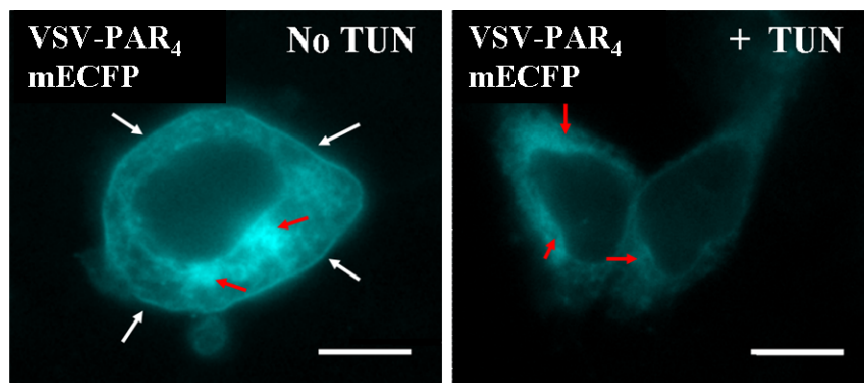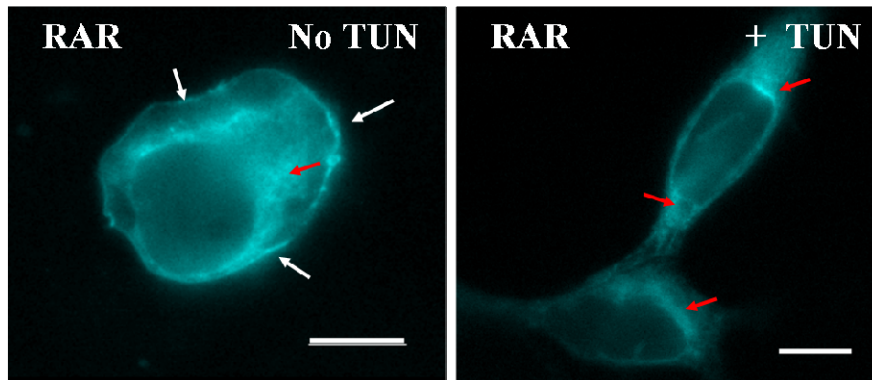
(D)
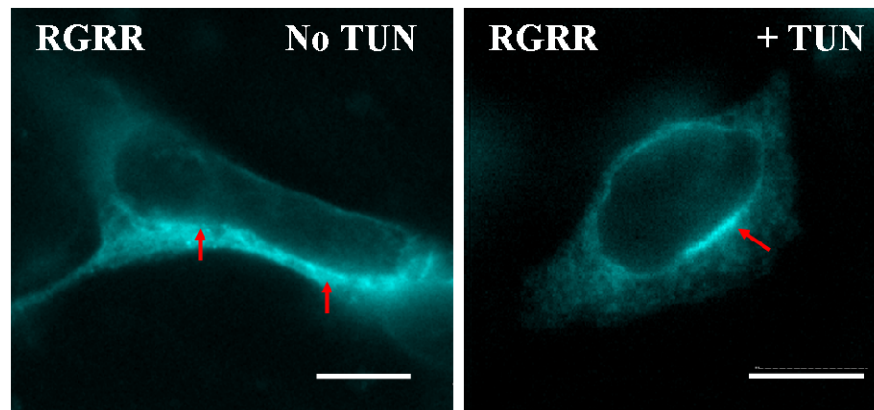
(E)
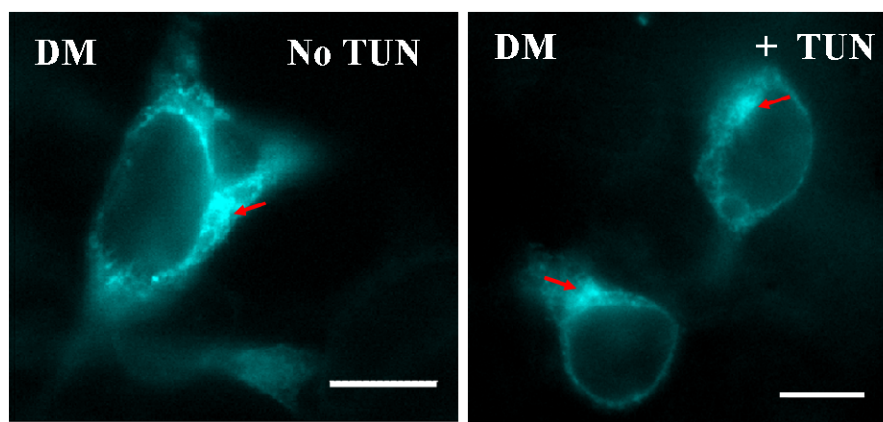
Figure 4.21. The effect of deglycosylation upon PAR$_4$ expression in HEK293 cells

HEK293 cells were grown in plates with and without coverslips then transiently transfected with VSV-PAR$_4$ mECFP or ER mutants (1 μg/ml) for 24 hours as described in Chapter 2.5. After which time the media was replaced with serum free media supplemented with tunicamycin (2 μg/ml) for 16 hours. Whole cell lysates were prepared and resolved by Western blotting as outlined in Chapter 2.8.2. (A) The expression of PAR$_4$ was detected through the use of a GFP antibody recognising the C-terminal ECFP fluorophore. (B) Cells grown on coverslips were prepared for epifluorescence microscopy as outlined in Chapter 2.6.1. Corresponding images -/+ TUN treatment (B-E) were acquired at 100x magnification for each mutant (scale bar = 10 μm). Blots and images are representative of at least two independent experiments.

168

4.8 Investigating possible interaction between PAR$_4$ and Calnexin in HEK293 cells.

The influence of deglycosylation upon PAR$_4$ localisation was clearly demonstrated in Section 4.7, thus highlighting that N-linked glycosylation may contribute in part to the expression of PAR$_4$ at the plasma membrane in HEK293 cells. With this in mind, it was therefore assessed to see if calnexin could play a role in the regulation of PAR$_4$ expression.

Interaction between PAR$_4$ and calnexin was assessed using co-immunoprecipitation and fluorescence-resonance energy transfer (FRET). Figure 4.22 (A) shows immunoprecipitation (IP) of calnexin followed by immunoblotting (IB) for calnexin and PAR$_4$ using a PAR$_4$-specific antibody and a GFP antibody. IP of calnexin (90 kDa) is clearly shown (top panel) with blotting for PAR$_4$ (middle panel) demonstrating co-immunoprecipitation of WT PAR$_4$ (38 kDa), PAR$_4$ mECFP and VSV-PAR$_4$CFP (~65 kDa) in HEK293 cells expressing these proteins. The corresponding GFP blot (bottom panel) distinctly shows PAR$_4$ mECFP and VSV-PAR$_4$ mECFP co-immunoprecipitation. The positive control loaded for the experiment was a whole cell lysate expressing PAR$_4$ mECFP. Based upon the bands resolved in this lane, the 65 kDa PAR$_4$ protein band appears to be the band that co-immunoprecipitated with calnexin, however, a small level of the upper PAR$_4$ band was also observed in the GFP blot.

The reciprocal IP of PAR$_4$ is shown in Figure 4.22 (B). Following the IP of PAR$_4$ from HEK293 cells expressing PAR$_4$, PAR$_4$ mECFP or VSV-PAR$_4$ mECFP, related IB results (top and bottom panels) clearly show that PAR$_4$ was successfully immunoprecipitated. Despite this, calnexin was shown to be equally co-immunoprecipitated in all wells, including in cells expressing empty vector. The ability of calnexin and PAR$_4$ to co-immunoprecipitate in NCTC-2544 cells was also assessed (C). IP of calnexin (top panel) and subsequent IB for PAR$_4$ using a GFP-specific antibody (bottom panel) resulted in successful co-immunoprecipitation of the 65 kDa protein band for PAR$_4$ mECFP.

As a further measure to ensure that interaction between PAR_4 and calnexin was bona fide and not an artefact of co-immunoprecipitation, FRET was used to detect interaction. In order for this to be carried out, EYFP and ECFP-calnexin constructs were used. Optimisation to determine the expression levels of these constructs was carried out through Western blotting and direct immunofluorescence by epifluorescence microscopy.

Increasing concentrations of ECFP-calnexin and EYFP-calnexin DNA (0-1 µg/ml) were transfected in HEK293 cells, as shown in Figure 4.23 (A) and (B) respectively. Proteins were resolved by Western blotting using both calnexin-specific and GFP antibodies to detect endogenous calnexin and the fluorescent calnexin constructs expressed in the cells. As the DNA transfected increased, so did the level of ECFP-calnexin and EYFP-calnexin expressed in the cells (117 kDa band), reaching maximal expression levels at 0.5 µg/ml of DNA. Comparable results were obtained from both of the antibodies used. Endogenous calnexin was detected in cells as a band resolved at 90 kDa, consistent with the fractionation experiments carried out in Section 4.2. (B) Epifluorescence microscopy of cells expressing the EYFP-calnexin construct identified intracellular expression of calnexin, which when co-localised with an ER tracker dye confirmed the expression of calnexin in the ER. This provided a good indication that the presence of the fusion protein did not alter the localisation of calnexin. With the confidence that the fluorescent constructs for calnexin were reliable, interaction between PAR_4 and calnexin was investigated using wide-field FRET microscopy, as shown in Section 4.9.

(A)
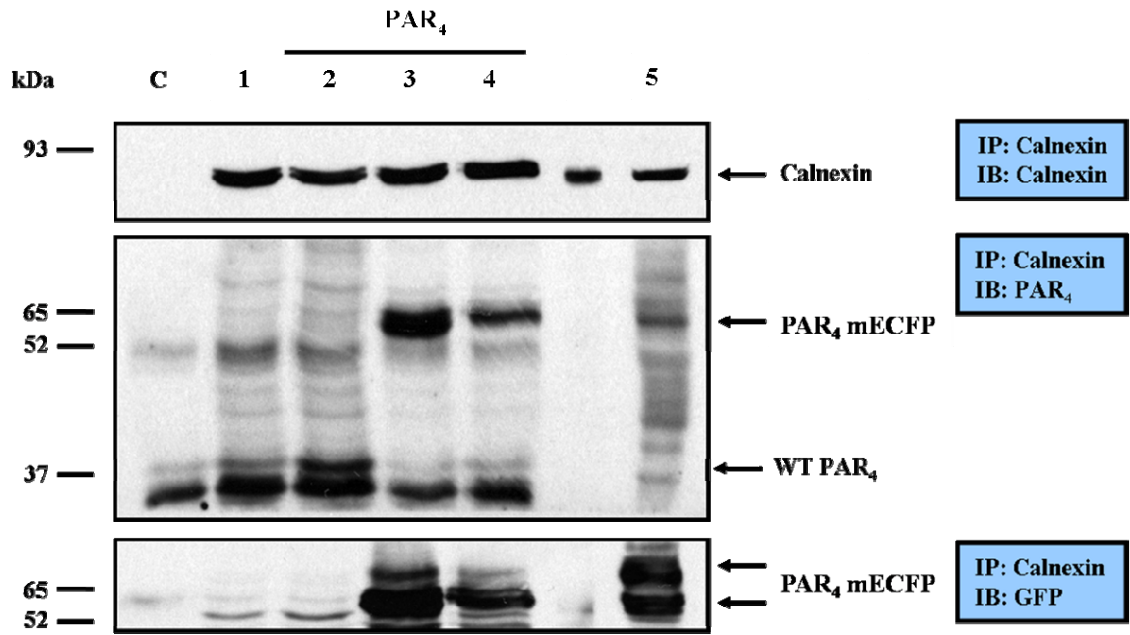
(B)
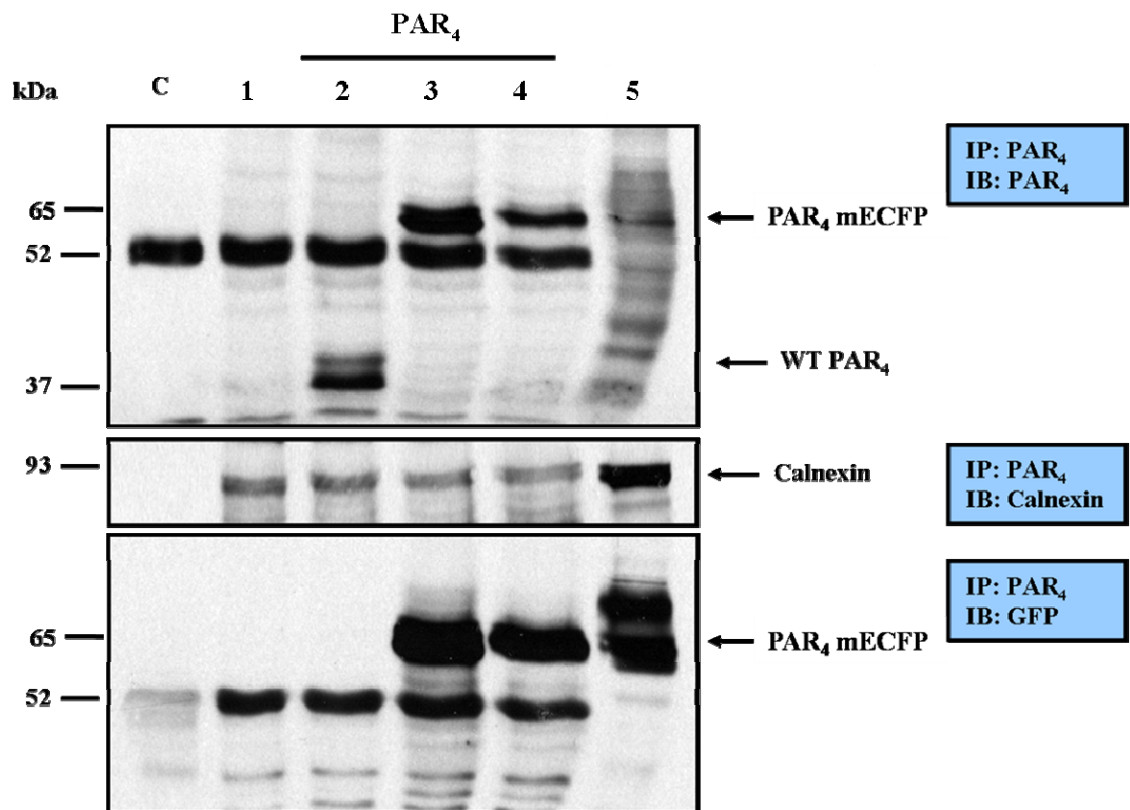
(C)
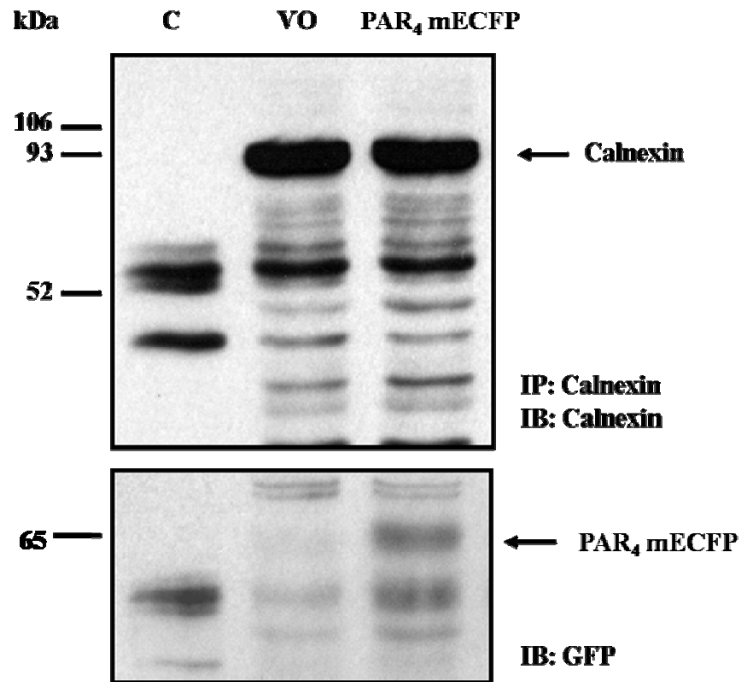
Figure 4.22. Co-immunoprecipitation of PAR$_4$ CFP with calnexin in HEK293 cells and NCTC-2544 cells

Cells were grown to 80% confluence in T75 flasks prior to transfection with empty vector pcDNA3.1 (1), WT PAR$_4$ in pcDNA3.1 (2), PAR$_4$ mECFP (3) or VSV-PAR$_4$ mECFP (4) plasmid DNA for 24 hours as outlined in Chapter 2.5. A HEK293 cell lysate expressing PAR$_4$ mECFP transfection was also loaded as a positive control (5) in addition to a control sample containing only the beads and antibody. Cells were serum starved for a further 24 hours then harvested in solubilisation buffer. Calnexin protein was immunoprecipitated (IP) with anti-calnexin antibody on protein G sepharose beads (HEK293 cells; A and NCTC-2544 cells; C) whilst PAR$_4$ was pulled down using a PAR$_4$-specific antibody on protein A sepharose beads (HEK293 cells; B), as described in Chapter 2.8.5. The samples were resolved through Western blotting as outlined in Chapter 2.8.2. Blots were probed for calnexin (~90kDa) and then re-probed for PAR$_4$ (WT ~38 kDa, tagged protein ~65 kDa) using both the PAR$_4$ and GFP antibodies as shown. Blots are representative of at least two independent experiments.

(A)

(B)

173
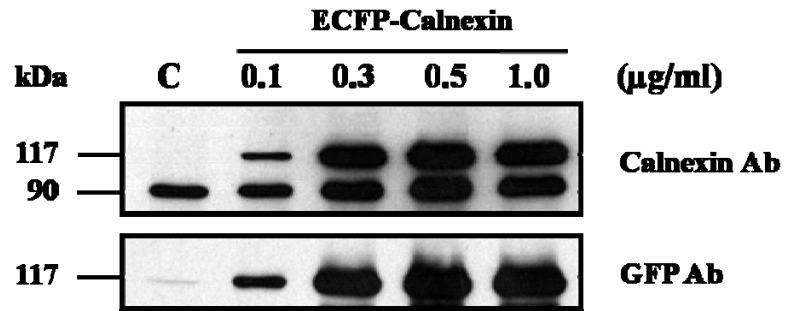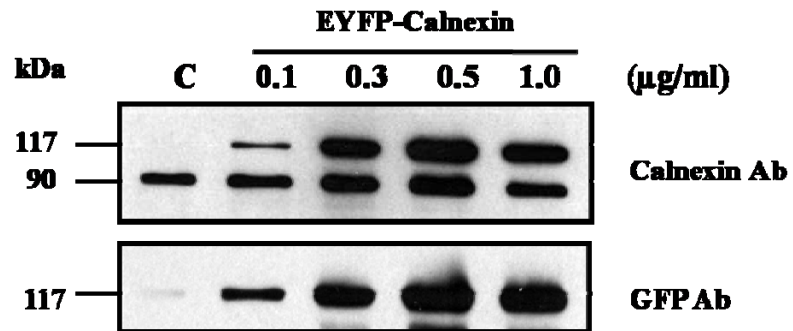
(C)
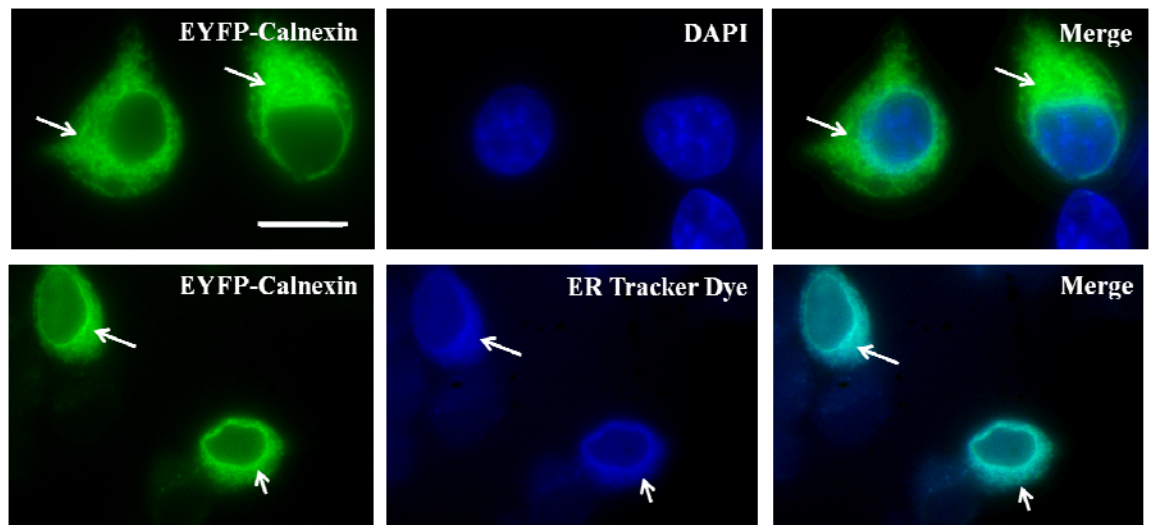
Figure 4.23. Characterisation of fluorescent calnexin constructs in HEK293 cells.

HEK293 cells were grown on plates with and without coverslips then transiently tranfected with ECFP-Calnexin (A) or EYFP-calnexin (B) at the given concentrations following the protocol in Chapter 2.5. Whole cell lysates were prepared and resolved by Western blotting as shown in Chapter 2.8.2. The expression of calnexin was detected through the use of an anti-calnexin (Calnexin ~90 kDa) and GFP antibodies (EYFP/ECFP-Calnexin ~117 kDa) as shown. (C) Cells transfected on coverslips were prepared for epifluorescence microscopy as described in Chapter 2.6.1. Images were acquired at 100x magnification (Scale bar = 10 µm). ER localisation of EYFP-calnexin was confirmed using an ER tracker dye (white arrows). Blots and images are representative of at least two independent experiments.

4.9 FRET analysis in HEK293

FRET analysis was performed using wide-field FRET microscopy in live HEK293 cells, as described in Chapter 2.7. The donor used for experimentation was mECFP or PAR$_4$ mECFP, whilst the acceptor used was mEYFP or EYFP-calnexin. These constructs were either co-expressed or expressed individually prior to FRET analysis.

4.9.1 FRET imaging in HEK293 cells expressing ECFP and EYFP controls

In order for interaction to be reliably measured, control experiments were carried out to measure the interaction between the fluorophore pairs, in the absence of PAR$_4$ or calnexin. This is regarded as potential collisional FRET (i.e. energy transfer based upon random collision of the fluorophore pair). Images were acquired for HEK293 cells transiently expressing mEYFP only and mECFP only (not shown), mECFP and mEYFP together (index of collisional FRET) and a tandem protein comprised of mECFP-mEYFP fused together (positive FRET control). Figure 4.24 (A) shows the images acquired for ECFP/Don (cyan), EYFP/Acc (yellow), uncorrected FRET (magenta) filter settings (uFRET) alongside the corrected FRET (cFRET) signal (pseudocolor), with corresponding ratiometric FRET values (RFRET) quantified and graphed (B). Representative images are shown for cells expressing mECFP and mEYFP (top panel) and the mECFP-mEYFP tandem protein (bottom panel). When mECFP and mEYFP were co-expressed in HEK293 cells, no fluorescence was in the cFRET image. However, images acquired for cells expressing the mECFP-mEYFP tandem (bottom panel) showed a strong signal detected in the cFRET image after bleedthrough correction of uFRET. The corresponding RFRET values recorded for the FRET experiments carried out in HEK293 cells (n=3) are shown as mean ± s.e.m, in Figure 4.24 (B). RFRET values were obtained for mECFP (0.995 ± 0.004), mEYFP (0.997 ± 0.003), mECFP and mEYFP (1.115 ± 0.033) and the mECFP-mEYFP tandem (5.148 ± 0.129). No difference in RFRET value was found for mECFP, mEYFP or mECFP and mEYFP expressing cells, however there was a significant increase in RFRET value obtained for the tandem protein, which corresponded well with the cFRET signal detected in the FRET images in (A, bottom panel).

4.9.2 Co-expression of PAR$_4$ mECFP and EYFP-calnexin in HEK293 cells.

Similar FRET analysis was carried out in cells expressing ECFP-calnexin/PAR$_2$ mEYFP, and PAR$_4$ mECFP/EYFP-calnexin donor/acceptor pairs. Figure 4.25 illustrates images acquired using the following filter sets; CFP/Don (cyan), YFP/Acc (yellow), uFRET and cFRET. No fluorescence was observed in the cFRET image in cells expressing only PAR$_4$ mECFP (A). Similar results were observed in cells expressing EYFP-calnexin (B). FRET imaging of PAR$_4$ mECFP and EYFP-calnexin co-expression in HEK293 cells is shown in (C). A considerable fluorescence signal was detected in the cFRET image when these proteins were co-expressed. This signal was not observed in cells co-expressing PAR$_2$ mEYFP and ECFP-calnexin (D). The RFRET values obtained for the data set were graphed (E). Similar to the control RFRET values observed in Figure 4.24, values obtained for both PAR$_4$ mECFP (0.998 ± 0.005) and EYFP-calnexin (0.995 ± 0.003) indicated no FRET. However a significant increase in RFRET value was observed between PAR$_4$ mECFP and EYFP-calnexin co-expression (1.400 ± 0.017). As a control, FRET between PAR$_2$ and calnexin was investigated alongside PAR$_4$ and calnexin FRET experiments. As the RFRET values show in Figure 4.25 (E), no interaction was observed between PAR$_2$ mEYFP and ECFP-calnexin (RFRET value 1.061 ± 0.010) relative to control RFRET values (~1 = no interaction).
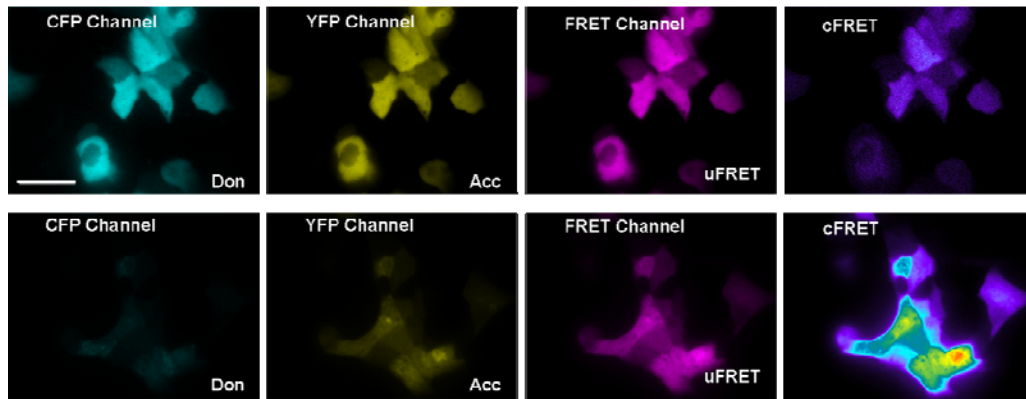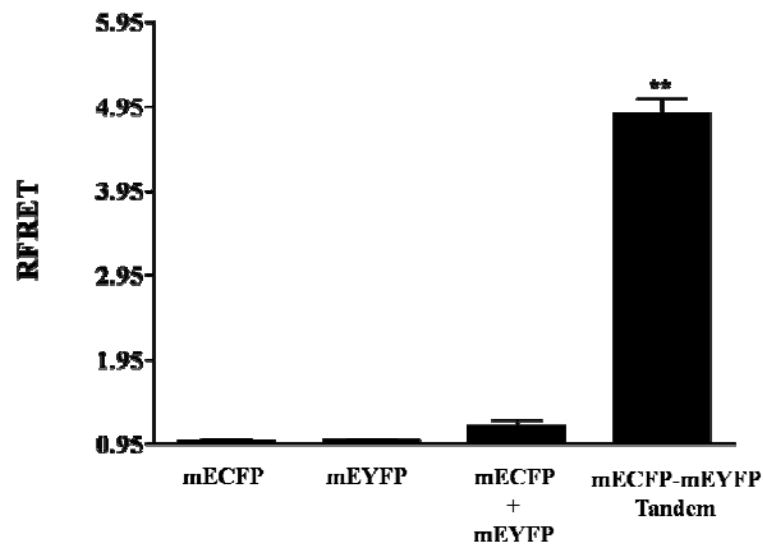
Figure 4.24. FRET imaging of mECFP, mEYFP and tandem control constructs. HEK293 cells were transfected with the indicated constructs for 24 hours prior to serum starvation for a further 24 hours. Wide-field FRET was performed as outlined in Chapter 2.7. Images were acquired in all three channels; CFP, YFP, and FRET, with the raw FRET signal (uFRET) corrected (cFRET) for spectral bleedthrough (scale bar = 50μm). The images shown in (A) reflect collisional FRET signal observed between mECFP and mEYFP (top panel) and a positive FRET signal obtained from the mECFP-mEYFP tandem (bottom panel). Ratiometric FRET values (RFRET) were quantified from the images acquired and graphed (B). Images are representative of three separate FRET experiments and with RFRET data expressed as mean ± s.e.m ($**p = <0.01$).
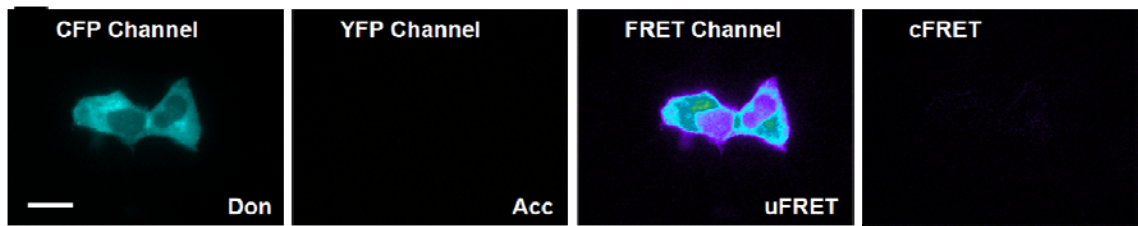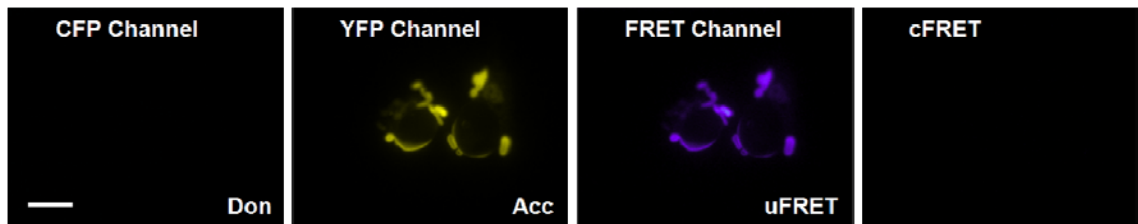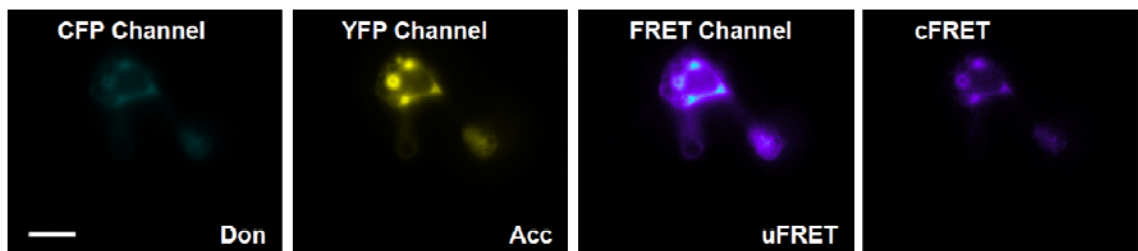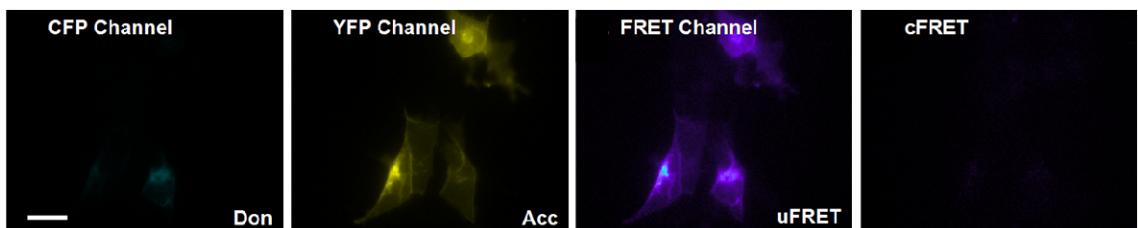
(E)
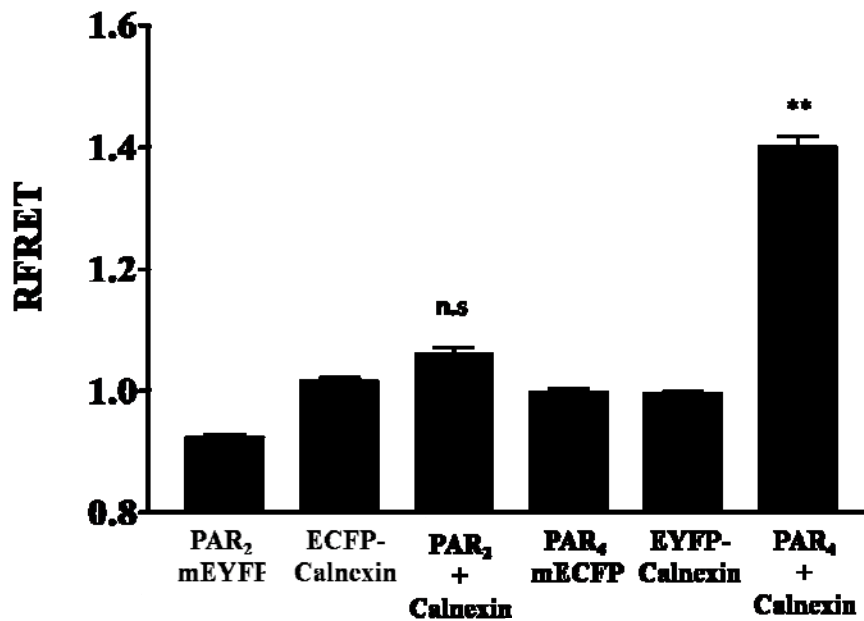
Figure 4.25. Confirmation of interaction between PAR$_4$ and calnexin in HEK293 cells using wide-field FRET microscopy.

PAR$_4$ mECFP, mEYFP-calnexin, PAR$_2$ mEYFP or ECFP-calnexin were transiently expressed individually or co-expressed in HEK293 cells for 24 hours prior to serum starvation for a further 24 hours. Wide-field FRET was carried out as outlined in Chapter 2.7. Images were acquired in all three channels; CFP, YFP, and FRET, with the raw FRET signal (uFRET) corrected (cFRET) for spectral bleedthrough (scale bar = 25 μm). The images reflect the FRET signal observed in cells expressing only (A) PAR$_4$ mECFP, (B) EYFP-calnexin or co-expressing PAR$_4$ mECFP and EYFP-calnexin (C) or PAR$_2$ mEYFP and ECFP-calnexin (D). Ratiometric FRET (RFRET) values were quantified from the images acquired from all FRET pairs tested and graphed (E). Images are representative of two separate FRET experiments (n=50 single cell measurements) and with RFRET data expressed as a mean ± s.e.m (**p=<0.01, n.s = not significant).

4.10 Discussion

Analysis of the protein sequence for PAR$_4$ provided an insight into the regulatory motifs that may dictate the subcellular localisation of PAR$_4$, The experiments carried out in Chapter 3 and Chapter 4, identified PAR$_4$ as a protein which is predominantly retained in the endoplasmic reticulum (ER), but with the capability of trafficking to the cell surface through various mechanisms. When PAR$_4$ mECFP was expressed in HEK23 cells, two distinct PAR$_4$ protein bands were resolved through Western blotting; one at 65 kDa and another band resolving slightly higher around 70-75 kDa. The expression of multiple protein bands for one GPCR is not unique to PAR$_4$. Western blotting of other GPCRs, for example the vasopressin V$_2$ receptors (Wüller *et al.,* 2004), identified multiple protein bands when expressed; reflecting both the core glycosylated protein at 55 kDa (immature receptor) and the complex glycosylated protein resolving at 70-75 kDa (mature receptor). Based upon the subcellular fractionation studies carried out for PAR$_4$, the 65 kDa protein may well represent the immature receptor expressed in the ER, whilst the 70-75 kDa protein band may reflect mature PAR$_4$ expressed at the plasma membrane, further work would be required to confirm immature/mature receptor expression. When expressed in the NCTC-2544 cells only the 65 kDa band was detected, which provided the basis for investigating the nature of PAR$_4$ ER retention and cell surface delivery.

Two potential arginine-based ER retention/retrieval motifs (R^{183}AR and R^{188}GRR) were found to exist within intracellular loop-2 of PAR$_4$, similar in sequence and location to the functional 'RAR' ER retention motifs present in 5HT$_{3B}$ channels (Boyd *et al.,* 2003) and KA2 receptors (Nasu-Nishimura *et al.,* 2006) and the 'RRGR' motif present in the intracellular loop of the vasopressin V$_2$ receptor (Hermosilla and Schülein*.,* 2001). The mutagenesis experiments carried out in this study found distinct differences in phenotype between the R^{183}AR and R^{188}GRR motifs when expressed in HEK293 and NCTC-2544 cells.

Mutation of the R^{183}AR motif did not affect the subcellular distribution of PAR$_4$ in HEK293 cells, with PAR$_4$ localised both in the ER and at the membrane similar to PAR$_4$ mECFP. However expression of this mutant in the NCTC-2544 cell model,

where PAR$_4$ is predominantly expressed in the ER, resulted in enhanced cell surface expression and the appearance of the upper protein band resolving at 70-75 kDa. Based upon these results, the potential to improve the receptor pharmacology of PAR$_4$ through mutation of this motif was explored. Despite efficient delivery of PAR$_4$ to the plasma membrane in cells expressing the R^{183}AR mutants, both thrombin and AYPGKF-NH$_2$ failed to stimulate any inositol phosphate response, with only a weak ERK response observed in comparison to responses observed for PAR$_4$ mECFP. Thus enhanced cell surface expression did not equate to increased cell signal transduction as previously proposed. This loss of function was also demonstrated in the HEK293 cells where expression of PAR$_4$ mECFP and the R^{183}AR mutant at the membrane was observed. However mutation did not appear to affect AYPGKF-NH$_2$-mediated JNK signalling, with elevated basal levels of phosphorylated p38 MAPK observed upon expression. Interestingly, mutation of this motif appeared to specifically affect PAR$_4$-G$\alpha_{q/11}$ coupled events, thus in addition to regulating PAR$_4$ localisation, these arginine residues may also be critical to efficient receptor-G$\alpha_{q/11}$ coupling. Further work is required to identify if this loss of function extends to other G-protein coupling, such as G$\alpha_{i/o}$ or G$\alpha_{12/13}$.

The arginine-based ER retention motifs that reside in intracellular loop-2 (ICL-2) of PAR$_4$ are within close proximity to the fourth transmembrane domain (TM4) of the receptor. In ICL-2, the highly conserved DRY motif exists proximal to the cytosolic side of the third transmembrane domain. In addition to its role in maintaining the conformational stability of GPCRs, the arginine residue within the DRY domain has been shown to facilitate in G-protein coupling (Binet *et al.,* 2007). In the present study, mutation of the R^{183}AR motif may have indirectly affected the DRY domain, thus resulting in the observed loss of function. However, the fact that mutation only affected G$\alpha_{q/11}$ coupling, without affecting JNK or P38 MAPK activation may implicate R^{183}AR as an important factor in the structural basis of PAR$_4$ -G$\alpha_{q/11}$ coupling. It may be possible that tethered ligand interaction with the extracellular loop-2 (ECL-2) domain during receptor activation may result in conformational changes to TM4, thus directing G-protein coupling at these sites. The arginine residue at position 183 (**R^{183}**AR) in PAR$_4$ present in muscarinic M1, M3 and M5

receptors, which enable these receptors to couple strongly with $G\alpha_{q/11}$. A methionine residue at the same position in M2 and M4 receptors allow preferential coupling of these receptors to $G\alpha_{i/o}$ (Blin *et al.,* 1995). Work by Jürgen Wess and colleagues found that substitution of the methionine residue for an arginine at the same 183 position of the M2 receptor resulted in the ability of M2 receptors to signal via $G\alpha_{q/11}$ (Blin *et al.,* 1995). Based on these findings it could therefore be possible that the arginine residue at the 183 position on PAR_4 may be pivotal to PAR_4 $G\alpha_{q/11}$ coupling and thus mutation of which resulted in loss of $G\alpha_{q/11}$-dependent signal transduction.

In addition to the role of $R^{183}AR$ in regulating PAR_4 localisation and cell signal transduction, another notable feature of $R^{183}AR$ mutation was the ability of cell surface PAR_4 to undergo agonist-mediated receptor internalisation. Even in the HEK293 cells where mature PAR_4 mECFP was expressed at the membrane, no internalisation was observed even when treated for prolonged periods of time with agonist. However when the $R^{183}AR$ mutant was expressed in the NCTC-2544 cell model, PAR_4 demonstrated the ability to traffic to the membrane where upon activation, the receptor efficiently internalised. Whilst the membrane trafficking of both PAR_1 and PAR_2 have been extensively studied, no such studies have been carried out for PAR_4. Studies in other Class A GPCRs have found that specific residues, including the arginine in the DRY motif and ten residues thereafter within ICL-2, are important for GPCR-β-arrestin binding (Marion *et al.,* 2006; Wilbanks *et al.,* 2002). In these studies, the presence of proline 6 residues distal to the DRY domain and alanine in ICL-2 were important in the regulation of β-arrestin binding. The ICL-2 of PAR_4 contains this proline residue distal to the DRY sequence, along with several alanines. For the purpose of elucidating a functional role for the $R^{183}AR$ sequence as a potential regulator of PAR_4 ER retention, the arginine residues were substituted for alanines. In doing so, this could have created receptor mutants that would favourably bind β-arrestin, thus explaining the gain of function.

Mutation of the $R^{188}GRR$ and $R^{183}AR/ R^{188}GRR$ double mutant resulted in loss of function in all parameters tested. In the HEK293 cells, where wild PAR_4 mECFP was observed at the cell surface, expression of these mutants completely abolished

delivery to the plasma membrane and subsequent PAR$_4$-mediated signalling events. Unlike R^{183}AR, mutation of this sequence did not improve cell surface expression of PAR$_4$ in the NCTC-2544 cells. Using Prosite (a protein motif software), it was discovered that an X-G-[RK]-[RK] sequence may also be indicative of an amidation site, which would give rise to post translational modification of the protein. Thus, mutation may have altered the ability of PAR$_4$ to undergo the necessary modification for membrane expression to be successfully achieved.

Further analysis of the PAR$_4$ protein sequence identified an N-linked glycosylation motif (N^{56}DS) at the N-terminal of the receptor, thus highlighting the potential for PAR$_4$ to undergo post-translational modification to enable membrane expression. Deglycosylation experiments carried out in HEK293 cells identified a clear role for N-glycosylation in the delivery of PAR$_4$ to the cell surface, with membrane expression abolished after treatment with tunicamycin. Previous studies have identified the ECL-2 domain of most GPCRs to be important in N-glycosylation (Lanctot *et al.,* 2005), however the site for PAR$_4$ is located at the N-terminal. Whilst no mutagenesis work has been carried out to confirm the involvement of this motif per se, with no other site within PAR$_4$ it is thought that the N^{56}DS site is responsible for directing glycoslyation. Interestingly, despite PAR$_4$ membrane localisation in HEK293 cells, the VSV antibody was unable to detect cell surface VSV- PAR$_4$ mECFP, which may further suggest that N-glycosylation occurs at the N-terminal of PAR$_4$, thus preventing antibody recognition of the N-terminal VSV epitope.

Despite the ability of PAR$_4$ to evade ER retention in HEK293 cells, the accumulation of PAR$_4$ in the ER was relatively high in these cells as well as the NCTC-2544 model. In addition to the motifs that facilitate in the ER retention of PAR$_4$, the ability of PAR$_4$ to interact with the ER chaperone calnexin was established. Calnexin specifically targets N-linked glycans (Ruddock and Molinari, 2006), like PAR$_4$, with the capability of retaining such proteins in the ER or sorting proteins for export to the membrane. This duality of function is poorly understood however a recent study has demonstrated that calnexin can interact in both a glycan dependent and independent nature to differentially regulate the intracellular trafficking of

dopamine D1 and D2 receptors (Free *et al.,* 2007). PAR_4 was able to interact with calnexin in both HEK293 cells and NCTC-2544 cells. As the FRET studies demonstrate, calnexin interacted with PAR_4, but not PAR_2, a receptor which is both heavily N-glycosylated (Compton *et al.,* 2001) and expressed at the plasma membrane. Without further studies being carried out, it is difficult to draw any firm conclusions as to its role in the regulation of PAR_4. However as interaction is observed in both cell types, in particular the NCTC-2544 cells where only 65 kDa ER retained PAR_4 is expressed, it is possible that the role of calnexin is to retain PAR_4 in the ER through an N-glycan independent mechanism.

These results confirm a functional motif responsible for ER retention of PAR_4; however, the mechanism through which PAR_4 evades ER retention in HEK293 cells, but not in NCTC-2544 cells, remains unknown.

CHAPTER 5
THE EFFECT OF PAR$_2$ EXPRESSION UPON PAR$_4$ LOCALISATION

5.1 INTRODUCTION

As Chapters 3 and 4 demonstrate, PAR_4 resides predominantly in the ER, with cell surface expression regulated through various mechanisms. ER retention was dictated in part due to the presence of an $R^{183}AR$ retention motif and possibly through interaction with calnexin, an ER resident chaperone protein that targets N-linked glycans. Mutation of the $R^{183}AR$ motif allowed PAR_4 to traffic to the cell surface whilst deglycosylation abolished PAR_4 expression at the membrane, implicating a role for N-linked glycosylation in membrane localisation. Of these results, an interesting feature of PAR_4 was the ability of the receptor to evade ER retention and travel to the cell surface in HEK293 cells but remain confined to the ER in NCTC-2544 cells.

Through the experiments carried out in Chapter 3, HEK293 cells were shown to respond to thrombin, trypsin and the PAR_2–specific activating peptide SLIGKV-OH, but not $AYPGKF-NH_2$, a PAR_4-specific activating peptide. These results confirmed the presence of endogenous PAR_1 and PAR_2 but not PAR_4. NCTC-2544 cells do not express PAR_2, PAR_3 or PAR_4, with only low levels of PAR_1 detectable (Kawabata *et al.,* 2004). Endogenous PAR expression may be a contributing factor in the differences in intracellular trafficking of PAR_4 observed in both cell systems.

Multimeric receptors possess the ability to evade ER retention through masking RxR ER retention motifs during protein assembly, thus allowing transport to the membrane (Zerangue *et al.*, 1999; Margeta-Mitrovic *et al.*, 2000; Boyd *et al.,* 2003). Such events are important for membrane expression of $GABA_{B1}/GABA_{B2}$ (Margeta-Mitrovic *et al.*, 2000) and 5-HT3$_A$/5-HT$_{3B}$ (Boyd *et al.,* 2003) heterodimers. GPCR dimerisation has been investigated in so many GPCR families now that it has become widely accepted as an important factor in GPCR expression and receptor function (Rios *et al.,* 2001 and Prinster *et al.,* 2005). Dimerisation has been demonstrated between members of the PAR family (Leger *et al.,* 2006b; McLaughlin *et al.,* 2007). As PAR_1 is expressed in both HEK293 and NCTC-2544 cells, it is highly unlikely that this receptor is responsible for the differences observed. However PAR_2 is only

expressed in the HEK293 model, not the NCTC cells, thus may be a contributing factor to PAR$_4$ localisation at the membrane.

The experiments carried out in this chapter aim to identify if the localisation of PAR$_4$ is altered during co-expression with PAR$_2$. In the absence of high quality PAR-specific antibodies FRET was used to identify if interaction takes place between PAR$_2$ mEYFP and PAR$_4$ mECFP when co-expressed in the HEK293 and NCTC2544 cell models. To simplify the interpretation of the FRET data; where no FRET takes place (i.e. no interaction), a typical RFRET value of ~1 would be obtained, whilst FRET occurrence the expected RFRET value would be >1 (for method see Chapter 2.7).

5.1. Investigating the effect of PAR$_2$ and PAR$_4$ co-expression in NCTC-2544 cells

So far in this project the localisation of both PAR$_2$ mEYFP and PAR$_4$ mECFP have been studied separately. Figure 5.1 highlights the localisation of PAR$_4$ mECFP during co-expression with PAR$_2$ mEYFP when visualised by confocal microscopy. Interestingly, unlike the previous experiments in NCTC-244 cells where PAR$_4$ was retained the ER, when PAR$_2$ mEYFP is expressed, PAR$_4$ is localised at the plasma membrane (white arrows) with minimal intracellular clustering.

In order to ensure that this was not an artefact of interaction between the two variant GFP proteins fused to PAR$_2$ and PAR$_4$, fundamental experiments were repeated in an NCTC-2544 clonal cell line that stably expresses PAR$_2$ (NCTC-PAR$_2$). Following transient expression of PAR$_4$ mECFP in NCTC-2544 cells, NCTC-PAR$_2$ cells and HEK293 cells as a control, Western blotting was performed to establish if there were any distinct differences in the pattern of the protein bands. As Figure 5.2 (A) shows, when PAR$_4$ mECFP is expressed in NCTC-2544 cells only the 65 kDa is resolved (PAR$_4$ 38 kDa with ~27 kDa ECFP protein). Interestingly when expressed in the NCTC-PAR$_2$ cells (NP$_2$), a second band is observed which corresponds well with the PAR$_4$ bands resolved in HEK293 cells. Parallel epifluorescence microscopy experiments were carried out in NCTC-2544 and NCTC-PAR$_2$ cells as shown in

Figure 5.2 (B). In the NCTC-2544 cells PAR_4 mECFP remained in the ER, however in the PAR_2 clonal cells PAR_4 mECFP was observed at the plasma membrane.

In order to identify if the protein bands observed in the Western blot experiments were indicative of ER/plasma membrane PAR_4 protein, subcellular fractionation experiments were carried out using the appropriate markers for plasma membrane, endosomal and ER fractions. When PAR_4 mECFP was expressed in the NCTC-PAR_2 cells, as shown in Figure 5.3, separation of the fractions clearly established that the upper band was localised in both endosomal and membrane fractions whilst the lower 65 kDa band remained confined to the ER/endosomal fractions with very low levels of protein detected in membrane fractions.
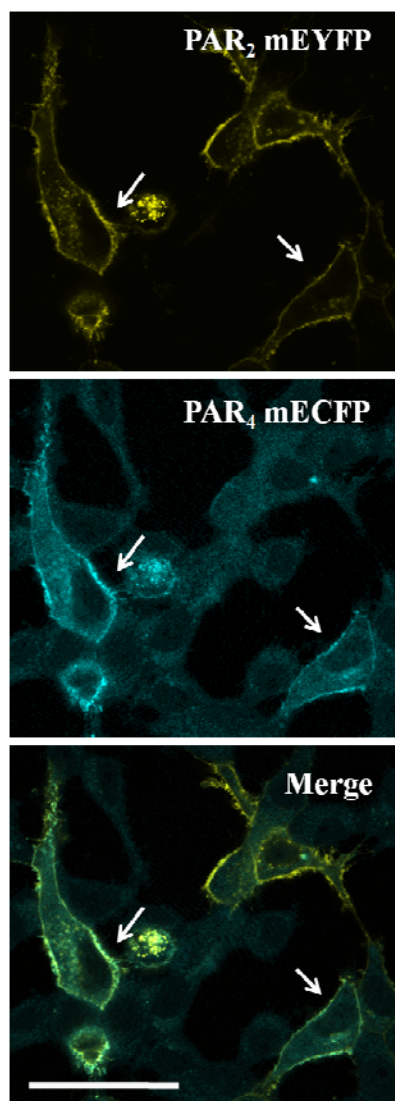
Figure 5.1. Co-expression of PAR$_2$ mEYFP and PAR$_4$ mECFP in NCTC-2544 cells.

NCTC-2544 cells were grown on coverslips and transiently co-transfected with PAR4 mECFP and PAR2 mEYFP for 24 hours prior to serum starvation for a further 24 hours. The cells were prepared for direct immunofluorescence as described in Chapter 2.6.1 and visualised at CFP and YFP wavelengths using confocal microscopy (scale bar = 25 µm). Membrane (white arrows) receptor expression is highlighted.   Images shown are representative of at least three independent experiments.

(A)
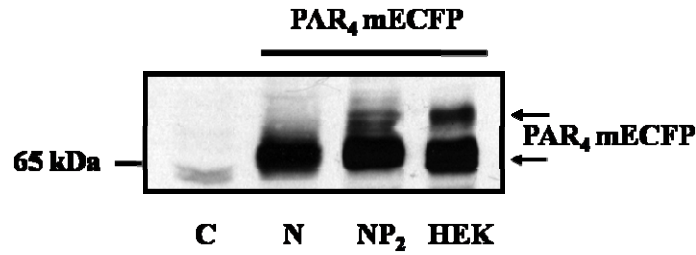
(B)
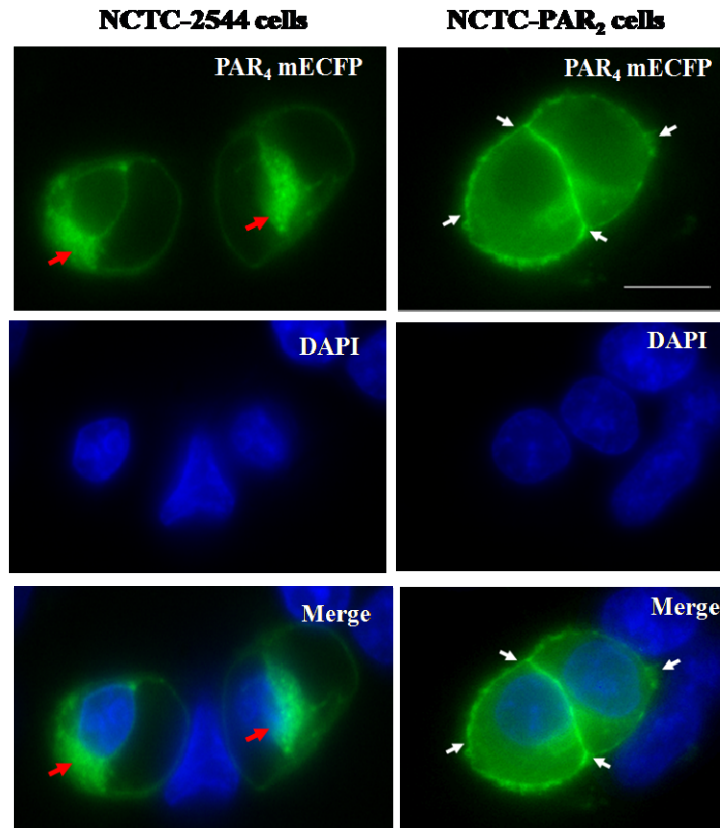
Figure 5.2. Expression of PAR₄ mECFP in NCTC-2544 and NCTC-PAR₂ cells.

PAR₄ mECFP was transiently transfected as indicated for 24 hours in (A) NCTC-2544 (**N**), NCTC-PAR₂ (**NP₂**) or HEK293 (**HEK**) cells prior to serum starvation for a further 24 hours. Whole cell lysates were prepared and resolved by Western blotting with PAR₄ mECFP detected using a GFP antibody. (B) The different receptor populations of PAR₄ mECFP were monitored by fluorescence microscopy in NCTC and NCTC-PAR₂ cells (scale bar = 10 μm). Membrane expression is highlighted by white arrows whilst the red arrows represent intracellular retained receptor. These blots and images are representative of at least three independent experiments.
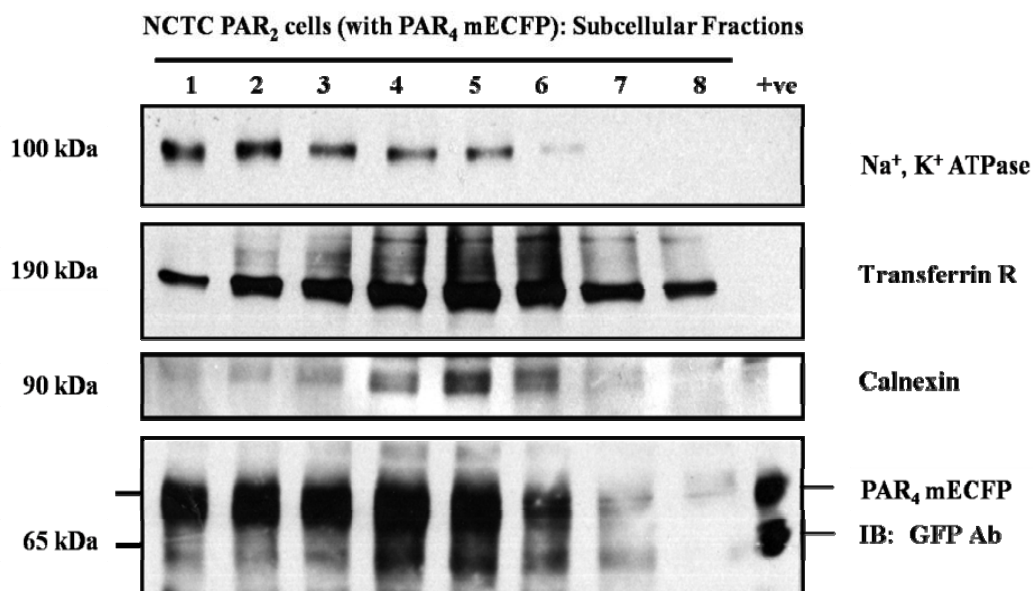
Figure 5.3. Subcellular fractionation (SCF) of plasma membrane, endosomal and endoplasmic reticulum (ER) compartments in NCTC-PAR$_2$ cells.

Subcellular fractionation was carried out in NCTC-PAR$_2$ cells expressing PAR$_4$ mECFP using differential ultra-centrifugation on a density gradient as outlined in Chapter 2.8.6. Fractions of 300 µl (1-8 shown above) were resolved by Western blotting. Na$^+$, K$^+$ ATPase (~100 kDa), transferrin receptor (~190 kDa) and calnexin (90 ~kDa) antibodies were used for the detection of membrane, endosomal and ER compartments respectively. PAR$_4$ mECFP was detected using a GFP antibody. A positive control (HEK293 cells expressing PAR$_4$ mECFP) was loaded as a control to indicate both immature ER PAR$_4$ (65kDa) and mature receptor (~70-75 kDa) bands. These blots are representative of at least two independent experiments.

5.2. The effect of PAR$_4$ ER motif mutants upon PAR$_2$-mediated translocation of PAR$_4$ in NCTC-2544 cells.

In previous studies carried out in Chapter 4, mutation of the ER motifs in PAR$_4$ resulted in different phenotypes when expressed in HEK293 cells and NCTC-2544 cells. Here the effect of motif mutation was explored when PAR$_4$ was expressed in NCTC-PAR$_2$ cells. Figure 5.4 demonstrates protein expression of PAR$_4$ mECFP and subsequent expression of R^{183}AR, R^{188}GRR and R^{183}AR/R^{188}GRR (DM) mutants using (A) Western blotting and (B) epifluorescence microscopy. These results show two PAR$_4$ bands (one 65 kDa and the upper 70-75 kDa band) following expression of the R^{183}AR mutant, with corresponding imaging results identifying distinct intracellular and cell surface PAR$_4$ similar to that observed for cells expressing PAR$_4$ mECFP. However, when the R^{188}GRR and DM mutants were expressed, only the 65 kDa was observed with PAR$_4$ localisation confined to intracellular compartments, presumably the ER.

(A)

(B)
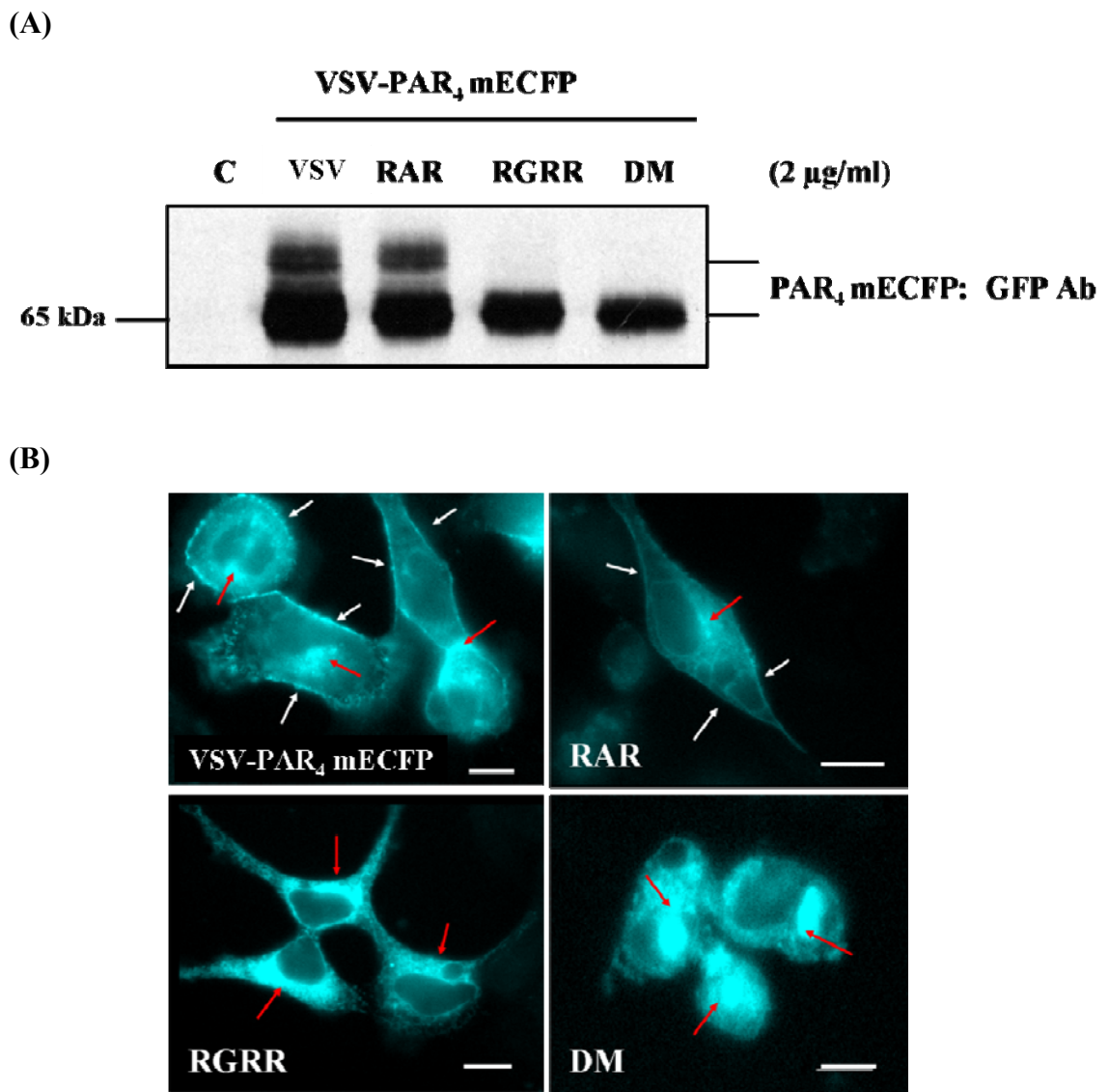
Figure 5.4. Expression of ER retention motif mutants in NCTC-PAR$_2$ cells.

NCTC- PAR$_2$ cells were grown in plates and on coverslips and transiently transfected with VSV-PAR$_4$ mECFP (VSV) or ER motif mutant constructs as indicated above, for 24 hours prior to serum starvation for a further 24 hours. (A) Whole cell lysates were prepared and resolved by Western blotting as outlined in Chapter 2.8.2. PAR$_4$ receptor expression was detected using a GFP antibody. (B) Transfected cells grown on coverslips were prepared for epifluorescence microscopy as outlined in Chapter 2.6.1. Corresponding images were acquired at 100x magnification (scale bar = 10 μm). The localisation of the ER mutants was compared to VSV-PAR$_4$ mECFP with membrane (white arrows) and intracellular expression (red arrows) highlighted.

5.3. FRET analysis between PAR$_4$ mECFP and PAR$_2$ mEYFP

One of the notable features of co-expression of PAR$_2$ and PAR$_4$ so far in this Chapter was the ability of PAR$_2$ to mediate PAR$_4$ membrane expression. In order to identify if PAR$_2$ and PAR$_4$ interact as possible heterodimers, FRET analysis was carried out in HEK293 cells and NCTC-2544 cells.

Wide field FRET was carried out in HEK293 cells (Figure 5.5) and in NCTC-2544 cells (Figure 5.6) expressing PAR$_2$ mEYFP (Acceptor) and PAR$_4$ mECFP (Donor). Three images were acquired for FRET analysis which included; a CFP/Donor image (in cyan), YFP/Acceptor image (in yellow) and an uncorrected FRET (uFRET) image (in magenta), which contains the raw FRET signal with spectral bleedthrough contamination. Once bleedthrough correction has been carried out, actual FRET can be determined and the uFRET image corrected (cFRET).

In Figure 5.5, when PAR$_4$ mECFP and PAR$_2$ mEYFP were expressed in HEK293 cells, fluorescence was detected in the cFRET image. When the images were processed and the FRET data analysed, ratiometric FRET (RFRET) values were determined for each sample tested. These are graphed in Figure 5.5 (B). Co-expression of PAR$_2$ mEYFP and PAR$_4$ mECFP resulted in a significant increase in RFRET (1.883 ± 0.003) when compared to the RFRET values obtained for PAR$_2$ mEYFP (0.952 ± 0.002), PAR$_4$ mECFP (0.989 ± 0.003) and cells co-expressing mEYFP and mECFP (1.173 ± 0.055); the benchmark for collisional FRET that accounts for fluorophore interaction. In order to minimise repetition of FRET data interpretation, the RFRET values obtained for other controls tested involved in these experiments have been tabulated (C). This includes values obtained for cells expressing mECFP and mEYFP in isolation, in addition to the positive control for FRET analysis; a tandem construct with mEYFP and mECFP fused together.

Parallel experiments were conducted in NCTC2544 cells, as shown in Figure 5.6. When PAR$_2$ mEYFP and PAR$_4$ mECFP were co-expressed, no fluorescence signal was detected in the cFRET image (A). The RFRET values were similarly quantified and graphed (B), with an overall RFRET value of 1.176 ± 0.029 obtained for PAR$_2$

mEYFP and PAR$_4$ mECFP. These values were consistent with control RFRET values for cells expressing each receptor in isolation; PAR$_2$ mEYFP only (RFRET 0.879 ± 0.023) and PAR$_4$ mECFP (RFRET 0.996 ± 0.004), and were not different from the collisional FRET value observed between mECFP and mEYFP expressing cells (RFRET 1.101 ± 0.008). The remaining control RFRET values are also shown (C).

.

Based upon the RFRET values obtained for PAR$_2$ mEYFP and PAR$_4$ mECFP in HEK293 cells, ratiometric FRET images were prepared to distinguish the localisation of peak RFRET signals. As shown in Figure 5.7, a strong FRET signal was observed in intracellular compartments, presumably the ER/Golgi secretory pathway. A weak signal was also observed at the plasma membrane.

Due to the lack of FRET interaction between PAR$_2$ mEYFP and PAR$_4$ mECFP, it was decided that similar analysis would be carried out in cells expressing PAR$_1$ mEYFP and PAR$_4$ mECFP. The RFRET values obtained for these experiments are shown in Figure 5.8. When PAR$_1$ mEYFP and PAR$_4$ mECFP were co-expressed, fluorescence was negligible in the cFRET image (A). Whilst an increase in the RFRET value for PAR$_1$ and PAR$_4$ co-expression was observed (RFRET 1.114 ± 0.023), when compared to the collisional mECFP and mEYFP RFRET value (1.113 ± 0.001), there was no significant difference.

(A)

(B)

(C)
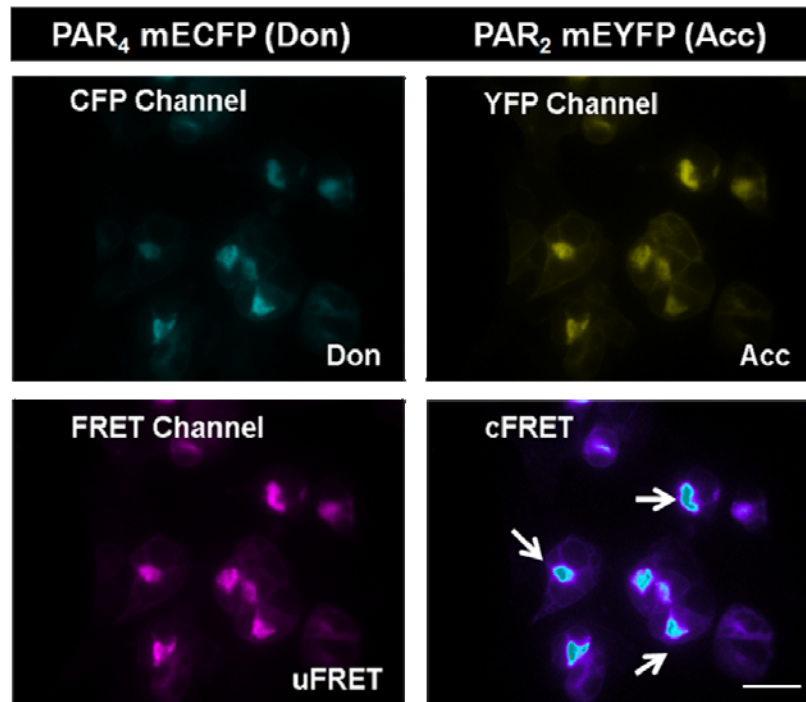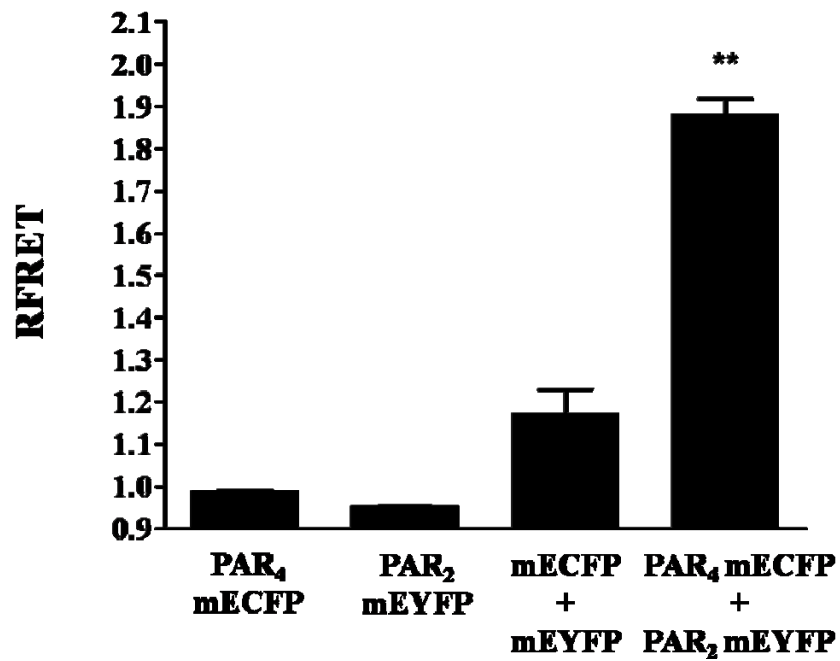
Controls	RFRET value ± s.e.m
mECFP only	0.999 ± 0.003
mEYFP only	1.005 ± 0.003
mECFP + mEYFP	1.173 ± 0.005
mECFP-mEYFP tandem	5.148 ± 0.129
PAR_4 mECFP only	0.989 ± 0.003
PAR_2 mEYFP only	0.955 ± 0.002
PAR_4 mECFP + PAR_2 mEYFP	1.883 ± 0.035

Figure 5.5. FRET imaging of PAR_4 and PAR_2 in HEK293 cells.

PAR_4 mECFP and PAR_2 mEYFP co-expressed in HEK293 cells. Wide field FRET was carried out on live cells as outlined in Chapter 2.7. (A) Images were acquired for CFP, YFP, uncorrected FRET (uFRET), with the uFRET channel corrected for spectral bleedthrough/contamination (cFRET). Ratiometric FRET (RFRET) values were then quantified, graphed (B) and tabulated (C). Tabulated data expressed as a mean ± s.e.m from three separate FRET experiments (n=72 single cell measurements), **p=0.001 one-way ANOVA with Dunnett's post test.

(A)

(B)

(C)
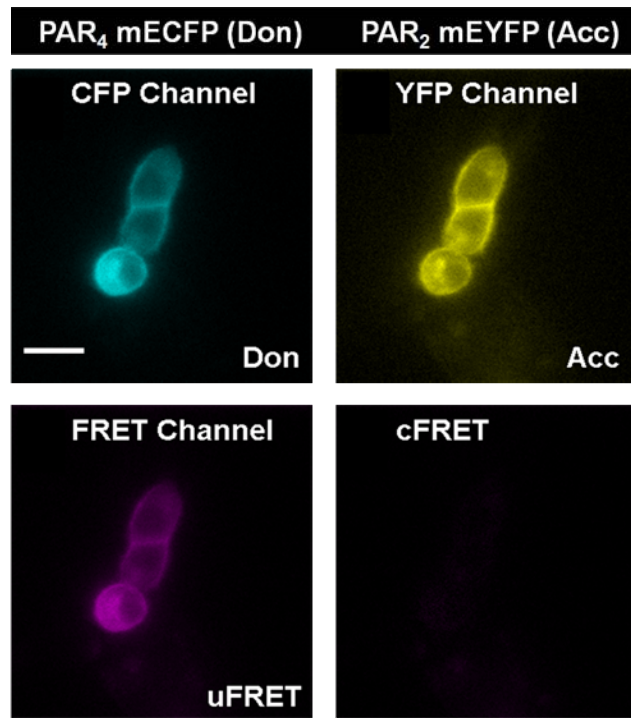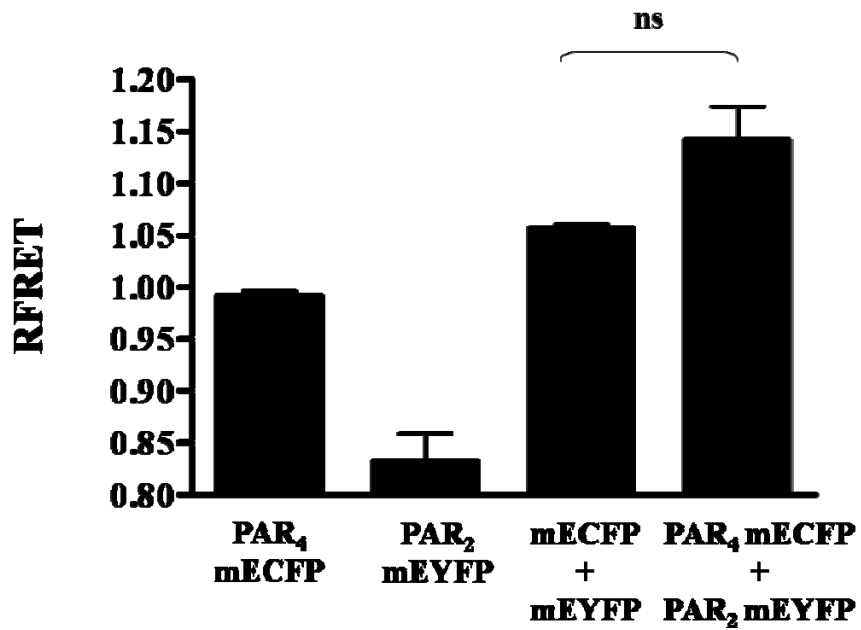
Controls	RFRET value ± s.e.m
mECFP only	1.001 ± 0.004
mEYFP only	0.986 ± 0.010
mECFP + mEYFP	1.101 ± 0.008
mECFP-mEYFP tandem	5.510 ± 0.081
PAR$_4$ mECFP only	0.996 ± 0.004
PAR$_2$ mEYFP only	0.879 ± 0.023
PAR$_4$ mECFP + PAR$_2$ mEYFP	1.176 ± 0.029

Figure 5.6. FRET imaging of PAR$_4$ and PAR$_2$ in NCTC-2544 cells.

PAR$_4$ mECFP and PAR$_2$ mEYFP co-expressed in NCTC-2544 cells (A). Wide field FRET was performed in live cells as outlined in Chapter 2.7. Images were acquired for CFP, YFP, uncorrected FRET (uFRET), with the uFRET channel corrected for spectral bleedthrough/contamination (cFRET). Ratiometric FRET (RFRET) values were then quantified, graphed (B) and tabulated (C). Tabulated data expressed as a mean ± s.e.m from three separate FRET experiments (n=72 single cell measurements), n.s. = not significant, one-way ANOVA.
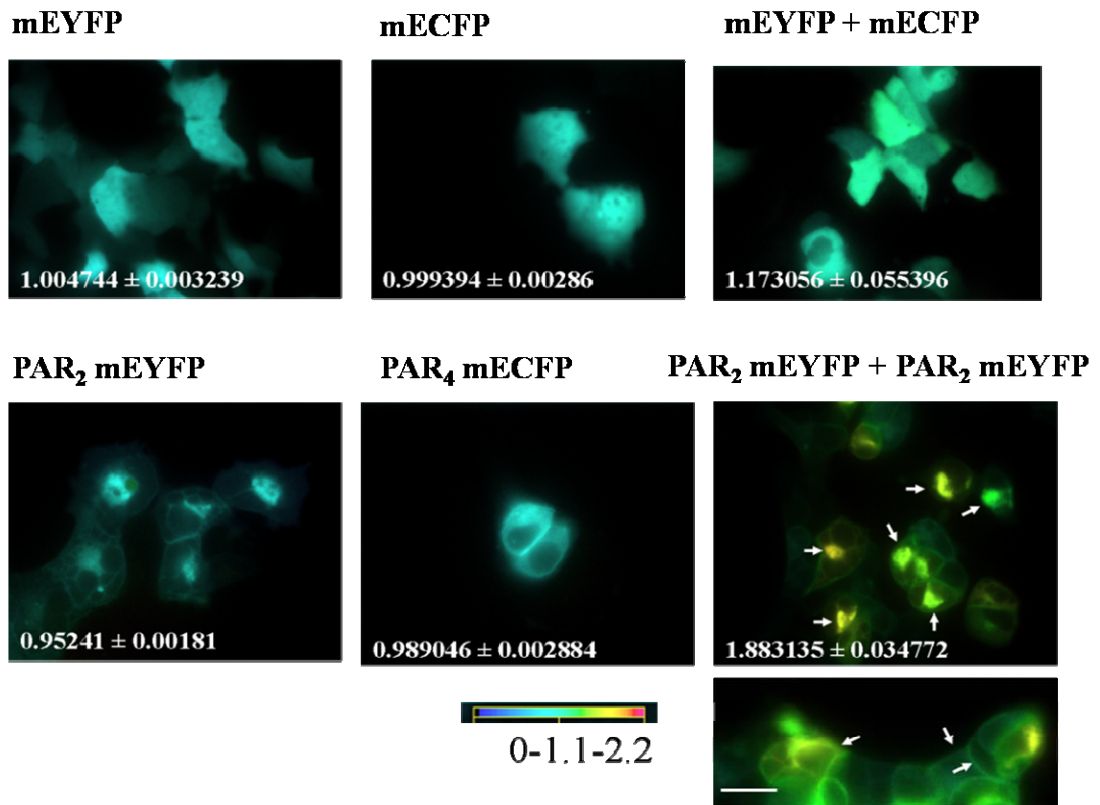
Figure 5.7. Ratiometric FRET images for FRET signal detected in HEK293 cells. RFRET images shows intensity-scaled images across all samples tested scaled to the positive FRET signal observed between PAR4 mECFP and PAR2 mEYFP. These images demonstrate the prominent intracellular distribution of the RFRET signal, with only a weak signal observed on the membrane. Images representative of three separate FRET experiments, scale bar = 25µm.

(A)
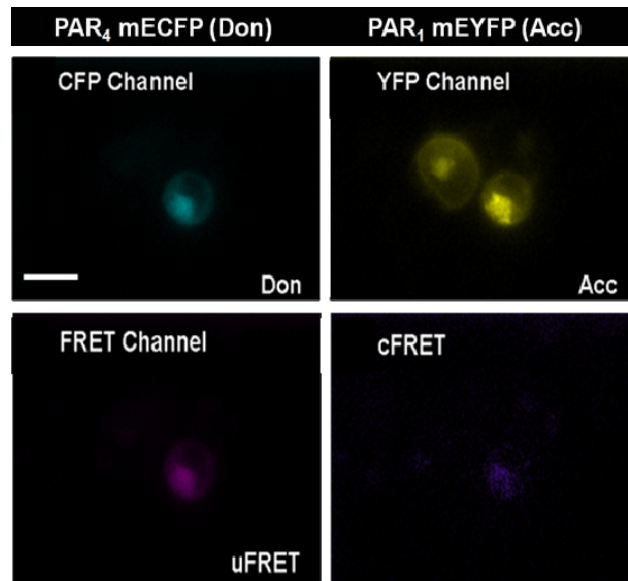
(B)
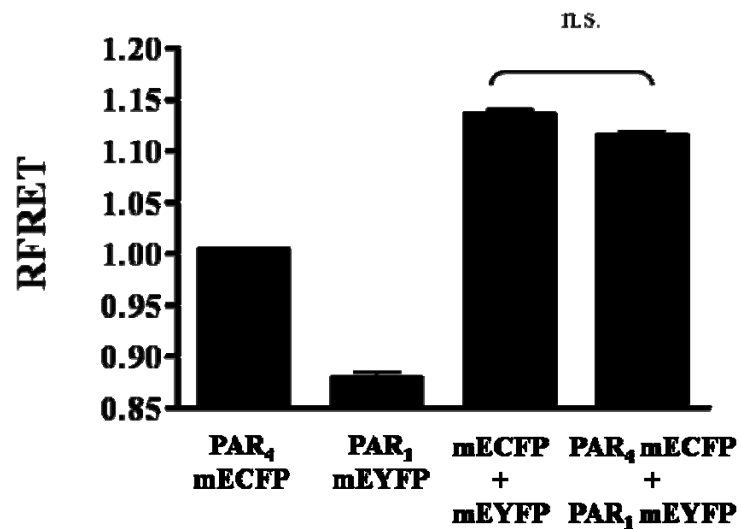
Figure 5.8. FRET imaging of PAR$_4$ and PAR$_1$ in NCTC-2544 cells.

PAR$_4$ mECFP and PAR$_1$ mEYFP co-expressed in NCTC-2544 cells. Wide field FRET was performed in live cells as outlined in Chapter 2.7. (A) Images were acquired for CFP, YFP, uncorrected FRET (uFRET), with the uFRET channel corrected for spectral bleedthrough/contamination (cFRET). Ratiometric FRET (RFRET) values were then quantified and graphed (B). n=72 single cell measurements over three independent experiments, n.s. = not significant, one-way ANOVA.

5.4 The effect of TNF alpha upon co-expression of PAR$_2$ mEYFP and PAR$_4$ mECFP in NCTC-2544 cells.

Despite previous experiments demonstrating clear translocation of PAR$_4$ to the membrane when co-expressed with PAR$_2$, no FRET was detected between these two receptors. Based on previous experiments conducted in the laboratory where upregulation of PAR$_2$ and PAR$_4$ was observed during prolonged treatment with TNFα (Ritchie *et al.,* 2007), the ability of PAR$_2$ mEYFP and PAR$_4$ mECFP to interact under similar conditions was examined. FRET analysis was carried out in NCTC-2544 cells co-expressing PAR$_2$ mEYFP and PAR$_4$ mECFP following treatment with TNFα (10 ng/ml) for 24 hours. As a comparison, parallel FRET experiments in cells expressing PAR$_1$ mEYFP and PAR$_4$ mECFP were also performed.

Figure 5.9 shows the effect of treatment in NCTC-2544 cells co-expressing PAR$_2$ mEYFP and PAR$_4$ mECFP. In the absence of TNFα, no fluorescence was observed in the cFRET image. However in the presence of TNFα, fluorescence was detected (A) with a significant increase in RFRET (1.406 ± 0.043) relative to the collisional FRET control (1.139 ± 0.02) as shown in Figure 5.9 (B). TNFα did not have any effect upon RFRET values obtained for the control samples with no difference observed in these values either in the presence or absence of TNFα (C).

The ability of TNFα to promote FRET between PAR$_1$ mEYFP and PAR$_4$ mECFP in NCTC-2544 cells was assessed. The RFRET values in Figure 5.10 clearly demonstrated that the effect of TNFα was specific to PAR$_2$/PAR$_4$, with no increase in RFRET observed between untreated (1.245 ± 0.023) and treated (1.14 ± 0.019) cells expressing PAR$_1$/PAR$_4$. In fact, a significant decrease in RFRET was observed in these cells.

A)

(B)

(C)
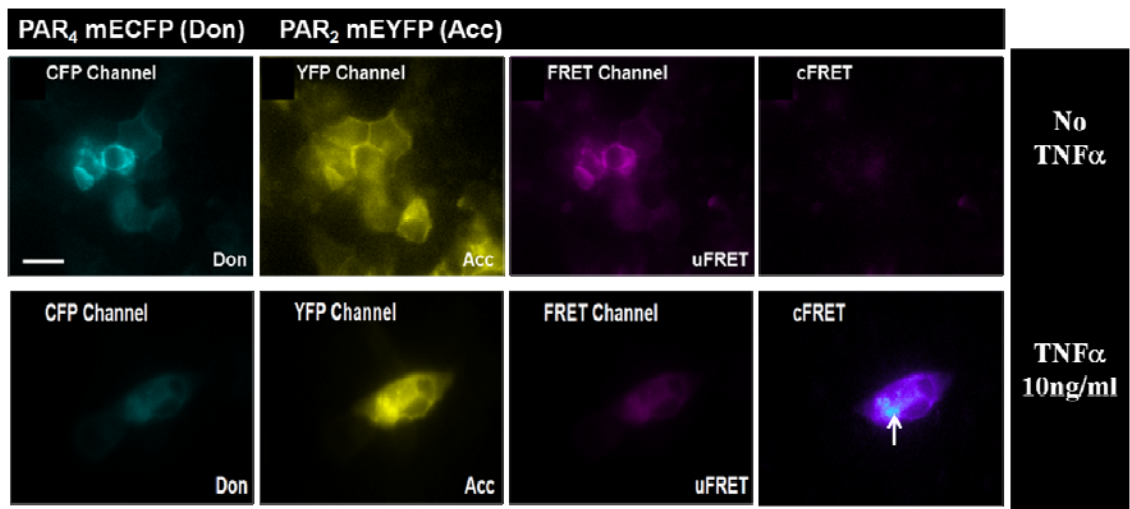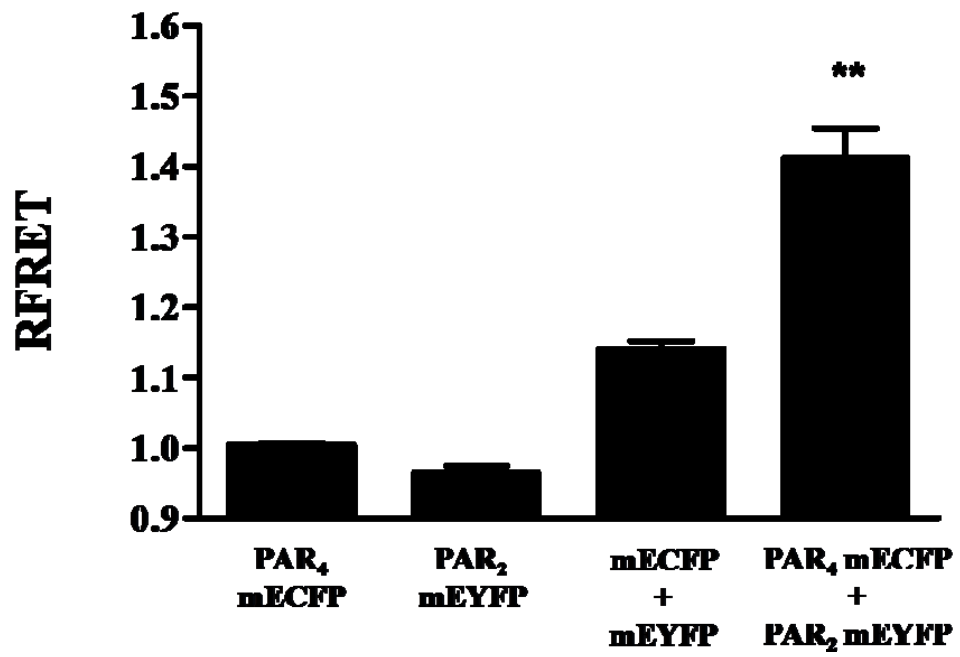
	No TNFα	+ TNFα (10 ng/ml)
Controls	RFRET	RFRET
mECFP only	1.000 ± 0.003	0.998 ± 0.003
mEYFP only	0.986 ± 0.010	0.996 ± 0.003
mECFP + mEYFP	1.110 ± 0.006	1.139 ± 0.002
mECFP-mEYFP tandem	5.502 ± 0.081	5.430 ± 0.021
PAR$_4$ mECFP only	1.00 ± 0.004	1.004 ± 0.003
PAR$_2$ mEYFP only	0.879 ± 0.023	0.964 ± 0.009
PAR$_4$ mECFP + PAR$_2$ mEYFP	1.169 ± 0.030	1.406 ± 0.043

Figure 5.9. FRET imaging of PAR$_4$ and PAR$_2$ in NCTC-2544 cells treated with TNFα.

PAR$_4$ mECFP and PAR$_2$ mEYFP co-expressed in NCTC-2544 cells for 24 hours prior to treatment with TNFα as indicated for a further 24 hours. Wide field FRET was performed in live cells as outlined in Chapter 2.7. (A) Images were acquired for CFP, YFP, uncorrected FRET (uFRET), with the uFRET channel corrected for spectral bleedthrough/contamination (cFRET). (B) Ratiometric FRET (RFRET) values were then quantified and graphed. RFRET values for all samples are shown in the table (C). n=72 single cell measurements over three independent experiments, **p=<0.001, one-way ANOVA with Dunnett's post test.
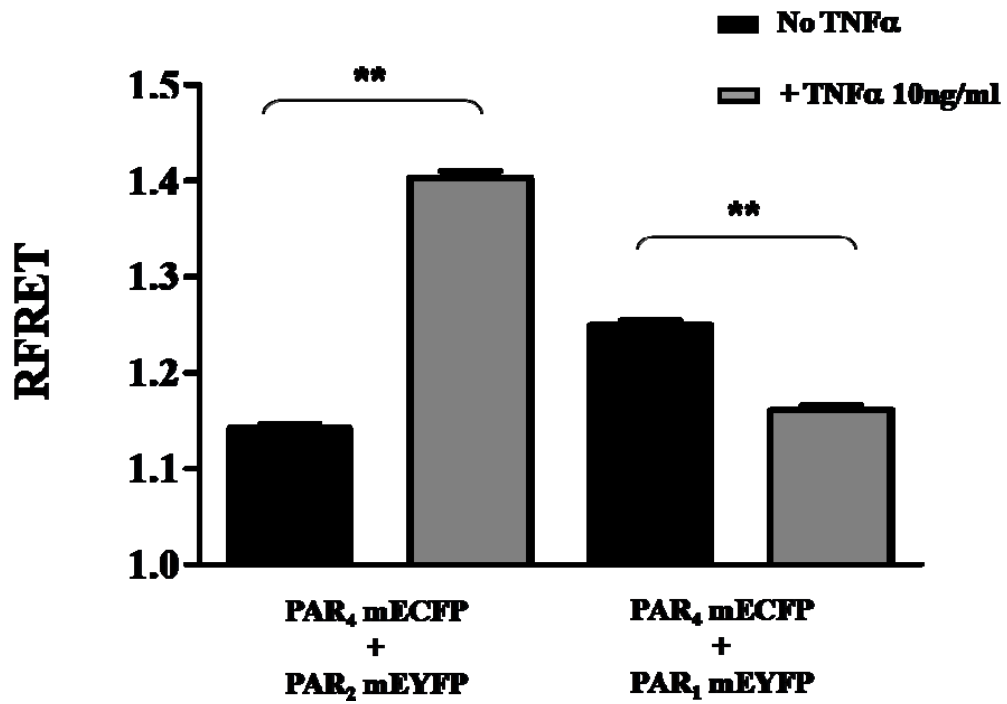
Figure 5.10. Comparing RFRET values of PAR$_4$/PAR$_2$ and PAR$_4$/PAR$_1$.
Wide field FRET was performed in NCTC-2544 cells co expressing either PAR$_2$ mEYFP/PAR$_4$ mECFP or PAR$_1$ mEYFP/PAR$_4$ mECFP following treatment with TNFα. (10 ng/ml) for 24 hours. The ratiometric FRET (RFRET) values obtained for these experiments were then quantified and graphed. n=72 single cell measurements, **p=<0.001, one-way ANOVA with Dunnett's post test.

5.5 The effect of ER motif mutation on PAR$_2$/PAR$_4$ FRET in HEK293cells

In both HEK293 cells and the NCTC-PAR$_2$ cells, mutation of the ER motifs within PAR$_4$ resulted in a loss of PAR$_4$ cell surface expression, and in the case of HEK293 cells a loss of function. Mutation of the R^{188}GRR and the double motif (DM) mutant confined PAR$_4$ to the ER in both of these cell systems. Here, the ability of these receptor mutants to influence PAR$_2$/PAR$_4$ FRET responses was observed in HEK293 cells. As Figure 5.11 shows, mutation of these motifs (RFRET values: R^{183}AR = 1.410 ± 0.023, R^{188}GRR = 1.383 ± 0.058, DM = 1.426 ± 0.040) did not alter RFRET between PAR$_2$/PAR$_4$ when compared with responses obtained from interaction between PAR$_2$ mECFP and wild type PAR$_4$ mECFP (1.496 ± 0.041). FRET between PAR$_2$ and PAR$_4$ remained intact.
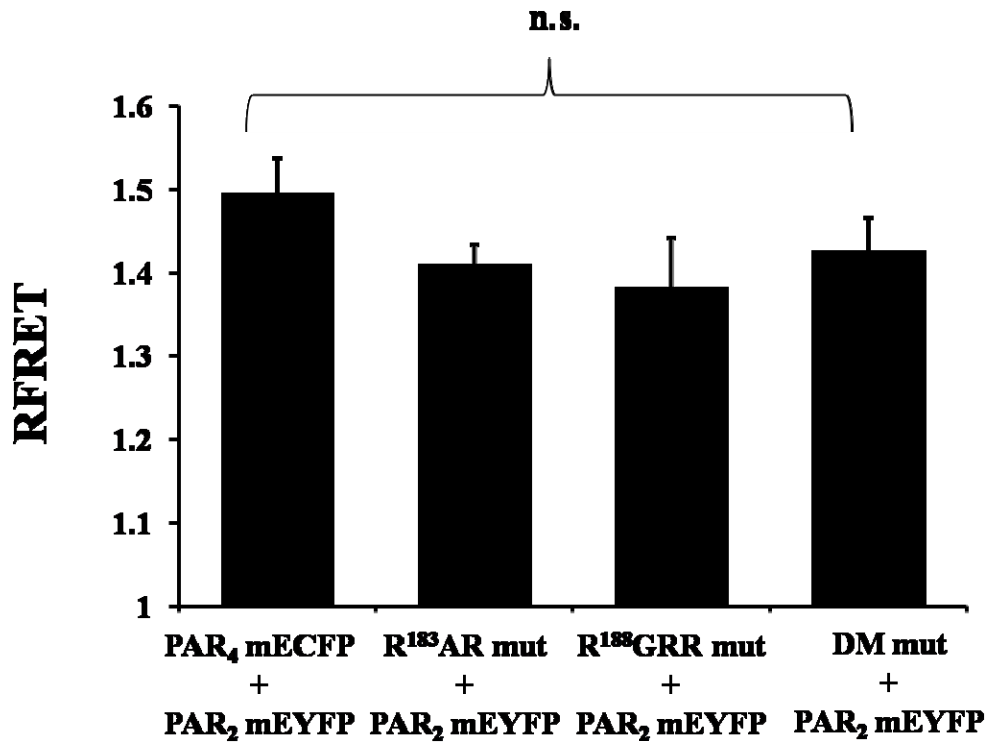
Figure 5.10. Comparing RFRET values of PAR$_4$/PAR$_2$ to those obtained from cells expressing PAR$_4$ ER motif mutants.

Wide field FRET was performed in NCTC-2544 cells co-expressing; PAR$_2$ mEYFP/PAR$_4$ mECFP, PAR$_2$ mEYFP/R^{183}AR mECFP mutant, PAR$_2$ mEYFP/R^{188}GRR mECFP mutant, or PAR$_2$ mEYFP/ R^{183}AR R^{188}GRR mECFP mutant (DM). The ratiometric FRET (RFRET) values obtained for these experiments were then quantified and graphed.   n=28 single cell measurements from two independent experiments, n.s. = not significant p>0.05, one-way ANOVA with Dunnett's post test.

5.6 Preliminary assessment of the effects of PAR$_2$/PAR$_4$ co-expression on PAR$_4$ mediated inositol phosphate responses.

Although FRET between PAR$_4$ mECFP and PAR$_2$ mEYFP was negligible in the NCTC-2544 cell system, the fact remained that co-expression of these receptors resulted in the delivery of PAR$_4$ to the plasma membrane. The effect of these events upon PAR$_4$ mediated cell signal transduction was explored. Due to time constraints, the only signalling parameters to be assessed were inositol phosphate responses. However work is currently ongoing to assess effects upon ERK, JNK, P38 MAPK activation, calcium mobilisation and NFκB responses.

As shown in Figure 5.11, in NCTC-2544 and NCTC-PAR$_2$ cells transiently expressing PAR$_4$ mECFP results in an increase in the basal inositol phosphate response (NCTC, 4.59 ± 0.45 fold; NCTC-PAR$_2$, 8.28 ± 0.65). When both cell systems were treated with the PAR$_4$ activating peptide, AYPGKF-NH$_2$, an increase in the inositol phosphate response was observed. When PAR$_4$ was expressed in NCTC-PAR$_2$ cells, a significant increase in response was observed (9.47 ± 2.45 and 21.16 ± 2.62 fold on NCTC-PAR$_2$ basal), relative to responses observed in NCTC-2544/PAR$_4$ cells (7.80 ± 0.46 and 9.47 ± 2.45 fold of NCTC basal).
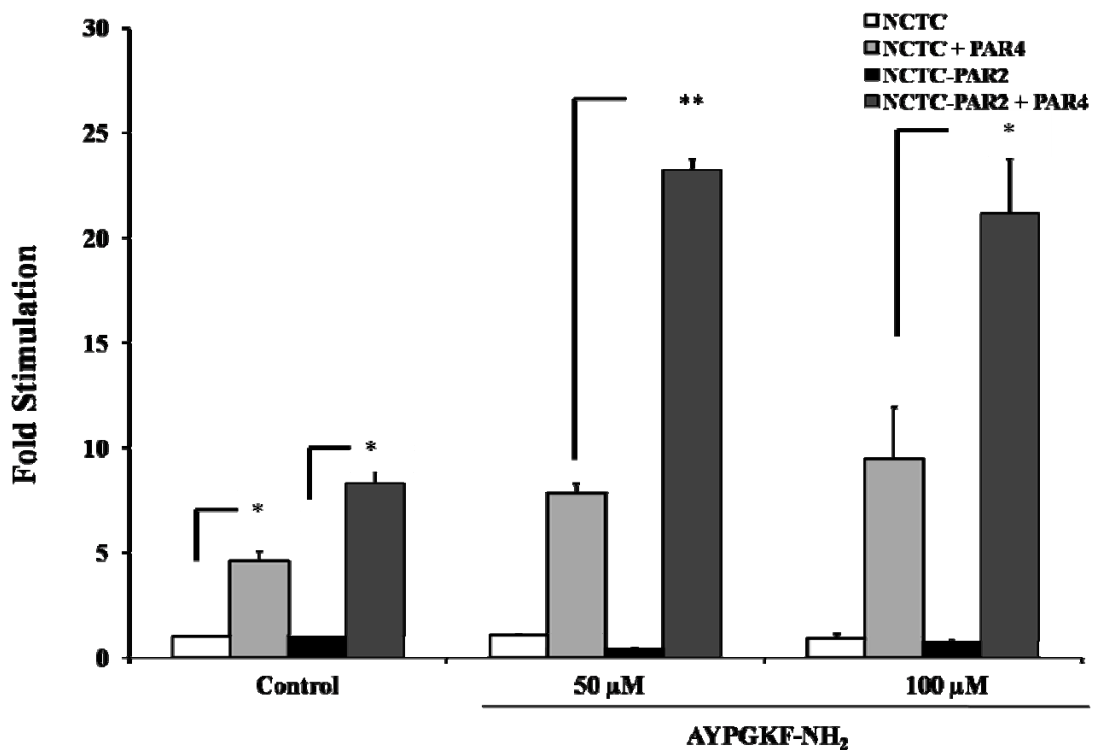
Figure 5.11. **PAR$_4$-mediated [^{3}H]-inositol phosphate accumulation in NCTC-2544 and NCTC-PAR$_2$ cells.**

Cells were transiently transfected for 24 hours with PAR$_4$ mECFP, as outlined in Chapter 2.5. The media was replaced with serum free growth media supplemented with 0.25 μCi of [^{3}H]-2-myo-inositol for a further 24 hours prior. Cells were pre-treated with 10 mM lithium chloride for 15 minutes prior to stimulation with AYPGKF-NH$_2$ for 45 minutes. Total inositol phosphate (InsP$_{1-4}$) accumulation was measured through anion exchange as described in Chapter 2.9. The data presented represent values taken in triplicate (mean ± s.e.m.) over three independent experiments (**p=<0.01).

5.7 Discussion

In Chapter 4 the events underlying PAR$_4$ ER retention were assessed, whilst the focus of Chapter 5 was to elucidate the mechanisms through which PAR$_4$ was able to reach the cell surface. The presence of a functional ER retention motif and subsequent interaction with an ER chaperone confirmed ER retention however the ability of PAR$_4$ to localise at the membrane in HEK293 cells but remain in the ER in the NCTC model highlighted the existence of an alternative regulatory pathway. In the secretory pathway, proper folding and assembly of GPCRs is essential for efficient export to the cell membrane and function (Lippincott-Schwartz *et al.,* 2000). A number of ER retained GPCRs manage to overcome this by forming complexes with other GPCRs to evade retention (Boyd *et al.,* 2003; Margeta-Mitrovic *et al.,* 2000). These studies show that GPCR dimerisation may be crucial for plasma membrane localisation and function. The ability of PAR$_4$ to interact with PAR$_2$ was explored as a mechanism to regulate intracellular trafficking to the membrane and subsequent cell signal transduction.

The NCTC-2544 cell system provided the ideal model to monitor PAR$_4$ localisation due to the lack of PAR activity observed in experiments carried out in the previous chapters. The experiments carried out in this chapter identified a novel interaction between PAR$_2$ and PAR$_4$; with a clear role for PAR$_2$ in the regulation of PAR$_4$ localisation. For FRET to occur between two fluorophore fused proteins, they must be within 1-100 Å of one another for energy from the donor to be efficiently transferred to the acceptor (Takanishi *et al.,* 2006). The fact that no FRET was observed in NCTC cells between PAR$_4$ mECFP (donor) and PAR$_2$ mEYFP (acceptor) could have been due to the limitations of the method used to detect interaction due to the presence of another protein in the complex. Whilst co-immunoprecipitation of PAR$_2$ and PAR$_4$ was attempted (not shown), these results were hindered by the lack of quality antibodies for the detection of PAR$_2$. Previously immunoprecipitation has been undertaken for PAR$_2$ however as this receptor is highly glycosylated (Compton *et al.,* 2001) many of these approaches use pharmacological deglycosylation agents such as tunicamycin to resolve receptor bands (Hasdemir *et al.,* 2009). The use of tunicamycin in the present study was shown to abolish cell surface expression of

PAR$_4$, therefore to use such conditions for immunoprecipitation may disrupt the regulatory interactions responsible for membrane localisation.

Endogenous PAR expression in the HEK293 cell model precluded the use of these cells for the purpose of investigating the intricate nature of cell surface delivery but provided another model to establish if PAR$_2$ and PAR$_4$ could form heterodimers in a different cell system. Fundamental differences in PAR$_2$ and PAR$_4$ expression in these cell systems were further highlighted by FRET analysis. In HEK293 cells, an intracellular FRET signal was observed between PAR$_4$ mECFP and PAR$_2$ mEYFP, indicating that they can form heterodimers when co-expressed. The assembly of GPCR dimers are thought to occur early in the protein synthesis pathway (Bouvier, 2001), thus this FRET signal may be representative of the early stage of dimer assembly in the ER. Based on this data it may be that the PAR$_2$ and PAR$_4$ heterodimer is one that is preformed in the ER, similar to the GABA$_{B1}$/GABA$_{B2}$ (Marshall *et al.,* 1999; Margeta-Mitrovic *et al.,* 2000), with the purpose of allowing PAR$_4$ to be expressed as a mature glycoprotein at the cell surface. A notable feature of the FRET analysis carried out between the two cell systems was the high level of intracellular PAR$_2$/PAR$_4$ observed in HEK293 cells when compared with co-expression of PAR$_2$/PAR$_4$ in the NCTC-2544 model. The lack of intracellular compartmentalisation of PAR$_2$/PAR$_4$ in NCTC-2544 cells may explain why constitutive PAR$_2$/PAR$_4$ FRET was readily observed in HEK293 cells and not in NCTC-2544 cells. Furthermore, the fact that FRET was not observed in the membrane may suggest that interaction between PAR$_2$/PAR$_4$ may only be required for ER export however once at the membrane; the two receptors may exist as separately functioning units. The structural determinants that dictate the transient/stable formation of GPCR dimers remains unclear.

Although it may be possible that the R^{183}AR sequence becomes masked during heterodimer assembly, when FRET analysis was carried out between PAR$_2$ and the PAR$_4$ ER mutants it was established that these ER retention sequences were not a factor that directly contributed towards PAR$_2$ and PAR$_4$ heterodimerisation. Mutation of these sequences did not affect energy transfer between PAR$_4$ mECFP and

PAR$_2$ mEYFP, thus the actual site of interaction between PAR$_2$ and PAR$_4$ remains unknown. Such studies investigating the dimer interface of Class A GPCRs have used cysteine crosslinking approaches, identifying transmembrane 4 (TM4) and TM5 (Guo *et al.,* 2003) and TM6 (Hebert *et al.,* 1996) to be crucial for the dimer stability. Using peptides derived from a region of TM6, Bouvier and colleagues identified that the L^{272}xxxGxxxGxxxL sequence in TM6 was a site of interaction for β$_2$ adrenoreceptor homodimer formation (Hebert *et al.,* 1996). In the TM6 of PAR$_4$ a G^{316}xxxG sequence is present however the significance of this sequence in interaction remains to be investigated. Using this peptide approach may be the key to the identification of key domains involved in PAR$_2$/PAR$_4$ interaction. Interaction between PAR$_3$ and PAR$_4$ has been identified, whereby the extracellular N-terminal domain of PAR$_3$ presents PAR$_4$ with a means to interact with thrombin with high affinity (Nakanishi-Matsui *et al.,* 2000). The very nature of PAR activation; proteolytic cleavage of the N-terminal to form a tethered ligand which intramolecularly interacts with ECL-2, presents a possible site which may be significant for PAR$_2$ and PAR$_4$ interaction. The availability of peptide agonists and blockers derived from the tethered ligand sequence of these receptors may provide a better understanding of interaction, and identify if interaction between ECL-2 domains of PAR$_2$ and PAR$_4$ exists. Furthermore, in HEK293 and NCTC-PAR$_2$ cell lines, the R^{188}GRR mutant resulted in immature PAR$_4$ expression, with no cell surface expression observed, however FRET between PAR$_2$ and this mutant was maintained. These effects implicate this sequence as a key feature to the membrane expression of PAR$_4$. Whilst mutation of this sequence may retain the complex in the ER, the use of cell permeable peptides to block this sequence, instead to the mutagenesis approach currently in use, may provide a better understanding of its role in intracellular trafficking.

Despite obvious translocation of PAR$_4$ to the membrane when co-expressed in NCTC cells with PAR$_2$, the fact that interaction was not observed in these cells between these two receptors was surprising. However, the ability of GPCRs to dimerise can be readily influenced by changes to the physiological environment in which that are expressed. Agonist-induced conformational changes in GPCRs can promote

dimerisation or even cause GPCR dimeric complexes to separate and form monomers. This is particularly true for members of the human somatostatin (hSSTR) receptors during treatment with SST-14 (Grant *et al.,* 2004) and treatment of dopamine D_1 receptor with cell permeable agonists (Kong *et al.,* 2006; Gines *et al.,* 2000) among other GPCR families. Whilst the ability of PAR_2 and PAR_4-specific agonists to influence PAR_2/PAR_4 interaction have not been demonstrated in this thesis, attempts were made using a dynamic FRET approach as described by Ponsioen *et al.,* 2004 (not shown). Quantification of the images acquired and processed from this method was greatly hindered by the level of receptor/cell movement observed during stimulation, thus reliable changes in fluorescence could not be achieved by this method. The use of a more sensitive time-resolved FRET, BRET or SNAP/CLIP (Maurel *et al.,* 2008) technique may be better tools for monitoring agonist-induced changes in PAR_2/PAR_4 interaction.

Previous studies have found an increase in PAR_2 and PAR_4 levels in endothelial cells under pro-inflammatory stress (Ritchie *et al.,* 2007; Hamilton *et al.,* 2001). In Chapter 5, a robust intracellular FRET response was observed between PAR_2 and PAR_4 in NCTC-2544 cells following treatment with TNFα. Furthermore this effect was only observed during co-expression of PAR_2 and PAR_4; a possible feature of dual upregulation. The fact that no FRET was observed between PAR_1 and PAR_4 indicate that this interaction was not an artefact of overexpression. Heterodimerisation between PAR_1 and PAR_4 has previously been identified by other laboratories in COS-7 fibroblasts using FRET (Leger *et al.,* 2006b). However as FRET analysis in the present study demonstrates, the ability of receptors to interact in one cell system does not mean interaction can be applied to all cellular environments where these receptors are expressed.

As the preliminary experiments investigating the functional significance of interaction between PAR_2 and PAR_4 show; an increase in PAR_4 membrane localisation during PAR_2 co-expression resulted in enhanced PAR_4-mediated inositol phosphate responses. So far functional analysis has been performed in a transient expression system however work is ongoing to develop a stable PAR_4 expression

system in NCTC-2544 cells in which PAR_2 is regulated under a doxycyline promoter. These cell systems are routinely used in the Milligan laboratory for the functional characterisation of the receptor pharmacology of GPCR dimmers (Ellis *et al.,* 2006; Sartania *et al.,* 2007; Lopez-Gimenez *et al.,* 2008; Canals and Milligan, 2008). Using these cells, the functional role of PAR_2-mediated cell surface delivery of PAR_4 will be further explored for JNK, P38 MAPK, ERK and NKκB signalling pathways.

Experiments carried out in the present study highlighted a potentially important role for TNFα in the regulation of PAR_2 and PAR_4 interaction. An increase in PAR_2 has been linked to the progression of chronic inflammation (Ferrell *et al.,* 2003), with a role for PAR_4 in acute inflammation being implicated in other arthritic models (Russell *et al.,* 2009; McDougall *et al.,* 2009). Co-expression of these receptors in these pathophysiological environments where TNFα is in abundance may be pivotal to the progression of a PAR_2/PAR_4 –mediated pro-inflammatory response. This is currently under investigation.

CHAPTER 6

GENERAL DISCUSSION

Trafficking of receptors from the endoplasmic reticulum (ER) to the plasma membrane is a highly coordinated process which in many cases involves multiple accessory proteins. The work presented in this thesis explored the mechanisms through which PAR_4 localisation was regulated. This work was undertaken in the attempt to provide a better understanding of the molecular pharmacology of proteinase-activated receptor 4 (PAR_4).

In this study, receptors fused with fluorescent proteins were relied upon to monitor receptor expression. Full characterisation of PAR_2 mEYFP and PAR_4 mECFP was carried out in Chapter 3 in order to assess if the function of PAR_2 and PAR_4 was intact in HEK293 cells and an epidermal keratinocyte-derived NCTC-2544 cell line when fused to mEYFP and mECFP respectively. Monitoring cell signal transduction of these constructs following protease and peptide agonist treatment confirmed that overexpression of the receptors retained the capacity to signal to ERK MAPK, inositol phosphate and mediate calcium responses comparable to wildtype receptor activation. These were consistent with responses documented in the literature for PAR_2 (Nystedt *et al.,*1995a and 1995b; Molino *et al.,* 1997; Seatter *et al.,*2004;) and parallel to the sustained responses observed following PAR_4 activation (Jardin *et al.,* 2007; Ando *et al.,* 2007; Bretschneider *et al.,* 2001; Covic *et al.,* 2000 and Shapiro *et al.,* 2000). The notable difference between the cell types tested in this study was the lower magnitude of response observed in the NCTC-2544 cells in comparison with HEK293 cells. The fluorescence microscopy and subcellular fractionation experiments conducted to monitor receptor expression identified key differences in the features of PAR_4 localisation between these two cell systems. In HEK293 cells, PAR_4 localised both in intracellular compartments and at the membrane as a mature glycoprotein, in many ways similar to PAR_2 (Böhm *et al.,* 1996; Déry *et al.* 1999), however no internalisation was observed following PAR_4 activation. In the NCTC-2544 cell line only intracellular receptor pools were observed.

Further assessment of the original protein sequence (Xu *et al.,* 1998) in Chapter 4 provided a rationale for the intracellular nature of PAR_4, with the identification of two potential ER retention sequences; $R^{183}AR$ and $R^{188}GRR$ respectively. These are

similar to the ER signal sequences observed in GABA$_{B1}$ (Margeta-Mitrovic *et al.,* 2000) 5HT$_{3B}$ (Boyd *et al.,* 2003), mGluR1 (Chan *et al.*, 2001), KA1 and KA2 (Ren *et al.,* 2003; Nasu-Nishimura *et al.,* 2006) and the vasopressin V2 (Hermosilla *et al.,* 2001) protein sequences which result in ER retention of these receptors. Mutagenesis of the R^{183}AR motif allowed PAR$_4$ to be expressed at the cell surface in NCTC-2544 cells, which was consistent with observations made when similar approaches were used to mutate the motifs present in other ER retained proteins such as the 5-HT$_{3B}$ receptors (Boyd *et al.* 2003). Localisation and interaction with the ER resident chaperone calnexin further confirmed the ER localisation of PAR$_4$. Calnexin targets N-linked glycoproteins but can serves as a chaperone to direct such proteins for ER export, however through a glycan independent mechanism it may also assist in retention of misfolded proteins in the ER (Vassilakos *et al.,* 1998). This duality of function has been described for the intracellular trafficking of dopamine D$_5$ (Karpa *et al.,* 1999), D$_1$ and D$_2$ (Free *et al.,* 2007) receptors. The exact role that calnexin plays in regulating PAR$_4$ localisation remains to be fully elucidated. Interaction between calnexin and PAR$_4$ was observed in both HEK293 and NCTC-2544 cells. In HEK293 cells PAR$_4$ was expressed both at the membrane and in the ER, whilst ER retention was predominantly observed in NCTC-2544 cells, thus calnexin interaction may implicate more of a role in ER retention rather than ER export.

Although deglycosylation of PAR$_4$ in the experiments in chapter 4 (section 4.7) demonstrated a loss of cell surface expression of PAR$_4$ in HEK293 cells, however if N-linked glycosylation was fully responsible for PAR$_4$ expression at the cell surface then these effects would have also been similarly observed in NCTC-2544 cells. As such, tunicamycin is a broad ranging deglycosylation agent therefore would affect expression of all glycosylated proteins in the cells. This in effect may have interfered with other proteins which may facilitate PAR$_4$ trafficking to the plasma membrane. An alternative strategy to assess the relative contribution of glycosylation would have been to mutate the putative N-linked glycosylation motif (N^{56}DS) at the N-terminal of the receptor and monitor subsequent changes in receptor localisation. Mutation of two such motifs within the structure of β$_2$

adrenoreceptors has been shown to result in inefficient delivery to the cell surface (Rands *et al.* 1990). However it should be noted that similar mutation may not affect receptor expression at all, as observed following motif mutation in early studies investigating glycosoylation in α_1 adrenoreceptors (Sawutz *et al.,* 1987). Such experiments may also identify if calnexin interacted via this N-linked glycosylation site or independent of this motif.

One of the most important regulatory mechanisms to be identified in this study was the novel interaction between PAR_2 and PAR_4. The ability of PAR_4 to evade ER retention was clearly demonstrated in the experiments of chapter 5, whereby co-expression with PAR_2 resulted in efficient delivery of PAR_4 to the plasma membrane. These events have been previously described for other proteins including the functional assembly of $GABA_{B1}/GABA_{B2}$ heterodimer and $5\text{-}HT_{3A}/5\text{-}HT_{3B}$ heterodimer, both of which assemble to mask the respective ER retention signals within $GABA_{B1}$ and $5\text{-}HT_{3B}$ to facilitate membrane delivery and restore receptor function (Margeta-Mitrovic *et al.,* 2000; Boyd *et al.,* 2003). To ensure that assembly with PAR_2 is an essential factor for PAR_4 cell surface mobilisation further work would be required. This may involve introducing ER retention sequences into PAR_2 to confine the receptor in the ER, similar to the ER trapping strategy routinely used in the Milligan laboratory (Wilson *et al.,* 2005). This would allow the functional consequences of PAR_2/PAR_4 heterodimerisation to be assessed. Alternatively, the localisation of PAR_4 could have been explored using PAR_2 deficient mice (Ferrell *et al.,* 2003) and compared to wild type mouse models. Such studies may prove to be extremely valuable to the future direction of this study, particularly in assessment of the receptor pharmacology of the PAR_2/PAR_4 complex. The preliminary experiments identified that enhanced cell surface expression of PAR_4 may translate to improved cell signalling following receptor activation. The use of cells derived from the mouse models previously described may allow PAR_4 responses to be assessed in its native environment, without the need for overexpression, in the presence and absence of PAR_2. The generation of signalling deficient receptor mutants may also provide a model to determine if any cooperativity exists between PAR_2 and PAR_4 signalling events. The loss of function observed for the PAR_4

R^{183}AR mutant observed in chapter 4 highlighted a potential site crucial for G$\alpha_{q/11}$ coupling, thus may provide an ideal opportunity to assess if co-expression with PAR$_2$ could present PAR$_4$ with an alternative mechanism to couple with G$\alpha_{q/11}$. Furthermore real-time analysis of receptor internalisation may indicate if PAR$_4$ can influence internalisation of PAR$_2$ and vice versa. These experiments are currently ongoing.

The very same structural determinants that facilitate ER retention may also contribute to export to the membrane. As the FRET experiments demonstrated, interaction between PAR$_2$ and PAR$_4$ was not readily observed in the NCTC-2544 cells, thus the translocation event may involve other proteins that scaffold to PAR$_2$ and PAR$_4$. Proteins such as the 14-3-3 isoforms in the ER/Golgi Intermediate compartment (ERGIC) and the coat protein I complex (COPI), can target proteins for retention through recognition and interaction RXR ER sequences (Aridor, 1995; Vivithanaporn, 2006), as demonstrated for retention of KA2 receptors (Vivithanaporn *et al.*, 2006). Similarly 14-3-3 proteins may also mask these motifs to direct ER/Golgi export of GPCR multimers (Shikano *et al.*, 2006). Interaction of 14-3-3, COPI and COPII proteins would be attractive candidates for further exploration of the intracellular regulation of PAR$_2$/PAR$_4$ to the plasma membrane. Small GTPase Rab proteins have been shown to be recruited by both 14-3-3 proteins and COPII vesicles to facilitate in ER/Golgi export (Shikano *et al.*, 2006). A role for Rab11a was identified in the trafficking of PAR$_2$ from Golgi stores to the plasma membrane (Roosterman *et al.*, 2003). Other approaches in use to detect protein-protein interaction in the PAR family include recent yeast two-hybrid screening. Such screening using a brain cDNA library identified a host of interacting proteins, such as Jab1 and the cargo protein p24A, that facilitate in the trafficking of PAR$_2$ (Luo *et al.*, 2006 and 2007). Interaction between PAR$_2$ and p24A at sites on the N-terminus of p24A and the ECL-2 of PAR$_2$ functions to temporarily retain PAR$_2$ in the Golgi. This interaction is disrupted upon PAR$_2$ activation, which in turn recruits the small GTPase, ADP-ribosylation factor-1 (ARF-1) to the Golgi, where it becomes activated by guanine nucleotide exchange factors (GEF). These events allow PAR$_2$ to be exported to the membrane (Luo *et al.*, 2007). These interactions

may prove to play an equally important role in the export of PAR$_2$/PAR$_4$ to the plasma membrane. Furthermore, using the second intracellular loop as bait, a yeast two-hybrid screen of PAR$_4$ could similarly identify potential interacting proteins with the RXR motif which may be important for intracellular trafficking of this receptor.

There are many examples in the literature where possession of the RXR retention signals can have deleterious effects upon protein folding and consequently contribute towards major pathophysiological conditions, including cystic fibrosis (Kopito *et al.,*1999; Gomes-Alves *et al.,* 2010) and nephrogenic diabetes insipidus (Hermosilla *et al.,* 2001). The consequence of PAR$_4$ ER retention remains to be defined, however in terms of the physiological relevance of PAR$_2$ and PAR$_4$ interaction, the most important revelation of the experiments carried out in chapter 5 was the ability of tumour necrosis factor (TNFα) to promote heterodimeristion between these receptors. TNFα is pivotal to the generation of inflammatory responses that underlie various chronic inflammatory disorders including rheumatoid arthritis (Popa *et al.,* 2007); a condition where both PAR$_2$ and more recently, PAR$_4$ activation have been clearly linked to (Ferrell *et al.,* 2003; McDougall *et al.,* 2009). At physiological levels, PAR$_2$ for example, is recognised to be protective (Cock *et al.,* 1999). Thus, TNFα may be acutely switching off PAR$_2$ in its protective mode whilst at the same time promoting increased expression of both receptors for subsequent pro-inflammatory signalling. This hypothesis may link with another recent finding, that PAR$_2$ activation is able to inhibit TNFα stimulated JNK signalling (McIntosh *et al.,* 2010). Therefore synergy at the level of signal transduction may be a consequence of the regulatory control TNFα displays upon PAR$_2$ and PAR$_4$ interaction. Other contexts where interaction of PAR$_2$/PAR$_4$ and subsequent regulation by TNFα may be important would be cells where both receptors are strongly expressed, such as leukocytes and vascular endothelium (Major et al., 2003). PAR$_4$ has long been associated with platelet activation and aggregation (Leger *et al.,* 2006a) and leukocyte rolling (Vergnolle *et al.,* 2002), with potential roles implicated in the progression of cardiovascular inflammation (Leger *et al.,* 2006b). Thus, the use of the PAR$_2$ deficient mice models and PAR-specific antagonist approaches (Kelso *et al.,* 2006; Kanke *et al.,*2009;

Kuliopolus *et al.,* 2003), may provide an ideal context in which PAR_4 localisation can be explored in physiology and pathophysiology in the presence and absence of PAR_2.

The work in this project has revealed for the first time that PAR_4 contains a functional ER retention sequence which dictates subcellular localisation and can interact with the ER chaperone, calnexin. A novel interaction between PAR_2 and PAR_4 was discovered, whereby PAR_2 can escort PAR_4 to the plasma membrane, possibly through masking of the ER retention motif within PAR_4.   These findings implicate a regulatory mechanism, distinct from PAR_1 and PAR_2, in the trafficking of PAR_4 to the plasma membrane and add to the knowledge of GPCR interactions but in a very unique way. PAR_2/PAR_4 interaction was shown to be regulated by the pro-inflammatory mediator, TNFα.   These findings may have important repercussions in the understanding of the roles of each receptor in inflammation. This understanding will provide the basis for future studies assessing the functional pharmacology of PAR_2/PAR_4 in the context of inflammatory diseases.

REFERENCES

ABE, K., ASLAM, A., WALLS, A., SATO, T. & INOUE, H. (2006) Up-regulation of protease-activated receptor-2 by bFGF in cultured human synovial fibroblasts. Life Sci, 79, 898-904.

AL-ANI, B., SAIFEDDINE, M., WIJESURIYA, S. & HOLLENBERG, M. (2002a) Modified proteinase-activated receptor-1 and -2 derived peptides inhibit proteinase-activated receptor-2 activation by trypsin. J Pharmacol Exp Ther, 300, 702-8.

AL-ANI, B., WIJESURIYA, S. & HOLLENBERG, M. (2002b) Proteinase-activated receptor 2: differential activation of the receptor by tethered ligand and soluble peptide analogs. J Pharmacol Exp Ther, 302, 1046-54.

ALEXANDER, S., MATHIE, A. & PETERS, J. (2007) Guide to Receptors and Channels (GRAC), 2nd edition (2007 Revision). Br J Pharmacol, 150 Suppl 1, S1-168.

ALEXANDER, S., MATHIE, A. & PETERS, J. (2008) Guide to Receptors and Channels (GRAC), 3rd edition. Br J Pharmacol, 153 Suppl 2, S1-209.

ANDO, S., OTANI, H., YAGI, Y., KAWAI, K., ARAKI, H., NAKAMURA, T., FUKUHARA, S. & INAGAKI, C. (2007) Protease-activated receptor 4-mediated Ca2+ signaling in mouse lung alveolar epithelial cells. Life Sci, 81, 794-802.

ARIDOR, M., BANNYKH, S., ROWE, T. & BALCH, W. (1995) Sequential coupling between COPII and COPI vesicle coats in endoplasmic reticulum to Golgi transport. J Cell Biol, 131, 875-93.

ARORA, P., RICKS, T. K. & TREJO, J. (2007) Protease-activated receptor signalling, endocytic sorting and dysregulation in cancer. J Cell Sci, 120, 921-8.

ASFAHA, S., CENAC, N., HOULE, S., ALTIER, C., PAPEZ, M., NGUYEN, C., STEINHOFF, M., CHAPMAN, K., ZAMPONI, G. & VERGNOLLE, N. (2007) Protease-activated receptor-4: a novel mechanism of inflammatory pain modulation. Br J Pharmacol, 150, 176-85.

ATTRAMADAL, H., ARRIZA, J., AOKI, C., DAWSON, T., CODINA, J., KWATRA, M., SNYDER, S., CARON, M. & LEFKOWITZ, R. (1992) Beta-arrestin2, a novel member of the arrestin/beta-arrestin gene family. J Biol

Chem, 267, 17882-90.

AYOUB, M., DAMIAN, M., GESPACH, C., FERRANDIS, E., LAVERGNE, O., DE WEVER, O., BANÈRES, J., PIN, J. & PRÉVOST, G. (2009) Inhibition of heterotrimeric G protein signaling by a small molecule acting on Galpha subunit. J Biol Chem, 284, 29136-45.

AYOUB, M., MAUREL, D., BINET, V., FINK, M., PRÉZEAU, L., ANSANAY, H. & PIN, J. (2007) Real-time analysis of agonist-induced activation of protease-activated receptor 1/Galphai1 protein complex measured by bioluminescence resonance energy transfer in living cells. Mol Pharmacol, 71, 1329-40.

BABICH, M., KING, K. & NISSENSON, R. (1990) Thrombin stimulates inositol phosphate production and intracellular free calcium by a pertussis toxin-insensitive mechanism in osteosarcoma cells. Endocrinology, 126, 948-54.

BARLOWE, C., D'ENFERT, C. & SCHEKMAN, R. (1993) Purification and characterization of SAR1p, a small GTP-binding protein required for transport vesicle formation from the endoplasmic reticulum. J Biol Chem, 268, 873-9.

BARLOWE, C., ORCI, L., YEUNG, T., HOSOBUCHI, M., HAMAMOTO, S., SALAMA, N., REXACH, M., RAVAZZOLA, M., AMHERDT, M. & SCHEKMAN, R. (1994) COPII: a membrane coat formed by Sec proteins that drive vesicle budding from the endoplasmic reticulum. Cell, 77, 895-907.

BAR-SAGI, D. & HALL, A. (2000) Ras and Rho GTPases: a family reunion. Cell, 103, 227-38.

BELHAM, C., TATE, R., SCOTT, P., PEMBERTON, A., MILLER, H., WADSWORTH, R., GOULD, G. & PLEVIN, R. (1996) Trypsin stimulates proteinase-activated receptor-2-dependent and -independent activation of mitogen-activated protein kinases. Biochem J, 320 (Pt 3), 939-46.

BENOVIC, J., KÜHN, H., WEYAND, I., CODINA, J., CARON, M. & LEFKOWITZ, R. (1987) Functional desensitization of the isolated beta-adrenergic receptor by the beta-adrenergic receptor kinase: potential role of an analog of the retinal protein arrestin (48-kDa protein). Proc Natl Acad Sci U S A, 84, 8879-82.

BENOVIC, J., PIKE, L., CERIONE, R., STANISZEWSKI, C., YOSHIMASA, T., CODINA, J., CARON, M. & LEFKOWITZ, R. (1985) Phosphorylation of the mammalian beta-adrenergic receptor by cyclic AMP-dependent protein kinase. Regulation of the rate of receptor phosphorylation and dephosphorylation by agonist occupancy and effects on coupling of the receptor to the stimulatory guanine nucleotide regulatory protein. J Biol Chem, 260, 7094-101.

BENOVIC, J., STRASSER, R., CARON, M. & LEFKOWITZ, R. (1986) Beta-adrenergic receptor kinase: identification of a novel protein kinase that phosphorylates the agonist-occupied form of the receptor. Proc Natl Acad Sci U S A, 83, 2797-801.

BERGERON, J., BRENNER, M., THOMAS, D. & WILLIAMS, D. (1994) Calnexin: a membrane-bound chaperone of the endoplasmic reticulum. Trends Biochem Sci, 19, 124-8.

BERNEY, C. & DANUSER, G. (2003) FRET or no FRET: a quantitative comparison. Biophys J, 84, 3992-4010.

BERNSTEIN, L., RAMINENI, S., HAGUE, C., CLADMAN, W., CHIDIAC, P., LEVEY, A. & HEPLER, J. (2004) RGS2 binds directly and selectively to the M1 muscarinic acetylcholine receptor third intracellular loop to modulate Gq/11alpha signaling. J Biol Chem, 279, 21248-56.

BERRIDGE, M. (1983) Rapid accumulation of inositol trisphosphate reveals that agonists hydrolyse polyphosphoinositides instead of phosphatidylinositol. Biochem J, 212, 849-58.

BERRIDGE, M., DAWSON, R., DOWNES, C., HESLOP, J. & IRVINE, R. (1983) Changes in the levels of inositol phosphates after agonist-dependent hydrolysis of membrane phosphoinositides. Biochem J, 212, 473-82.

BHATTACHARYA, M., BABWAH, A. & FERGUSON, S. (2004) Small GTP-binding protein-coupled receptors. Biochem Soc Trans, 32, 1040-4.

BIKLE, D., NG, D., TU, C., ODA, Y. & XIE, Z. (2001) Calcium- and vitamin D-regulated keratinocyte differentiation. Mol Cell Endocrinol, 177, 161-71.

BINET, V., DUTHEY, B., LECAILLON, J., VOL, C., QUOYER, J., LABESSE, G., PIN, J. & PRÉZEAU, L. (2007) Common structural requirements for

heptahelical domain function in class A and class C G protein-coupled receptors. J Biol Chem, 282, 12154-63.

BLACKHART, B., EMILSSON, K., NGUYEN, D., TENG, W., MARTELLI, A., NYSTEDT, S., SUNDELIN, J. & SCARBOROUGH, R. (1996) Ligand cross-reactivity within the protease-activated receptor family. J Biol Chem, 271, 16466-71.

BLIN, N., YUN, J. & WESS, J. (1995) Mapping of single amino acid residues required for selective activation of Gq/11 by the m3 muscarinic acetylcholine receptor. J Biol Chem, 270, 17741-8.

BÖHM, S., KHITIN, L., GRADY, E., APONTE, G., PAYAN, D. & BUNNETT, N. (1996) Mechanisms of desensitization and resensitization of proteinase-activated receptor-2. J Biol Chem, 271, 22003-16.

BOODEN, M., ECKERT, L., DER, C. & TREJO, J. (2004) Persistent signaling by dysregulated thrombin receptor trafficking promotes breast carcinoma cell invasion. Mol Cell Biol, 24, 1990-9.

BOUTON, M., JANDROT-PERRUS, M., MOOG, S., CAZENAVE, J., GUILLIN, M. & LANZA, F. (1995) Thrombin interaction with a recombinant N-terminal extracellular domain of the thrombin receptor in an acellular system. Biochem J, 305 (Pt 2), 635-41.

BOUVIER, M. (2001) Oligomerization of G-protein-coupled transmitter receptors. Nat Rev Neurosci, 2, 274-86.

BOYD, G., DOWARD, A., KIRKNESS, E., MILLAR, N. & CONNOLLY, C. (2003) Cell surface expression of 5-hydroxytryptamine type 3 receptors is controlled by an endoplasmic reticulum retention signal. J Biol Chem, 278, 27681-7.

BRASS, L., MANNING, D., WILLIAMS, A., WOOLKALIS, M. & PONCZ, M. (1991) Receptor and G protein-mediated responses to thrombin in HEL cells. J Biol Chem, 266, 958-65.

BREIT, A., LAGACÉ, M. & BOUVIER, M. (2004) Hetero-oligomerization between beta2- and beta3-adrenergic receptors generates a beta-adrenergic signaling unit with distinct functional properties. J Biol Chem, 279, 28756-65.

BRETSCHNEIDER, E., KAUFMANN, R., BRAUN, M., NOWAK, G., GLUSA, E.

& SCHRÖR, K. (2001) Evidence for functionally active protease-activated receptor-4 (PAR-4) in human vascular smooth muscle cells. Br J Pharmacol, 132, 1441-6.

BRETSCHNEIDER, E., KAUFMANN, R., BRAUN, M., WITTPOTH, M., GLUSA, E., NOWAK, G. & SCHRÖR, K. (1999) Evidence for proteinase-activated receptor-2 (PAR-2)-mediated mitogenesis in coronary artery smooth muscle cells. Br J Pharmacol, 126, 1735-40.

BUDDENKOTTE, J., STROH, C., ENGELS, I., MOORMANN, C., SHPACOVITCH, V., SEELIGER, S., VERGNOLLE, N., VESTWEBER, D., LUGER, T., SCHULZE-OSTHOFF, K. & STEINHOFF, M. (2005) Agonists of proteinase-activated receptor-2 stimulate upregulation of intercellular cell adhesion molecule-1 in primary human keratinocytes via activation of NF-kappa B. J Invest Dermatol, 124, 38-45.

BÜNEMANN, M., FRANK, M. & LOHSE, M. (2003) Gi protein activation in intact cells involves subunit rearrangement rather than dissociation. Proc Natl Acad Sci U S A, 100, 16077-82.

BUSHELL, T., PLEVIN, R., COBB, S. & IRVING, A. (2006) Characterization of proteinase-activated receptor 2 signalling and expression in rat hippocampal neurons and astrocytes. Neuropharmacology, 50, 714-25.

CAMERER, E., HUANG, W. & COUGHLIN, S. (2000) Tissue factor- and factor X-dependent activation of protease-activated receptor 2 by factor VIIa. Proc Natl Acad Sci U S A, 97, 5255-60.

CANALS, M. & MILLIGAN, G. (2008) Constitutive activity of the cannabinoid CB1 receptor regulates the function of co-expressed Mu opioid receptors. J Biol Chem, 283, 11424-34.

CASSEL, D. & SELINGER, Z. (1977) Mechanism of adenylate cyclase activation by cholera toxin: inhibition of GTP hydrolysis at the regulatory site. Proc Natl Acad Sci U S A, 74, 3307-11.

CHALFIE, M., TU, Y., EUSKIRCHEN, G., WARD, W. & PRASHER, D. (1994) Green fluorescent protein as a marker for gene expression. Science, 263, 802-5.

CHAN, W., SOLOVIEV, M., CIRUELA, F. & MCILHINNEY, R. (2001) Molecular

determinants of metabotropic glutamate receptor 1B trafficking. Mol Cell Neurosci, 17, 577-88.

CHAO, B., KALKUNTE, S., MARAGANORE, J. & STONE, S. (1992) Essential groups in synthetic agonist peptides for activation of the platelet thrombin receptor. Biochemistry, 31, 6175-8.

CHAPMAN, S., OPARKA, K. & ROBERTS, A. (2005) New tools for in vivo fluorescence tagging. Curr Opin Plant Biol, 8, 565-73.

CHEN, C., PAING, M. & TREJO, J. (2004) Termination of protease-activated receptor-1 signaling by beta-arrestins is independent of receptor phosphorylation. J Biol Chem, 279, 10020-31.

CHEN, J., ISHII, M., WANG, L., ISHII, K. & COUGHLIN, S. (1994) Thrombin receptor activation. Confirmation of the intramolecular tethered ligating hypothesis and discovery of an alternative intermolecular ligating mode. J Biol Chem, 269, 16041-5.

CHUANG, T., IACOVELLI, L., SALLESE, M. & DE BLASI, A. (1996) G protein-coupled receptors: heterologous regulation of homologous desensitization and its implications. Trends Pharmacol Sci, 17, 416-21.

CHUNG, S., FUNAKOSHI, T. & CIVELLI, O. (2008) Orphan GPCR research. Br J Pharmacol, 153 Suppl 1, S339-46.

CIRINO, G. & VERGNOLLE, N. (2006) Proteinase-activated receptors (PARs): crossroads between innate immunity and coagulation. Curr Opin Pharmacol, 6, 428-34.

COCKCROFT, S. & GOMPERTS, B. (1985) Role of guanine nucleotide binding protein in the activation of polyphosphoinositide phosphodiesterase. Nature, 314, 534-6.

COCKCROFT, S., HOWELL, T. & GOMPERTS, B. (1987) Two G-proteins act in series to control stimulus-secretion coupling in mast cells: use of neomycin to distinguish between G-proteins controlling polyphosphoinositide phosphodiesterase and exocytosis. J Cell Biol, 105, 2745-50.

COCKS, T., FONG, B., CHOW, J., ANDERSON, G., FRAUMAN, A., GOLDIE, R., HENRY, P., CARR, M., HAMILTON, J. & MOFFATT, J. (1999) A protective role for protease-activated receptors in the airways. Nature, 398,

156-60.

COCKS, T. & MOFFATT, J. (2001) Protease-activated receptor-2 (PAR2) in the airways. Pulm Pharmacol Ther, 14, 183-91.

COMPTON, S., RENAUX, B., WIJESURIYA, S. & HOLLENBERG, M. (2001) Glycosylation and the activation of proteinase-activated receptor 2 (PAR(2)) by human mast cell tryptase. Br J Pharmacol, 134, 705-18.

CONNOLLY, A., ISHIHARA, H., KAHN, M., FARESE, R. J. & COUGHLIN, S. (1996) Role of the thrombin receptor in development and evidence for a second receptor. Nature, 381, 516-9.

CONNOLLY, T., CONDRA, C., FENG, D., COOK, J., STRANIERI, M., REILLY, C., NUTT, R. & GOULD, R. (1994) Species variability in platelet and other cellular responsiveness to thrombin receptor-derived peptides. Thromb Haemost, 72, 627-33.

COORAY, S., CHAN, L., WEBB, T., METHERELL, L. & CLARK, A. (2009) Accessory proteins are vital for the functional expression of certain G protein-coupled receptors. Mol Cell Endocrinol, 300, 17-24.

COTECCHIA, S., SCHWINN, D., RANDALL, R., LEFKOWITZ, R., CARON, M. & KOBILKA, B. (1988) Molecular cloning and expression of the cDNA for the hamster alpha 1-adrenergic receptor. Proc Natl Acad Sci U S A, 85, 7159-63.

COTTRELL, G., AMADESI, S., GRADY, E. & BUNNETT, N. (2004) Trypsin IV, a novel agonist of protease-activated receptors 2 and 4. J Biol Chem, 279, 13532-9.

COVIC, L., GRESSER, A. & KULIOPULOS, A. (2000) Biphasic kinetics of activation and signaling for PAR1 and PAR4 thrombin receptors in platelets. Biochemistry, 39, 5458-67.

COVIC, L., GRESSER, A., TALAVERA, J., SWIFT, S. & KULIOPULOS, A. (2002) Activation and inhibition of G protein-coupled receptors by cell-penetrating membrane-tethered peptides. Proc Natl Acad Sci U S A, 99, 643-8.

DAY, R. & SCHAUFELE, F. (2005) Imaging molecular interactions in living cells. Mol Endocrinol, 19, 1675-86.

DE VRIES, L. & GIST FARQUHAR, M. (1999) RGS proteins: more than just GAPs for heterotrimeric G proteins. Trends Cell Biol, 9, 138-44.

DEFEA, K., SCHMIDLIN, F., DÉRY, O., GRADY, E. & BUNNETT, N. (2000a) Mechanisms of initiation and termination of signalling by neuropeptide receptors: a comparison with the proteinase-activated receptors. Biochem Soc Trans, 28, 419-26.

DEFEA, K., ZALEVSKY, J., THOMA, M., DÉRY, O., MULLINS, R. & BUNNETT, N. (2000b) beta-arrestin-dependent endocytosis of proteinase-activated receptor 2 is required for intracellular targeting of activated ERK1/2. J Cell Biol, 148, 1267-81.

DÉRY, O. & BUNNETT, N. (1999) Proteinase-activated receptors: a growing family of heptahelical receptors for thrombin, trypsin and tryptase. Biochem Soc Trans, 27, 246-54.

DÉRY, O., THOMA, M., WONG, H., GRADY, E. & BUNNETT, N. (1999) Trafficking of proteinase-activated receptor-2 and beta-arrestin-1 tagged with green fluorescent protein. beta-Arrestin-dependent endocytosis of a proteinase receptor. J Biol Chem, 274, 18524-35.

DESSAUER, C., POSNER, B. & GILMAN, A. (1996) Visualizing signal transduction: receptors, G-proteins, and adenylate cyclases. Clin Sci (Lond), 91, 527-37.

DIXON, R., KOBILKA, B., STRADER, D., BENOVIC, J., DOHLMAN, H., FRIELLE, T., BOLANOWSKI, M., BENNETT, C., RANDS, E. & DIEHL, R. (1986) Cloning of the gene and cDNA for mammalian beta-adrenergic receptor and homology with rhodopsin. Nature, 321, 75-9.

DOHLMAN, H. & THORNER, J. (1997) RGS proteins and signaling by heterotrimeric G proteins. J Biol Chem, 272, 3871-4.

DONG, C., FILIPEANU, C., DUVERNAY, M. & WU, G. (2007) Regulation of G protein-coupled receptor export trafficking. Biochim Biophys Acta, 1768, 853-70.

DONG, C. & WU, G. (2006) Regulation of anterograde transport of alpha2-adrenergic receptors by the N termini at multiple intracellular compartments. J Biol Chem, 281, 38543-54.

DORSAM, R., KIM, S., JIN, J. & KUNAPULI, S. (2002) Coordinated signaling through both G12/13 and G(i) pathways is sufficient to activate GPIIb/IIIa in human platelets. J Biol Chem, 277, 47588-95.

DOWAL, L., PROVITERA, P. & SCARLATA, S. (2006) Stable association between G alpha(q) and phospholipase C beta 1 in living cells. J Biol Chem, 281, 23999-4014.

EASON, M., MOREIRA, S. & LIGGETT, S. (1995) Four consecutive serines in the third intracellular loop are the sites for beta-adrenergic receptor kinase-mediated phosphorylation and desensitization of the alpha 2A-adrenergic receptor. J Biol Chem, 270, 4681-8.

ELLIS, J., PEDIANI, J., CANALS, M., MILASTA, S. & MILLIGAN, G. (2006) Orexin-1 receptor-cannabinoid CB1 receptor heterodimerization results in both ligand-dependent and -independent coordinated alterations of receptor localization and function. J Biol Chem, 281, 38812-24.

FARUQI, T., WEISS, E., SHAPIRO, M., HUANG, W. & COUGHLIN, S. (2000) Structure-function analysis of protease-activated receptor 4 tethered ligand peptides. Determinants of specificity and utility in assays of receptor function. J Biol Chem, 275, 19728-34.

FERGUSON, S., BARAK, L., ZHANG, J. & CARON, M. (1996a) G-protein-coupled receptor regulation: role of G-protein-coupled receptor kinases and arrestins. Can J Physiol Pharmacol, 74, 1095-110.

FERGUSON, S., ZHANG, J., BARAK, L. & CARON, M. (1996b) G-protein-coupled receptor kinases and arrestins: regulators of G-protein-coupled receptor sequestration. Biochem Soc Trans, 24, 953-9.

FERRELL, W., LOCKHART, J., KELSO, E., DUNNING, L., PLEVIN, R., MEEK, S., SMITH, A., HUNTER, G., MCLEAN, J., MCGARRY, F., RAMAGE, R., JIANG, L., KANKE, T. & KAWAGOE, J. (2003) Essential role for proteinase-activated receptor-2 in arthritis. J Clin Invest, 111, 35-41.

FILMORE & DAVID (2004) It's a GPCR world. Modern Drug Discovery, 7, 24-28.

FOORD, S., BONNER, T., NEUBIG, R., ROSSER, E., PIN, J., DAVENPORT, A., SPEDDING, M. & HARMAR, A. (2005) International Union of Pharmacology. XLVI. G protein-coupled receptor list. Pharmacol Rev, 57,

279-88.

FOTIADIS, D., LIANG, Y., FILIPEK, S., SAPERSTEIN, D., ENGEL, A. & PALCZEWSKI, K. (2004) The G protein-coupled receptor rhodopsin in the native membrane. FEBS Lett, 564, 281-8.

FOX, M., HARRIOTT, P., WALKER, B. & STONE, S. (1997) Identification of potential activators of proteinase-activated receptor-2. FEBS Lett, 417, 267-9.

FREDERICKS, Z., PITCHER, J. & LEFKOWITZ, R. (1996) Identification of the G protein-coupled receptor kinase phosphorylation sites in the human beta2-adrenergic receptor. J Biol Chem, 271, 13796-803.

FREE, R., HAZELWOOD, L., CABRERA, D., SPALDING, H., NAMKUNG, Y., RANKIN, M. & SIBLEY, D. (2007) D1 and D2 dopamine receptor expression is regulated by direct interaction with the chaperone protein calnexin. J Biol Chem, 282, 21285-300.

FREEDMAN, N., LIGGETT, S., DRACHMAN, D., PEI, G., CARON, M. & LEFKOWITZ, R. (1995) Phosphorylation and desensitization of the human beta 1-adrenergic receptor. Involvement of G protein-coupled receptor kinases and cAMP-dependent protein kinase. J Biol Chem, 270, 17953-61.

FUJIWARA, M., JIN, E., GHAZIZADEH, M. & KAWANAMI, O. (2005) Activation of PAR4 induces a distinct actin fiber formation via p38 MAPK in human lung endothelial cells. J Histochem Cytochem, 53, 1121-9.

FUNG, J. J., DEUPI, X., PARDO, L., YAO, X. J., VELEZ-RUIZ, G. A., DEVREE, B. T., SUNAHARA, R. K. & KOBILKA, B. K. (2009) Ligand-regulated oligomerization of beta(2)-adrenoceptors in a model lipid bilayer. EMBO J, 28, 3315-28.

GASSMANN, M., HALLER, C., STOLL, Y., AZIZ, S., BIERMANN, B., MOSBACHER, J., KAUPMANN, K. & BETTLER, B. (2005) The RXR-type endoplasmic reticulum-retention/retrieval signal of GABAB1 requires distant spacing from the membrane to function. Mol Pharmacol, 68, 137-44.

GEORGE, S., FAN, T., XIE, Z., TSE, R., TAM, V., VARGHESE, G. & O'DOWD, B. (2000) Oligomerization of mu- and delta-opioid receptors. Generation of novel functional properties. J Biol Chem, 275, 26128-35.

GERSHENGORN, M. & OSMAN, R. (2001) Minireview: Insights into G protein-

coupled receptor function using molecular models. Endocrinology, 142, 2-10.

GETHER, U. (2000) Uncovering molecular mechanisms involved in activation of G protein-coupled receptors. Endocr Rev, 21, 90-113.

GILMAN, A. (1987) G proteins: transducers of receptor-generated signals. Annu Rev Biochem, 56, 615-49.

GINÉS, S., HILLION, J., TORVINEN, M., LE CROM, S., CASADÓ, V., CANELA, E., RONDIN, S., LEW, J., WATSON, S., ZOLI, M., AGNATI, L., VERNIERA, P., LLUIS, C., FERRÉ, S., FUXE, K. & FRANCO, R. (2000) Dopamine D1 and adenosine A1 receptors form functionally interacting heteromeric complexes. Proc Natl Acad Sci U S A, 97, 8606-11.

GOH, F., NG, P., NILSSON, M., KANKE, T. & PLEVIN, R. (2009) Dual effect of the novel peptide antagonist K-14585 on proteinase-activated receptor-2-mediated signalling. Br J Pharmacol, 158, 1695-704.

GOMES-ALVES, P., COUTO, F., PESQUITA, C., COELHO, A. & PENQUE, D. (2010) Rescue of F508del-CFTR by RXR motif inactivation triggers proteome modulation associated with the unfolded protein response. Biochim Biophys Acta.

GOODMAN, O. J., KRUPNICK, J., GUREVICH, V., BENOVIC, J. & KEEN, J. (1997) Arrestin/clathrin interaction. Localization of the arrestin binding locus to the clathrin terminal domain. J Biol Chem, 272, 15017-22.

GOON GOH, F., SLOSS, C., CUNNINGHAM, M., NILSSON, M., CADALBERT, L. & PLEVIN, R. (2008) G-protein-dependent and -independent pathways regulate proteinase-activated receptor-2 mediated p65 NFkappaB serine 536 phosphorylation in human keratinocytes. Cell Signal, 20, 1267-74.

GRAILHE, R., MEROLA, F., RIDARD, J., COUVIGNOU, S., LE POUPON, C., CHANGEUX, J. & LAGUITTON-PASQUIER, H. (2006) Monitoring protein interactions in the living cell through the fluorescence decays of the cyan fluorescent protein. Chemphyschem, 7, 1442-54.

GRAND, R., TURNELL, A. & GRABHAM, P. (1996) Cellular consequences of thrombin-receptor activation. Biochem J, 313 (Pt 2), 353-68.

GRANT, M., COLLIER, B. & KUMAR, U. (2004) Agonist-dependent dissociation of human somatostatin receptor 2 dimers: a role in receptor trafficking. J Biol

Chem, 279, 36179-83.

GUO, W., SHI, L. & JAVITCH, J. (2003) The fourth transmembrane segment forms the interface of the dopamine D2 receptor homodimer. J Biol Chem, 278, 4385-8.

GUREVICH, V., DION, S., ONORATO, J., PTASIENSKI, J., KIM, C., STERNE-MARR, R., HOSEY, M. & BENOVIC, J. (1995) Arrestin interactions with G protein-coupled receptors. Direct binding studies of wild type and mutant arrestins with rhodopsin, beta 2-adrenergic, and m2 muscarinic cholinergic receptors. J Biol Chem, 270, 720-31.

GUREVICH, V. & GUREVICH, E. (2004) The molecular acrobatics of arrestin activation. Trends Pharmacol Sci, 25, 105-11.

HAMILTON, J., FRAUMAN, A. & COCKS, T. (2001a) Increased expression of protease-activated receptor-2 (PAR2) and PAR4 in human coronary artery by inflammatory stimuli unveils endothelium-dependent relaxations to PAR2 and PAR4 agonists. Circ Res, 89, 92-8.

HAMILTON, J., MOFFATT, J., FRAUMAN, A. & COCKS, T. (2001b) Protease-activated receptor (PAR) 1 but not PAR2 or PAR4 mediates endothelium-dependent relaxation to thrombin and trypsin in human pulmonary arteries. J Cardiovasc Pharmacol, 38, 108-19.

HARPER, M. & SAGE, S. (2006) Actin polymerisation regulates thrombin-evoked Ca(2+) signalling after activation of PAR-4 but not PAR-1 in human platelets. Platelets, 17, 134-42.

HARRISON, C. & VAN DER GRAAF, P. (2006) Current methods used to investigate G protein coupled receptor oligomerisation. J Pharmacol Toxicol Methods, 54, 26-35.

HART, M., JIANG, X., KOZASA, T., ROSCOE, W., SINGER, W., GILMAN, A., STERNWEIS, P. & BOLLAG, G. (1998) Direct stimulation of the guanine nucleotide exchange activity of p115 RhoGEF by Galpha13. Science, 280, 2112-4.

HASDEMIR, B., MURPHY, J., COTTRELL, G. & BUNNETT, N. (2009) Endosomal deubiquitinating enzymes control ubiquitination and down-regulation of protease-activated receptor 2. J Biol Chem, 284, 28453-66.

HEBERT, D. & MOLINARI, M. (2007) In and out of the ER: protein folding, quality control, degradation, and related human diseases. Physiol Rev, 87, 1377-408.

HEBERT, T., MOFFETT, S., MORELLO, J., LOISEL, T., BICHET, D., BARRET, C. & BOUVIER, M. (1996) A peptide derived from a beta2-adrenergic receptor transmembrane domain inhibits both receptor dimerization and activation. J Biol Chem, 271, 16384-92.

HEIN, L., ISHII, K., COUGHLIN, S. & KOBILKA, B. (1994) Intracellular targeting and trafficking of thrombin receptors. A novel mechanism for resensitization of a G protein-coupled receptor. J Biol Chem, 269, 27719-26.

HENDERSON, R. & SCHERTLER, G. (1990) The structure of bacteriorhodopsin and its relevance to the visual opsins and other seven-helix G-protein coupled receptors. Philos Trans R Soc Lond B Biol Sci, 326, 379-89.

HENDERSON, R. & UNWIN, P. (1975) Three-dimensional model of purple membrane obtained by electron microscopy. Nature, 257, 28-32.

HERMOSILLA, R. & SCHÜLEIN, R. (2001) Sorting functions of the individual cytoplasmic domains of the G protein-coupled vasopressin V(2) receptor in Madin Darby canine kidney epithelial cells. Mol Pharmacol, 60, 1031-9.

HILLION, J., CANALS, M., TORVINEN, M., CASADO, V., SCOTT, R., TERASMAA, A., HANSSON, A., WATSON, S., OLAH, M., MALLOL, J., CANELA, E., ZOLI, M., AGNATI, L., IBANEZ, C., LLUIS, C., FRANCO, R., FERRE, S. & FUXE, K. (2002) Coaggregation, cointernalization, and codesensitization of adenosine A2A receptors and dopamine D2 receptors. J Biol Chem, 277, 18091-7.

HIRANO, K., NOMOTO, N., HIRANO, M., MOMOTA, F., HANADA, A. & KANAIDE, H. (2007) Distinct Ca2+ requirement for NO production between proteinase-activated receptor 1 and 4 (PAR1 and PAR4) in vascular endothelial cells. J Pharmacol Exp Ther.

HIRSCH, C., GAUSS, R., HORN, S., NEUBER, O. & SOMMER, T. (2009) The ubiquitylation machinery of the endoplasmic reticulum. Nature, 458, 453-60.

HOFFMANN, C., GAIETTA, G., BÜNEMANN, M., ADAMS, S., OBERDORFF-MAASS, S., BEHR, B., VILARDAGA, J., TSIEN, R., ELLISMAN, M. &

LOHSE, M. (2005) A FlAsH-based FRET approach to determine G protein-coupled receptor activation in living cells. Nat Methods, 2, 171-6.

HOLLENBERG, M. (2002) PARs in the stars: proteinase-activated receptors and astrocyte function. Focus on "Thrombin (PAR-1)-induced proliferation in astrocytes via MAPK involves multiple signaling pathways". Am J Physiol Cell Physiol, 283, C1347-50.

HOLLENBERG, M. & HOULE, S. (2005) Proteinases as hormone-like signal messengers. Swiss Med Wkly, 135, 425-32.

HOLLENBERG, M., SAIFEDDINE, M., AL-ANI, B. & KAWABATA, A. (1997) Proteinase-activated receptors: structural requirements for activity, receptor cross-reactivity, and receptor selectivity of receptor-activating peptides. Can J Physiol Pharmacol, 75, 832-41.

HOLLINGER, S. & HEPLER, J. (2002) Cellular regulation of RGS proteins: modulators and integrators of G protein signaling. Pharmacol Rev, 54, 527-59.

HOOGERWERF, W., ZOU, L., SHENOY, M., SUN, D., MICCI, M., LEE-HELLMICH, H., XIAO, S., WINSTON, J. & PASRICHA, P. (2001) The proteinase-activated receptor 2 is involved in nociception. J Neurosci, 21, 9036-42.

HOU, L., KAPAS, S., CRUCHLEY, A., MACEY, M., HARRIOTT, P., CHINNI, C., STONE, S. & HOWELLS, G. (1998) Immunolocalization of protease-activated receptor-2 in skin: receptor activation stimulates interleukin-8 secretion by keratinocytes in vitro. Immunology, 94, 356-62.

HOWELLS, G., MACEY, M., CHINNI, C., HOU, L., FOX, M., HARRIOTT, P. & STONE, S. (1997) Proteinase-activated receptor-2: expression by human neutrophils. J Cell Sci, 110 (Pt 7), 881-7.

HOXIE, J., AHUJA, M., BELMONTE, E., PIZARRO, S., PARTON, R. & BRASS, L. (1993) Internalization and recycling of activated thrombin receptors. J Biol Chem, 268, 13756-63.

HUBBARD, K. & HEPLER, J. (2006) Cell signalling diversity of the Gqalpha family of heterotrimeric G proteins. Cell Signal, 18, 135-50.

INGLESE, J., FREEDMAN, N. J., KOCH, W. J. & LEFKOWITZ, R. J. (1993)

Structure and mechanism of the G protein-coupled receptor kinases. J Biol Chem, 268, 23735-8.

ISHIHARA, H., CONNOLLY, A., ZENG, D., KAHN, M., ZHENG, Y., TIMMONS, C., TRAM, T. & COUGHLIN, S. (1997) Protease-activated receptor 3 is a second thrombin receptor in humans. Nature, 386, 502-6.

ISHII, K., GERSZTEN, R., ZHENG, Y., WELSH, J., TURCK, C. & COUGHLIN, S. (1995) Determinants of thrombin receptor cleavage. Receptor domains involved, specificity, and role of the P3 aspartate. J Biol Chem, 270, 16435-40.

ISHII, K., HEIN, L., KOBILKA, B. & COUGHLIN, S. (1993) Kinetics of thrombin receptor cleavage on intact cells. Relation to signaling. J Biol Chem, 268, 9780-6.

IWATA, K., ITO, K., FUKUZAKI, A., INAKI, K. & HAGA, T. (1999) Dynamin and rab5 regulate GRK2-dependent internalization of dopamine D2 receptors. Eur J Biochem, 263, 596-602.

JAAKOLA, V., GRIFFITH, M., HANSON, M., CHEREZOV, V., CHIEN, E., LANE, J., IJZERMAN, A. & STEVENS, R. (2008) The 2.6 angstrom crystal structure of a human A2A adenosine receptor bound to an antagonist. Science, 322, 1211-7.

JACQUES, S. & KULIOPULOS, A. (2003) Protease-activated receptor-4 uses dual prolines and an anionic retention motif for thrombin recognition and cleavage. Biochem J, 376, 733-40.

JARDIN, I., BEN AMOR, N., BARTEGI, A., PARIENTE, J., SALIDO, G. & ROSADO, J. (2007) Differential involvement of thrombin receptors in Ca2+ release from two different intracellular stores in human platelets. Biochem J, 401, 167-74.

JORDAN, B. & DEVI, L. (1999) G-protein-coupled receptor heterodimerization modulates receptor function. Nature, 399, 697-700.

KAHN, M., NAKANISHI-MATSUI, M., SHAPIRO, M., ISHIHARA, H. & COUGHLIN, S. (1999) Protease-activated receptors 1 and 4 mediate activation of human platelets by thrombin. J Clin Invest, 103, 879-87.

KAHN, M., ZHENG, Y., HUANG, W., BIGORNIA, V., ZENG, D., MOFF, S.,

FARESE, R. J., TAM, C. & COUGHLIN, S. (1998) A dual thrombin receptor system for platelet activation. Nature, 394, 690-4.

KANEIDER, N., LEGER, A., AGARWAL, A., NGUYEN, N., PERIDES, G., DERIAN, C., COVIC, L. & KULIOPULOS, A. (2007) 'Role reversal' for the receptor PAR1 in sepsis-induced vascular damage. Nat Immunol, 8, 1303-12.

KANEIDER, N., LEGER, A. & KULIOPULOS, A. (2006) Therapeutic targeting of molecules involved in leukocyte-endothelial cell interactions. FEBS J, 273, 4416-24.

KANKE, T., ISHIWATA, H., KABEYA, M., SAKA, M., DOI, T., HATTORI, Y., KAWABATA, A. & PLEVIN, R. (2005a) Binding of a highly potent protease-activated receptor-2 (PAR2) activating peptide, [3H]2-furoyl-LIGRL-NH2, to human PAR2. Br J Pharmacol, 145, 255-63.

KANKE, T., KABEYA, M., KUBO, S., KONDO, S., YASUOKA, K., TAGASHIRA, J., ISHIWATA, H., SAKA, M., FURUYAMA, T., NISHIYAMA, T., DOI, T., HATTORI, Y., KAWABATA, A., CUNNINGHAM, M. & PLEVIN, R. (2009) Novel antagonists for proteinase-activated receptor 2: inhibition of cellular and vascular responses in vitro and in vivo. Br J Pharmacol, 158, 361-71.

KANKE, T., MACFARLANE, S., SEATTER, M., DAVENPORT, E., PAUL, A., MCKENZIE, R. & PLEVIN, R. (2001) Proteinase-activated receptor-2-mediated activation of stress-activated protein kinases and inhibitory kappa B kinases in NCTC 2544 keratinocytes. J Biol Chem, 276, 31657-66.

KANKE, T., TAKIZAWA, T., KABEYA, M. & KAWABATA, A. (2005b) Physiology and pathophysiology of proteinase-activated receptors (PARs): PAR-2 as a potential therapeutic target. J Pharmacol Sci, 97, 38-42.

KARPA, K., LIDOW, M., PICKERING, M., LEVENSON, R. & BERGSON, C. (1999) N-linked glycosylation is required for plasma membrane localization of D5, but not D1, dopamine receptors in transfected mammalian cells. Mol Pharmacol, 56, 1071-8.

KATAOKA, H., HAMILTON, J., MCKEMY, D., CAMERER, E., ZHENG, Y., CHENG, A., GRIFFIN, C. & COUGHLIN, S. (2003) Protease-activated receptors 1 and 4 mediate thrombin signaling in endothelial cells. Blood, 102,

3224-31.

KAWABATA, A. (2003) Gastrointestinal functions of proteinase-activated receptors. Life Sci, 74, 247-54.

KAWABATA, A., KANKE, T., YONEZAWA, D., ISHIKI, T., SAKA, M., KABEYA, M., SEKIGUCHI, F., KUBO, S., KURODA, R., IWAKI, M., KATSURA, K. & PLEVIN, R. (2004) Potent and metabolically stable agonists for protease-activated receptor-2: evaluation of activity in multiple assay systems in vitro and in vivo. J Pharmacol Exp Ther, 309, 1098-107.

KAWABATA, A. & KURODA, R. (2000) Protease-activated receptor (PAR), a novel family of G protein-coupled seven trans-membrane domain receptors: activation mechanisms and physiological roles. Jpn J Pharmacol, 82, 171-4.

KAWABATA, A., KURODA, R., NAKAYA, Y., KAWAI, K., NISHIKAWA, H. & KAWAO, N. (2001) Factor Xa-evoked relaxation in rat aorta: involvement of PAR-2. Biochem Biophys Res Commun, 282, 432-5.

KAWABATA, A., OONO, Y., YONEZAWA, D., HIRAMATSU, K., INOI, N., SEKIGUCHI, F., HONJO, M., HIROFUCHI, M., KANKE, T. & ISHIWATA, H. (2005) 2-Furoyl-LIGRL-NH2, a potent agonist for proteinase-activated receptor-2, as a gastric mucosal cytoprotective agent in mice. Br J Pharmacol, 144, 212-9.

KELLY, E., BAILEY, C. & HENDERSON, G. (2008) Agonist-selective mechanisms of GPCR desensitization. Br J Pharmacol, 153 Suppl 1, S379-88.

KELSO, E., LOCKHART, J., HEMBROUGH, T., DUNNING, L., PLEVIN, R., HOLLENBERG, M., SOMMERHOFF, C., MCLEAN, J. & FERRELL, W. (2006) Therapeutic promise of proteinase-activated receptor-2 antagonism in joint inflammation. J Pharmacol Exp Ther, 316, 1017-24.

KENWORTHY, A. (2001) Imaging protein-protein interactions using fluorescence resonance energy transfer microscopy. Methods, 24, 289-96.

KOBILKA, B. (2007) G protein coupled receptor structure and activation. Biochim Biophys Acta, 1768, 794-807.

KOBILKA, B., DIXON, R., FRIELLE, T., DOHLMAN, H., BOLANOWSKI, M., SIGAL, I., YANG-FENG, T., FRANCKE, U., CARON, M. & LEFKOWITZ, R. (1987) cDNA for the human beta 2-adrenergic receptor: a protein with

multiple membrane-spanning domains and encoded by a gene whose chromosomal location is shared with that of the receptor for platelet-derived growth factor. Proc Natl Acad Sci U S A, 84, 46-50.

KOHOUT, T., LIN, F., PERRY, S., CONNER, D. & LEFKOWITZ, R. (2001) beta-Arrestin 1 and 2 differentially regulate heptahelical receptor signaling and trafficking. Proc Natl Acad Sci U S A, 98, 1601-6.

KONG, M., FAN, T., VARGHESE, G., O'DOWD, B. & GEORGE, S. (2006) Agonist-induced cell surface trafficking of an intracellularly sequestered D1 dopamine receptor homo-oligomer. Mol Pharmacol, 70, 78-89.

KOPITO, R. (1999) Biosynthesis and degradation of CFTR. Physiol Rev, 79, S167-73.

KOSTENIS, E., WAELBROECK, M. & MILLIGAN, G. (2005) Techniques: promiscuous Galpha proteins in basic research and drug discovery. Trends Pharmacol Sci, 26, 595-602.

KRAPIVINSKY, G., KRAPIVINSKY, L., WICKMAN, K. & CLAPHAM, D. (1995) G beta gamma binds directly to the G protein-gated K+ channel, IKACh. J Biol Chem, 270, 29059-62.

KRUPNICK, J., SANTINI, F., GAGNON, A., KEEN, J. & BENOVIC, J. (1997) Modulation of the arrestin-clathrin interaction in cells. Characterization of beta-arrestin dominant-negative mutants. J Biol Chem, 272, 32507-12.

KULIOPULOS, A. & COVIC, L. (2003) Blocking receptors on the inside: pepducin-based intervention of PAR signaling and thrombosis. Life Sci, 74, 255-62.

KUMAR, P., LAU, C., MATHUR, M., WANG, P. & DEFEA, K. (2007) Differential effects of beta-arrestins on the internalization, desensitization and ERK1/2 activation downstream of protease activated receptor-2. Am J Physiol Cell Physiol, 293, C346-57.

LANCTOT, P., LECLERC, P., CLÉMENT, M., AUGER-MESSIER, M., ESCHER, E., LEDUC, R. & GUILLEMETTE, G. (2005) Importance of N-glycosylation positioning for cell-surface expression, targeting, affinity and quality control of the human AT1 receptor. Biochem J, 390, 367-76.

LAPORTE, S., OAKLEY, R., HOLT, J., BARAK, L. & CARON, M. (2000) The interaction of beta-arrestin with the AP-2 adaptor is required for the

clustering of beta 2-adrenergic receptor into clathrin-coated pits. J Biol Chem, 275, 23120-6.

LAPORTE, S., OAKLEY, R., ZHANG, J., HOLT, J., FERGUSON, S., CARON, M. & BARAK, L. (1999) The beta2-adrenergic receptor/betaarrestin complex recruits the clathrin adaptor AP-2 during endocytosis. Proc Natl Acad Sci U S A, 96, 3712-7.

LAVOIE, C., MERCIER, J., SALAHPOUR, A., UMAPATHY, D., BREIT, A., VILLENEUVE, L., ZHU, W., XIAO, R., LAKATTA, E., BOUVIER, M. & HÉBERT, T. (2002) Beta 1/beta 2-adrenergic receptor heterodimerization regulates beta 2-adrenergic receptor internalization and ERK signaling efficacy. J Biol Chem, 277, 35402-10.

LEFKOWITZ, R. & SHENOY, S. (2005) Transduction of receptor signals by beta-arrestins. Science, 308, 512-7.

LEFKOWITZ, R. & WHALEN, E. (2004) beta-arrestins: traffic cops of cell signaling. Curr Opin Cell Biol, 16, 162-8.

LEGER, A., COVIC, L. & KULIOPULOS, A. (2006a) Protease-activated receptors in cardiovascular diseases. Circulation, 114, 1070-7.

LEGER, A., JACQUES, S., BADAR, J., KANEIDER, N., DERIAN, C., ANDRADE-GORDON, P., COVIC, L. & KULIOPULOS, A. (2006b) Blocking the protease-activated receptor 1-4 heterodimer in platelet-mediated thrombosis. Circulation, 113, 1244-54.

LIGGETT, S., OSTROWSKI, J., CHESNUT, L., KUROSE, H., RAYMOND, J., CARON, M. & LEFKOWITZ, R. (1992) Sites in the third intracellular loop of the alpha 2A-adrenergic receptor confer short term agonist-promoted desensitization. Evidence for a receptor kinase-mediated mechanism. J Biol Chem, 267, 4740-6.

LIPPINCOTT-SCHWARTZ, J., ROBERTS, T. & HIRSCHBERG, K. (2000) Secretory protein trafficking and organelle dynamics in living cells. Annu Rev Cell Dev Biol, 16, 557-89.

LIPPINCOTT-SCHWARTZ, J., SNAPP, E. & KENWORTHY, A. (2001) Studying protein dynamics in living cells. Nat Rev Mol Cell Biol, 2, 444-56.

LOHSE, M., HEIN, P., HOFFMANN, C., NIKOLAEV, V., VILARDAGA, J. &

BÜNEMANN, M. (2008a) Kinetics of G-protein-coupled receptor signals in intact cells. Br J Pharmacol, 153 Suppl 1, S125-32.

LOHSE, M. & KLENK, C. (2008) Blocking them all: beta-arrestins inhibit cellular signaling. Mol Cell, 31, 619-21.

LOHSE, M., NIKOLAEV, V., HEIN, P., HOFFMANN, C., VILARDAGA, J. & BÜNEMANN, M. (2008b) Optical techniques to analyze real-time activation and signaling of G-protein-coupled receptors. Trends Pharmacol Sci, 29, 159-65.

LOPEZ-GIMENEZ, J., CANALS, M., PEDIANI, J. & MILLIGAN, G. (2007) The alpha1b-adrenoceptor exists as a higher-order oligomer: effective oligomerization is required for receptor maturation, surface delivery, and function. Mol Pharmacol, 71, 1015-29.

LOPEZ-GIMENEZ, J., VILARÓ, M. & MILLIGAN, G. (2008) Morphine desensitization, internalization, and down-regulation of the mu opioid receptor is facilitated by serotonin 5-hydroxytryptamine2A receptor coactivation. Mol Pharmacol, 74, 1278-91.

LUO, W., WANG, Y., HANCK, T., STRICKER, R. & REISER, G. (2006) Jab1, a novel protease-activated receptor-2 (PAR-2)-interacting protein, is involved in PAR-2-induced activation of activator protein-1. J Biol Chem, 281, 7927-36.

LUO, W., WANG, Y. & REISER, G. (2007) p24A, a type I transmembrane protein, controls ARF1-dependent resensitization of protease-activated receptor-2 by influence on receptor trafficking. J Biol Chem, 282, 30246-55.

LUTTRELL, L. (2002) Activation and targeting of mitogen-activated protein kinases by G-protein-coupled receptors. Can J Physiol Pharmacol, 80, 375-82.

LUTTRELL, L. & LEFKOWITZ, R. (2002) The role of beta-arrestins in the termination and transduction of G-protein-coupled receptor signals. J Cell Sci, 115, 455-65.

MA, L. & PEI, G. (2007) Beta-arrestin signaling and regulation of transcription. J Cell Sci, 120, 213-8.

MA, Y., ZHANG, B., QIAN, R., LU, C., ZHAO, F. & YIN, L. (2006) Tryptase activates PKB in inflammatory reaction in ECV304 cells. Biochim Biophys

Acta, 1763, 313-21.

MACFARLANE, S., SEATTER, M., KANKE, T., HUNTER, G. & PLEVIN, R. (2001) Proteinase-activated receptors. Pharmacol Rev, 53, 245-82.

MACFARLANE, S., SLOSS, C., CAMERON, P., KANKE, T., MCKENZIE, R. & PLEVIN, R. (2005) The role of intracellular Ca2+ in the regulation of proteinase-activated receptor-2 mediated nuclear factor kappa B signalling in keratinocytes. Br J Pharmacol, 145, 535-44.

MAGGIO, R., VOGEL, Z. & WESS, J. (1993) Coexpression studies with mutant muscarinic/adrenergic receptors provide evidence for intermolecular "cross-talk" between G-protein-linked receptors. Proc Natl Acad Sci U S A, 90, 3103-7.

MAJOR, C., SANTULLI, R., DERIAN, C. & ANDRADE-GORDON, P. (2003) Extracellular mediators in atherosclerosis and thrombosis: lessons from thrombin receptor knockout mice. Arterioscler Thromb Vasc Biol, 23, 931-9.

MARGETA-MITROVIC, M., JAN, Y. & JAN, L. (2000) A trafficking checkpoint controls GABA(B) receptor heterodimerization. Neuron, 27, 97-106.

MARINISSEN, M., SERVITJA, J., OFFERMANNS, S., SIMON, M. & GUTKIND, J. (2003) Thrombin protease-activated receptor-1 signals through Gq- and G13-initiated MAPK cascades regulating c-Jun expression to induce cell transformation. J Biol Chem, 278, 46814-25.

MARION, S., OAKLEY, R., KIM, K., CARON, M. & BARAK, L. (2006) A beta-arrestin binding determinant common to the second intracellular loops of rhodopsin family G protein-coupled receptors. J Biol Chem, 281, 2932-8.

MARSHALL, F., JONES, K., KAUPMANN, K. & BETTLER, B. (1999a) GABAB receptors - the first 7TM heterodimers. Trends Pharmacol Sci, 20, 396-9.

MARSHALL, F., WHITE, J., MAIN, M., GREEN, A. & WISE, A. (1999b) GABA(B) receptors function as heterodimers. Biochem Soc Trans, 27, 530-5.

MAUREL, D., COMPS-AGRAR, L., BROCK, C., RIVES, M., BOURRIER, E., AYOUB, M., BAZIN, H., TINEL, N., DURROUX, T., PRÉZEAU, L., TRINQUET, E. & PIN, J. (2008) Cell-surface protein-protein interaction analysis with time-resolved FRET and snap-tag technologies: application to GPCR oligomerization. Nat Methods, 5, 561-7.

MCDOUGALL, J., ZHANG, C., CELLARS, L., JOUBERT, E., DIXON, C. & VERGNOLLE, N. (2009) Triggering of proteinase-activated receptor 4 leads to joint pain and inflammation in mice. Arthritis Rheum, 60, 728-37.

MCINTOSH, K., CUNNINGHAM, M., CADALBERT, L., LOCKHART, J., BOYD, G., FERRELL, W. & PLEVIN, R. (2010) Proteinase-activated receptor-2 mediated inhibition of TNFalpha-stimulated JNK activation - A novel paradigm for G(q/11) linked GPCRs. Cell Signal, 22, 265-73.

MCINTOSH, K., PLEVIN, R., FERRELL, W. & LOCKHART, J. (2007) The therapeutic potential of proteinase-activated receptors in arthritis. Curr Opin Pharmacol, 7, 334-8.

MCLAUGHLIN, J., PATTERSON, M. & MALIK, A. (2007) Protease-activated receptor-3 (PAR3) regulates PAR1 signaling by receptor dimerization. Proc Natl Acad Sci U S A, 104, 5662-7.

MCLAUGHLIN, J., SHEN, L., HOLINSTAT, M., BROOKS, J., DIBENEDETTO, E. & HAMM, H. (2005) Functional selectivity of G protein signaling by agonist peptides and thrombin for the protease-activated receptor-1. J Biol Chem, 280, 25048-59.

MELLOR, H. & PARKER, P. (1998) The extended protein kinase C superfamily. Biochem J, 332 (Pt 2), 281-92.

MICHELSEN, K., YUAN, H. & SCHWAPPACH, B. (2005) Hide and run. Arginine-based endoplasmic-reticulum-sorting motifs in the assembly of heteromultimeric membrane proteins. EMBO Rep, 6, 717-22.

MILLIGAN, G. (2007) G protein-coupled receptor dimerisation: molecular basis and relevance to function. Biochim Biophys Acta, 1768, 825-35.

MILLIGAN, G. & KOSTENIS, E. (2006) Heterotrimeric G-proteins: a short history. Br J Pharmacol, 147 Suppl 1, S46-55.

MILLIGAN, G., PEDIANI, J., CANALS, M. & LOPEZ-GIMENEZ, J. (2006) Oligomeric structure of the alpha1b-adrenoceptor: comparisons with rhodopsin. Vision Res, 46, 4434-41.

MOLINO, M., BARNATHAN, E., NUMEROF, R., CLARK, J., DREYER, M., CUMASHI, A., HOXIE, J., SCHECHTER, N., WOOLKALIS, M. & BRASS, L. (1997a) Interactions of mast cell tryptase with thrombin receptors

and PAR-2. J Biol Chem, 272, 4043-9.

MOLINO, M., WOOLKALIS, M., REAVEY-CANTWELL, J., PRATICÓ, D., ANDRADE-GORDON, P., BARNATHAN, E. & BRASS, L. (1997b) Endothelial cell thrombin receptors and PAR-2. Two protease-activated receptors located in a single cellular environment. J Biol Chem, 272, 11133-41.

MOMOTA, F., HIRANO, K., HIRANO, M., NISHIMURA, J. & KANAIDE, H. (2006) Involvement of Gi/o in the PAR-4-induced NO production in endothelial cells. Biochem Biophys Res Commun, 342, 365-71.

NAKANISHI-MATSUI, M., ZHENG, Y., SULCINER, D., WEISS, E., LUDEMAN, M. & COUGHLIN, S. (2000) PAR3 is a cofactor for PAR4 activation by thrombin. Nature, 404, 609-13.

NANEVICZ, T., ISHII, M., WANG, L., CHEN, M., CHEN, J., TURCK, C., COHEN, F. & COUGHLIN, S. (1995) Mechanisms of thrombin receptor agonist specificity. Chimeric receptors and complementary mutations identify an agonist recognition site. J Biol Chem, 270, 21619-25.

NASU-NISHIMURA, Y., HURTADO, D., BRAUD, S., TANG, T., ISAAC, J. & ROCHE, K. (2006) Identification of an endoplasmic reticulum-retention motif in an intracellular loop of the kainate receptor subunit KA2. J Neurosci, 26, 7014-21.

NATHANS, J. & HOGNESS, D. (1983) Isolation, sequence analysis, and intron-exon arrangement of the gene encoding bovine rhodopsin. Cell, 34, 807-14.

NYSTEDT, S., EMILSSON, K., LARSSON, A., STRÖMBECK, B. & SUNDELIN, J. (1995a) Molecular cloning and functional expression of the gene encoding the human proteinase-activated receptor 2. Eur J Biochem, 232, 84-9.

NYSTEDT, S., EMILSSON, K., WAHLESTEDT, C. & SUNDELIN, J. (1994) Molecular cloning of a potential proteinase activated receptor. Proc Natl Acad Sci U S A, 91, 9208-12.

NYSTEDT, S., LARSSON, A., ABERG, H. & SUNDELIN, J. (1995b) The mouse proteinase-activated receptor-2 cDNA and gene. Molecular cloning and functional expression. J Biol Chem, 270, 5950-55.

NYSTEDT, S., RAMAKRISHNAN, V. & SUNDELIN, J. (1996) The proteinase-

activated receptor 2 is induced by inflammatory mediators in human endothelial cells. Comparison with the thrombin receptor. J Biol Chem, 271, 14910-5.

OAKLEY, R., LAPORTE, S., HOLT, J., CARON, M. & BARAK, L. (2000) Differential affinities of visual arrestin, beta arrestin1, and beta arrestin2 for G protein-coupled receptors delineate two major classes of receptors. J Biol Chem, 275, 17201-10.

O'BRIEN, P., PREVOST, N., MOLINO, M., HOLLINGER, M., WOOLKALIS, M., WOULFE, D. & BRASS, L. (2000) Thrombin responses in human endothelial cells. Contributions from receptors other than PAR1 include the transactivation of PAR2 by thrombin-cleaved PAR1. J Biol Chem, 275, 13502-9.

O'DOWD, B., JI, X., ALIJANIARAM, M., RAJARAM, R., KONG, M., RASHID, A., NGUYEN, T. & GEORGE, S. (2005) Dopamine receptor oligomerization visualized in living cells. J Biol Chem, 280, 37225-35.

OFFERMANNS, S., LAUGWITZ, K., SPICHER, K. & SCHULTZ, G. (1994) G proteins of the G12 family are activated via thromboxane A2 and thrombin receptors in human platelets. Proc Natl Acad Sci U S A, 91, 504-8.

OWEN, W. (2003) PAR-3 is a low-affinity substrate, high affinity effector of thrombin. Biochem Biophys Res Commun, 305, 166-8.

PAING, M., JOHNSTON, C., SIDEROVSKI, D. & TREJO, J. (2006) Clathrin adaptor AP2 regulates thrombin receptor constitutive internalization and endothelial cell resensitization. Mol Cell Biol, 26, 3231-42.

PAING, M., STUTTS, A., KOHOUT, T., LEFKOWITZ, R. & TREJO, J. (2002) beta -Arrestins regulate protease-activated receptor-1 desensitization but not internalization or Down-regulation. J Biol Chem, 277, 1292-300.

PALCZEWSKI, K., KUMASAKA, T., HORI, T., BEHNKE, C., MOTOSHIMA, H., FOX, B., LE TRONG, I., TELLER, D., OKADA, T., STENKAMP, R., YAMAMOTO, M. & MIYANO, M. (2000) Crystal structure of rhodopsin: A G protein-coupled receptor. Science, 289, 739-45.

PLEVIN, R., KELLOCK, N., WAKELAM, M. & WADSWORTH, R. (1994) Regulation by hypoxia of endothelin-1-stimulated phospholipase D activity in

sheep pulmonary artery cultured smooth muscle cells. Br J Pharmacol, 112, 311-5.

POLLOK, B. A. & HEIM, R. (1999) Using GFP in FRET-based applications. Trends Cell Biol, 9, 57-60.

PONSIOEN, B., ZHAO, J., RIEDL, J., ZWARTKRUIS, F., VAN DER KROGT, G., ZACCOLO, M., MOOLENAAR, W., BOS, J. & JALINK, K. (2004) Detecting cAMP-induced Epac activation by fluorescence resonance energy transfer: Epac as a novel cAMP indicator. EMBO Rep, 5, 1176-80.

POPA, C., NETEA, M., VAN RIEL, P., VAN DER MEER, J. & STALENHOEF, A. (2007) The role of TNF-alpha in chronic inflammatory conditions, intermediary metabolism, and cardiovascular risk. J Lipid Res, 48, 751-62.

PREMONT, R., INGLESE, J. & LEFKOWITZ, R. (1995) Protein kinases that phosphorylate activated G protein-coupled receptors. FASEB J, 9, 175-82.

PRENZEL, N., ZWICK, E., DAUB, H., LESERER, M., ABRAHAM, R., WALLASCH, C. & ULLRICH, A. (1999) EGF receptor transactivation by G-protein-coupled receptors requires metalloproteinase cleavage of proHB-EGF. Nature, 402, 884-8.

PRINSTER, S., HAGUE, C. & HALL, R. (2005) Heterodimerization of g protein-coupled receptors: specificity and functional significance. Pharmacol Rev, 57, 289-98.

PROCTOR, K., MILLER, S., BRYANT, N. & GOULD, G. (2006) Syntaxin 16 controls the intracellular sequestration of GLUT4 in 3T3-L1 adipocytes. Biochem Biophys Res Commun, 347, 433-8.

RALLABHANDI, P., NHU, Q., TOSHCHAKOV, V., PIAO, W., MEDVEDEV, A., HOLLENBERG, M., FASANO, A. & VOGEL, S. (2008) Analysis of proteinase-activated receptor 2 and TLR4 signal transduction: a novel paradigm for receptor cooperativity. J Biol Chem, 283, 24314-25.

RANDS, E., CANDELORE, M., CHEUNG, A., HILL, W., STRADER, C. & DIXON, R. (1990) Mutational analysis of beta-adrenergic receptor glycosylation. J Biol Chem, 265, 10759-64.

RASMUSSEN, S., CHOI, H., ROSENBAUM, D., KOBILKA, T., THIAN, F., EDWARDS, P., BURGHAMMER, M., RATNALA, V., SANISHVILI, R.,

FISCHETTI, R., SCHERTLER, G., WEIS, W. & KOBILKA, B. (2007) Crystal structure of the human beta2 adrenergic G-protein-coupled receptor. Nature, 450, 383-7.

RASMUSSEN, U., VOURET-CRAVIARI, V., JALLAT, S., SCHLESINGER, Y., PAGÈS, G., PAVIRANI, A., LECOCQ, J., POUYSSÉGUR, J. & VAN OBBERGHEN-SCHILLING, E. (1991) cDNA cloning and expression of a hamster alpha-thrombin receptor coupled to Ca2+ mobilization. FEBS Lett, 288, 123-8.

REN, Z., RILEY, N., GARCIA, E., SANDERS, J., SWANSON, G. & MARSHALL, J. (2003) Multiple trafficking signals regulate kainate receptor KA2 subunit surface expression. J Neurosci, 23, 6608-16.

RIOS, C., JORDAN, B., GOMES, I. & DEVI, L. G-protein-coupled receptor dimerization: modulation of receptor function. Pharmacol Ther, 92, 71-87.

RITCHIE, E., SAKA, M., MACKENZIE, C., DRUMMOND, R., WHEELER-JONES, C., KANKE, T. & PLEVIN, R. (2007) Cytokine upregulation of proteinase-activated-receptors 2 and 4 expression mediated by p38 MAP kinase and inhibitory kappa B kinase beta in human endothelial cells. Br J Pharmacol, 150, 1044-54.

ROCHEVILLE, M., LANGE, D., KUMAR, U., PATEL, S., PATEL, R. & PATEL, Y. (2000) Receptors for dopamine and somatostatin: formation of hetero-oligomers with enhanced functional activity. Science, 288, 154-7.

RODBELL, M. (1971) In vitro assays of adenyl cyclase. Acta Endocrinol Suppl (Copenh), 153, 337-47.

ROOSTERMAN, D., SCHMIDLIN, F. & BUNNETT, N. (2003) Rab5a and rab11a mediate agonist-induced trafficking of protease-activated receptor 2. Am J Physiol Cell Physiol, 284, C1319-29.

ROTH, N., CAMPBELL, P., CARON, M., LEFKOWITZ, R. & LOHSE, M. (1991) Comparative rates of desensitization of beta-adrenergic receptors by the beta-adrenergic receptor kinase and the cyclic AMP-dependent protein kinase. Proc Natl Acad Sci U S A, 88, 6201-4.

ROY, A., BARAGLI, A., BERNSTEIN, L., HEPLER, J., HÉBERT, T. & CHIDIAC, P. (2006) RGS2 interacts with Gs and adenylyl cyclase in living cells. Cell

Signal, 18, 336-48.

RUDDOCK, L. & MOLINARI, M. (2006) N-glycan processing in ER quality control. J Cell Sci, 119, 4373-80.

RUSSO, A., SOH, U., PAING, M., ARORA, P. & TREJO, J. (2009) Caveolae are required for protease-selective signaling by protease-activated receptor-1. Proc Natl Acad Sci U S A, 106, 6393-7.

SABO, T., GURWITZ, D., MOTOLA, L., BRODT, P., BARAK, R. & ELHANATY, E. (1992) Structure-activity studies of the thrombin receptor activating peptide. Biochem Biophys Res Commun, 188, 604-10.

SABRI, A., GUO, J., ELOUARDIGHI, H., DARROW, A., ANDRADE-GORDON, P. & STEINBERG, S. (2003) Mechanisms of protease-activated receptor-4 actions in cardiomyocytes. Role of Src tyrosine kinase. J Biol Chem, 278, 11714-20.

SABRI, A., MUSKE, G., ZHANG, H., PAK, E., DARROW, A., ANDRADE-GORDON, P. & STEINBERG, S. (2000) Signaling properties and functions of two distinct cardiomyocyte protease-activated receptors. Circ Res, 86, 1054-61.

SABRI, A., SHORT, J., GUO, J. & STEINBERG, S. (2002) Protease-activated receptor-1-mediated DNA synthesis in cardiac fibroblast is via epidermal growth factor receptor transactivation: distinct PAR-1 signaling pathways in cardiac fibroblasts and cardiomyocytes. Circ Res, 91, 532-9.

SAMBRANO, G., HUANG, W., FARUQI, T., MAHRUS, S., CRAIK, C. & COUGHLIN, S. (2000) Cathepsin G activates protease-activated receptor-4 in human platelets. J Biol Chem, 275, 6819-23.

SANTULLI, R., DERIAN, C., DARROW, A., TOMKO, K., ECKARDT, A., SEIBERG, M., SCARBOROUGH, R. & ANDRADE-GORDON, P. (1995) Evidence for the presence of a protease-activated receptor distinct from the thrombin receptor in human keratinocytes. Proc Natl Acad Sci U S A, 92, 9151-5.

SARTANIA, N., APPELBE, S., PEDIANI, J. & MILLIGAN, G. (2007) Agonist occupancy of a single monomeric element is sufficient to cause internalization of the dimeric beta2-adrenoceptor. Cell Signal, 19, 1928-38.

SAWUTZ, D., LANIER, S., WARREN, C. & GRAHAM, R. (1987) Glycosylation of the mammalian alpha 1-adrenergic receptor by complex type N-linked oligosaccharides. Mol Pharmacol, 32, 565-71.

SCARBOROUGH, R., NAUGHTON, M., TENG, W., HUNG, D., ROSE, J., VU, T., WHEATON, V., TURCK, C. & COUGHLIN, S. (1992) Tethered ligand agonist peptides. Structural requirements for thrombin receptor activation reveal mechanism of proteolytic unmasking of agonist function. J Biol Chem, 267, 13146-9.

SCHMIDT, V., NIERMAN, W., MAGLOTT, D., CUPIT, L., MOSKOWITZ, K., WAINER, J. & BAHOU, W. (1998) The human proteinase-activated receptor-3 (PAR-3) gene. Identification within a Par gene cluster and characterization in vascular endothelial cells and platelets. J Biol Chem, 273, 15061-8.

SCHULTE, G. & BRYJA, V. (2007) The Frizzled family of unconventional G-protein-coupled receptors. Trends Pharmacol Sci, 28, 518-25.

SCHWEIZER, A., FRANSEN, J., MATTER, K., KREIS, T., GINSEL, L. & HAURI, H. (1990) Identification of an intermediate compartment involved in protein transport from endoplasmic reticulum to Golgi apparatus. Eur J Cell Biol, 53, 185-96.

SEACHRIST, J., ANBORGH, P. & FERGUSON, S. (2000) beta 2-adrenergic receptor internalization, endosomal sorting, and plasma membrane recycling are regulated by rab GTPases. J Biol Chem, 275, 27221-8.

SEATTER, M., DRUMMOND, R., KANKE, T., MACFARLANE, S., HOLLENBERG, M. & PLEVIN, R. (2004) The role of the C-terminal tail in protease-activated receptor-2-mediated Ca2+ signalling, proline-rich tyrosine kinase-2 activation, and mitogen-activated protein kinase activity. Cell Signal, 16, 21-9.

SHAN, D., CHEN, L., WANG, D., TAN, Y., GU, J. & HUANG, X. (2006) The G protein G alpha(13) is required for growth factor-induced cell migration. Dev Cell, 10, 707-18.

SHAPIRO, M. & COUGHLIN, S. (1998) Separate signals for agonist-independent and agonist-triggered trafficking of protease-activated receptor 1. J Biol

Chem, 273, 29009-14.

SHAPIRO, M., TREJO, J., ZENG, D. & COUGHLIN, S. (1996) Role of the thrombin receptor's cytoplasmic tail in intracellular trafficking. Distinct determinants for agonist-triggered versus tonic internalization and intracellular localization. J Biol Chem, 271, 32874-80.

SHAPIRO, M., WEISS, E., FARUQI, T. & COUGHLIN, S. (2000) Protease-activated receptors 1 and 4 are shut off with distinct kinetics after activation by thrombin. J Biol Chem, 275, 25216-21.

SHI, X., GANGADHARAN, B., BRASS, L., RUF, W. & MUELLER, B. (2004) Protease-activated receptors (PAR1 and PAR2) contribute to tumor cell motility and metastasis. Mol Cancer Res, 2, 395-402.

SHIKANO, S., COBLITZ, B., WU, M. & LI, M. (2006) 14-3-3 proteins: regulation of endoplasmic reticulum localization and surface expression of membrane proteins. Trends Cell Biol, 16, 370-5.

SIBLEY, D., BENOVIC, J., CARON, M. & LEFKOWITZ, R. (1987) Regulation of transmembrane signaling by receptor phosphorylation. Cell, 48, 913-22.

SNOW, B., HALL, R., KRUMINS, A., BROTHERS, G., BOUCHARD, D., BROTHERS, C., CHUNG, S., MANGION, J., GILMAN, A., LEFKOWITZ, R. & SIDEROVSKI, D. (1998) GTPase activating specificity of RGS12 and binding specificity of an alternatively spliced PDZ (PSD-95/Dlg/ZO-1) domain. J Biol Chem, 273, 17749-55.

STALHEIM, L., DING, Y., GULLAPALLI, A., PAING, M., WOLFE, B., MORRIS, D. & TREJO, J. (2005) Multiple independent functions of arrestins in the regulation of protease-activated receptor-2 signaling and trafficking. Mol Pharmacol, 67, 78-87.

STEINBERG, S. (2005) The cardiovascular actions of protease-activated receptors. Mol Pharmacol, 67, 2-11.

STERNE-MARR, R., LEAHEY, P. A., BRESEE, J. E., DICKSON, H. M., HO, W., RAGUSA, M. J., DONNELLY, R. M., AMIE, S. M., KRYWY, J. A., BROOKINS-DANZ, E. D., ORAKWUE, S. C., CARR, M. J., YOSHINO-KOH, K., LI, Q. & TESMER, J. J. (2009) GRK2 activation by receptors: role of the kinase large lobe and carboxyl-terminal tail. Biochemistry, 48, 4285-

93.

STRATHMANN, M. & SIMON, M. (1990) G protein diversity: a distinct class of alpha subunits is present in vertebrates and invertebrates. Proc Natl Acad Sci U S A, 87, 9113-7.

STREB, H., IRVINE, R., BERRIDGE, M. & SCHULZ, I. (1983) Release of Ca2+ from a nonmitochondrial intracellular store in pancreatic acinar cells by inositol-1,4,5-trisphosphate. Nature, 306, 67-9.

SUNAHARA, R., DESSAUER, C., WHISNANT, R., KLEUSS, C. & GILMAN, A. (1997) Interaction of Gsalpha with the cytosolic domains of mammalian adenylyl cyclase. J Biol Chem, 272, 22265-71.

SUO, Z., WU, M., CITRON, B., PALAZZO, R. & FESTOFF, B. (2003) Rapid tau aggregation and delayed hippocampal neuronal death induced by persistent thrombin signaling. J Biol Chem, 278, 37681-9.

SWIFT, S., SHERIDAN, P., COVIC, L. & KULIOPULOS, A. (2000) PAR1 thrombin receptor-G protein interactions. Separation of binding and coupling determinants in the galpha subunit. J Biol Chem, 275, 2627-35.

TADROSS, M., PARK, S., VEERAMANI, B. & YUE, D. (2009) Robust approaches to quantitative ratiometric FRET imaging of CFP/YFP fluorophores under confocal microscopy. J Microsc, 233, 192-204.

TAKANISHI, C., BYKOVA, E., CHENG, W. & ZHENG, J. (2006) GFP-based FRET analysis in live cells. Brain Res, 1091, 132-9.

TAKASAKI, J., SAITO, T., TANIGUCHI, M., KAWASAKI, T., MORITANI, Y., HAYASHI, K. & KOBORI, M. (2004) A novel Galphaq/11-selective inhibitor. J Biol Chem, 279, 47438-45.

TANABE, S., KREUTZ, B., SUZUKI, N. & KOZASA, T. (2004) Regulation of RGS-RhoGEFs by Galpha12 and Galpha13 proteins. Methods Enzymol, 390, 285-94.

TERRILLON, S., BARBERIS, C. & BOUVIER, M. (2004) Heterodimerization of V1a and V2 vasopressin receptors determines the interaction with beta-arrestin and their trafficking patterns. Proc Natl Acad Sci U S A, 101, 1548-53.

TERRILLON, S. & BOUVIER, M. (2004) Roles of G-protein-coupled receptor

dimerization. EMBO Rep, 5, 30-4.

TERRILLON, S., DURROUX, T., MOUILLAC, B., BREIT, A., AYOUB, M., TAULAN, M., JOCKERS, R., BARBERIS, C. & BOUVIER, M. (2003) Oxytocin and vasopressin V1a and V2 receptors form constitutive homo- and heterodimers during biosynthesis. Mol Endocrinol, 17, 677-91.

TIRUPPATHI, C., YAN, W., SANDOVAL, R., NAQVI, T., PRONIN, A., BENOVIC, J. & MALIK, A. (2000) G protein-coupled receptor kinase-5 regulates thrombin-activated signaling in endothelial cells. Proc Natl Acad Sci U S A, 97, 7440-5.

TOPIOL, S. & SABIO, M. (2009) X-ray structure breakthroughs in the GPCR transmembrane region. Biochem Pharmacol, 78, 11-20.

TREJO, J., ALTSCHULER, Y., FU, H., MOSTOV, K. & COUGHLIN, S. (2000) Protease-activated receptor-1 down-regulation: a mutant HeLa cell line suggests novel requirements for PAR1 phosphorylation and recruitment to clathrin-coated pits. J Biol Chem, 275, 31255-65.

TREJO, J., HAMMES, S. & COUGHLIN, S. (1998) Termination of signaling by protease-activated receptor-1 is linked to lysosomal sorting. Proc Natl Acad Sci U S A, 95, 13698-702.

URBAN, J., CLARKE, W., VON ZASTROW, M., NICHOLS, D., KOBILKA, B., WEINSTEIN, H., JAVITCH, J., ROTH, B., CHRISTOPOULOS, A., SEXTON, P., MILLER, K., SPEDDING, M. & MAILMAN, R. (2007) Functional selectivity and classical concepts of quantitative pharmacology. J Pharmacol Exp Ther, 320, 1-13.

VASSILAKOS, A., MICHALAK, M., LEHRMAN, M. & WILLIAMS, D. (1998) Oligosaccharide binding characteristics of the molecular chaperones calnexin and calreticulin. Biochemistry, 37, 3480-90.

VAUGHAN, D., MILLMAN, E., GODINES, V., FRIEDMAN, J., TRAN, T., DAI, W., KNOLL, B., CLARK, R. & MOORE, R. (2006) Role of the G protein-coupled receptor kinase site serine cluster in beta2-adrenergic receptor internalization, desensitization, and beta-arrestin translocation. J Biol Chem, 281, 7684-92.

VERGNOLLE, N. (2000) Review article: proteinase-activated receptors - novel

signals for gastrointestinal pathophysiology. Aliment Pharmacol Ther, 14, 257-66.

VERGNOLLE, N., BUNNETT, N., SHARKEY, K., BRUSSEE, V., COMPTON, S., GRADY, E., CIRINO, G., GERARD, N., BASBAUM, A., ANDRADE-GORDON, P., HOLLENBERG, M. & WALLACE, J. (2001) Proteinase-activated receptor-2 and hyperalgesia: A novel pain pathway. Nat Med, 7, 821-6.

VERGNOLLE, N., DERIAN, C., D'ANDREA, M., STEINHOFF, M. & ANDRADE-GORDON, P. (2002) Characterization of thrombin-induced leukocyte rolling and adherence: a potential proinflammatory role for proteinase-activated receptor-4. J Immunol, 169, 1467-73.

VERRIER, S., WILLMANN, M., WENZEL, D., WINTER, U., VON MOLLARD, G. & SÖLING, H. (2008) Members of a mammalian SNARE complex interact in the endoplasmic reticulum in vivo and are found in COPI vesicles. Eur J Cell Biol, 87, 863-78.

VILARDAGA, J., BÜNEMANN, M., KRASEL, C., CASTRO, M. & LOHSE, M. (2003) Measurement of the millisecond activation switch of G protein-coupled receptors in living cells. Nat Biotechnol, 21, 807-12.

VILARDAGA, J. P., BUNEMANN, M., FEINSTEIN, T. N., LAMBERT, N., NIKOLAEV, V. O., ENGELHARDT, S., LOHSE, M. J. & HOFFMANN, C. (2009) GPCR and G proteins: drug efficacy and activation in live cells. Mol Endocrinol, 23, 590-9.

VIVITHANAPORN, P., YAN, S. & SWANSON, G. (2006) Intracellular trafficking of KA2 kainate receptors mediated by interactions with coatomer protein complex I (COPI) and 14-3-3 chaperone systems. J Biol Chem, 281, 15475-84.

VOSS, T., DEMARCO, I. & DAY, R. (2005) Quantitative imaging of protein interactions in the cell nucleus. Biotechniques, 38, 413-24.

VU, T., HUNG, D., WHEATON, V. & COUGHLIN, S. (1991a) Molecular cloning of a functional thrombin receptor reveals a novel proteolytic mechanism of receptor activation. Cell, 64, 1057-68.

VU, T., WHEATON, V., HUNG, D., CHARO, I. & COUGHLIN, S. (1991b)

Domains specifying thrombin-receptor interaction. Nature, 353, 674-7.

WANAMAKER, C. & GREEN, W. (2005) N-linked glycosylation is required for nicotinic receptor assembly but not for subunit associations with calnexin. J Biol Chem, 280, 33800-10.

WANG, Y., ZHOU, Y., SZABO, K., HAFT, C. & TREJO, J. (2002) Down-regulation of protease-activated receptor-1 is regulated by sorting nexin 1. Mol Biol Cell, 13, 1965-76.

WARNE, T., SERRANO-VEGA, M., BAKER, J., MOUKHAMETZIANOV, R., EDWARDS, P., HENDERSON, R., LESLIE, A., TATE, C. & SCHERTLER, G. (2008) Structure of a beta1-adrenergic G-protein-coupled receptor. Nature, 454, 486-91.

WEI, H., AHN, S., SHENOY, S., KARNIK, S., HUNYADY, L., LUTTRELL, L. & LEFKOWITZ, R. (2003) Independent beta-arrestin 2 and G protein-mediated pathways for angiotensin II activation of extracellular signal-regulated kinases 1 and 2. Proc Natl Acad Sci U S A, 100, 10782-7.

WIELAND, T. & MITTMANN, C. (2003) Regulators of G-protein signalling: multifunctional proteins with impact on signalling in the cardiovascular system. Pharmacol Ther, 97, 95-115.

WILBANKS, A., LAPORTE, S., BOHN, L., BARAK, L. & CARON, M. (2002) Apparent loss-of-function mutant GPCRs revealed as constitutively desensitized receptors. Biochemistry, 41, 11981-9.

WILLETS, J., MISTRY, R., NAHORSKI, S. & CHALLISS, R. (2003) Specificity of g protein-coupled receptor kinase 6-mediated phosphorylation and regulation of single-cell m3 muscarinic acetylcholine receptor signaling. Mol Pharmacol, 64, 1059-68.

WILSON, S., WILKINSON, G. & MILLIGAN, G. (2005) The CXCR1 and CXCR2 receptors form constitutive homo- and heterodimers selectively and with equal apparent affinities. J Biol Chem, 280, 28663-74.

WISE, A., JUPE, S. & REES, S. (2004) The identification of ligands at orphan G-protein coupled receptors. Annu Rev Pharmacol Toxicol, 44, 43-66.

WOLFE, B. & TREJO, J. (2007) Clathrin-dependent mechanisms of G protein-coupled receptor endocytosis. Traffic, 8, 462-70.

WÜLLER, S., WIESNER, B., LÖFFLER, A., FURKERT, J., KRAUSE, G., HERMOSILLA, R., SCHAEFER, M., SCHÜLEIN, R., ROSENTHAL, W. & OKSCHE, A. (2004) Pharmacochaperones post-translationally enhance cell surface expression by increasing conformational stability of wild-type and mutant vasopressin V2 receptors. J Biol Chem, 279, 47254-63.

XIANG, Y., MASUKO-HONGO, K., SEKINE, T., NAKAMURA, H., YUDOH, K., NISHIOKA, K. & KATO, T. (2006) Expression of proteinase-activated receptors (PAR)-2 in articular chondrocytes is modulated by IL-1beta, TNF-alpha and TGF-beta. Osteoarthritis Cartilage, 14, 1163-73.

XIAO, K., MCCLATCHY, D., SHUKLA, A., ZHAO, Y., CHEN, M., SHENOY, S., YATES, J. R. & LEFKOWITZ, R. (2007) Functional specialization of beta-arrestin interactions revealed by proteomic analysis. Proc Natl Acad Sci U S A, 104, 12011-6.

XIE, G. X. & PALMER, P. P. (2007) How regulators of G protein signaling achieve selective regulation. J Mol Biol, 366, 349-65.

XU, J., HE, J., CASTLEBERRY, A., BALASUBRAMANIAN, S., LAU, A. & HALL, R. (2003) Heterodimerization of alpha 2A- and beta 1-adrenergic receptors. J Biol Chem, 278, 10770-7.

XU, W., ANDERSEN, H., WHITMORE, T., PRESNELL, S., YEE, D., CHING, A., GILBERT, T., DAVIE, E. & FOSTER, D. (1998) Cloning and characterization of human protease-activated receptor 4. Proc Natl Acad Sci U S A, 95, 6642-6.

YANG, F., MOSS, L. & PHILLIPS, G. J. (1996) The molecular structure of green fluorescent protein. Nat Biotechnol, 14, 1246-51.

YAO, X., VÉLEZ RUIZ, G., WHORTON, M., RASMUSSEN, S., DEVREE, B., DEUPI, X., SUNAHARA, R. & KOBILKA, B. (2009) The effect of ligand efficacy on the formation and stability of a GPCR-G protein complex. Proc Natl Acad Sci U S A, 106, 9501-6.

YUAN, H., MICHELSEN, K. & SCHWAPPACH, B. (2003) 14-3-3 dimers probe the assembly status of multimeric membrane proteins. Curr Biol, 13, 638-46.

YUFU, T., HIRANO, K., BI, D., HIRANO, M., NISHIMURA, J., IWAMOTO, Y. & KANAIDE, H. (2005) Rac1 regulation of surface expression of protease-

activated receptor-1 and responsiveness to thrombin in vascular smooth muscle cells. Arterioscler Thromb Vasc Biol, 25, 1506-11.

ZACHARIAS, D., VIOLIN, J., NEWTON, A. & TSIEN, R. (2002) Partitioning of lipid-modified monomeric GFPs into membrane microdomains of live cells. Science, 296, 913-6.

ZANIA, P., GOURNI, D., APLIN, A., NICOSIA, R., FLORDELLIS, C., MARAGOUDAKIS, M. & TSOPANOGLOU, N. (2009) Parstatin, the cleaved peptide on proteinase-activated receptor 1 activation, is a potent inhibitor of angiogenesis. J Pharmacol Exp Ther, 328, 378-89.

ZERANGUE, N., SCHWAPPACH, B., JAN, Y. & JAN, L. (1999) A new ER trafficking signal regulates the subunit stoichiometry of plasma membrane K(ATP) channels. Neuron, 22, 537-48.

ZHANG, J., BARAK, L., ANBORGH, P., LAPORTE, S., CARON, M. & FERGUSON, S. (1999) Cellular trafficking of G protein-coupled receptor/beta-arrestin endocytic complexes. J Biol Chem, 274, 10999-1006.

ZHANG, J., BARAK, L., WINKLER, K., CARON, M. & FERGUSON, S. (1997) A central role for beta-arrestins and clathrin-coated vesicle-mediated endocytosis in beta2-adrenergic receptor resensitization. Differential regulation of receptor resensitization in two distinct cell types. J Biol Chem, 272, 27005-14.

ZHANG, J., CAMPBELL, R. E., TING, A. Y. & TSIEN, R. Y. (2002) Creating new fluorescent probes for cell biology. Nat Rev Mol Cell Biol, 3, 906-18.

ZHENG, B., DE VRIES, L. & GIST FARQUHAR, M. (1999) Divergence of RGS proteins: evidence for the existence of six mammalian RGS subfamilies. Trends Biochem Sci, 24, 411-4.

ZIDAR, D. A., VIOLIN, J. D., WHALEN, E. J. & LEFKOWITZ, R. J. (2009) Selective engagement of G protein coupled receptor kinases (GRKs) encodes distinct functions of biased ligands. Proc Natl Acad Sci U S A, 106, 9649-54.

ZOUDILOVA, M., KUMAR, P., GE, L., WANG, P., BOKOCH, G. & DEFEA, K. (2007) Beta -arrestin-dependent regulation of the cofilin pathway downstream of protease-activated receptor-2. J Biol Chem, 282, 20634–20646.

Book Chapter Reference

CHEN, Y., ELANGOVAN, M., PERIASAMY, A. (2005) FRET Data Analysis: The Algorithm. **In** A. Perisamy & R. N. Day (Ed.) Molecular Imaging FRET Microscopy and Spectroscopy (pp. 126-145). Oxford University Press Inc.